

5. Automotive Metals - Steel

A. Advanced High Strength Steel Joining Technologies Project

Principal Investigator: John C. Bohr
General Motors
Global ME Body
30300 Mound Road – Mail Code 480-109-164
Warren, MI 48090
(810) 602-8276; e-mail: johnc.bohr@gm.com

Principal Investigator: Ted Coon
Ford Motor Company
Manufacturing Development Center
6000 Mercury Drive, Cube BH015
Dearborn, MI 48126
(313) 805-6485; e-mail: tcoon@ford.com

Technology Area Development Manager: William Joost
(202) 287-6020; e-mail: william.joost@ee.doe.gov

Contractor: United States Automotive Materials Partnership(USAMP¹)
Contract No.: DE-FC05-02OR22910 through the National Energy Technology Laboratory

Objective

- Provide welding and joining expertise to support A/SP project teams to facilitate increased use of Advanced High-Strength Steels (AHSS).
- Augment the existing welding and joining technical knowledge pertaining to AHSS through applied research.
- Utilize A/SP research data to prepare industry weldability and weld quality acceptance standards.

Approach

- Anticipate needs of the A/SP lightweighting projects and conduct applied research to address identified barriers and technology gaps.
- Determine welding parameters to produce quality welds, then statically and dynamically test welds produced at these parameters to quantify individual weld structural performance. Tensile shear strength, impact energy and fatigue life are typically evaluated.

- Utilize commercially-available equipment or equipment typically found in existing manufacturing facilities for AHSS feasibility assessments. Utilize other, new technologies as necessary for lightweighting implementation.
- Focus on materials classified as International Iron and Steel Institute (IISI) Group 3 and 4 as well as specific materials recommended by the A/SP member companies.
- Investigate the use of process finite-element modeling to predict weld quality characteristics and optimize weld process parameters. Utilize simulation for future projects to develop weld process optimization and weldability assessments. Validate simulation results with experimental data.

Accomplishments

- Completed Phase II of a comprehensive study on joint efficiency that will allow joining process comparisons for weld repair or substitution. Joint efficiency is defined as joint strength/parent material strength. The Joint Efficiency project is intended only to compare processes. Data are also available for energy comparisons and for stiffness comparisons.
- Created and published results of a Between Spot Weld Buckling Project that assessed the influence of weld pitch and structural adhesive on the load characteristics of hexagonal sections.
- Supported development of an automotive industry AHSS resistance spot weld material characterization (AWS D8.9M:200X) and provided technical support for development of a software application to support common deployment and analysis of the AHSS Design of Experiment test method. This American National Standard has started the balloting process heading towards publication.
- Created and published Weld Bond Adhesive Guidelines for the Future Generation Passenger Compartment and Lightweight Chassis Project Teams.
- Completed extensive finite-element modeling and laboratory experimentation to develop and validate starting resistance spot weld schedules for advanced high strength steel applications.
- Completed finite-element modeling and laboratory experimentation for a FEM web based application for automotive arc welding utilizing the E-Weld Predictor tool developed by the Edison Welding Institute and the Ohio Super-Computer Center.

Future Direction

Future team activities include supporting welding development for the A/SP AHSS Application Guidelines Project Team and developing welding parameter and joint performance data for specific applications on AHSS automotive body prototypes. Future project work also includes:

- Developing arc weld procedures for various weld filler metals and AHSS joints, including determining and ranking the hot-cracking susceptibility and filler metal compatibility of sheet AHSS materials.
- Completing Phase III of the Weld Repair and Joint Efficiency Study to create an application to quantify manufacturing costs for various automotive welding and joining processes.

- Enhancing the FEM application for automotive arc welding utilizing the E-Weld Predictor tool developed by the Edison Welding Institute and the Ohio Super-Computer Center.
- Addressing common misconceptions and myths associated with spot welding AHSS.

Introduction

The primary objective of the High-Strength Steel Joining Technologies project team is to provide welding and joining expertise to the Auto/Steel Partnership (A/SP) light weighting projects to facilitate the increased use of Advanced High-Strength Steels (AHSS). Additional project objectives include augmenting the technical knowledge pertaining to welding of AHSS through applied research and development of industry standards for quality acceptance and weldability testing of AHSS. The purpose of this project is to evaluate the weldability of the new advanced high-strength steels currently being considered by the automotive companies as a solution to lightweighting without compromising cost or structural strength. The project intent is to evaluate various grades, thicknesses, and joining processes.

A secondary purpose of the project is to identify and remove barriers for application of Advanced High-Strength Steels in order to allow automotive manufacturers to reduce vehicle weight and enhance Body-In-White performance. To accomplish this goal the project provides welding parameters and joint performance data for future applications of AHSS.

Weld Repair and Joint Efficiency Project – Phase II

This study is the second phase of the 2008 A/SP Joining Technology Committee Joint Efficiency and Repair Welding project. This work is a comprehensive study on various grades of steels, which quantifies peak load, joint efficiency, energy up to peak load, and joint stiffness for a variety of joining methods. The data allows comparisons to be made for production welding and joining processes and repair substitutions.

Mild steel and four advanced high strength steels were tested. Materials studied were 1.2 mm galvanized mild steel, 1.2 mm electro-galvanized HSLA, 1.2mm galvanized DP600, 1.0 mm galvanized DP780, and 1.0 mm electro-galvanized M190. A wide variety of joining processes were used in this study. Categories included resistance spot welding, gas metal arc welding and brazing, laser welding and brazing, mechanical fasteners, and adhesive bonding. Lap and coach joints were studied.

Load/displacement curves were generated using a tensile test machine. Joint efficiency was calculated from tensile test data as the peak load of the joint divided by the peak load of the parent material, expressed as a percentage. Energy was calculated as the area under the load/displacement curve up to peak load. Joint stiffness was calculated as the slope of the best fit line in the elastic region of the load/displacement curve. For comparison purposes, joint energy and stiffness were normalized to the parent metal energy and stiffness and expressed as percentages.

It was observed that AHSS are weldable and joinable by most of the processes studied in this project. Various joining processes resulted in different strength metrics. There appears to be no common correlation between joint efficiency, energy, and stiffness for the material and process combinations tested.

Joint efficiency decreased as material strength increased for most of the processes studied. This shows that peak load and corresponding joint strength does not generally increase in proportion to parent material strength increase. There appears to be no correlation between normalized energy or stiffness and material strength (See [Figure1](#)).

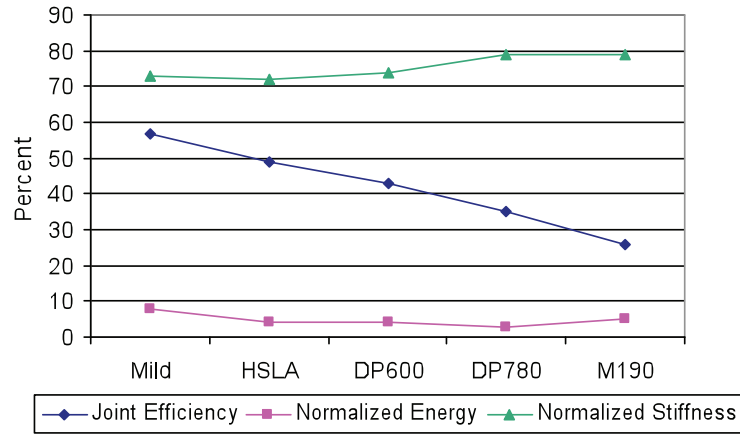


Figure 1. Lap Shear Average Joint Efficiency, Normalized Energy, and Stiffness (All Processes Combined)

Coach joints typically showed significantly lower joint efficiencies and stiffness than lap joints. Comparing all processes, some may produce relatively high joint efficiencies in lap joints but low joint efficiencies in coach joints. Therefore, joint configuration should be considered when selecting joining processes.

In general, few processes produced high joint efficiency, stiffness, and energy for all coupon configurations and materials. Metrics varied substantially among different processes, joint configurations, and materials. Therefore, it is important to carefully consider all factors, based on the intended application and required performance. A pivot table was created to facilitate the review of various joining processes against the desired performance (See Figure 2).

Material	Coupon Configuration	Joining Process	Peak Load (N)	Joint Efficiency	Normalized Energy	Normalized Stiffness
DP780	LS	Arc Braze (25mm lap fillet) LS	11,339	29.0%	0.5%	77.8%
		GMAW (AWS D8.8M - 25mm fillet) LS	19,562	50.0%	1.8%	86.7%
		Laser (25mm lap) LS	20,633	52.8%	2.9%	88.7%
		Laser Braze (25mm lap fillet) LS	8,075	20.7%	0.2%	81.6%
Mild Steel	LS	Arc Braze (25mm lap fillet) LS	7,855	54.0%	3.1%	77.0%
		GMAW (AWS D8.8M - 25mm fillet) LS	9,908	68.2%	7.9%	81.3%
		Laser (25mm lap) LS	10,139	69.8%	9.8%	83.0%
		Laser Braze (25mm lap fillet) LS	6,657	45.8%	1.0%	73.0%

Figure 2. Pivot Table Example for DP780

Weld Bonding Simulation Study

The Joining Team in cooperation with the University of Michigan completed a weld bonding applied research project to study the influence of weld pitch and structural adhesive between spot weld buckling.

This project focused on the axial load deflection characteristics of hexagonal sections. A Gurson shell model was utilized in this study. Sections with and without adhesives were analyzed.

The responses studied included maximum load, the average force taken over the entire displacement and the average force calculated between 25mm to 255mm displacements. Comparisons were made at the extreme corners of the section design on each of four materials (HSLA 350, DP 590, IHS140, and DP 890).

This work concluded that an adhesive bonded flange can precipitate an unstable crush mode for sections with slender plates, spot weld pitch does not have a strong influence on mean crush force improvement with adhesive, and plate slenderness is an important indicator for mean crush force (See Figures 3 and 4).

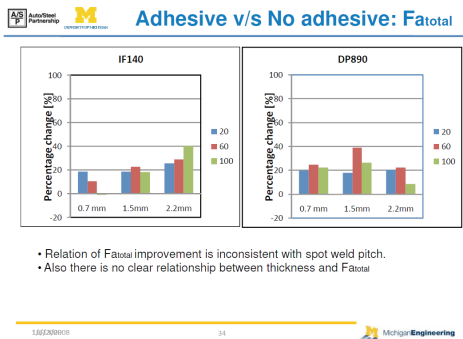


Figure 3: Spot Weld Pitch Effect

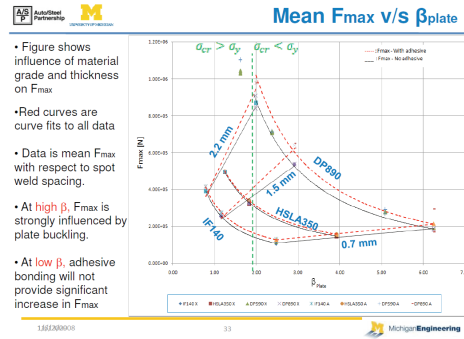


Figure 4: Material Influence

An Online Weld Modeling Tool for Automotive Arc Welding Lap Joints

On-line software tool, E-Weld Predictor, has been developed to predict temperature, microstructure, stress, and distortion for arc welding processes by combining the power of numerical weld modeling and high performance computational hardware. It provides users with easy access to advanced modeling tools over the internet to quickly explore various welding scenarios. This project created the software structure, user implementation, and the application of E-Weld Predictor for automotive lap joint applications. The new development of predicting weld sizes, microstructure, weld residual stress, and distortion for arc welding processes will provide benefit to automotive industries.

Gas Metal Arc Welding of steel sheets in the lap joint configuration is one of the most common welding scenarios used in the automotive industry. The interface and backend solver of E-Weld was customized based on the requirements from automotive companies. Material coating and detailed welding procedures were taken into account in the model. A weld bead predictor was developed with the help from experimental trials to predict the weld size for given welding parameters, geometry and materials. It will help design engineers to better design welded structures and help manufacturing engineers to qualify and optimize welding processes.

Weld Bond Adhesive Guidelines

A Weld Bond Task Group of the Joining Team created a Weld Bond Adhesive Design Guide for use by the OEM engineering organizations. The guide, in addition to providing design information for the A/SP lightweighting projects, also provides information for body structure design engineers and for modeling engineers working on vehicle designs utilizing structural adhesives.

The information on the Weld Bond Adhesive Guide pertains to pumpable adhesives and is applicable for NVH, durability or crash analysis.

Topics addressed include; Flange widths, Bead “Wet-Out” recommendations, joint gap conditions, loading conditions, bead length, and distance between spot welds or mechanical fasteners when utilizing adhesive bonding.

Starting Resistance Spot Weld (RSW) Schedules for AHSS

The OEMs currently have starting point resistance spot weld (RSW) schedule matrices for resistance spot welding mild and HSLA production materials (steels classified as IISI Groups 1 and 2) that are based on governing metal thickness (GMT) and type of material coating. These starting-point weld schedules are used for material weldability testing as well as during product launch for set-up of resistance spot welding equipment.

The purpose of this Auto/Steel Partnership Joining Technologies Project was to determine whether these existing AC and DC weld schedules were suitable for Advanced High Strength Steels (AHSS) classified as IISI Group 3 and 4 materials. Verification of these weld schedules for Group 3 and 4 steels was accomplished by:

1. Finite Element Modeling via SORPAS Version 7.0 software, and
2. Limited welding of 2T and 3T stack-ups with available material.

Two-thickness (2T) and three-thickness (3T) stack-up combinations were considered. The IISI Group 3 and Group 4 steels included; TRIP 800, DP 600, DP 980, and uncoated hot-stamped boron. Mild steels were used in 3T stack-up modeling including AISI 1006 and BH 210. Finite element modeling for both AC and DC RSW consisted of the following 3 types of thickness combinations:

1. 2T stack-up, Group 3 and 4 steel welded to itself.
2. 2T stack-up, Group 3 and 4 steel welded to itself with a thickness ratio of 1:2.5.
3. 3T stack-up, Group 3 and 4 steel welded to itself along with an 0.64 to 1.08 mm mild steel.

The test constraints for verification were as follows: maximum 6.0 mm total stack-up thickness, 2.1 mm maximum gage for a coated steel, 3.0 mm for uncoated steel, and a worst-case thickness ratio equal to 1 to 2.5. The governing metal thickness was the 2nd thickest sheet. Additionally, for 3T stack-ups, the worst-case welding situation was thin to thick to thick. The criteria was that the minimum weld size (MWS) as per AWS D8.1M:2007 (Specification for Automotive Weld Quality-Resistance Spot Welding of Steel) was obtained.

The results from finite-element modeling indicated that the AC starting-point weld schedules met the MWS requirement stated above. The initial DC weld schedules proved to be “hot” and required adjustments which were then simulated. The final DC weld schedules also met the MWS requirement.

The following materials at various gages were scheduled to be welded using the AC and DC weld schedules that were verified through finite element modeling: DP 600, DP 590R, DP 750, DP780, DP 980, and TRIP 800. Welding with actual steel consisted of the following:

1. 2T stack-up, Group 3 and 4 steel welded to itself.
2. 2T stack-up, Group 3 and 4 steel welded to itself at different thicknesses.
3. 3T stack-up, Group 3 and 4 steel welded to itself along with thinner mild steel.

Testing of the welded samples included destructive peel, shear tension, cross tension, and metallography. Results were compared to the requirements of AWS D8.1M:2007.

The results are published as a one-page set of tables entitled, “A/SP Starting Resistance Spot Weld Schedules.”

Conclusions

Additional welding issues will be addressed during 2010, by the Joining Technologies Team, funded by USAMP Lightweighting Initiatives and as member company in-kind contributions.

Presentations and Publications

Paul Davidson – University of Michigan, “Between Spot Weld Buckling Project”

Presented to the 2009 Great Designs in Steel Conference, on May 13, 2009

John Bohr – General Motors

“A Comparative Study of Joint Efficiency for Advanced High Strength Steels”

Presented at the 2009 Great Designs in Steel Conference, on May 13, 2009

Yu-Ping Yang – Edison Weld Institute

“Development of Online Weld Modeling Tool for Automotive Applications”

Presented at the 2009 International Automotive Body Congress (IABC), on November 4, 2009

¹Denotes project 070 of the Auto/Steel Partnership (A/SP), the automotive-focus arm of the American Iron and Steel Institute (AISI). See www.a-sp.org The A/SP co-funds projects with the DOE through a Cooperative Agreement between DOE and the United States Automotive Materials Partnership (USAMP), one of the formal consortia of the United States Council for Automotive Research (USCAR), set up by Chrysler LLC, Ford Motor Company and General Motors Corporation to conduct joint, pre-competitive research and development. See www.uscar.org.

B. Hydroforming Materials and Lubricants

Principal Investigator: Ronald Soldaat
ArcelorMittal USA
1330 Burlington Street East
P.O. Box 2460
Hamilton, Ontario; Canada L8N 3J5
(905)548-7200 ext. 2664; e-mail: ronald.soldaat@arcelormittal.com

Technology Area Development Manager: William Joost
(202)287-6020; e-mail: william.joost@ee.doe.gov

Contractor: United States Automotive Materials Partnership (USAMP)
Contract No.: DE-FC05-02OR22910 through the National Energy Technology Laboratory

Objective

- Develop mechanical test procedures and forming limit diagrams (FLDs) for steel, hydroformed tubes.
- Improve the accuracy and confidence in finite element modeling (FEM) of tubular hydroforming.
- Investigate the fabricating and performance characteristics of tailor welded tubes (TWTs).
- Develop an understanding of steel and lubricant requirements for hydroforming using a combination of experiments and FEM.
- Develop an improved understanding of the structural and cost benefits of hydroformed components.
- Support the work of other A/SP project teams when they investigate hydroformed structural components.
- Validate the performance benefits of hydroforming in automotive structures.

Approach

The approach taken on this project is to initially gain a basic understanding of the hydroforming process and potential issues and to then extend learning to real world applications of increasing complexity. The investigation encompasses various steel grades with a focus on advanced high strength steel (AHSS) and gauges of steel tubing, including tailor welded tubes (TWTs), in free expansion and corner fill processes using several types of lubricants. Project plans are developed based on identified knowledge gaps, barriers to implementation and technology needs as follows:

- Limited in-depth understanding of hydroforming and associated processes.
Effect of process variables such as lubrication at each operation on subsequent operations.
Forming operations prior to hydroforming include tube making, prebending and pre-forming.
Forming limits (e.g. FLDs) and other failure criterion.
- Experience with AHSS in hydroforming applications is limited.

Attitude is conservative toward new materials and envelope-pushing applications.

Need to demonstrate the benefits of tube hydroforming through projects focused on real world applications

- Limited computer modeling knowledge and lack of validated tools for automotive design process.

Milestone, Metrics and Accomplishments

During the report period (October 1, 2008 – September 30, 2009) the following objectives were accomplished:

Hydroforming of DP600 and IF Bent Tubes with Welded End Caps

- Completed work on the final report on the Influence of Bending parameters on Hydroforming of interstitial free (IF) and dual phase 600 MPa tensile strength (DP600) Tubes with welded end caps.
- Welded end caps eliminated uncontrolled and unwanted tube end feeding associated with conical end sealing.

Study on the Forming Characteristics of Tailor Welded Tubes (TWTs)

- Completed a project to obtain strain and thickness measurements during the hydroforming process of the above TWTs.
- Final report has been prepared and has been reviewed by the A/SP Hydroform team.

AHSS Hydroform TWT Lightweight Front Rails

- In March 2005 the team was challenged to demonstrate the manufacturability of advanced high-strength steel (AHSS) hydroform TWT lightweight automotive front rails.
- While the fabrication and preform bending of the AHSS tailor welded tubes was successfully completed, the team was unable to overcome technical issues encountered during the hydroforming process of these TWTs. No robust manufacturing process could be developed. After a significant effort to achieve a properly formed part, the team concluded that its objective of demonstrating the advantages of hydroformed lightweight front rails could not be reasonably achieved. The expenditure of additional funds in pursuit of this goal was not deemed justified. The project team terminated further efforts toward this objective.
- Final report has been prepared by Schuler Hydroforming and has been reviewed by the A/SP Hydroform team.

Investigation of Fabricating Dual Phase and TRIP Steel Tube from an ERW Production Line

- All the experimental testing and analysis on this project was completed at CANMET using their laboratory tube high-frequency induction tube welding draw bench.
- Final report has been prepared by CANMET and has been reviewed by the A/SP Hydroform team.

Numerical Modeling of Straight Tailor Welded Tube Hydroforming and Pre-Bent Tubular Hydroforming

- This project has been deleted.

Characterizing Material Response during Tube Hydroforming

- This project has been re-assigned to a newly formed project team. The Hydroform Team will not pursue this effort.

Other – Dissemination of Project Learning

- A technical paper was prepared for and presented at the 2009 SAE World in Detroit on April 23, 2009. The paper reviewed results and learning from the start of the project with a focus on experimental forming limits of steel tubes and effect of bending and lubrication on hydroforming of IF and DP600 steel tubes without and with welded end caps.

Future Direction

The Hydroforming Materials and Lubricant Team will be closed out at the end of December 2009. The last project meeting of the team was April 22, 2009. The tasks to be completed during the remainder of 2009 are:

- Wrap up the remaining technology transfer actions.

Publish IRDI hydroforming TWT, IRDI hydroforming of DP600 and IF bent tubes with welded end caps, CANMET fabricating DP and TRIP steel tube from an ERW production line and Schuler AHSS hydroform TWT lightweight front rail reports.

- USAMP closeout report.

Introduction

Hydroformed steel tubes have been used in the automotive industry to form components that meet structural objectives, particularly strength and rigidity, at optimal mass. One of the most significant advantages of tubes is that they are monolithic closed sections and, as such, exhibit many times more stiffness in torsion than conventional open sections, such as “C” and “hat” shapes. Their use is limited largely by a lack of knowledge about the capabilities and parameters of hydroforming processes and the effects of the processes on the tubes.

This project was undertaken to investigate and quantify the capabilities and parameters of various hydroforming processes so that automotive designers and engineers can utilize the tube configurations that are available and predict the performance of components made by hydroforming. Hydroformed tubes and tailor welded tubes made from high strength and advanced high strength steels (AHSS) are of particular interest because of the potential reduction of mass associated with materials of higher strength and optimal thickness.

The Hydroforming Process

Hydroforming is a process in which a tube is placed into a die which is shaped to develop the desired configuration of the tube. Water is introduced into the tube under very high pressure causing the tube to expand inside the die. The tube ends can be held stationary or moved inward during the process to end feed material into the die cavity.

The process has two distinct stages, shown in [Figure 1](#). The first stage is free expansion, (Figure 1a). The free expansion phase continues until the tube contacts the die wall (Figure 1b). In the second stage, the corner filling phase, the tube is in contact with the surface of the die which

constrains subsequent deformation (Figure 1c). During this stage, the tube expands into the corners of the cavity, accomplishing corner fill. A tube that has been hydroformed is shown with the die in Figure 2. Note that the test was continued until the tube failed.

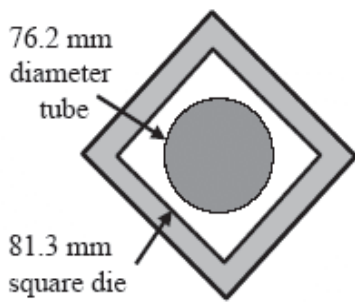


Figure 1a. Free expansion stage.

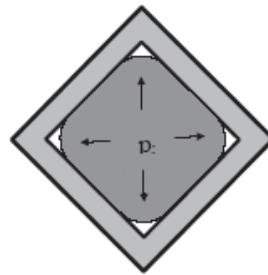


Figure 1b. Contact with the die wall.

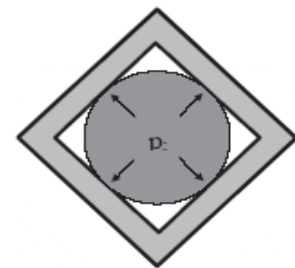


Figure 1c. Corner filling.

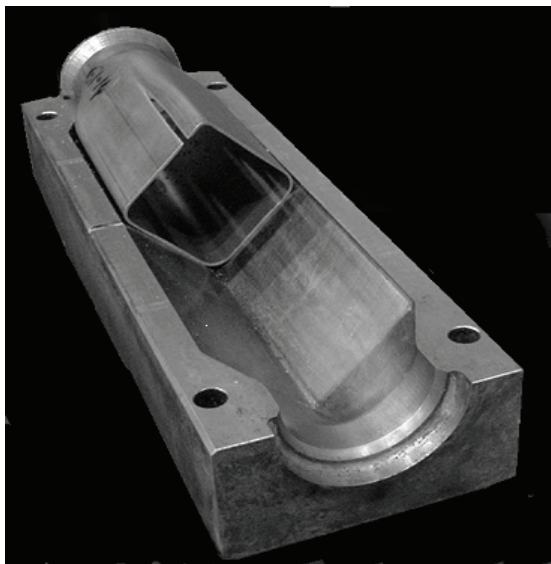


Figure 2. Hydroformed tube and die (the test was run to failure of the tube).

During corner fill, the tube slides against the die. Friction between the tube and die affects the process. The lubricant used in the process is a significant parameter.

During both stages, the tube undergoes plastic strain. The amount of plastic strain that can occur before the material fractures is predicted in stamping processes that utilize flat sheet steel by using a forming limit diagram (FLD). The FLD is determined by the properties of the material. The hydroforming process is preceded by tube forming and sometimes pre-bending of the tube, both of which induce strains in the material and alter its properties. Before an FLD can be developed for the hydroforming process, the strain history, that is the strain induced in the material prior to hydroforming, must be known.

Project Discussion

Tailor-Welded Tubes

Tailor-welded blanks are used for sheet steel stampings in numerous automotive applications. Their use enables the development of components with varying material thicknesses and mechanical properties to achieve the required structural performance at optimal mass. These same advantages can be achieved in tubes by utilizing the expertise currently available for producing tailor welded blanks.

The Hydroforming Team recognized that optimal performance can be achieved only when the parameters of fabricating and hydroforming tubes with varying thicknesses and/or material properties are understood. For example, when a sheet steel blank of a given thickness and grade is joined to a blank with greater thickness and/or strength, the former sheet will tend to expand farther than the latter. The tendency for differential expansion imposes loads on the interface of the sheets, namely the weld, where there can be no differential expansion.

Tubes are usually formed before hydroforming in bending operations which progressively bend the tube to the desired radius along its length. Bending parameters may need to be adjusted

to move progressively over tube sections with varying thickness and material properties.

To assess the parameters associated with these conditions, the Hydroforming Team developed a test plan that will allow direct comparison of tailor welded tube characteristics by forming five sets of tubes, 12 tubes per set. The first set is a baseline tube made from one blank. The other four are made from two laser welded blanks, as follows:

1. One-piece tube as a baseline: 1.5 mm DP 600.
2. Same material, same thickness: 1.5 mm DP. 600 welded to 1.5 mm DP 600.
3. Same material, different thickness: 1.2 mm. DP 600 welded to 1.5 mm DP 600.
4. Different material, same thickness: 1.5 mm. HSLA 350 welded to 1.5 mm DP 600.
5. Different material, different thickness: 1.5 mm. HSLA 350 welded to 1.2 mm DP 600.

Tailor Welded Tubes (TWTs) Project - Results and Discussion

The TWTs were manufactured by laser welding the dissimilar sheet steels together in the flat to produce a laser/tailor welded blank (LWB/TWB) that was then formed into a cylinder and laser tube seam welded. A visual inspection of the as-received TWTs revealed that the laser weld quality was poor, particularly the longitudinal laser seam welds which were done on the formed cylinders, compared to the normal appearance of welded tubes received for experimental work from continuous electric resistance welded (ERW) tube making facilities. The metal appeared to have been 'bent' rather than rolled into the tube shape. The weld areas were rough and often one side of the weld was higher than the other side. Three tubes from each series were chosen for measurement of tube wall thickness and ovality. Wall thickness measurements were within normal variations. However, the ovality of the tubes was not consistent and varied from 0.13 mm to 2.01 mm.

Free expansion tests with a six inch expansion length were performed on four tubes from each series. Initial tests were with one non-circle gridded TWT from each series to compare burst performance of the five combinations. Unfortunately, three of the TWTs (Series B, C and E) failed on the longitudinal weld. The radial expansion at burst was similar for Series A and D and as expected the pressure at burst was higher for A than for D. The burst pressure was 3986 psi for Series A and 3318 psi for Series D with bursting occurring in the 1.5 mm HSLA350 steel.

Free expansion tests with a fifteen inch expansion length were also performed on two non circle gridded and one circle gridded TWT from each series. Results are shown in [Table 1](#) below. Four of the fifteen tested TWTs failed at a weld location. The greatest expansion and burst location occurred in the thinner DP600 when it was mated with a thicker wall DP600 or in the 1.5 mm HSLA350 when mated with either the 1.2 mm or 1.5 mm DP600.

Table 1. Free Expansion Data Chart for Fifteen-Inch TWTs – Average Values for Tubes that did not Fail on the Weld

Free Expansion Hydroforming Data - Average Values for Tubes that did not Fail on the Weld (15-in. Tubes)					
Tube Series	Material		Avg. Burst Pressure (psi)	Avg. Laser Exp. (mm)	Comments - Burst Location
A	1.5 mm DP600		3765	5.29	1.5 mm DP600
B	1.5 mm DP600	1.5 mm DP600	3874	2.60	1.5 mm DP600
C	1.2 mm DP600	1.5 mm DP600	3100	0.82	1.2 mm DP600
D	1.5 mm HSLA350	1.5 mm DP600	2986	0.55	1.5 mm HSLA350
E	1.5 mm HSLA350	1.2 mm DP600	3024	2.51	1.5 mm HSLA350

Straight tube corner fill hydroforming tests were performed on five eighteen inch long TWTs from each series. Two of the five TWTs from each series were circle gridded. Sixteen of the twenty-five TWTs failed in the longitudinal weld. Four of the nine TWTs that did not fail in the laser weld were from Series A. Internal pressure versus corner expansion results for TWTs that did not fail in the laser weld are shown in Figure 3.

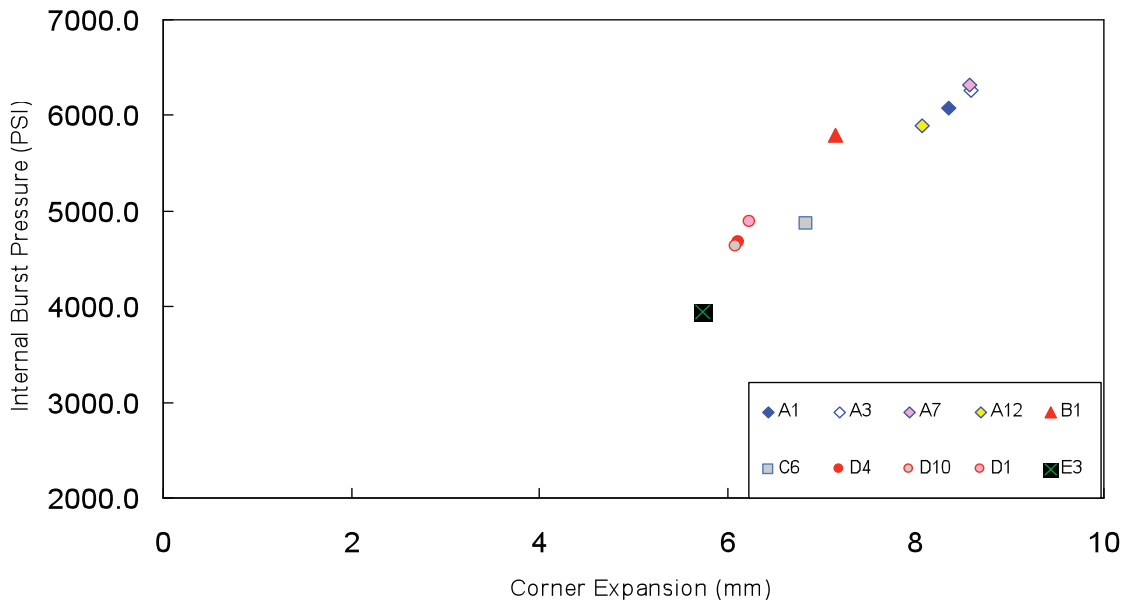


Figure 3. Internal Pressure versus Corner Expansion for each of the TWTs tested in the corner fill hydroforming test that did not burst at a weld area

Independent of whether or not the failure was on a weld, the greatest expansion was consistently observed in the thinner sheet steel when identical alloys were welded together and in the DP600 steel for both series D and E. This occurred even though for series E the thickness of DP600 was 1.2 and the thickness of HSLA350 was 1.5 mm.

Thickness and circle grid surface strain measurements were made on all gridded TWTs. The strain data was not analyzed but is available for finite element analysis (FEA) for other A/SP projects.

Photographs were taken of all TWTs that were tested by either the free expansion or the corner fill hydroforming tests. Failure locations are visible in the photographs (see [Figure 4](#)).



Figure 4: Example of a Burst Tube Used for Strain Measurements.

The condition of the TWTs produced for testing, in terms of both ovality and poor longitudinal laser weld quality, resulted in less reliable data than expected from these evaluations. It is clear that the TWT forming process and the welding of the TWTs is critical. In spite of this, the pattern of greater expansion occurring in either DP600 (more formable) or thinner sheet steel was evident. However, in order to sufficiently determine the effect that the radial (circumferential) laser weld has on the formability, weld integrity is necessary to prevent premature failure in the longitudinal laser seam weld.

Hydroforming with Welded End Caps

During hydroforming operations, expansion of the tubes causes “end feeding”, wherein the ends of the tube move inward toward the expanding area due to metal flow in the workpiece. End feeding affects the strain patterns in the tube. In some hydroforming operations, deliberate end feeding is performed under controlled parameters in relationship to other parameters, such as water pressure, to enhance metal flow. End feeding can be prevented by welding the tubes to the end caps (interface between the tube and the area where water is introduced) and fixing the caps rigidly in the hydroforming tool. The Hydroforming Team determined that the effects of end feeding on strain patterns in the hydroformed tubes could be better understood by performing tests with no end feeding. Welded end caps were used in all tests.

Conclusions

Work conducted during this reporting period indicated that:

- The fabrication of AHSS tubes (DP and TRIP) on an ERW production line appears feasible. A rich chemistry steel design and an optimized welding schedule are required to prevent heat affected zone (HAZ) softening.
- The fabrication and perform bending of AHSS TWTs is difficult, but achievable.
- No currently available process could be identified which is capable of economically hydroforming a complex AHSS TWT front rail.

Presentations and Publications

1. "Hydroforming Group," Auto/Steel Partnership Program Review, Department of Energy, September 21, 2005.
2. "Hydroforming Committee," A/SP SPARC financial planning review, July 18, 2006.
3. "Hydroforming Materials and Lubricants," Auto/Steel Partnership Department of Energy Peer Review meeting was conducted on Friday, December 1, 2006.
4. "Influence of Lubricant in Bending & Hydroforming Evaluations" presentation by Jean Reid at ASTM D02 Petroleum Products and Lubricants Committee workshop/symposium on Tribological Challenges of Metal Deformation Fluids, Florida, June 17, 2007.
5. "Tube Hydroforming Phase V: Experimental Forming Limits of Steel Tubes" IRDI report, March 2007.
6. "Influence of Bending Parameters on the Hydroforming of IF and DP 600 Tubes" IRDI report, March 2007.
7. "Hydroforming Materials and Lubricants (ASP060) - Project Description Sheet, Statement of Project Objectives and Presentation," A/SP Project Review and Budget meeting, July 17, 2007.
8. Reid, J., et al "Hydroforming Tailor Welded Tubes", A/SP Hydroforming Materials and Lubricants final project report, July 2008 (awaiting publication by A/SP Technology Transfer Team). (* Project contracted to IRDI.)
9. "Hydroforming Materials and Lubricants (ASP060) – Project Description Sheet, Statement of Project Objectives and Presentation," A/SP Project Review and Budget meeting, August 19, 2008.
10. Reid, J., et al "Hydroforming of DP600 and IF Bent Tubes with Welded End Caps", A/SP Hydroforming Materials and Lubricants final project report, July 2008 (awaiting publication by A/SP Technology Transfer Team). (* Project contracted to IRDI.)
11. Soldaat, R.J., Alghanem, J., Chen, M., Kernosky, S.K, Stoughton, T.B. and Tervo, L "Results of Auto/Steel Partnership (A/SP) Steel Tube Hydroforming Materials and Lubricants Experimental Projects", SAE Technical Paper # 2009-01-1390, April 2009. (* Presented at 2009 SAE World Congress – Detroit, Michigan, April 23, 2009.)
12. Rashid, M. and Martin, P. "Investigation of Fabricating DP and TRIP Steel Tubes from an ERW Production Line", A/SP Hydroforming Materials and Lubricants final project report, September 2009 (awaiting publication by A/SP Technology Transfer Team). (* Project contracted to CANMET.)
13. Soman, P. "Advanced High Strength Steel (AHSS) Hydroform Tailor Welded Tube (TWT) Lightweight Front Rail", A/SP Hydroforming Materials and Lubricants final project report, September 2009 (awaiting publication by A/SP Technology Transfer Team). (* Project contracted to Schuler Hydroforming)

¹Denotes project 060 of the Auto/Steel Partnership (A/SP), the automotive-focus arm of the American Iron and Steel Institute (AISI). See www.a-sp.org The A/SP co-funds projects with the DOE through a Cooperative Agreement between DOE and the United States Automotive Materials Partnership (USAMP), one of the formal consortia of the United States Council for Automotive Research (USCAR), set up by Chrysler LLC, Ford Motor Company and General Motors Corporation to conduct joint, pre-competitive research and development. See www.uscar.org.

C. Sheet Steel Fatigue Characteristics Project

Principal Investigator: A.K. Khosrovaneh
General Motors Company
30200 Mound Road; MC 480-111-S60
Warren, Michigan 48090-9010
586-907-5726; email:ak.khosrovaneh@gm.com

Technology Area Development Manager: William Joost
(202) 287-6020; e-mail: william.joost@ee.doe.gov

Contractor: U.S. Automotive Materials Partnership
Contract No.: DE-FC05-02OR22910

Objective

- Provide automotive manufacturers with the sheet steel fatigue and durability information necessary to help them reduce vehicle weight and improve fuel economy.
- Investigate the fatigue life both of parent metal and that of joints formed in mild steels, high strength steels (HSS) and advanced high strength steels (AHSS) by spot welding, adhesive bonding and weld bonding (a combination of welding and adhesive bonding).
- Explore the fatigue response of AHSS steels after being subjected to metal inert gas (MIG) and laser-welded joining and compare this behavior with that of standard automotive steels.
- Make the test data generated in the current and previous phases of the program available to the automotive engineering community.
- Assist the Joining Technology team in identifying optimum welding parameters for laser and MIG welded joints by the development of a fatigue test program and the use of fatigue response as a performance measure.

Approach

- Investigate the fatigue characteristics of resistance spot welding using an approach that recognizes the process and its effects on the weld and the metals being joined.
- Investigate the fatigue characteristics of adhesive bonding which substitutes an entirely different material in place of the weld to act as the load bearing connection. The adhesive must adhere to the metals being joined and resist fatigue failure at the adhesive/metal interface and within itself.
- Investigate the fatigue characteristics of weld bonding, a combination of adhesive bonding and spot welding. The investigation studies the characteristics of the welding and bonding processes and their interaction in the weld bonding process.
- Investigate the previously little known factors for welds behavior such as microstructure, fracture interface and microhardness of materials that are expected to either improve or impact durability and facilitate modeling and simulation.
- Reduce the spot weld, adhesive bonded and weld bonded test data to a form that is useful to design engineers who perform vehicle structural analysis and publish it on the A/SP website.

- Develop a test program to investigate the fatigue characteristics of Metal Inert Gas (MIG) welding, a fusion process that introduces a third “filler” metal, forms alloy microstructures different from the metals being joined, and produces continuous joints.
- Identify the parameters of Metal Inert Gas (MIG) welded joints including metal grades, metal thicknesses, coatings and joint configurations that impact fatigue.

Current Project:

Fatigue Behavior of MIG Weld

- The MIG weld fatigue test program has two phases, Phase 1A and Phase 1B:

The Phase 1A weld fatigue test program consisted of fatigue tests of MIG joints for DP590 GA, SAE 1008, HSLA HR 420, DP600 HR, Boron, DQSK, TRIP780 GI, and DP780 GI sheet steels. Some welded joints tested are constructed using combinations of DP590GA and SAE1008, DP600 and SAE1008, TRIP780 and SAE1008, and DP780 and SAE1008. The specimen geometry included single lap-shear, double lap-shear, butt weld, start-stop, and perch mount.

The Phase 1B test program includes fatigue testing of HSLA, DP590, Boron, DP780, and Boron/HSLA joints of single-lap, double-lap, and/or start-stop specimen geometry.

A variability study that includes the identification of sources of test result variation and measurement of key geometric parameters of the welded specimens used in both the Phase 1A and Phase 1B.

Milestone, Metrics and Accomplishments

- Completed work on the Phase 1A MIG Weld Fatigue Test project.
- Presented (and published) two papers at the SAE 2009 Congress on the Phase 1A project.
- Initiated work to define the requirements for the Phase 1B portion of the weld fatigue test project.
- Identified a vendor to fabricate the weld fatigue test specimens.
- Provided technical support to the A/SP Joining Technologies project team in the area of vehicle durability studies. (we need to specify the team here)
- Initiated contracts with two institutions for manufacturing and testing of welded coupons for Phase 1B program.
- Completed geometric variability study of specimens tested under Phase 1A program.

Future Direction

- Complete Phase 1B fatigue testing.
- Complete a comprehensive report summarizing Phase 1A and 1B test results and variability study.

Introduction

Future and near-future vehicle designs are faced with several stringent requirements that impose conflicting demands on the vehicle designers. Safety must be improved while weight and cost are contained. Advanced high-strength steels, judiciously selected and applied, are currently the best candidates offering low-cost (compared with aluminum, magnesium and plastics/composites), reliable materials for meeting these mandates. As structural components are optimized and thinner gauge, higher strength materials are assessed, fatigue life of the component and the areas where loads are transferred become increasingly important considerations. To assess the performance of a component in the design phase, the fatigue characteristics of the base material and the joints, where loads are transferred, must be known. This project has essentially completed testing various grades of steel that have been spot welded, adhesively bonded and weld bonded, and is currently supplementing those tests with additional tests on commercial quality (CQ) steel CQ and boron steel. Testing of Metal Inert Gas (MIG) joints is under way.

Discussion

Spot Weld, Adhesive Bonding and Weld Bond Testing

The effort to evaluate the fatigue characteristics of spotwelds began in the 2002 fiscal year with presentations by key researchers on the current state of the work at Chrysler LLC, Ford Motor Company and General Motors Corporation. Based on these presentations, the Sheet Steel Fatigue Project Team has produced results beneficial to all three companies. Early in the planning stage, the Auto/Steel Partnership (A/SP) Joining Technologies Team was consulted, and that team prepared the samples to be tested. This interaction ensured that the samples were joined using procedures that were properly controlled and in adherence to the best current practices in sheet metal joining.

The following test parameters were agreed upon by the team:

Two modes of testing: tensile shear (Figure 1) and coach peel (Figure 2).

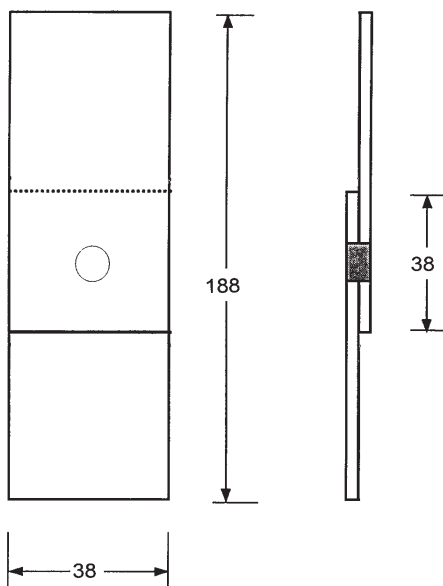


Figure 1. Tensile shear spot weld test specimen (units in mm).

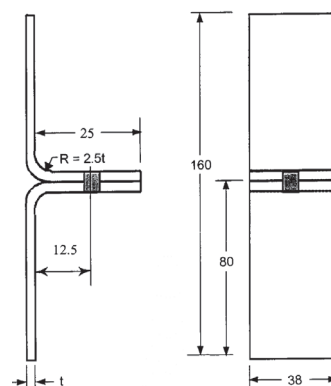


Figure 2. Coach peel spot weld test specimen (units in mm).

- Since weld fatigue performance is independent of metal thickness for mild steels, high-strength low-alloy (HSLA) grades and advanced high-strength steels (AHSS), tests on these grades utilized only one metal thickness (1.6mm).
- Because no such data were available for advanced HSS, several grades in this class were tested at two thicknesses (1.6mm and 0.7mm).
- Testing was done at two R ratios: 0.1 and 0.3. The stress ratio R is defined as the ratio of the minimum stress to the maximum stress in the test cycle. Maximum and minimum values are algebraic, with tension designated as positive and compression negative.

To date, eleven different steel grades have been tested, and two remain. Most of the testing was performed on spot welded joints. Many tests were also performed on adhesive bonded and weld bonded joints.

As the testing progressed and results were analyzed, the following tests were added for comparison purposes:

1. Testing at specified R ratios means that the maximum and minimum loads are constant throughout a given test. However, as the maximum load is increased to generate fatigue curve data, the minimum loads also increase. This process is valuable for establishing baseline data. However, in the real world, loads can be expected to vary. For this reason, automotive spectrum load tests, set to different predetermined load scaling, were run.
2. Two studies were performed on samples with a different welding schedule that produced a smaller weld button.
3. In concert with the Joining Technologies Team, the fatigue of very wide samples (125 mm vs. the standard 38 mm) was studied in order to investigate mean stress.

Laser Welded Joints

Laser welded joints were studied jointly with the Sheet Steel Fatigue project team High Strength Steel Joining Technologies project team in FY2005-6. A discussion of this work can be found in the High Strength Steel Joining Technologies Project FY2006 and FY2007 Annual Reports.

Metal Inert Gas (MIG) Welded Joints

MIG welding is the second most common welding process used on vehicle structures, and applications are expected to increase. MIG welds are used not only on body members and passenger vehicle sub-frames but also in frames for larger passenger vehicles, light trucks and sport-utility vehicles (SUV). Therefore, the test samples will be made from two thickness ranges: 1.6 mm for body applications and 3.4 mm for frame applications (boron body steel will be tested at 1.8 mm thickness).

Frame members do not generally require as much formability as body members, and they offer excellent opportunities for mass reduction through downgaging. Therefore, tests on frame joints may address higher strength materials than those specific to body members.

The Team agreed to four modes of testing: butt weld ([Figure 3](#)), single lap shear ([Figure 4](#)), double lap shear ([Figure 5](#)), and perch mount ([Figure 6](#)).

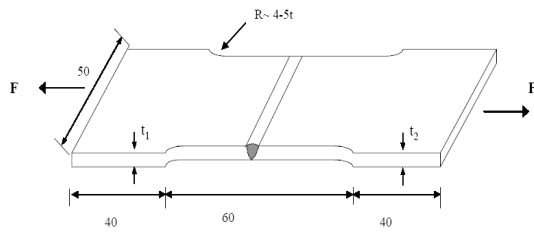


Figure 3. Butt weld MIG test specimen (units in mm).

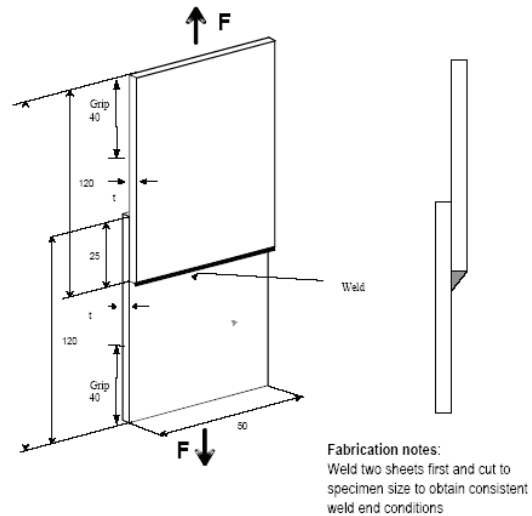


Figure 4. Single lap shear MIG test specimen (units in mm)

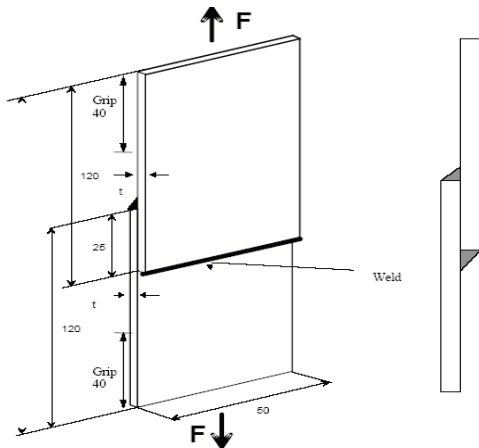


Figure 5. Double lap shear MIG test specimen (units in mm).

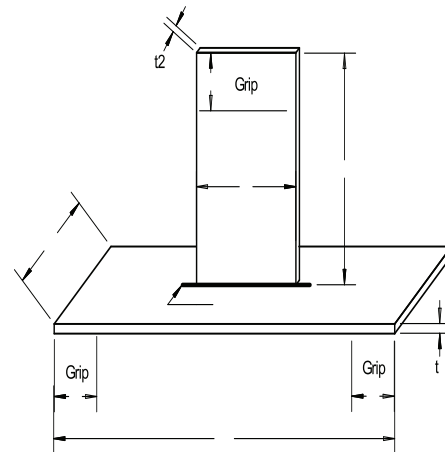


Figure 6. Perch mount MIG test specimen (units in mm).

Based on the Phase 1A effort, it was determined that, regardless of specimen configuration, base material strength played no role in the fatigue performance of these joints. Additional conclusions include:

- Given both that the welds were reasonably geometrically consistent (within a given base metal thickness) and that the cross-sectional geometry was not optimized, parent metal strength does not affect the fatigue strength of the welded joints – the fatigue curves for the strongest and weakest materials can reasonably be said to overlay each other for any given thickness/specimen configuration. For a given joint configuration and specimen thickness, fatigue lives usually collapsed into a fairly narrow band, regardless of parent metal strength. However, the 1.6mm materials were certainly more subject to scatter – especially the R=0.3 DP590GA single lap-shear tests. The results for double-lap shear specimens are shown in Figures 7 and 8, while that for single-lap shear specimens are shown in Figure 9.

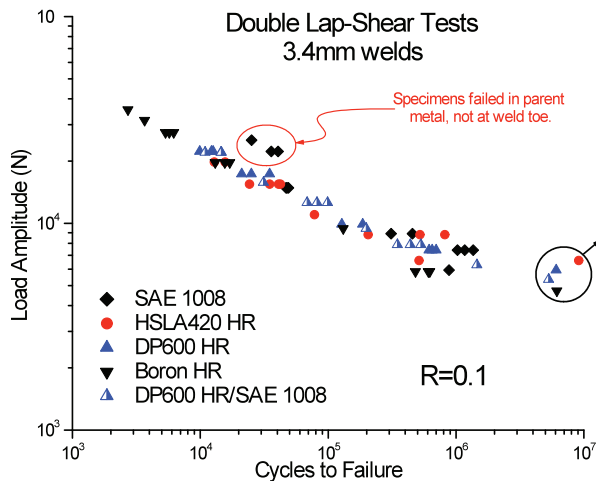


Figure 7. Double lap-shear tests of welds of 3.4mm thick materials. Monolithic welds (same to same materials).

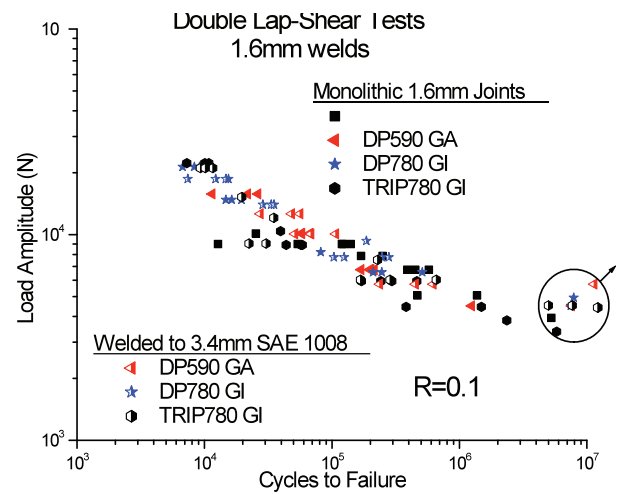


Figure 8. Double lap shear R=0.1 fatigue tests involving 1.6mm thick materials.

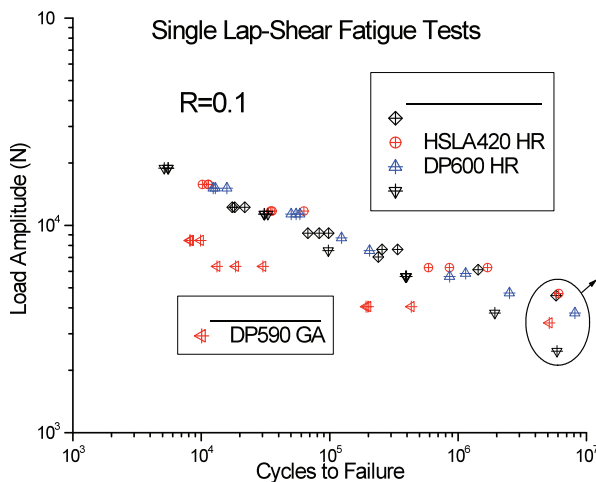


Figure 9. All R=0.1 single lap-shear fatigue tests.

- Given a consistent weld geometry, sheet thickness is a more dominant factor in the fatigue strength of MIG joints than any other factor in this study, largely because of the attendant change in nominal stress and the introduction of a welding gap in the 1.6mm materials. This observation holds true regardless of specimen type and base metal strength.

- Unlike in base metal tests, mean stress was not influential on weld fatigue life. This result is limited to the two R-ratios tested (R=0.1 and R=0.3) and the two materials examined (1.6mm DP590 GA and 3.4mm DP600 HR). The exception to this conclusion was the start-stop weld specimens (and to a very minor extent, perch mount specimens tested under shear loading) which behaved as parent metals do.

- Weld stops and starts, when included in the test section, did not significantly impact joint fatigue performance over joints with no starts or stops. The presence of these defects did, however, greatly increase the scatter in life.
- Scatter was greater in joints made of thinner materials, and was particularly bad in welds constructed of dissimilar thickness base metals. This is, in part, due to the difficulty in MIG welding of very thin sheet.

Conclusions

Analysis of test results indicates that the fatigue performance of a MIG weld is largely independent of the materials being welded. This finding supports the initial understanding that the melting and resolidification processes associated with MIG welding form micro-structures different from the parent metal and make the properties and coating of the material(s) being joined, and the welding parameters, relatively insignificant contributors to overall fatigue performance. Details of the tests and tests resulted have been published in two SAE publications.

Future Directions

Upon completion of the Phase 1B weld fatigue test program and the variability study, the Sheet Steel Fatigue project will be concluded. The project team will finish the remaining technology transfer steps and make the end-of-project reports to DOE, USAMP and A/SP management.

Presentations and Publications

“Sheet Steel Fatigue Group”, Auto/Steel Partnership Program Review, Department of Energy, September 21, 2005.

“A/SP Sheet Steel Fatigue Committee”, Joint Policy Board, Feb. 1, 2006.

J.J.F. Bonnen, Hari Agrawal, Mark A. Amaya, Raj Mohan Iyengar, HongTae Kang, A. K. Khosrovaneh, Todd M. Link, Hua Chu Shih, Matt Walp, Benda Yan, “Fatigue of Advanced High Strength Steel Spot Welds,” 2006, Society of Automotive Engineers, SAE-2006-01-0978, pp. 19. Republished in 2006 SAE Transactions.

Kang, HongTae, “Evaluation of Spot Weld Fatigue Damage Parameters” 2006, Society of Automotive Engineers, SAE-2006-01-0978, pp. 19. Republished in 2006 SAE Transactions.

“Spot Welds, MIG Welds and their effect on the fatigue of AHSS steels,” Mar. 10, 2006 (A/SP Frame group).

“Sheet Steel Fatigue Committee,” A-S/P SPARC financial planning review, July 18, 2006.

“Spot Welds, MIG Welds and their effect on the fatigue of AHSS steels,” Mar. 10, 2006 (Joining group).

“Fatigue of MIG Welds” AISI Wheel Task force meeting, Nov 18, 2005.

ASP Team Review, Dec. 15, 2005.

“Fatigue of AHSS SpotWelds,” 2nd Annual Ford AHSS Conference, Oct. 18, 2005.

J.J.F. Bonnen and R. Mohan-Iyengar, “Fatigue of Spot Welds in Low-Carbon, High-Strength Low-Alloy, and Advanced High-Strength Steels and Fatigue of Fusion Welds in Advanced High-Strength Steels,” 2006 Proceedings of the International Automotive Body Congress (IABC 2006), pp 12, 2006.

H.-T. Kang, J. J. F. Bonnen, and R. Mohan Iyengar, “Sources of Variability in the Fatigue Strength of Spot Welded Specimens,” Proceedings of Materials Science & Technology Conference, Detroit, September 2007.

J. J. F. Bonnen and R. Mohan Iyengar, “Fatigue Performance of Conventional and Advanced High-Strength Steel Spot Welds,” presented at the special symposium marking the 20th Anniversary of Auto-Steel Partnership, held as part of the Materials Science & Technology Conference, Detroit, September 2007.

Publication SAE 2006-01-0978 “Fatigue of Advanced High Strength Steel Spotwelds”. Presented at the SAE World Congress and Exposition, April 2006. Published 2006 in SAE SP-2031.

Mohan Iyengar, R.; Bonnen, J.J.F.; Young, E.; Maatz Jr., D. F.; Soter, M.; Amaya, M.; Citrin, K.; Khosrovaneh, A.; Link, T.; Schillaci, N.; and Shih, H.-S., (2009) "Influence of Weld Process Parameters on the Geometric Variability of the Gas-Metal Arc Welds," SAE Technical Paper Series 2009-01-1549, 2009 SAE World Congress Detroit, MI.

J. J. F. Bonnen, Raghuram Mandapati, HongTae Kang, Raj Mohan Iyengar, A.K. Khosrovaneh, Mark A. Amaya, Ken Citrin, Hua-Chu Shih, 2009, "Durability of Advanced High Strength Steel Gas Metal Arc Welds," SAE Paper No. 2009-01-0257, SAE, Warrendale, PA.

D. Tribology

Principal Investigator: Tareena Mulholland
General Motors Corporation
Manufacturing Engineering
30001 Van Dyke Avenue, Mail Code 480-210-Y25
Warren, Michigan 48090
(248) 640-8881; e-mail:tareena.mulholland@gm.com

Technology Area Development Manager: William Joost
(202) 287-6020; e-mail: william.joost@ee.doe.gov

Contractor: United States Automotive Materials Partnership (USAMP)
Contract No.: DE-FC05-02OR22910 through the National Energy Technology Laboratory

Objective

- Identify the tribological factors that contribute to successful stamping of AHSS. This includes minimized tool wear and minimized galling/die pick-up.
- Identify the most effective pierce clearance (burr height) when piercing AHSS.
- Determine optimal die material and coating performance for tooling stamping AHSS.

Approach

- A progressive die with 12 stations has been constructed. Each station of the die is removable to allow for testing of different types of die work (trim, flange, etc.) as well as materials and surface treatments.

Phase I – Run 100,000 hits of 1.2mm uncoated DP980 through progressive die to test several materials, coatings, and designs in form, flange, trim, and pierce functions in a production type environment.

Phase II – While Phase I identified several designs, materials and surface treatments that are durable, there are many others yet to be tested. Therefore, 100,000 hits of 1.3-1.4mm uncoated and coated DP780, TRIP780, DP980, and DP Low Carbon Equivalent (LCE) will be stamped through trim and pierce functions in the progressive die.

- A coating fatigue test is a new type of coating test which differs from the typical “pin-on-disc” experiments by adding impact forces to the test samples.

Phase I – Determine the correlation of the coating fatigue test using impact to the results from the production type environment of the progressive die test.

Phase II – Add sliding friction forces to the impact fatigue test and determine correlation with the progressive die wear test.

Milestones and Accomplishments

- Phase I of Progressive Die Wear Project was completed and some best practice materials and coatings were identified.

- Developed design for Phase II of Progressive Die Wear Project and began construction of die changes for continuous improvement investigation.
- Phase I of the Coating Fatigue Test supported the conclusions from Phase I of the Progressive Die Wear Project.

Future Direction

Phase II of the Progressive Die Test will be using several different grades of material; DP780, TRIP780, DP980, and DP980 LCE. The die has been redesigned to include only trim and pierce test stations.

Phase II of the Coating Fatigue Test will be compared to the results of Phase I of not only the coating fatigue test but the Phase I of the Progressive Die Wear Test (DWT) as well.

Use the results from this project to continuously improve die design standards to provide cost effective quality stamping tools, and prevent a situation in which tooling for stamping AHSS is too costly to manufacture.

Introduction

The ability to fully realize the benefits of advanced high-strength steels depends upon the ability to aggressively form these steels into challenging parts. These steels have been shown to cause die failures in early implementations. This project is intended to improve the tribological understanding of the interaction between advanced high-strength steels (AHSS), tooling, coatings, and the forming process so that the proper system can be selected to successfully manufacture automotive parts.

Effective trimming of advanced high-strength steel parts has recently been noted as among the most challenging manufacturing operations for these materials, particularly Dual Phase (DP) steels with tensile strengths greater than 750 MPa. Accelerated wear of trim steels has lowered productivity and adversely affected part quality. There are many developments occurring in trim steel materials, but no effective method of screening the newly available material is available.

The work hardening effects of advanced high-strength steel have also introduced excessive temperatures and wear on the forming and flanging operations. The challenge arises to determine what materials, surface treatments, and die conditions are optimal for producing high quality, cost effective parts.

The Auto/Steel Partnership (A/SP) Tribology Team's interest is to determine durable die materials and surface treatments for manufacturing automotive parts. A/SP Tribology members designed a progressive die in which each of the aforementioned operations is inserted in a way that the die can test a myriad of different design conditions, materials, and surface treatments.

While there are many die materials available, there are many more coatings and surface treatments options to extend the life of the die. Typical tests such as the "pin-on-disc" test and Center for Precision Forming (CPF) tool on sheet have seen discrepancies when the results have been applied in a production environment.

A laboratory test would determine the effectiveness of a coating or surface treatment more efficiently and cost effectively than production. A coating fatigue test will be performed to determine if there is any correlation between the laboratory and progressive die experiment.

Main Sections - Progressive Die Project

Phase I

Phase I of the Progressive Die Project tested form, flange, trim, and pierce operations. The die contained materials standardized by the American Iron and Steel Institute (AISI) and the North American Automotive Metric Standards (NAAMS), as well as trademarked materials. Evaluated surface treatments included Ion Nitride, Hard Chrome, Microplasma, Chemical Vapor Deposition (CVD) TiC coating, Physical Vapor Deposition (PVD) TiAlN coating, PVD CrN, PVD TiCN, and Ion Nitride + PVD CrN. After some minor adjustments to the designs, the first phase was completed in May 2009. The strip is found in [Figure 1](#).

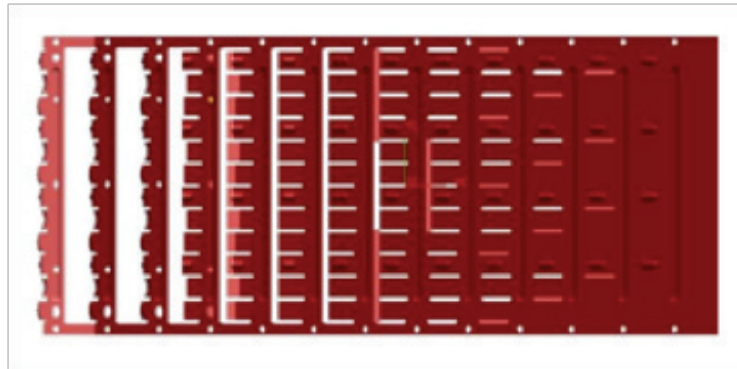


Figure 1. Phase I Strip

The first function added four (4) form beads in order to add strain. The work hardening resulting from the form helped reveal which materials formed best in the latter die stations.

The next three (3) stations added pierce with clearances varying from 5% to 30% in 5% increments. Phase I determined that the optimal pierce clearance is between 5-15%. As seen in [Figure 2](#), the 10% clearance is the cleanest pierced slot with no burrs and a clean edge.

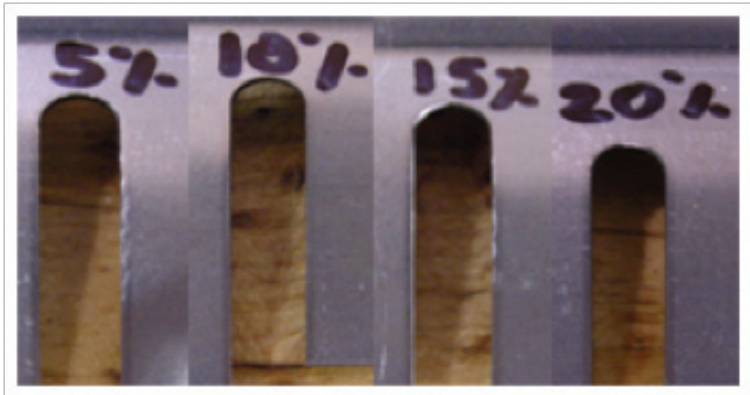


Figure 2. Phase I Pierce Results

The next two (2) stations used long pierce steels for part trimming, but did not give any visible results. A specialty pierce station with five (5) shaped pierce punches also did not generate visible results.

After a forming station that tilted the part up 20°, the part was trimmed. Of the seven (7) viable test materials, the AISI D2 and AISI S7 performed the best. The NAAMS G25HP and Caldie™ did not perform as well. The successful AISI D2 upper trim steel results are seen in [Figure 3](#), and the less successful Caldie™ upper trim steel results in [Figure 4](#).

Figure 3. Phase I Trim Results - AISI D2





Figure 4. Phase I Trim Results - Caldie™

The last working station was the flange station where it was quickly noticed that the die materials without surface treatments or coatings did not perform well. After very few hits, coatings and surface treatments were added to each of the steels. Of the five (5) materials and eight (8) coatings / surface treatments, AISI D2 + CVD TiC and Carmo® + Ion Nitride + PVD CrN (found in Figure 5) performed the best, while AISI M4 + Hard Chrome (found in Figure 6) and Vanadis® 4E + Microplasma performed the worst.



Figure 5. Phase I Flange Results - Carmo® + Ion Nitride + PVD CrN



Figure 6. Phase I flange Results - AISI M4 + Hard Chrome

Phase II

Phase II of the Progressive Die Project will test only trim and pierce (Figure 7). A myriad of AHSS sheet metals will be tested that include coated and uncoated materials. Stamping experience from the A/SP tribology team identified that coated steel would not generate form and flange operation results as readily as trim and pierce results.

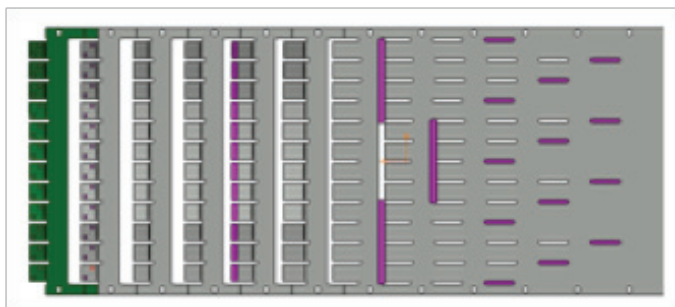


Figure 7. Phase II Strip

From phase I, there were some results that could not be analyzed visually. Optical profilometry will be used in Phase II to determine if a particular standard decreases the wear inflicted from AHSS when there is no visible wear.

The pierce in the first stations will now test 8%, 10%, 12%, and 15% to determine which design allows for the smallest wear rate.

The trim station angle now varies from -30° to 30° in 5° increments, and there will be two (2) pierce punches added in the last station piercing at the same angle. These angled test pierce punches will also be testing the benefits of an engineered radius vs. a sharp edge on each of the pierce.

Phase II is scheduled to run in December 2009 and January 2010.

Coating Fatigue Test

Phase I

The Coating Fatigue Test used an impact force to “wear” the coating. It is suspected that a coating fails internally from fatigue stress causing cracking, fails at the adhesion to the surface from stress or strain cracks in the substrate, or fails to uniformly adhere to the substrate from poor surface finish. The test is shown in Figure 8.

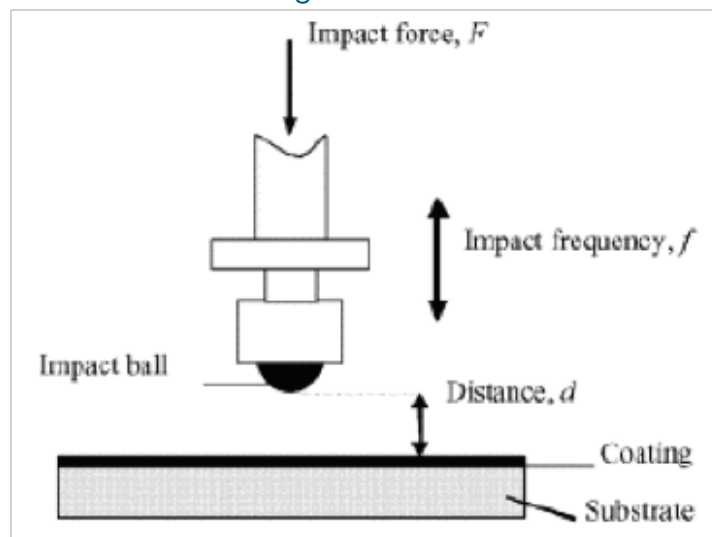


Figure 8. Coating Fatigue Test Phase I Apparatus

Phase I tested six (6) coatings from different vendors and was completed in September 2009. The results are similar to the progressive die test as seen in Figure 9.

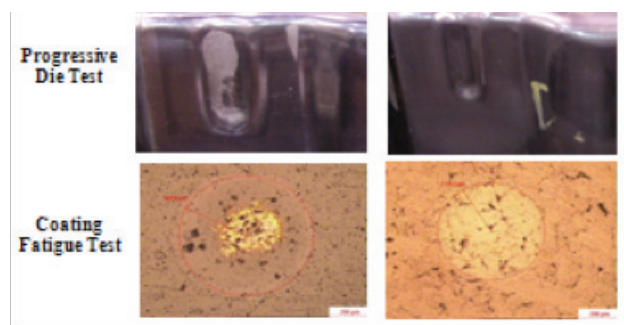


Figure 9. Test Comparison

Phase II

While Phase I results were similar to the DWT, there is still one element missing. The second phase of the coating fatigue test will add friction to the already present fatigue stress and strain. Phase II will run in December 2009 and the design of the apparatus is found in Figure 10.

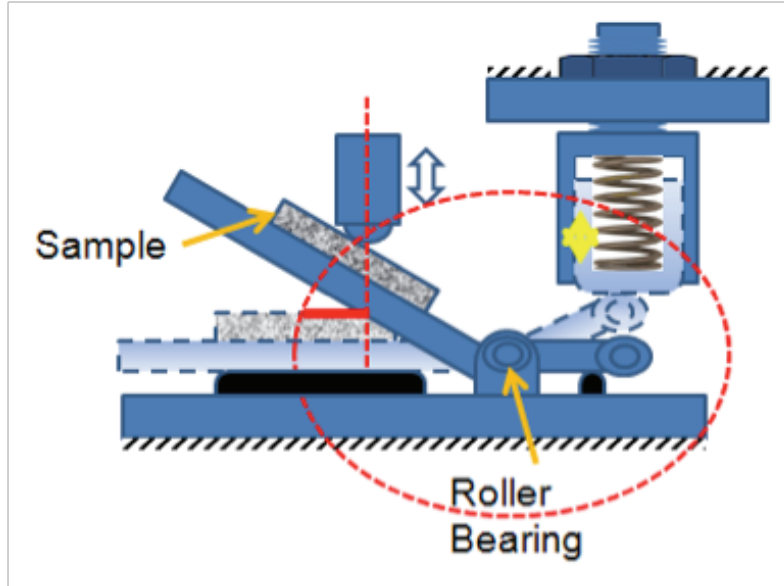


Figure 10. Coating Fatigue Test Phase II Apparatus

Conclusions

The Progressive Die Wear Test is a cost effective test tool from which standards can be continuously improved. The original design that permits stations to be altered and/or replaced allows the tool to continue testing the multitude of conditions seen in stamping AHSS parts.

A valuable lesson was learned concerning the limitations of forming AHSS in Phase I of the progressive die test. The intended form station had to be removed because there was not enough press tonnage or die capacity to stamp the panel. However there were a few valuable conclusions that were determined.

Piercing:

Optimal pierce clearance is between 5-15%

Trimming:

AISI D2 and AISI S7 performed the best

Flanging:

AISI D2 + CVD TiC and Carmo® + Ion Nitride + PVD CrN performed the best

The initial results from these tests are already being implemented, and their continuous improvements are critical to the successful application of AHSS.

The Coating Fatigue Test adds components missing in most coating wear tests – stress and strain from fatigue. Once both phases of the test have been proven, it will assist in narrowing the search for cost effective, quality coatings.

Presentations/Publications/Patents

1. Darryl Young, Ford Motor Company “Investigation of Tooling Durability for Advanced High-Strength Steel” Presented at the 2009 Great Designs in Steel Seminar, May 13, 2009, Livonia, Michigan
2. One (1) technical paper will be written from the Progressive Die work and expected to be made available to various trade publications.
3. Two (2) technical papers will be written from the Coating Fatigue Test Phases I and II. The correlation to the Progressive Die work will be included in that technical paper.

¹Denotes project 230 of the Auto/Steel Partnership (A/SP), the automotive-focus arm of the American Iron and Steel Institute (AISI). See www.a-sp.org. The A/SP co-funds projects with the DOE through a Cooperative Agreement between DOE and the United States Automotive Materials Partnership (USAMP), one of the formal consortia of the United States Council for Automotive Research (USCAR), set up by Chrysler LLC, Ford Motor Company and General Motors Corporation to conduct joint, pre-competitive research and development. See www.uscar.org.

E. AHSS Stamping Project

Principal Investigator: James Fekete
General Motors Corporation
Global Die & Press Center
30001 Van Dyke Avenue
Warren, Michigan 48090
(586) 201-9520; e-mail: jim.fekete@gm.com

Principal Investigator: Changqing Du
Chrysler LLC
800 Chrysler Drive
Auburn Hills, Michigan 48326
(248) 576-6680; e-mail: CD4@chrysler.com

Technology Area Development Manager: William Joost
(202) 287-6020; e-mail: william.joost@ee.doe.gov

Contractor: United States Automotive Materials Partnership (USAMP)
Contract No.: DE-FC05-95OR22363 through the National Energy Technology Laboratory

Objectives

- Determine how to accurately predict and control the amount of springback and other deviations from the desired stamping geometry for parts made from advanced high-strength steel (AHSS) prior to construction of production tooling.
- Develop part design and manufacturing process guidelines that can be recommended to automotive design and manufacturing engineers for the purpose of reducing springback and other part distortions.
- Investigate and analyze fractured materials for the purpose of understanding the fracture mechanism in terms of material properties and processing effects. Develop the ability to predict the onset of shear fracture in stamping processes.

Approach

The approach of the AHSS Stamping Project is to:

- Predict AHSS stamping springback through finite element analysis (FEA).
- Control AHSS stamping springback by developing knowledge of part design geometries that affect flange springback and die processes that control springback.
- Develop predictive tools related to fracture in AHSS based upon an investigation and analysis of fractured material properties and micro structural characterization.

Accomplishments

The significant accomplishments of The Auto/Steel Partnership AHSS Stamping Group are as follows:

- Modified tooling for stretch-forming processes of AHSS auto body structural components to neutralize the residual stresses that cause springback and sidewall curl. Predictable results have been shown for HSLA 350, DP600 MPa, DP780 MPa and DP980 MPa. Panel measurements and data analysis have been reported. The use of stiffening beads and other part shape modifications as well as control of key process variables are being recommended to product designers for control of twist, undercrown, and springback based upon these results.
- The study to evaluate springback compensation technology developed in the DOE-supported “Die Face Engineering” project continued. A previously evaluated part (GM B-Pillar) was re-evaluated, and numerical technology was used to develop a new die face which is expected to compensate for springback and lead to a dimensionally acceptable part. The modified die was used to successfully form parts from several different AHSS grades, and the parts were measured to evaluate shape. Good results were obtained for flange, sidewall and longitudinal springback, but twist was underpredicted. Additional work will be undertaken to understand this result.
- One additional case study of AHSS part development was completed by working through the OEMs. The part was a DP600 component used on a full size pickup truck. The volume “Advanced High-Strength Product and Process Applications Guidelines” was updated, using the information developed from the case studies and other project activities.
- The investigation of shear fracture of AHSS at Edison Welding Institute (EWI), in cooperation with the Ohio State University was completed. The results of the project included new constitutive materials models and new damage-based formability models, aimed at improving the correlation of FEA failure prediction to actual test results.
- New tasks were started to perform more systematic evaluations of edge stretching, based on experiments to be conducted with a new, flexible laboratory-scale tooling set, and a production scale tool aimed at large radius features. Plans are in place to utilize specialized material characterization, to study orientation effects and non-tensile loading paths on performance of AHSS materials.
- Additional work is underway to evaluate material behavior at deformation levels beyond uniform elongation and close to failure. The team is utilizing strain measurement accomplished with Digital Image Correlation (DIC). The team is also studying the effect of test direction (relative to material rolling direction) as an additional step in understanding if microstructural inhomogeneity has significant influence in the fracture performance of AHSS materials.

Future Direction

Additional applications guidelines case studies are being compiled, with a focus on parts at the 980 MPa strength level and above.

A significant new effort, most likely in a new project, will be focused on evaluating the 3rd generation AHSS steels currently under development. The timing of this project will be driven by availability of appropriate test material, and this is expected to be no sooner than FY2012.

Introduction

Advanced high-strength steels (AHSS) combining high-strength and superior formability compared to conventional high-strength steels are increasingly being used to deliver superior vehicle safety performance, while at the same time provide opportunities for mass reduction. AHSS have high initial work hardening rates as well as high tensile strengths. These characteristics,

which make the material attractive to design engineers, also create challenges in the stamping and manufacturing processes; especially in terms of dimensional control and fracture prediction.

FEA has been widely used in automotive industry for vehicle designs and manufacturing feasibility. Over a period of 20 years, a high level of confidence has been achieved using FEA to predict splits and wrinkling in metal forming processes. However, it remains a challenge to accurately predict springback, particularly for those parts with twists and sidewall curls. Numerous studies have been carried out to correlate computer prediction to experimental results. The material model, element formulation, friction and contact algorithm are important parameters affecting simulation accuracy. Other studies have also demonstrated the sensitivity of springback predictions to other numerical parameters, such as mesh size, number of through-thickness integration points, tooling travel speed, contact interface parameters, etc. During the last decade, FEA software developers and users have been investing much effort into the solution of springback prediction problems. A steady improvement has been seen in the prediction capability and methodology.

Prediction of splits using FEA has also been complicated with the emergence of shear fracture in AHSS stamping. Shear fractures are not predicted using conventional FEA analysis techniques, and this has resulted in significant issues during tryout of AHSS parts.

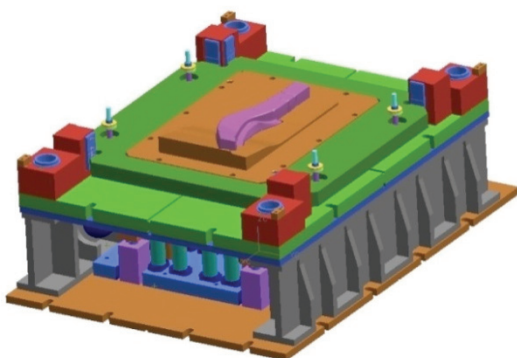
To address these issues, the A/SP initiated enabler projects, focusing on stamping experiments using production-intent tooling, with the results being compared to analyses using computer (FEA) models. To date, various classes of automotive parts have been studied, which were fabricated from AHSS with tensile strengths varying from 600 to 980 MPa. Stamping experiments included various forming process variables, including pad forces, blank holder forces and die configurations (drawing versus crash forming). Simulations were carried out using various numerical parameters (mass scaling, adaptive levels and mesh coarsening) in order to study their effects on the prediction accuracy. Experimental results were compared to the corresponding FEA simulations.

Discussion

Most experiments have been conducted with a multi-process research die with sub-die inserts (Figure 1) to produce various automotive structural components by a variety of processes. This die has the necessary higher holding pressures and controlled processes required for working the higher strength materials.

A programmable hydraulic pressure cushion is the main component of this system that provides the means of stretch forming the metal and controlling springback.

Sub-die inserts in the multi-process master shoe die enable stamping of underbody, cross-car and body side structural components with a variety of stamping processes.



The latest results of the experiments are described below.

Figure 1. Lower Half of Multi-Process Die.

Body Side Center Pillar Sub-Die

A sub-die for a Body Center Pillar was modified through tryout to optimize results (Figure 2). This part is crucial to the body side structure for meeting side impact requirements. It is also typically difficult to stamp in medium strength grades due to springback, twist, and undercrown. The higher strength grades increased the manufacturing difficulties.



Figure 2. Body Side Center Pillar.

During the now completed first phase of the project, several features were added to the part to enable stamping in DP780 material. Changes were made to the product shape to take up excess metal and features were added to stiffen the part. Split and fracture free stampings were then made from both DP780 and DP980 material. Parts have been scanned and dimensional analysis has been completed.

Phase two of the project is utilizing the dimensional evaluation of both untrimmed and trimmed parts. This information, FEA analysis, and computer guided compensation was used to re-cut the die to achieve dimensional accuracy of the part when manufactured from DP780 steel.

Press trials were completed during the reporting period. DP780 was used to produce panels for subsequent dimensional characterization for comparison to the analysis. DP980, TRIP700 and TRIP780 were also used to produce split and fracture-free panels.

The results of these trials were mixed. Figure 3 shows color maps that describe the position of the actual parts vs. the desired nominal target. Good results were obtained for flange, sidewall, and longitudinal springback; however, there was a significant component of twist in the part that was under predicted

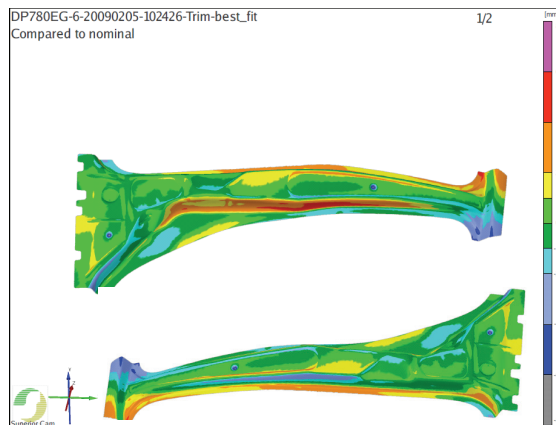


Figure 3. Color Map Describing Deviation of Actual Part from Nominal Target for DP780 Material.

Additional work is underway to determine if the problem is caused by the compensation process or the FE model itself. A detailed review of the FE model is being carried out. Following that, another iteration of the compensation software will be made, and the b-pillar die will be re-cut based on these results and parts resulting from the tryout of the re-compensated die will be evaluated.

Shear Fracture Project

Beginning in 2007 the A/SP AHSS Stamping Team contracted with Edison Welding Institute (EWI), in association with The Ohio State University (OSU), to conduct a three year project for shear fracture characterization, draw bend formability (DBF) testing and fracture criteria development of AHSS. Shear fracture has emerged as a common and unpredictable failure mechanism in production of AHSS parts. An example is shown in Figure 4.

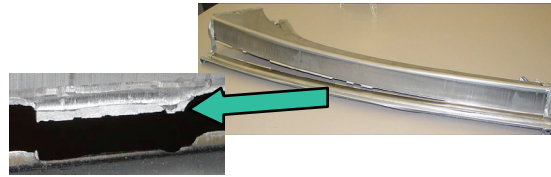


Figure 4. AHSS Shear Fracture Phenomenon.

The work at OSU focused on correlation of results of draw bend formability testing to FEA modeling. A picture of the draw bend tester is shown in Figure 5. Draw bend formability testing to date has been completed on DP 590, DP780, TRIP 780 and DP980 steel in 1.4mm and 1.75mm gauges.

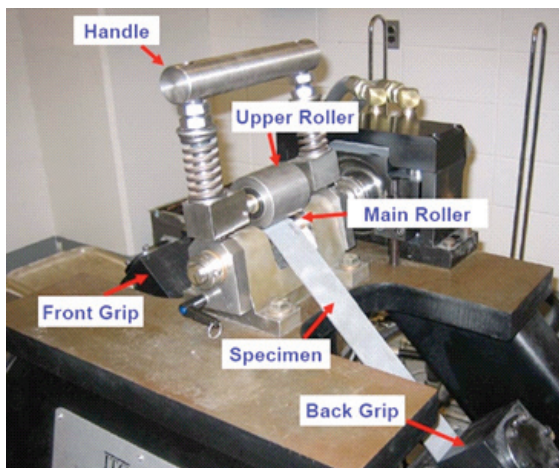


Figure 5. Draw Bend Formability Tester at OSU.

A key finding of the OSU work was that the heat generated during the deformation of the sample has a significant influence on the hardening behavior of the material, and should be taken into account for the most accurate simulations. The OSU investigators accounted for this behavior through development of a new constitutive materials model, which accounts for the reduction in hardening that occurs with the temperature increases measured during draw bend testing.

Using this method, the investigators were able to improve their ability to predict the displacement to failure, and also were able to predict the types of fracture (shear fracture vs. conventional tensile-type failure) (Figure 6 –A and Figure 6-B).

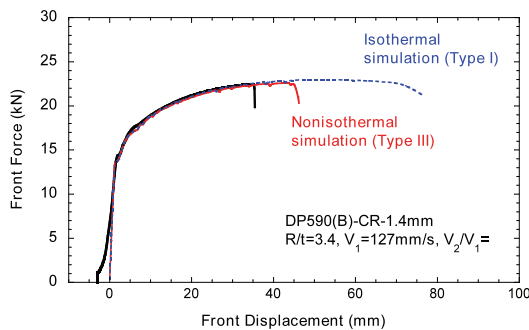


Figure 6-A. Comparison of predicted vs. measured fracture behavior in a stretch-draw test.

		$V_2/V_1=0$							
R/t		2.3	3.4	4.5	5.7	6.8	7.9	10.2	13.6
D	13mm/s	III (II)	III (II)	III (II)	I (I)	I (I)	I (I)	I (I)	I (I)
	2.5mm/s	III (II)	I (II)	I (I)	I (I)	I (I)	I (I)	I (I)	I (I)
DP780(D)	13mm/s	III (II)	III (II)	III (II)	III (I)	I (I)	I (I)	I (I)	I (I)
	2.5mm/s	III (II)	I (I)	I (I)	I (I)	I (I)	I (I)	I (I)	I (I)
DP980(D)	13mm/s	III (II)	III (II)	III (II)	III (I)	I (I)	I (I)	I (I)	I (I)
	2.5mm/s	III (II)	III (II)	I (I)	I (I)	I (I)	I (I)	I (I)	I (I)

Values in the parentheses are predicted ones.

Figure 6-B. Failure types: Simulation vs. Experiments.

All the tested materials had isotropic mechanical properties, and in all but one case, the draw bend formability was similarly isotropic. However, one material showed a distinct difference in behavior when tested transverse to the rolling direction compared to results from testing

longitudinal to the rolling direction. The reasons for this observation are not known, but microstructure likely plays a role.

The investigators at EWI used microstructural damage-based methods to approach the problem, including application of the Normalized Cockrel-Latham (NCL) model, which is a stress-triaxiality-strain based method. The model parameters were developed by correlating analysis results of tensile tests to actual tensile test behavior (Figure 7).

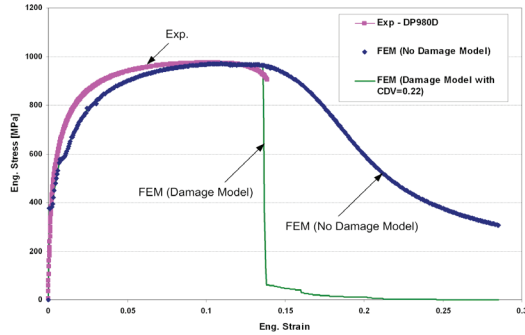


Figure 7. Comparison of DP980 Tensile Test Results to Analysis Results Using Normalized Cockrel-Latham Model.

Subsequently, the NCL model was used to predict results from the draw bend formability test. The model gave reasonable agreements with draw bend test results of various DP steels at different test conditions.

Once a successful correlation to tensile results was achieved, the NCL model was also applied (using LS-DYNA) to the B-pillar simulations. Figure 8 shows an example of the results, comparing actual B-pillar stampings containing shear fractures with the results from the NCL model. The maximum damage locations plotted by the NCL model showed good correlations with shear fracture locations on the B-pillar part.

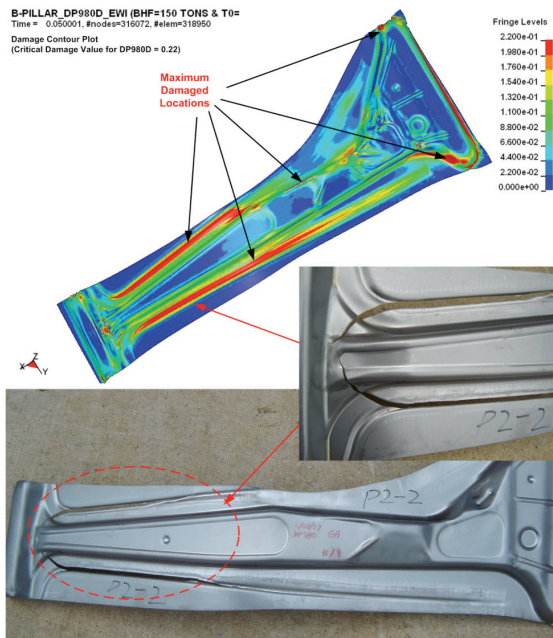


Figure 8. Comparison of Actual B-Pillar Stampings to Predictions of Highly Damaged Areas Based On NCL Model.

A microstructure damage-based approach was also evaluated. The chosen model was the Gurson-Tvergaard-Needleman (GTN) model, which depends on knowledge of micro-void nucleation, growth and coarsening. The model parameters were evaluated based on micro-structural evaluations of stopped-tensile tests on the subject materials. These results were subsequently used to successfully predict results of tensile tests, as shown in Figure 9.

At this time, the high computational requirements of this method preclude its use in industrial formability simulations. Future work will focus on improving the efficiency of the method.

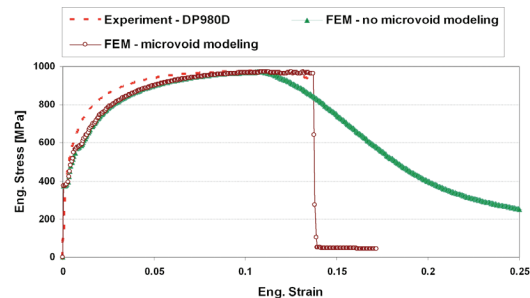


Figure 9. Comparison of DP980 Tensile Test Results to Analysis based on Gurson-Tvergaard-Needleman Model.

Flange Shear Affected Zone Study

A project to develop the empirical failure criterion of AHSS edge fracture under drawing (in-plane stretch) conditions has been started, including understanding the effect of sheared edge conditions on the failure criterion. Two objectives are defined for this project. First, the empirical failure criterion for the draw edge fracture of AHSS will be established on the basis of laboratory testing results. The plan of the experiment study is to use the flat punch hole expanding test and cut edge tensile test to study the AHSS edge fracture limits under various geometric, edge trimming and material thickness conditions. In addition, industrial experience has shown that the failure criteria for small plan-view radius features (e.g. stretched and flanged holes) can be different when compared to larger radius features (e.g. flanges on body panel cutouts). For this reason, experiments will also be conducted, using the same materials, for an industrial scale stamping with radii typical of large body panels (Figure 10).

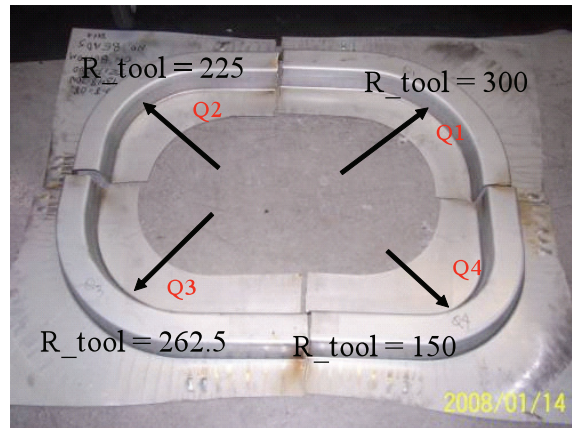


Figure 10. Stamping Used To Evaluate Stretched-Edge Behavior of AHSS In Large Radius Conditions

The effects of microstructures on the failure criterion and sheared edge conditions will also be investigated to help explain the results

Additional Materials Characterization Initiatives

Two additional tasks are underway, aimed at improving the understanding of the basic mechanical properties of AHSS under non-tensile load paths, and as a function of sheet orientation.

The first additional task is the measurement of tensile properties using Digital Image Correlation (DIC) strain measurement. The uniform elongation for AHSS is low; usually less than 15%, while the deformation in actual stamping in the fracture zone is higher and the equivalent strain can be higher than 50%. Stress-strain curves from conventional uniaxial tensile test cannot fully represent the 2-D forming deformation. An extrapolation is necessary to provide full curves for FEA simulations. Due to the varying shapes of AHSS stress-strain curves, such as DP780 vs. TRIP780; it is difficult to find a proper way for extrapolation. Using the DIC technique, full field strain distribution in the diffuse neck region can be captured. Strain data beyond uniform elongation can be obtained, which will provide guideline for the extrapolation of conventional stress-strain curves.

This task is largely complete. 6 quasi-static cases have been completed, for DP, TRIP and HSLA materials. A typical result is shown in Figure 11, which compares the tensile curve measured by an extensometer to that extended by the use of DIC.

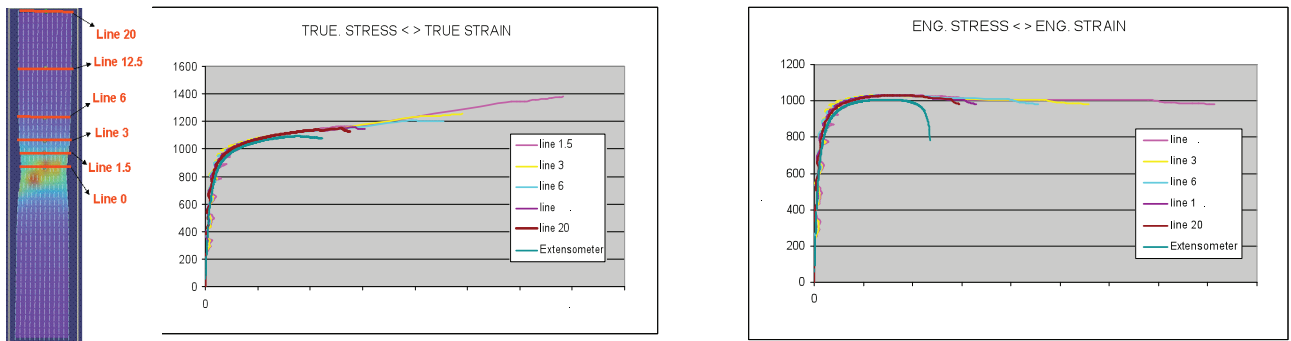


Figure 11. Comparison of Stress Strain Curves with Strain Measured by Extensometer and by DIC

The second task is the evaluation of the effect of sheet orientation on plane strain fracture. Some AHSS display a certain sensitivity of their formability to sheet rolling orientation in the cases of (A) small radius bending; (B) edge stretch; and (C) plane-strain stretch during tube hydro-bulging. This project is experimentally testing and measuring plane strain forming limit (FLD_0) using simple plane strain tension test on both the rolling direction and transverse direction. Strains are being measured using the DIC technique, and texture analysis is also planned to help explain the results.

Preliminary results have been achieved for materials up to DP780. The results have confirmed that acceptable plane strain conditions have been achieved. Modifications to the method are required for DP980 materials, to compensate for the very high strength of the material. An example of a successful test is shown in Figure 12.



Figure 12. Successful Plane Strain Test of an AHSS Material

AHSS Case Studies and Applications Guidelines

The work of this team was leveraged with evaluations of actual production parts. These detailed case studies include part designs, materials selections, stamping processes, analysis results, and lessons learned. One additional case study was completed during this reporting period. A total of 10 case studies are now available at www.a-sp.org/publications.htm.

In addition the “Advanced High-Strength Steel Applications Guidelines,” publication was revised and expanded with new information from other projects. The new document is available at the website described above.

Summary and Conclusions

The team is in the process of evaluating the latest generation of FEA technology for springback prediction. The B-pillar die face has been re-cut based on FEA technology. The parts made with the resulting tool were improved, but not completely dimensionally correct. The evaluation will continue in the next reporting period.

Elements of the experimental work, combined with the results of the case studies have been compiled into a volume entitled: “Advanced High-Strength Product and Process Applications Guidelines”

The EWI/OSU Shear Fracture Project is complete, and a final report has been written. Results show that stretch-bending fracture type can be predicted with knowledge of material and process variables. The FEA simulation results, using OSU proposed thermo-mechanical constitutive model, duplicated the fracture types observed in stretch-bending experiments within acceptable accuracy. Microstructural damage occurs as a result of these processes, and its influence on fracture is currently under investigation. FEA modeling at the microstructural level is also being investigated to determine if it provides value in predicting these fractures. New work aimed at establishing edge fracture criteria was started in this reporting period.

Data to improve constitutive modeling capability, utilizing the DIC method and applying it to conventional and plane strain tensile testing are underway. These data will provide more detailed tensile behavior prior to failure for improving the fidelity of constitutive models used in analysis.

Presentations and Publications

Two papers were presented at the International Deep Drawing Research Group meeting in Golden, CO.

“Failure analysis of advanced high-strength steels (AHSS) during draw bending,” Hyunok Kim¹, Alexander Bandar², Yu-Ping Yang¹, Ji Hyun Sung³, Robert Wagoner³, ¹Edison Welding Institute (EWI), United States, ²Scientific Forming Technologies Corporation (SFTC), United States, ³The Ohio State University, United States

1. “Sheet metal cutting process and edge characterization of dual phase steels by mechanical shearing,” Xiaoming Chen¹, Changqing Du², Xin Wu³, Xinghai Zhu⁴, Sheng-Dong Liu⁵, ¹United States Steel, ²Chrysler, LLC, ³Wayne State University, ⁴LSTC, ⁵Generalety, LLC

In addition, a presentation was made at the Great Designs in Steel seminar:

1. “Fracture Analysis of Advanced High-Strength Steels (AHSS) in Stretch Bending,” Hyunok Kim¹, Alexander R. Bandar², Yu-Ping Yang¹, Jihyun Sung³ and Robert H. Wagoner^{3,1} Edison Welding Institute, ²Scientific Forming Technologies Corporation, ³Ohio State University.
2. A report entitled “Developing a Spreadsheet for Predicting limit Strain in Stretching a Sheared Edge” by C. Van Tyne and B. S. Levy was completed.

¹Denotes project 050 of the Auto/Steel Partnership (A/SP), the automotive-focus arm of the American Iron and Steel Institute (AISI). See www.a-sp.org. The A/SP co-funds projects with the DOE through a Cooperative Agreement between DOE and the United States Automotive Materials Partnership (USAMP), one of the formal consortia of the United States Council for Automotive Research (USCAR), set up by Chrysler LLC, Ford Motor Company and General Motors Corporation to conduct joint, pre-competitive research and development. See www.uscar.org.

F. Strain Rate Characterization

Principal Investigator: Kangping (Kathy) Wang
General Motors Corporation
30200 Mound Rd
Warren, Michigan 48090-9010
(586) 986-1173; e-mail: kathy.wang@gm.com

Lead Scientist: Srdjan Simunovic
Oak Ridge National Laboratory (ORNL)
Oak Ridge, Tennessee 37831-6359
(865) 241-3863; e-mail: simunovics@ornl.gov

Lead Scientist: Susan Hill
University of Dayton Research Institute
Dayton, Ohio 45469-0133
(937) 229-4704; e-mail: Susan.Hill@udri.udayton.edu

Technology Area Development Manager: William Joost
(202) 287-6020; e-mail: william.joost@ee.doe.gov

Contractor: United States Automotive Materials Partnership (USAMP)
Contract No.: DE-FC05-02OR22910 through the National Energy Technology Laboratory

Objectives

- Develop new experimental methods for characterization of crashworthiness and strain-rate sensitivity of both advanced high-strength steels (AHSS) and structural designs.
- Replicate impact conditions that occur in automotive impact by simpler and more manageable experiments in order to generate meaningful data for computer modeling.
- Initiate new, robust spot-weld finite-element formulation procedures for modeling various modes of spot-weld failure as a function of impact, welding conditions and materials while maintaining the current computational efficiency.
- Establish an experimental database on the performance of resistance spot weld in AHSS components during impact.
- Determine the effect of paint baking on the static and dynamic material response of selected AHSS.
- Develop representative material data sets for selected AHSS, which can be used in CAE modeling.

Accomplishments

- Developed procedure for new crashworthiness characterization test based on parallel-plates buckling.
- Developed and conducted constant-velocity crash experiments on circular tubes.
- Developed hydraulic tests for strain rate characterization of high-strength steel (HSS).

- Developed www database for display and analysis of coupon, spot-weld, and tube crush experiments
- Develop test method for investigation of strain-rate effects of spot welds.
- Determined the effects of bake-hardening on the static and dynamic tensile behavior of DP600 and DP780 dual- phase steels.
- Results from tensile tests (DP600 and DP780) were used to create representative material response data sets suitable for input into impact modeling programs.
- Generated high rate tube crush data for as received and baked tubes (DP780).
- Presented two technical papers to SAE2009 World Congress: Dynamic Spot Weld Testing & Bake Hardening Effect of Dual Phase Steels.

Future Direction

- Project team was wrapped up as of March 2009
- Proposed new project team: Advanced Modeling of AHSS for Crashworthiness
- Support Oak Ridge National Lab to complete high rate experiment development and phase II spot weld project.

Introduction

Crashworthiness characterization of AHSS requires testing of materials and structures under increased strain rates, large plastic strains, and large displacements that are characteristic of actual impact events. The AHSS characterization involves testing at several different length scales. The intrinsic material properties are investigated using the coupon-level specimens where the material is exposed to simple stress states that can be reduced to the equivalent stress and strain measures used in formulation of constitutive models. The coupon tests involve uniaxial tension and compression in plane-stress conditions. High-speed hydraulic equipment is used to impose constant velocity in order to determine material response to different loading rates. At a higher length scale, the characteristic plastic hinge mechanism responsible for crash energy absorption in AHSS structures is investigated using the double-plate test. This test has shown that the strain-rate sensitivity of AHSS in bending under out-of-plane compression exhibit trends that cannot be fully explained using the plate bending models derived from material behavior under uniaxial plane stress. At the component level, AHSS properties in tubular structures are investigated using specialized hydraulic equipment that allows constant crush speeds up to 8 m/s. In automotive design, the structural integrity of AHSS components is primarily provided by spot welds. The response of spot welds under different loading velocities and loading states have also been characterized in this project.

The above experiments provide high-quality data for development of material and structural FEM models for AHSS and, thereby, enable more accurate modeling and design of lightweight, crashworthy vehicles. The developed experiment technology is also directly relevant to other automotive materials as it provides a systematic approach to characterization and comparison of crashworthiness of new automotive materials.

It is important to determine the behavior of advanced high strength steels (AHSS) under impact conditions in order to use the correct material properties in crash simulations. As previously reported, the material responses of specific AHSS were investigated to provide material data for FEM analysis. Tensile tests on DP600 and DP780 dual-phase steels were conducted for

as-received and baked samples to examine the effect of baking on the static and dynamic material response. In the latest reporting period, these material responses were digested into representative curves and data sets were generated suitable for input into crash simulations.

Additional crush tests were performed on DP780 tubes in the as-received and bake hardened conditions. An analysis method was developed to accommodate crush test data from facilities and test fixture designs.

Design of Experiments

The experiments conducted under this project have been compiled into interactive databases that are accessible over the World Wide Web. The portal page for the experiments is shown in Figure 1.



Figure 1. Web portal for AHSS experiments

The experiments data are integrated with the other project components and provide mechanisms for data analysis and collaboration between project participants.

Strain Rate Characterization in Sub-Hopkinson Regime

In support of the Auto/Steel Partnership (A/SP), Strain-Rate Characterization Project, Oak Ridge National Laboratory researchers are conducting a high-rate experimental tests and analysis of base material specimens in uniaxial tension configuration. The objective of the test program

is to provide the necessary experimental data in support of the A/SP efforts to determine high-strain-rate mechanical properties of AHSS. The test program consists of testing tensile specimens under strain rates of quasi-static, 0.1/, 1/, 10/, 100/s and maximum strain rates achievable in full open-loop configuration (1000/s) and the selected gage length. Among the unique features of the current approach is the ability to conduct tests across all speeds on the same apparatus and thereby, eliminate variability associated with using different testing methods and actuators.

The dynamic testing procedures from recent studies [1- 4] are followed and further enhanced using the new measurement techniques and synchronization. The multiple measurement methods of both forces and displacements allow for correlation of the results and verification of the different instrumentation techniques. Schematic representation of the test specimen and the measurement locations is shown in Figure 2. The specimen geometry for Dual Phase 780 MPa (DP780) steel is shown in Figure 3.

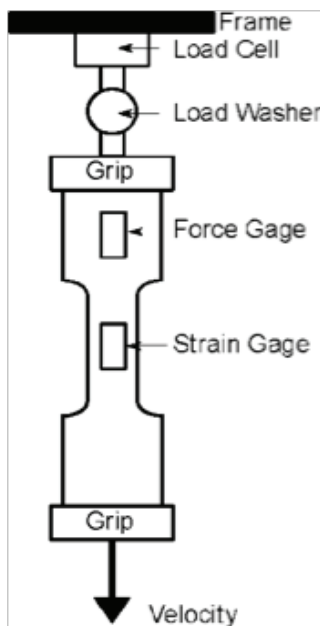


Figure 3. High strain-rate specimen geometry

Figure 2. High strain-rate rate test setup

The horizontal lines in the gage area were added to allow for optical-measurement correlation with the data from actuator displacement and electrical resistance strain gage in the gage area. All the measurements are synchronized using the central trigger. High-speed video recording is used to provide detailed record of the test and to correlate optical measurement with the mechanical output data.

As shown in Figure 3, the ratio between the grip (tab) and gage widths is 2:1. Although it has been widely used and recommended, this width ratio does not seem sufficient for high rate tests. Our experiments have shown discrepancy between the measured forces based on Force Gage and Load Washer and Load Cells, for some materials. The measured strains in the tab showed permanent deformation that indicates plastic deformation out of the desired region.

In order to develop optimal measurement procedures we are currently investigating effects of increasing the above width ratio and using multiple strain gages in the tab area. We are also investigating using the full bridge instrumentation for the Force Gages. Possible bending during the test is evaluated by strain gages on both sides of the specimen. The primary tests indicate that the increase of the width ratio to 3:1 and higher may be necessary, especially for damage prone materials.

Bake-Hardening Effect of Dual Phase Steels in Quasi-Static and High Strain Rate

The University of Dayton Research Institute conducted tensile tests to establish the effects of baking, pre-strain, and strain rate on AHSS: DP600 and DP780.

Examples of summary stress-strain curves showing as-received DP600 with 2% pre-strain across the test rates (0.001/, 10/, 500/s) are shown in Figure 4. The ultimate tensile strength and yield strength of both DP600 and DP780 increased at least 40 MPa with each increase in test rate for both the 0% and 2% pre-strain.

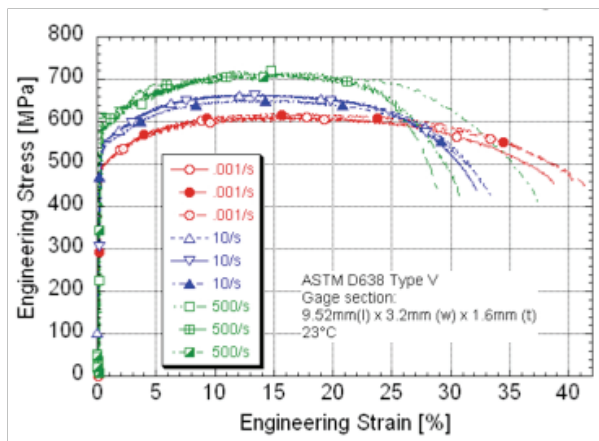


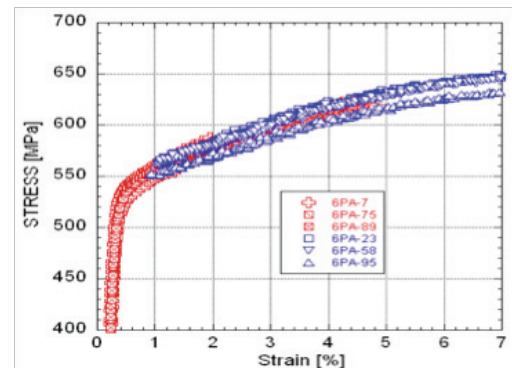
Figure 4. Stress-strain response of as-received DP600 with 2% pre-strain across the test rates

Representative Curve Generation

A representative curve was generated at each rate, derived to reflect the median response of the material at each test condition. The initial part of the representative curve was based on the strain-gauged responses since these specimens were compensated for potential bending. In addition, the resolution of the strain gages was better than the extensometer-based data at low values of strain. The extensometer-based curves were used as the baseline beyond ~2% strain. The data for DP600, as-received, 2% pre-strain are used as an example.

The data sets for a given test condition were combined onto one graph (Figure 5). Polynomial curves were fit to sections of the overall data set (Figure 6). The order of the best-fit curve varied depending on the strain range for the curve fit. Data were calculated at discrete values of strain based on the best-fit curve. The increment between the strain values varied, gradually increasing after yield as seen in Figure 7. The overlapping regions of the fit were reconciled and smoothed.

Figure 5. Data set for DP600, as-received, 2% pre-strain, used for representative curve generation.



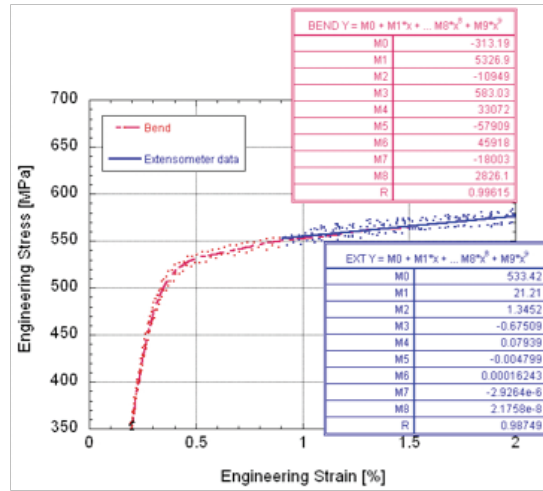


Figure 6. Best-fit polynomial curves for initial part of stress-strain curve.

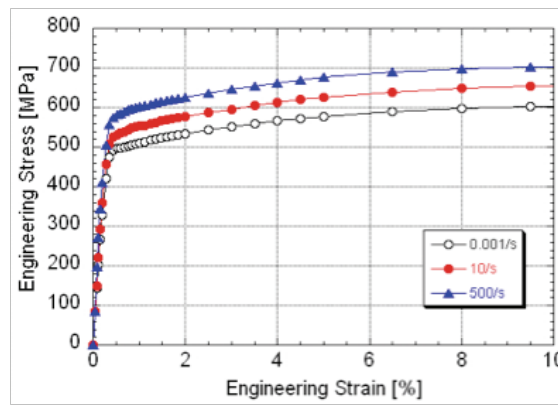


Figure 7. Increasing strain increments for representative curve.

The resultant curves were superimposed onto the data sets at each rate to check if the results were consistent (Figure 8). Some of the data points may have been adjusted to reflect the overall trends noted in the material with increasing rate. The ringing component noted for some of the runs at 500/s was visually or mathematically filtered, as seen in Figure 8.

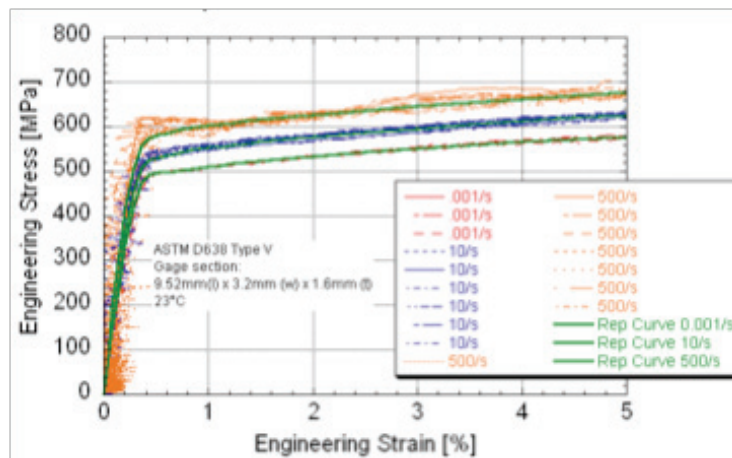
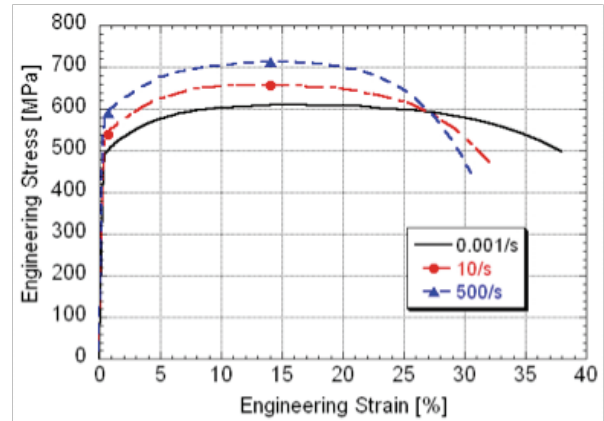


Figure 8. Representative curves and test data.

The same values of strain were used for all of the representative curves for a given material. Each curve contained 37 to 60 data pairs, depending on the failure strain. An example set of final representative curves are shown in Figure 9.

Figure 9. Final representative engineering stress-strain curves for DP600, as-received, 2% pre-strain.



Update on Tube Crush Testing

Room temperature compression tests were performed on as-received and bake-hardened DP780 tubes. Tubes for the 0.254 mm/s and 25.4 mm/s tests were compressed under 977 KN four-post MTS servo-hydraulic test station at UDRI. The tubes with the 2° taper were tested at 0.254 mm/s in the MTS station and at 7250 m/s with a VIA sled at Ford Motor Company.

The initial crush behavior was different for the two test set-ups, as seen in Figure 10. The differences had lessened by the onset of the first fully developed fold. The average crush load and energy absorption from this point out to a net displacement of 75 mm was used to compare the rate and heat treatment effects. Photographs of a typical crushed specimen are shown in Figure 11.

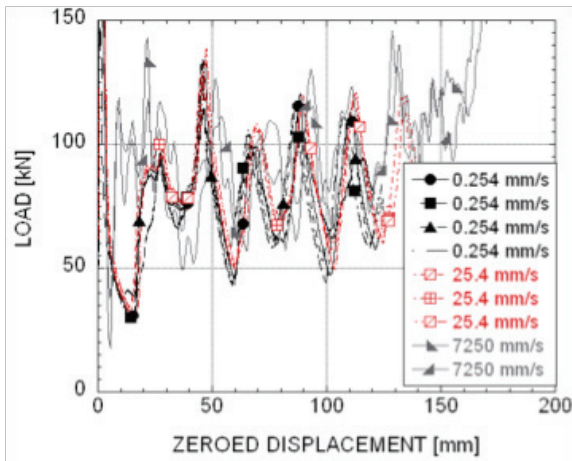


Figure 10. Comparison of behavior at three rates for as-received DP780 tubes.



Figure 11. Baked DP780 tube tested at 25.4 mm/s

The effect of bake-hardening and increasing test rates on the average crush load can be seen graphically in Figure 12. The effects of increasing test rates are in Tables 1 and 2. The average crush load and energy absorption increased with rate for the as-received tubes. Bake-hardening effects are in Table 3. Bake-hardening increased the average crush load and energy absorption by 3%. However, the increase between 25.4 mm/s and 7250 mm/s was not statistically significant because of a large amount of spread in the baked tube data at the high rate.

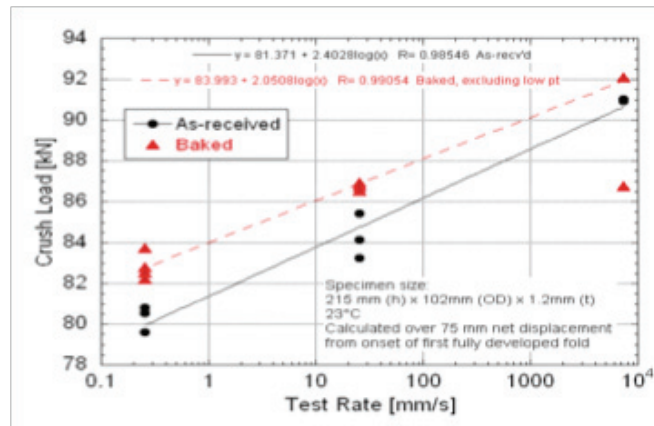


Figure 12. Average crush load versus test rate for as-received and baked DP780 tubes.

Table 1. Change in average crush load of DP780 tubes due to increased test rates. Values taken across net displacement of 75 mm from onset of first fully developed fold.

	From 0.254 mm/s to 25.4 mm/s		From 25.4 mm/s to 7250 mm/s	
	kN	%	kN	%
As-received	4.14#	5.16#	6.69#	7.36#
Baked	3.91#	4.72#	2.68*	3.09*
#Statistically significant, one-sided t-test, alpha=0.05				
*Positive trend but not statistically significant due to large spread in data.				

Table 2. Change in average energy absorption of DP780 tubes due to increased test rates. Values taken across net displacement of 75 mm from onset of first fully developed fold.

	From 0.254 mm/s to 25.4 mm/s		From 25.4 mm/s to 7250 mm/s	
	kJ	%	kJ	%
As-received	0.31#	5.10#	0.78#	12.4#
Baked	0.26#	4.21#	0.01*	0.12*
#Statistically significant, one-sided t-test, alpha=0.05				
*Positive trend but not statistically significant due to large spread in data.				

Table 3. Change in average DP780 tube properties due to bake-hardening. Values taken across net displacement of 75 mm from onset of first fully developed fold.

Test Rate [mm/s]	Crush Load		Energy	
	kN	%	kJ	%
0.254	2.69#	3.36#	0.22#	3.60#
25.4	2.47#	2.93#	0.17#	2.72#
7250	-1.54*	-1.70*	-0.60*	-8.47*

#Statistically significant, one-sided t-test, alpha=0.05
 *Positive trend but not statistically significant due to large spread in baked tube data.

Conclusions

A new method for characterization of strain-rate sensitivity under automotive strain rates has been developed. This method uses multiple measurements of material response in a single testing apparatus. It enables the correlation of the measurements and identification of test areas for further improvement. The new specimen configurations for plate materials are under development.

Tensile tests performed on DP600 and DP780 dual-phase steels established the effects of pre-straining, bake hardening, and increasing test rate. The results from the tensile tests were used to generate representative curves of the material response. The tabulated data from the curves can be used as input for finite element analyses of DP600 and DP780.

Crush tests were performed on DP780 tubes in the as-received and baked conditions at multiple strain rates. An analytical methodology was developed to enable analysis of crush data from dissimilar test setups. Trends showed a 3% increase with bake hardening in the average crush load and energy absorbed across a test rate of 0.254mm/s to 7250mm/s.

Acknowledgments

Support from the Auto/Steel Partnership Strain-Rate Characterization Team is acknowledged.

Future Work

The future work on the project will focus on the following topics:

1. Improvement of accuracy of strain and force measurements at strain rates larger than 100/s.
2. Development of integrated measurement system that automatically processes and correlates measurements.
3. Development of the specification for the testing of materials in the automotive strain rates regime.
4. Strain-rate sensitivity measurements for the new AHSS.

5. Digital image correlation measurement methods for out of plane compression problems and bending.
6. Development of new coupon-level crash characterization experiments for AHSS fracture under impact.

References

1. Recommendations for Dynamic Tensile Testing of Sheet Steels, International Iron and Steel Institute, 2005.
2. C. Wong, IISI-AutoCo Round-Robin Dynamic Tensile Testing Project, International Iron and Steel Institute, 2005.
3. D. Matlock, J. Speer, Constitutive Behavior of High Strength Multiphase Sheet Steels Under High Strain Rate Deformation, AISI/DOE Technology Roadmap Program, Report TRP 9904, 2005.
4. D.M. Bruce, “Dynamic Tensile Testing of Sheet Steels and Influence of Strain Rate on Strengthening Mechanisms in Sheet Steels”, Ph. D. Thesis # MT-SRC-003- 018, Colorado School of Mines, 2003.
5. B.M. Hance, T.M. Link and D.P. Hoydick, “Bake Hardenability of Multi-phase High-Strength Sheet Steels.” 45th MWSP (MS&T) Conference Proceedings. Vol. XLI, 2003
6. R. S. Kircher, A.K. De, J.G. Speer, and K. K. Matlock, “The Effects of Strain Rate on the Deformation Behavior of High-Strength IF and Bake-Hardenable Sheet Steels for Automotive Applications”, MS&T 2004 Conference Proceedings.

¹Denotes project 190 of the Auto/Steel Partnership (A/SP), the automotive-focus arm of the American Iron and Steel Institute (AISI). See www.a-sp.org. The A/SP co-funds projects with the DOE through a Cooperative Agreement between DOE and the United States Automotive Materials Partnership (USAMP), one of the formal consortia of the United States Council for Automotive Research (USCAR), set up by Chrysler LLC, Ford Motor Company and General Motors Corporation to conduct joint, pre-competitive research and development. See www.uscar.org.

G. Future Generation Passenger Compartment Phase 2 - Validation

Principal Investigator: Jody R. Shaw
Manager, Automotive Marketing
United States Steel Corporation
5850 New King Court
Troy, Michigan 48098-2608
(248) 267-260; e-mail: jrshaw@uss.com

Principal Investigator: Joe Polewarczyk
General Motors Corporation
Body Systems & Closures
Engineering West
Mail Code 480-11-W13
30200 Mound Road
Warren, Michigan 48092-2025
(586) 986-2157; e-mail: joseph.m.polewarczyk@gm.com

Principal Investigator: Shawn Morgans
Ford Motor Company
Body Structure – Technical Leader
Product Development Center
20910 Oakwood Boulevard
Cube-2F-C11
Dearborn, MI 48212

Technology Area Development Manager: William Joost
(202) 287-6020; e-mail: william.joost@ee.doe.gov

Contractor: United States Automotive Materials Partnership (USAMP)
Contract No.: DE-FC05-02OR22910 through the National Energy Technology Laboratories

Objective

- Validate the findings of the FGPC Phase 1 project on a 5-passenger 4-door high production volume donor vehicle reducing passenger compartment mass by 25% or greater with cost parity relative to baseline while maintaining the structural performance in crash safety, stiffness and durability while maintaining architectural constraints.
- Mass Efficient Architecture for Roof Strength (MEARS) project is the concept development of a large truck cab with no B-pillar that comprehends the increase from 1.5 to 2.5 times vehicle curb mass roof-strength criteria with weight parity.
- Comprehend manufacturing feasibility in advanced manufacturing.
- Comprehend opportunities and influence of mass compounding.
- Identify opportunities for additional mass reduction with continuous joining.

Approach

- Aggressive use of advance high-strength steels (AHSS), advanced manufacturing and computer aided topology, grade, gauge and geometry optimization techniques.
- Comprehend secondary mass reduction of vehicle systems with empirical regression analysis of production vehicle data.

Accomplishments

- Developed concepts for reducing sedan donor vehicle passenger compartment mass by 15% at cost parity while maintaining baseline structural performance criteria, passenger requirements, and vehicle architecture.
- Confirmed mass reduction associated with continuous joining, increasing mass reduction of passenger compartment from 15% to 20% at cost parity while maintaining all performance attributes.
- Developed three concepts for a truck cab with no B-pillar that satisfy FMVSS 216 (3 times roof-strength criteria) with minimal mass gains of 7.5 to 10.5kg and \$80.00 cost increase.
- Identified potential for secondary mass reductions on the order of 1.5 times the primary mass savings in clean-sheet vehicle architectural executions due to mass compounding.

Future Direction

- Develop vehicle structure with radical architectural changes and mass compounding to achieve structural mass reductions up to 50%.

Introduction

Initially FGPC- Phase 2 (Validation) Project was divided into eight tasks but upon request from the Auto/Steel Partnership (A/SP) Tasks 2.5, 8.0a and 8.0b were added to the project. An individual report is provided for each task, which includes its own appendices.

- Task 1.0: Calibration
- Task 2.0: Optimization
- Task 2.5: Parts Consolidation
- Task 3.0: Concept Design
- Task 4.0: Concept Design Validation
- Task 5.0: Final Optimization
- Task 6.0: Final Concept Design
- Task 7.0: Final Concept Design Validation
- Task 8.0a: Sensitivity Part 1 (Seat Position & Pole Impact to MMV targets)
- Task 8.0b: Sensitivity Part 2 (Continuous Joining)

Project Background

FGPC-Phase 2 (Validation) is the second part of a research project that aims to create a lightweight passenger compartment utilizing modern high strength steels. The first part of the project, FGPC-Phase 1, developed an optimization strategy, which was applied to the ULSAB-AVC (UltraLight Steel Auto Body - Advanced Vehicle Concepts) vehicle which achieved the requirements of the crashworthiness loadcases considered, while reducing the mass of the passenger compartment by 30% relative to reference vehicles through the use of high strength steel. The second part of the project, FGPC-Phase 2 (Validation), applies the Phase 1 findings to a current production vehicle called the Donor Vehicle.

Project Strategy

FGPC-Phase 1 clearly demonstrated that AHSS (Advanced High Strength Steel) can be effectively utilized in automotive lightweighting, or mass avoidance strategies, to provide the required performance at a lower overall cost.

FGPC-Phase 1 did successfully prove the following strategy:

1. Efficient use of geometry to define the loadpath that meets crashworthiness and stiffness requirements, while absorbing energy through total system topology optimization.
2. Investigate the usage of AHSS materials and manufacturing techniques, such as tailor-welded blanks, to reduce vehicle mass and increase its performance.
3. Reduce the vehicle mass by using topology and shape optimization.

FGPC-Phase 2 (Validation) aims to develop a robust design with a long-term perspective of 10 years. Hence this means developing concepts that would require manufacturing components from materials not traditionally applied to such components or in gauges that current design practice would not view as practical.

FGPC Structure

The strategy implemented by this project concentrated primarily upon multi-disciplinary loadpath optimization, which addressed all the crashworthiness, stiffness and NVH loadcases under consideration. When considering another material such as composite, aluminum or multi-material vehicle, the knowledge and technology developed by the load path optimization in this project is still valid. However, the FGPC project has demonstrated, the geometry, gauge and the impact of manufacturing, joining and assembly must be considered for each material proposal.

Lessons Learned From FGPC-Phase 2- (Validation)

General Comments

- The Donor Vehicle is/was a current production vehicle and so represents a fully matured design. Thus architectural constraints played an important role in constraining the degree of change available to the optimization.

Loadpath Optimization, Part Consolidation, Shape Optimization,

- Project investigates alternative loadpaths in the body structure that proved very effective at mitigating crash loads while enable mass reduction. Loadpath optimization is an essential ingredient in the project’s optimization process that enables the AHSS steels under consideration to reduce structural mass through down gauging and parts consolidation.
- Project investigates the opportunity for part consolidation with advance material processing. This improves the structure performance of the components and reduces mass by leveraging this improvement and elimination of weld flanges.
- Structural component geometries were optimized for improved performance enable mass reduction.
- The optimization did not automatically reduce the mass of all parts. In fact in some cases it increased their mass. The optimization balanced the performance of the complete structure in order to achieve the necessary performance. This is what enabled it to create the minimum mass solution.
- The mass of certain components was driven by torsional stiffness requirements. Since this is a stiffness loadcase, upgrading the material choice of such a component to a higher strength will not increase its stiffness. Without changing its geometry, only a change in gauge could achieve this, consequently increasing the overall mass.

Conclusions

Mass Reduction

The optimization methods applied to the FGPC- Phase 2 (Validation) project achieved a 39.8kg (-15%) mass reduction in the optimized components of the combined passenger compartment and doors compared to the Donor Vehicle.

Figure 1 shows the effect of applying these results to the complete passenger compartment, a 12% mass reduction and to the full BIW, a 9% mass reduction.

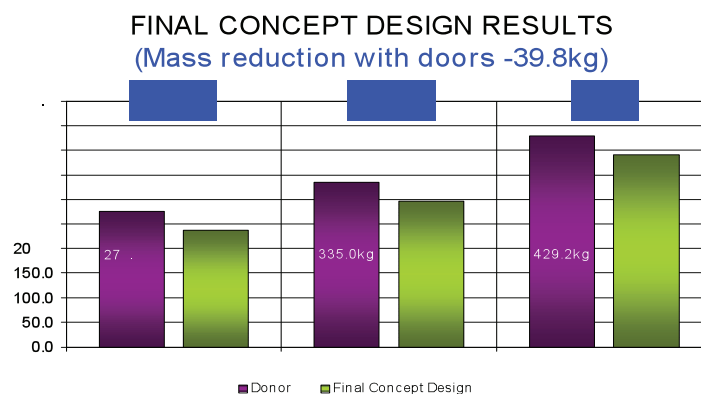


Figure 1. Final Concept Design – Mass reduction including effect of doors.

Sensitivity Studies

Three sensitivity studies were performed on the Final Concept Design. These were:

1. Seat Position Sensitivity
2. Pole Impact Sensitivity using the MMV (Multi-Material Vehicle) targets
3. Continuous Joining Sensitivity

Seat Position Sensitivity

The seat cross-member is a primary loadpath for IIHS Side and Pole Impacts developed by this project. During the course of the optimization both the driver's and passenger side seats were placed in the 5th Percentile position as defined by the IIHS test definition. As the placement of the seat cross-member changes with seat position what impact will this have on the loadpath's effectiveness?

This sensitivity study addresses this concern by evaluating the Final Concept Design's IIHS Side Impact performance for a variety of seat position combinations (Figure 2).

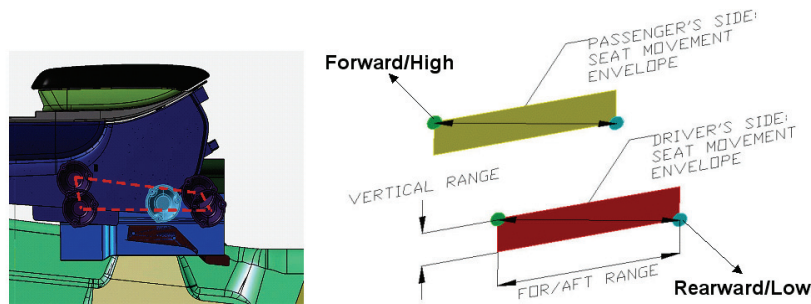


Figure 2. IIHS Side Impact Sensitivity – Range of Driver and Passenger Seat Positions.

In all the combinations of seat positions considered, the structure achieved the required performance by a comfortable margin (Table 1). This demonstrates that the vehicle's IIHS Side Impact performance is insensitive to seat position.

Table 1. IIHS Side Impact Sensitivity Results

Driver's Seat Position	Loadcase	Passenger's Seat Position	IIHS Side Impact Survival Space (Target: 83mm)*	Target Achieved
Forward/High	1	Forward/High	116mm	ü
	2	Rearward/Low	101mm	ü
Rearward/Low	3	Forward/High	98mm	ü
	4	Rearward/Low	99mm	ü

*The Final Concept Design was optimized at the IIHS 5th Percentile position for both seats and achieved a survival space of 115mm.

Pole Impact Sensitivity Using the MMV Target

The Final Concept Design was optimized to meet a Donor Vehicle pole impact capability of 83mm. With the replacement of the seat mount cross member the survival space target used was 125mm. In total they added 4.18kg to the mass of the passenger compartment. However,

it should be noted that the purpose of this study is not to optimize their added mass or performance but simply to determine if the increased survival space target of 125mm could be achieved.

Continuous Joining Sensitivity

The Final Concept Design is primarily a spot-welded structure. The first objective of this sensitivity study was defined the baseline performance of both a continuous laser welded and continuous adhesive bonded variants of the Final Concept Design. The performances of both types were measured for IIHS side impact, IIHS front crash 40% ODB, roof crush and pole impact. The second objective selected one continuous joining method and optimized it any additional mass reduction. This was achieved by optimizing the gauge of the major components in the passenger compartment.

Summarizing the performance of all five loadcases considered both joining methods showed a significant improvement over the Final Concept Design (Table 2). However, the adhesive model was selected for gage reduction optimization back to baseline performance because its increased performance over the laser joining enabled greater potential for mass reduction.

Table 2. Summary of Laser Welded & Adhesive Bonded Performance improvement.

LOADCASE	PERFORMANCE IMPROVEMENT	
	FINAL CONCEPT LASER	FINAL CONCEPT-ADHESIVE
IIHS Side Impact	2%	16%
IIHS Front Impact ODB	16% to 44%	22% to 60%
Roof Crush	15%	25%
Torsion	10%	15%
Bending	13%	20%

Optimization of the Continuous Adhesive Bonded model resulted in a revised selection of gauges for the components considered resulting in 18.7kg (-8%) mass reduction compared to the Final Concept Design a total of 59kg (-21%) mass reduction of the optimized components compared to the Donor Vehicle (Figure 3).

Full Joint Optimization Results

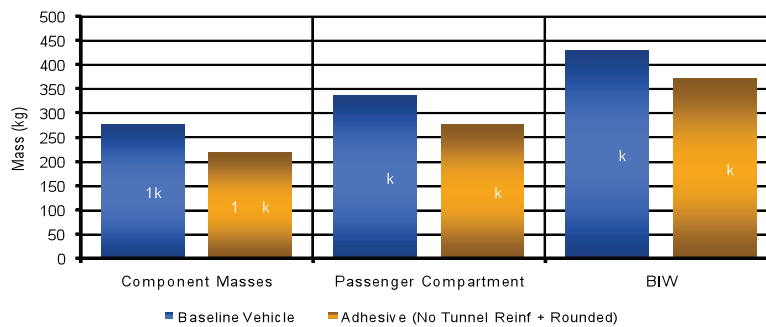


Figure 3. Joint Optimization Results – Comparison to Baseline Vehicle

FGPC Cost Model

A manufacturing cost model was developed that compared the baseline donor vehicle with the FGPC baseline solution and the optimized continuously joined solution. Results are shown in Figure 4.

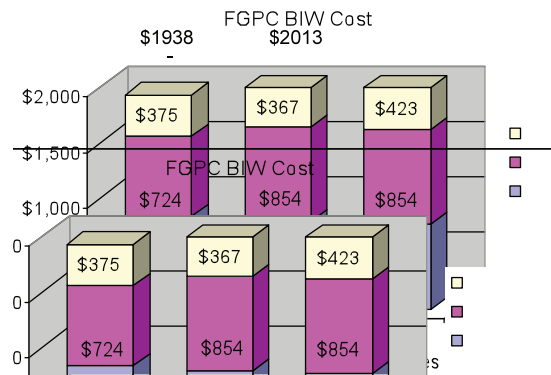


Figure 4. FGPC Cost Model Result

Mass Efficient Architecture for Roof Strength (MEARS) Project:

A related project was conducted to develop a mass efficient roof structure on a B-pillarless light truck cab structure. The MEARS Phase 1 final design concept model was validated in terms of the overall load carrying capability. This final concept model allowed the roof structure to hold a 40% higher normalized load.

The goal of the Phase II project was to continue to develop a mass efficient roof structure on the B-pillar-less, light truck structure. These goals included:

- Providing a mass efficient design of the roof structure by further optimizing the Phase I Composite Insert Nylon Steel Design through use of analytical multi-objective optimization.
- Developing designs that continue to meet the enhanced FMVSS 216 roof strength requirements as proposed by the MEARS team.
- Investigation of alternate steel only design concepts that would meet the requirements in a mass efficient manner.
- Investigation of continuous bonding methods including laser welding and weld bonding to gain further mass efficiencies.
- Providing a final design concept that is manufacturing feasible by conducting metal forming simulations and process evaluations on parts that are new or use ultra high strength steels like Boron Steel or Dual Phase Steels.
- Developing a cost model and performing a detailed cost analysis of the final design concept accounting for the manufacturing process and assembly changes in the design.
- Presenting a final design concept that represents an Optimal Design Concept of Mass Efficient Architecture for Roof Strength Performance.

Phase I Study Findings

The Phase I final design concept model was validated in terms of the overall load carrying capability at the beginning of the Phase II study. With the use of advanced high strength steels throughout the greenhouse, and the introduction of Composite Nylon Inserts in key areas, the Phase I final concept model was able to carry a normalized load of 3.06. Through design optimization, the mass of the steel components in the roof structure reduced by 5.2 kg. The overall mass of the roof structure including the nylon inserts was 1.3 kg higher than the donor model. More significantly, this Phase I final concept model allowed the roof structure to hold a 40% higher normalized load. **Table 3** details the metrics of these two models.

Table 3. Donor Model and Phase I Final Concept Model - Comparison Table.

M	Normalized Load	Mass of Roof Structure (kg)
Donor	.	3 .
Phase I Final Design Concept	3.06	37.4

Optimization of the Steel Design with Composite Nylon Inserts

The Phase I Final Concept Model was used as the baseline for this study. The composite inserts that were developed in Phase I were optimized for size and shape as was the surrounding greenhouse structure. The five concepts developed all met the load requirements and had varying degrees of mass savings and cost efficiencies. **Table 4** shows the results.

Table 4. Composite Nylon Insert Steel Design Concepts – Mass Comparison.

Model	Normalized Load	Mass of Roof Structure (kg)	Mass Savings (kg)
Phase I Final Design Concept	3.06	37.4	N/A
Phase II Composite Nylon Insert Steel Design Concept #1	3.0	32.2	5.2
Phase II Composite Nylon Insert Steel Design Concept #2	3.0	36.4	1.0
Phase II Composite Nylon Insert Steel Design Concept #3	3.0	36.7	0.7
Phase II Composite Nylon Insert Steel Design Concept #4	3.0	36.3	1.1
Phase II Composite Nylon Insert Steel Design Concept #5	3.0	31.7	5.7

Composite Body Solutions Correlation Data

Overall, material development and partial bonding modeling techniques are still being enhanced. For this project the data that has been established is correlated back to a variety of three point bend tests, along with some full vehicle tests.

The effects of partial bonding were examined and it has been determined that when a composite body solution was not fully bonded, the performance of the overall structure could be reduced significantly. Generally, there was no clear methodology to predict a ratio of performance (stiffness) compared to the percent of bonding for a specific composite body solution. It was determined that if areas of partial bonding are known and incorporated into an analysis model, then good correlation can be achieved between a physical structure and analytical results.

Optimization of an Alternate Steel Only Design

Due to the higher costs generally associated with using composite body solutions, a roof structure design that used only steel was considered as an affordable, reduced risk and more widely acceptable solution. The Phase I Final Design Concept Model was used as a baseline and starting point for this study. The Composite Nylon Inserts were removed, and the gauge and material grade were optimized to develop design concepts that met the overall roof strength load requirements. The solution meets the load requirement, but a slight mass increase occurred when compared to the Phase I Final Concept Model. The design was 1.4kg heavier, and used an extensive amount of Ultra High-Strength Steels (UHSS) in order to achieve this minimal increase in overall mass of the roof structure at considerable cost savings.

Table 5. Alternate Steel Design Concept Solution – Mass Comparison.

M	Normalized Load	Mass of Roof Structure (kg)	Mass Penalty (kg)
Phase I Final Design Concept	3.06	37.4	N/A
Phase II Alternate Steel Design Concept #1	.	3 .	1.4

Linear Statics Based Optimization

Linear statics based optimization showed a lot of initial promise, though many factors limited our overall ability to use this method to guide our design optimization process. Topology optimization showed results very similar to our non-linear optimization efforts. It indicated that higher gauges and design changes to improve stiffness in the C-Pillar area were critical to the structure meeting the load requirements. Similarly, the volume topology showed to be a quick way of establishing the nylon insert locations. Lastly, the shape optimization provided an interesting approach for developing shape changes and identifying shape variables for optimization.

In conclusion, linear statics based optimization for complex non-linear problem is a relatively new approach with a lot of research activity in the recent years, some providing very interesting results.

Cost Study

A cost study conducted at the end of the design phase indicated that the Phase II Final Concept Model has an added cost of \$69.48 when compared to the Donor Model. The steel components of the Phase II Model accounted for \$30 of the cost while the remaining was attributed to Composite Nylon Inserts. However, the Phase II Final Concept Model has a roof structure that is 4.4kg lighter than the Donor Model.

Lastly, the Phase II Final Concept Model roof was able to withstand a load that is 40% greater than the Donor Model under the enhanced FMVSS 216 requirement.

Manufacturing Feasibility Studies

Formability assessment of the greenhouse components utilizing ultra high strength steels were conducted for the Phase II Final Design Concept with CAE forming simulations. The team determined the Phase II Final Design Concept was feasible to manufacture.

Mears Phase 2 Project Conclusions

The Phase II Final Design Concept Model had a mass savings of 5.7kg when compared to the Phase I Final Concept Model and 4.4kg compared to the Donor Model. In order to achieve the mass savings, a combination of design changes, advanced and ultra high steel materials, additional spot welds and composite nylon inserts were included in the design. Composite Nylon Inserts and Boron Steel, coupled with design changes were used to help strengthen this area, allowing gauge reductions and material substitutions to occur throughout the greenhouse structure to achieve the final mass savings. **Table 6** compares the Phase II Final Design Concept with the Donor Model for load capability and mass of the roof structure.

Table 6. Phase II Final Design Concept Summary

M	Normalized Load	Mass of Roof Structure (kg)
Donor	.	3 .
Phase II Final Design Concept	.	3 .

FGPC and the Effects of Mass Compounding:

Phase 1 of FGPC found mass body structure mass savings would increase from 30% to 40% when the curb weight was reduced by 20%; identified as mass compounding. The objective of this task was to develop a more comprehensive tool for evaluating the mass compounding effect. Mass compounding behavior may be modeled using subsystem mass influence coefficients—the incremental change in subsystem mass for a unit change in gross vehicle mass. In setting targets for future vehicles, it is helpful to recognize this compounding behavior.

Vehicle design engineers intuitively know that an unplanned mass increase in a component during vehicle design has a ripple effect throughout the vehicle; other components need to be resized increasing vehicle mass even more. The phrase *mass begets mass* describes this phenomenon. A more encouraging view of this behavior is considering a reduction in the mass of a component enabled by a new technology resulting in a greater mass saving for the overall vehicle. These secondary mass changes can be considerable—estimated at an additional 0.7 to 1.8 times the initial—primary—mass change.

A means to quantify the secondary mass change is with a *mass compounding model*. In this model, each subsystem (denoted by *i*) is assigned an *influence coefficient*. The influence coefficient is the change in the subsystem mass when gross vehicle mass undergoes a unit change. The physical interpretation of the influence coefficient is each subsystem is sized to some degree by the mass of the vehicle, and as the vehicle mass changes the subsystem must also be resized.

Description of the Study

In this study, mass data collected by A2Mac1 was analyzed. (Since 1997, A2Mac1 has been providing benchmarking services to manufacturers and suppliers.

Summary of Results

When all subsystems can be resized, the secondary mass savings is approximately 1.5kg/kg. When the powertrain has been fixed and is not available for resizing, the secondary mass savings is approximately 0.6kg/kg. These results have been implementing into an effective excel design tool to enable preliminary designs to take advantage of mass compounding.

References

1. *Preliminary Vehicle Mass Estimation Using Empirical Subsystem Influence Coefficients*, D. E. Malen and K. Reddy, GDIS, 2008.
2. *A2mac1 Automotive Benchmarking*, www.a2mac1.com

¹Denotes project 241 of the Auto/Steel Partnership (A/SP), the automotive-focus arm of the American Iron and Steel Institute (AISI). See www.a-sp.org. The A/SP co-funds projects with the DOE through a Cooperative Agreement between DOE and the United States Automotive Materials Partnership (USAMP), one of the formal consortia of the United States Council for Automotive Research (USCAR), set up by Chrysler Group LLC, Ford Motor Company and General Motors Corporation to conduct joint, pre-competitive research and development. See www.uscar.org.

H. Lightweight Rear Chassis Structure

Principal Investigator: Jamal Alghanem, PhD
Chrysler Group LLC
800 Chrysler Drive - CIMS 484-01-09
Auburn Hills, MI 48326
(248)576-0849; e-mail: ga5@chrysler.com

Principal Investigator: Michael Gulas
ArcelorMittal
P.O. Box 2460, 1330 Burlington St .E.
Hamilton, ON, Canada L8N 3J5
(905)548-4719; e-mail: michael.gulas@arcelormittal.com

Technology Area Development Manager: William Joost
(202) 287-6020; e-mail: william.joost@ee.doe.gov

Contractor: U.S. Automotive Materials
Contract No.: DE-FC05-02OR22910

Objectives

- Obtain a minimum mass reduction of 25% for a baseline passenger car rear chassis structure with no more than a 9% cost premium.
- Address the technology gaps associated with the use of Advanced High-Strength Steel (AHSS) in chassis structures.

Approach

- Phase 1: Material optimization. Through material substitution and minimal size and shape changes, reduce the mass of the baseline chassis structure by 15%. Build and test prototypes.
- Phase 2: Design optimization. Through a clean-sheet redesign, obtain a minimum mass reduction of 25% with no more than a 9% cost premium.
- Phase 3: Communications. Transfer the technology developed in the project to Auto/Steel Partnership (A/SP) member companies and Tier 1 chassis structure designers.

Accomplishments

- Reduced the mass of the baseline chassis structure by 28% while maintaining cost parity (Reference 1).
- Identified and addressed five technology gaps, which hinder the use of AHSS in chassis structures: Availability, Forming, Welding, Corrosion Resistance and Fatigue Resistance (Reference 2).
- Published *Gas Metal Arc Welding (GMAW) Weld Design Guidelines for Chassis Structures* (Reference 3).

- Established corrosion protection methods for AHSS < 2.0 mm in thickness (Reference 4).
- Developed a fatigue simulation method that may be used to predict the fatigue life of chassis structures (Reference 5).
- Determined that a 20% reduction in gross vehicle weight results in an 8% mass reduction of a rear chassis structure.

Future Direction

Transfer the technology through road shows to A/SP member companies and Tier 1 suppliers.

Introduction

A typical vehicle has about one-third of its weight in the body, one-third in the chassis and one-third in the powertrain. Considerable work has been done to reduce the weight of the body through the application of AHSS. A/SP recognized that a similar effort should be undertaken on the chassis. Thus, it implemented the Lightweight Rear Chassis Structure Project in order to reduce the mass of chassis structures through the use of AHSS, the use of new chassis architecture and the use of new manufacturing technology. A/SP's Lightweight Chassis Structures Project Team was assigned this activity.

The Team selected the rear chassis structure in a donor vehicle as the baseline for the project (Figures 1 and 2).

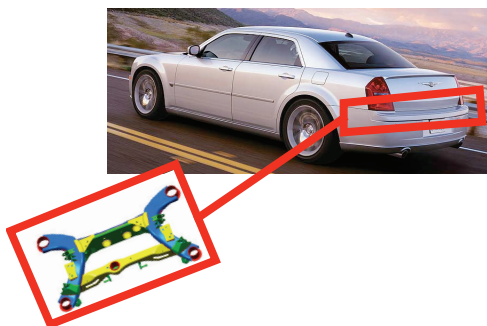


Figure 1. Donor vehicle and baseline structure

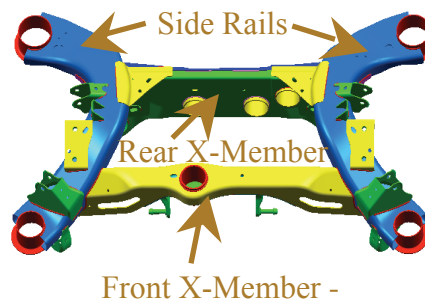


Figure 2. Baseline structure detail

Phase 1: Material Optimization

The OEM of the donor vehicle provided Computer-Aided Drafting (CAD) and Finite Element (FE) models for the baseline and four load cases for the baseline. Altair Engineering was retained to identify areas where AHSS could be substituted for the material in the baseline in order to reduce the mass of the baseline.

Ten prototypes were fabricated using DP590 and TRIP780 steels (Figure 3) in order to address the technology gaps associated with the use of AHSS in chassis structures. The prototypes have a mass of 21.74kg compared to the 25.81kg mass of the baseline. Thus, a mass reduction of 15.8% was achieved.



Figure 3. Phase 1 prototype

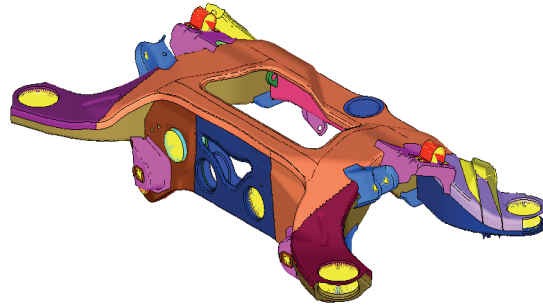


Figure 4. Phase 2 Final Design

Phase 1 Technology Gap Analysis Summary

Five technology gaps that hinder the use of AHSS in chassis structures were identified. Through the implementation of sub-projects, a major result from this project is the successful resolution of the identified technology gaps as discussed below.

Availability of AHSS

The Team concluded that the websites of A/SP steel member companies should be consulted for information on the global availability of AHSS and typical properties for AHSS.

Forming of AHSS

The Team concluded that globally available AHSS grades may be formed into satisfactory chassis structure parts.

Welding of AHSS

The Team collaborated with A/SP's Joining Team to develop a *GMAW Weld Design Guideline for Chassis Structures*.

Corrosion Resistance

The Team concluded that E-Coat and galvanized sheet steel can be used to protect AHSS parts less than 2.0 mm in thickness. Alternately, the entire chassis structure can be hot dip galvanized after fabrication using the Electropoli process.

Fatigue Resistance

The Team concluded that the FE-Safe and the Verity module may be used to predict the fatigue life of chassis structures.

Phase 2: Design Optimization

Martinrea International developed a conceptual Phase 2 design, which Altair Engineering optimized (Figure 4). The Final Design maintains the performance requirements of the baseline and can replace the baseline chassis structure without any major assembly or packaging issues. By utilizing a new architecture, AHSS, laser welded blanks and optimization techniques, the Team was able to create a chassis structure 28% lighter than the baseline (18.59kg compared to 25.81kg). Through the use of the Massachusetts Institute of Technology (MIT) cost model (Reference 1, Section 6.0), the Team determined that the Final Design has cost parity with the baseline.

Future Work

The successful use of AHSS in chassis structures revolves around the design and location of arc welds as outlined in Reference 3. HAZ softening, which depends on steel chemistry, is more pronounced in higher strength steels. This softening reduces joint efficiency and must be taken into account when designing a chassis structure. However, the use of AHSS in all arc welded structures, including chassis structures, would be enhanced if the softening issue is overcome, perhaps by new steel making technology.

Conclusions

The technology gaps that hinder the use of AHSS to achieve mass reduction in chassis structures have been addressed. The Team has demonstrated that the mass of chassis structures can be reduced by at least 25% by using AHSS and advanced manufacturing and design methods.

Normally, it takes from 2-3 years for new automotive innovations to reach production. Already, automotive chassis structures that incorporate AHSS have reached production. A significant increase in the use of AHSS to reduce the mass of chassis structures is predicted.

References

1. ASP 601 Lightweight Rear Chassis Project – *Phase 2 Final Report*; August 31, 2009; www.a-sp.org.
2. ASP 601 Lightweight Rear Chassis Project – *Phase 1 Final Report*; August 19, 2009; www.a-sp.org.
3. A/SP, *GMAW Weld Design Guidelines for Chassis Structures*; November 16, 2007; www.a-sp.org.
4. ASP 601 Lightweight Rear Chassis Project – *Corrosion Protection for Thin Chassis Structure Members*; August 19, 2009; www.a-sp.org.
5. ASP 601 Lightweight Rear Chassis Project – *As-Built Models and Development of Fatigue Analysis*; February 24, 2009; www.a-sp.org.

I. Characterization of Thermo-Mechanical Behaviors of Advanced High- Strength Steels (AHSS): Formability, Weldability and Performance Evaluations of AHSS Parts for Automotive Structures

Principal Investigator: Xin Sun
Pacific Northwest National Laboratory
Richland, WA 99352
(509) 372-6489; e-mail: xin.sun@pnl.gov

Technology Area Development Manager: William Joost
(202)287-6020; e-mail: william.joost@ee.doe.gov

Field Technical Manager: Mark T. Smith
(509)375-4478; e-mail: mark.smith@pnl.gov

Industry Consultants: Ford, General Motors, Chrysler, Auto/Steel Partnership

Contractor: Pacific Northwest National Laboratory
Contract No.: DE-AC05-76RL01830

Objective

- Investigate the formability of advanced high-strength steels (AHSS) with emphases on loading temperature, loading paths, and secondary deformation effects on part residual strength and microstructure.
- Develop a fundamental understanding of the transformation kinetics of AHSS steels by analyzing the crystallographic and morphological features of the phase transformations subject to different thermal and mechanical loading paths from forming and welding.
- Provide performance data and constitutive models for formed AHSS parts.
- Investigate the weldability of AHSS under various welding processes and parameter conditions applicable to auto production environment.
- Generate weld performance data including static strength, formability, impact strength, and fatigue life as a function of welding processes and parameters.
- Investigate welding techniques for improved AHSS weld performance and benchmark the performance against the current welding practices for roll- and hydro-formed AHSS frame and underbody structure applications.
- Develop design guidelines on AHSS to assist rapid structure design and prototyping.

Approach

- Investigate the formability and weldability of AHSS. This task includes forming under complex loading paths (uniaxial and biaxial) and quantification of formability and weldability for various grades of AHSS based on their chemistries and corresponding thermal-mechanical processes.

- Investigate the interdependency of manufacturing processes which includes both the weldability of a formed part and the formability of a welded part.
- Develop a transformation kinetics model and macroscopic constitutive relationships for AHSS (dual phase [DP], transformation-induced plasticity [TRIP] and complex phase [CP]).
- Systematically evaluate the effects of various welding processes and process parameters on microstructure and weld property. Welding processes include gas metal arc, laser, hybrid laser-arc, and resistance spot. Metallurgical and process models will be used to analyze the microstructure evolution. The properties will be measured as a function of geometry, composition, process, and process parameters. A performance evaluation procedure will be developed that allows for quantifying the performance improvement, weight, and cost savings associated with the use of AHSS.
- Evaluate the structural performance of formed and welded parts made of AHSS. This task will provide automotive design engineers with accurate material performance data for design verification of AHSS structural parts.

Milestones, Metrics, and Accomplishments

- Final report on modeling and characterization of thermal mechanical properties of AHSS. (Completed September 2009). A final report documenting project work on modeling of the effects of thermal treatments and deformation histories on the mechanical properties of AHSS was completed and provided to industry participants.
- Identified a new failure mechanism for DP steels that is different from the conventional ductile failure mechanism.
- Defined an approximate range of martensite volume fraction in DP steels where the new failure mechanism can apply.
- Completed examining the effects of austenite stability and various material parameters on the overall behaviors of TRIP steels.
- Completed the micromechanics-based fracture toughness modeling of TRIP800.
- Completed evaluation of the stacking fault energy (SFE) of a twinning induced plasticity (TWIP) steel with consideration of influence of aluminum.
- Completed quantification of the evolution of the micro-twin volume fraction during deformation of TWIP steels.
- Developed a phenomenological constitutive model for TWIP steels.
- Identified nano-size precipitates (Mo and Ti) along the grain boundary and inside the grains from preliminary transmission electron microscope (TEM) analyses of nano-size precipitates strengthening steels (NPSS).
- Completed electron backscatter diffraction (EBSD) experiments for identification of strengthening mechanism for NPSS.

Future Direction

- This project has been completed.

Introduction

This project is a collaborative effort between the U.S. Department of Energy, Pacific Northwest National Laboratory (PNNL), Oak Ridge National Laboratory, and the U.S. Automotive Materials Partnership of the U.S. Council for Automotive Research. The work began in October 2005.

Because of their excellent strength and formability combinations, advanced high-strength steels (AHSS) are being used in vehicle body structures to reduce vehicle weight and improve crash performance. Currently, technical barriers hindering wider applications of AHSS in the domestic auto industry are as follows:

- The fundamental behaviors of AHSS parts subject to different thermal and mechanical loading paths (forming and welding) are not fully understood and quantified.
- The constitutive behaviors for the formed parts are not available to computer-aided engineers for rapid prototyping.
- Welding induced complex microstructures and the effects of different welding processes and welding parameters on weld performance are not well understood.

In order to address these issues, PNNL's role in this project includes investigating the formability of AHSS with emphases on loading temperature, loading paths, and secondary deformation effects on part residual strength and microstructure. The project also develops a fundamental understanding of the transformation kinetics of AHSS steels by analyzing the crystallographic and morphological features of the phase transformations subject to different thermal and mechanical loading paths from forming. The goal is to provide automotive design engineers with accurate material performance data and constitutive models for design evaluations and verification of AHSS structural parts.

Approach

Key Factors Influencing Ductile Fractures of DP Steels

In this study, we examine the key factors influencing the ductile failure of various grades of dual phase (DP) steels using the microstructure-based modeling approach. For this purpose, various microstructure-based finite element models are generated based on the actual microstructures of DP steels with different martensite volume fractions. **Figure 1** shows an example of one of the various finite element models used in this study.

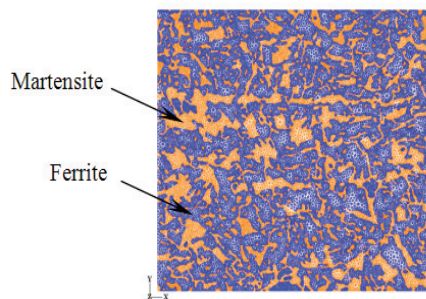


Figure 1. Finite element model based on the microstructure of a DP steel. Volume fraction martensite ($V_{f,M}$) in this model is 38%.

The adopted mechanical properties for the ferrite and martensite phases are based on the results in Sun et al. (2009). Next, we investigated the influence of ferrite ductility as well as the voids in the ferrite phase on the overall ductility of DP steels. **Figure 2** compares the ultimate ductility of all the representative volume elements (RVEs) as a function of the martensite volume fraction for different input strain ranges of the ferrite phase (ϵ_f). The results in Figure 2 indicate that failure of DP steels with the martensite volume fraction between 15% and 40% appears to be dominated by a different failure mechanism, rather than the conventional ductile failure, since

the ductility of DP steels shows no dependence on the ductility of the ferrite phase in this region except for the case that the input strain range of ferrite is only 30%. Figures 3 and 4, respectively, show the engineering stress-strain curves and failure modes of selected RVEs with and without voids. Based on these figures, it seems that voids do not have a noticeable influence on the ultimate ductility and/or failure modes of DP steels when the martensite volume fraction in DP steels is larger than about 15%.

From these observations, there seems to be a range of martensite volume fraction, approximately between 15% and 40%, where the overall ductility of DP steels shows negligible dependence on the ductility of the ferrite phase and the existence of micro voids in the microstructure. In this range of martensite volume fraction, the ductile failure of DP steels is governed primarily by the instability induced by the phase inhomogeneity between the hard and the soft phases (Figure 2). In other words, these results suggest that the growth and coalescence of the conventional micro voids is no longer the key failure driving mechanism for these DP steels. For example, the fracture surface of a DP800 in Figure 5 shows the ductile failure in the ferrite matrix (dimples) combined with the brittle, flat failure surfaces cutting through the martensite grains.

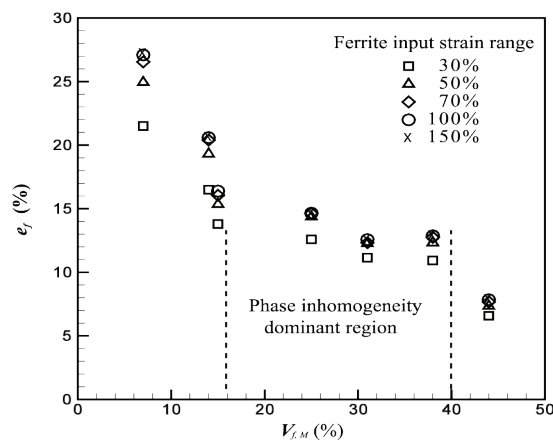


Figure 2. Ultimate ductility of DP steels as function of martensite volume fraction for different input strain ranges of ferrite.

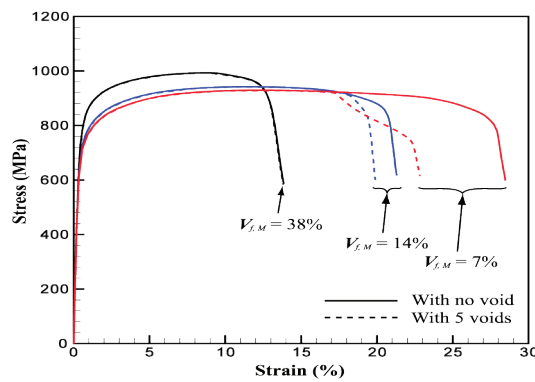


Figure 3. Engineering stress-strain curves based on three different RVEs with and without voids.

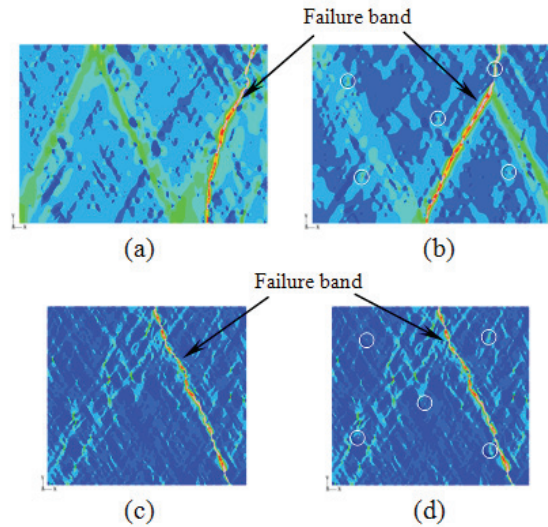


Figure 4. Failure modes of RVEs: (a) DP ($V_{f,M}=7\%$) w/o voids, (b) DP ($V_{f,M}=7\%$) with 5 voids, (c) DP ($V_{f,M}=38\%$) w/o voids and (d) DP ($V_{f,M}=38\%$) with 5 voids. Circles represent the void positions.

Figure 6 also validates our finding of the existence of a phase inhomogeneity-dominant region. In this figure, as the martensite volume fractions increase, fewer (very little) micro voids are observed near the fracture surface. This means that, for the DP steels with higher martensite volume fractions, the microstructure-level phase inhomogeneity can serve as the initial seeds for strain localization in the microstructure leading to final ductile fracture. The results suggest that the microstructure-based modeling methodology adopted in this study can be applied to DP steels within this phase inhomogeneity-dominant region to tailor DP steel design for its intended purpose and desired properties.

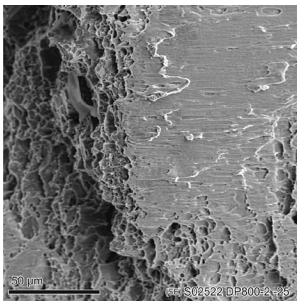


Figure 5. Failure Surface of DP800 showing combined ductile and brittle failure in ferrite and martensite.

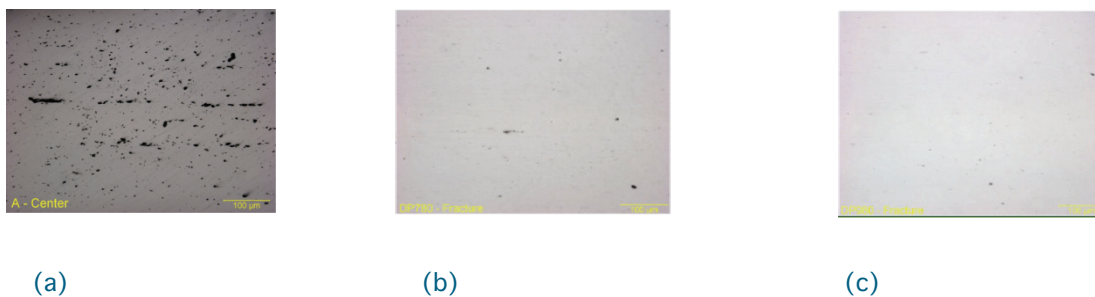


Figure 6. Microscopic pictures of the cross sections near the fracture surface. (a) DP600, (b) DP780 and (c) DP980 (Yang and Kim, 2008).

Effects of Austenite Stability and Various Material Parameters on Behaviors of TRIP Steels

In transformation-induced plasticity (TRIP) steels, the stability (i.e., resistance to phase transformation) of retained austenite is generally influenced by different parameters such as carbon content, grain size, morphology, nature of surrounding matrix, etc.. Among those parameters, the carbon content in the retained austenite phase can be relatively easily controlled by changing the bainite transformation time in the continuous annealing process. In this sense, assuming that austenite stability is governed only by the carbon content and all the austenite phase in a TRIP steel has the same carbon content, we can examine the effects of austenite stability on the behaviors of TRIP steels based on our microstructure-based modeling method, which is detailed in Choi et al. (2009).

Figure 7 shows a microstructure-based finite element model developed for investigating the austenite stability effect. The material properties of the constituent phases and other material parameters are based on the work of Choi et al. (2009). The austenite stability is varied by changing the magnitudes of critical value Π_c for the transformation yield function adopted in Choi et al. (2009)

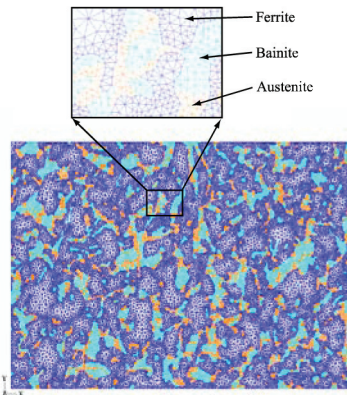


Figure 7. A microstructure-based finite element model used for the RVE of a TRIP800.

Figures 8(a) and 8(b), respectively, show the macroscopic engineering stress-strain curves and the volume fraction of the retained austenite as functions of the macroscopic equivalent plastic strains of the RVE for three different Π_c .

Figure 8(b) indicates that the different austenite stability induces quite different volume fraction evolutions of the retained austenite phase, leading to different macroscopic stress-strain curves, especially in initial hardening and ductility (Figure 8(a)). In summary, the delayed martensitic transformation from higher austenite stability is helpful to increase ductility, and this improvement in ductility can result in better formability, as shown in the pseudo-forming limit diagram predicted based on different loading conditions to the RVE (Figure 9).

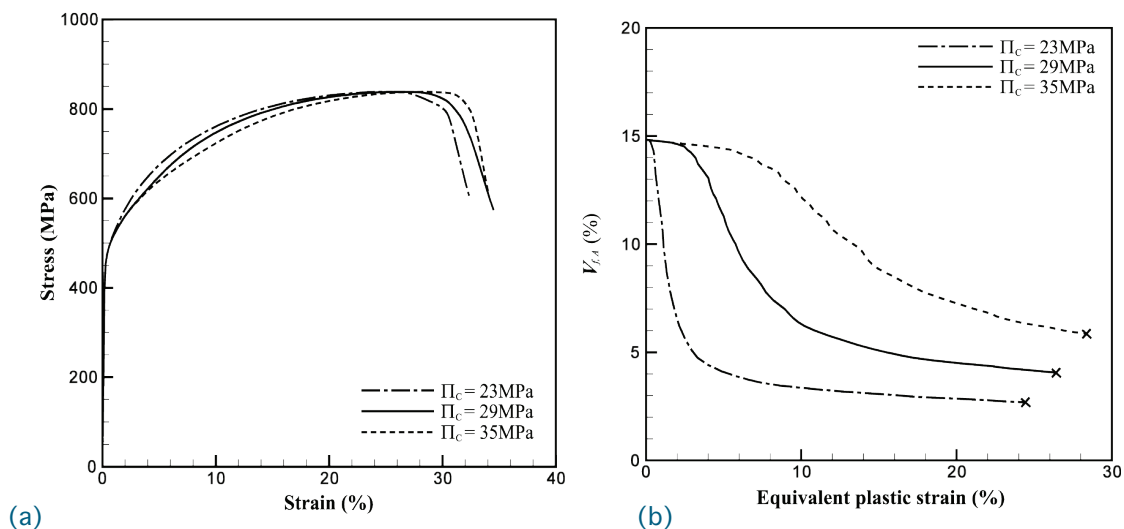


Figure 8. (a) Macroscopic responses of the RVE under uniaxial tension with different stabilities of austenite phase and (b) volume fractions of retained austenite as functions of the macroscopic equivalent plastic strain of the RVE under different loading conditions for different austenite stabilities.

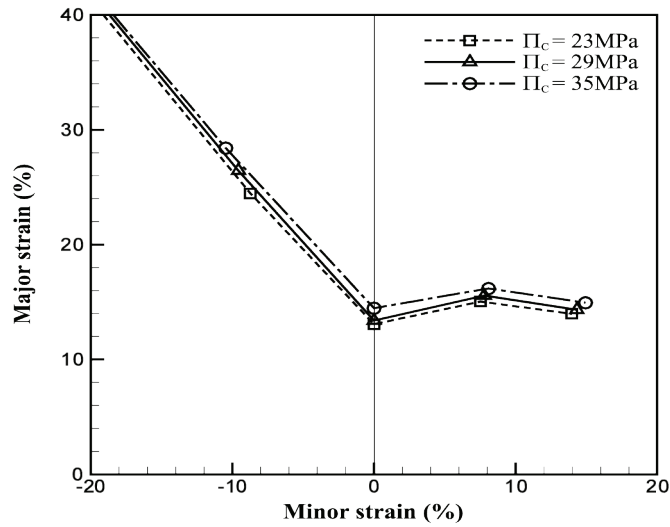


Figure 9. Pseudo-forming limit diagram based on the RVE for different austenite stabilities.

In this study, the effects of several other material parameters on the overall behavior of TRIP steels are also examined for development of high-performance TRIP steels. For this purpose, several RVEs with different retained austenite volume fractions are generated, and in these RVEs, only ferrite and retained austenite phases are assumed to initially exist. Some key results are presented here based on the RVEs with $V_{f,A}^0 = 31$ and 38%. Figure 10 indicates that either the increase of the austenite volume fraction ($V_{f,A}^0 = 38\%$) or the strengthening of the ferrite phase with the increased austenite volume fraction ($V_{f,A}^0 = 38\%$, Case 1) can only increase the strength of TRIP steels, resulting in a detrimental decrease of ductility. To improve ductility, both the austenite strength and stability need to be increased for gradual and delayed martensitic transformation ($V_{f,A}^0 = 38\%$, Case 2). Since a lower strength disparity between phases may be helpful to improve ductility, lower strength of the newly formed martensite phase also seems to be beneficial for better performance of TRIP steels ($V_{f,A}^0 = 38\%$, Case3). Note that the trend of the stress-strain curve in this case ($V_{f,A}^0 = 38\%$, Case 3) is similar to those of new high-performance TRIP steels in Merwin (2007).

In summary, several different material parameters must be combined and adjusted together in a way to increase the ductility as well as the ultimate tensile strength.

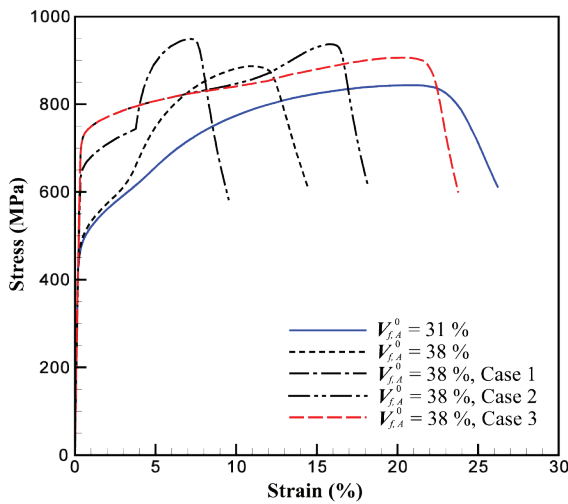


Figure 10. Effects of different parameters on engineering stress-strain curves.

Development of Phenomenological Constitutive Model for TWIP Steels

Recently, twinning induced plasticity (TWIP) steels have gained much attention as a candidate for automotive applications for their excellent combination of high strength and good ductility compared to second-generation AHSS. These exceptional characteristics of TWIP steels are achieved by the complex deformation mechanism involving interactions between gliding, mechanical twinning, and martensitic transformation.

In general, twinning, the favorable deformation mode, occurs in the materials with low stacking fault energy (SFE). SFE depends on the material chemical composition (mainly C and Mn contents) and the temperature. Note that high temperature facilitates gliding through thermal activation and inhibits twinning by increasing the SFE. Table 1 lists the chemical composition of the TWIP steel in this study.

Empirical models were proposed in the past to evaluate SFE in Fe–Mn–C austenitic alloys under different temperatures (Allain et al. 2004). As the TWIP steel here includes a large amount of Al, the influence of Al was additionally considered in evaluating the SFE of the TWIP steel. For the material studied here, Fe-17.5%wt. Mn-0.56%wt. C, the SFE values versus temperature are plotted in Figure 11. Three stages can be distinguished for the SFE. When the SFE value is below 12 mega-Joules/ m², (mJ/m²), martensitic transformation is favored. Twinning and gliding mechanisms are predominant when the SFE is higher than 12 mJ/m² but less than 23 mJ/m² while gliding is observed when the SFE is higher than 23 mJ/m².

Table 1. Chemical composition of the TWIP steel in this study.

C	Mn	Si	Al	P	S	Nb	V	Fe
0.56	17.5	0.24	1.39	0.023	0.0007	0.029	0.1	Balance

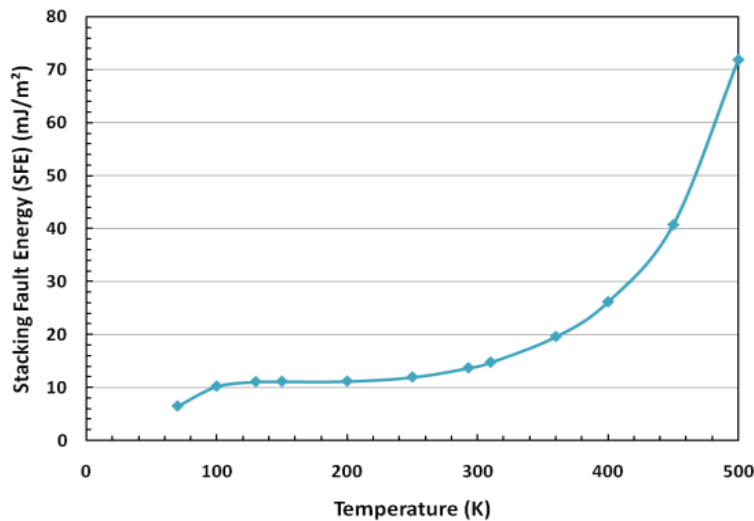


Figure 11. Calculated SFE for the TWIP steel.

Tensile tests were also conducted on this TWIP steel. Figure 12 represents scanning electron microscopy (SEM) pictures of the deformed specimen at different strain levels. We can observe more mechanical twins in the microstructure deformed at 20%. The TWIP steel here has relatively fine grains ($\approx 10\mu\text{m}$). Twins, resulting from the tensile test, can also be observed within these

fine grains. Figure 13(a) shows the stress-strain curve obtained from the tensile tests. We can see the work hardening of the material due to mechanical twinning and also the excellent ductility achieved in this case (55%).

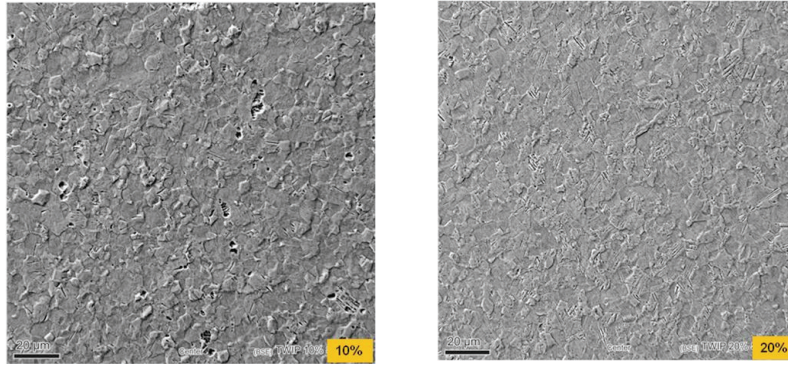


Figure 12. SEM pictures for the TWIP steel Fe-17.5 wt.% Mn-0.56 wt.% C deformed at different strain levels.

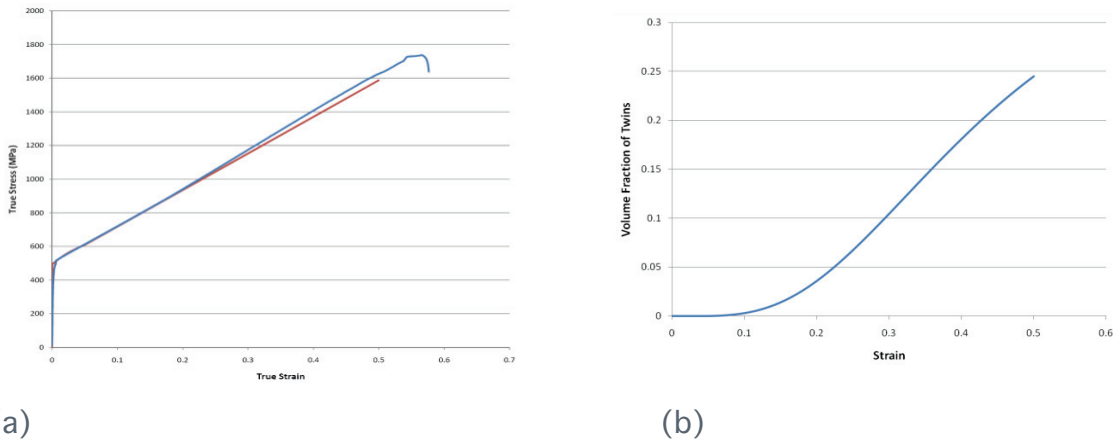


Figure 13. (a) Comparison of the stress-strain curves from experiment and the model in the case of tensile loading (b) volume fraction of twins estimated by the model.

A phenomenological constitutive model for TWIP steels is developed in this study. In our model, an energetic criterion is considered to describe the twinning kinetics. A thermo-dynamic driving force F must overcome a critical force F_c to allow twinning to occur in the model. This driving force F is expressed as

$$F = \tau \cdot \gamma_{tw} - \beta T \quad (1)$$

Here, τ is the shear stress, γ_{tw} is the twinning strain, β is a numerical constant, and T is the temperature. The critical force, F_c , is related to the SFE, and the volume fraction of the previously formed twins, and is expressed as

$$F_c = \eta \Gamma - h(1 - \exp(-\phi \dot{\epsilon}^p))^f - \chi \ln(1 - f) \quad (2)$$

Here, Γ is the SFE, $\dot{\epsilon}^p$ is the equivalent plastic strain rate, f is the twin volume fraction, and η , h , ϕ , χ are material constants to be identified. The details of the model are not explained in this report. In summary, this phenomenological model is based on the physics behind the twinning and gliding mechanisms. It contains internal variables (dislocation density, volume fraction of twins) that contain information on the microstructure. The advantage of such a model is that it is simple to implement in a finite element code as a subroutine and hence can be used to

simulate the forming process of TWIP steel sheets. The physical assumptions used to formulate the constitutive equations are limited to the case of face-centered cubic (FCC) austenitic steels with TWIP effect: (1) the freshly formed mechanical twins are effective obstacles to dislocation motion, (2) twinning occurs when a thermodynamic force reaches a critical value (function of the SFE), and (3) twins nucleation causes an additional “twinning” shear strain.

The simulation results of this model are in good agreement with the experimental data obtained from the tensile test performed on the Fe–17.5 wt.% Mn–0.56 wt.% C steel. The model is able to capture the excellent work hardening of TWIP steel by considering the mechanical twins as additional obstacles to the dislocations motion. Figure 13(a) represents a stress-strain comparison between the model and the experiment while Figure 13(b) represents the volume fraction of twins from the model.

Characterization of microstructure and mechanical properties of NPSS

Nano-size precipitates strengthening steels (NPSS) are single-phase ferritic steels hardened by precipitates refined to the size of several nanometers. For their excellent combination of mechanical properties, NPSS are also under consideration for use as various vehicle components in the automotive industry. In this section, preliminary studies on NPSS are discussed to explore possible directions for the development of third-generation AHSS.

Figure 14 show the engineering stress-strain curves of the NPSS. The examined NPSS demonstrates good combinations of ultimate tensile strength (UTS) and ductility due to the presence of nano-precipitates. Note here that thermal stability is also an important aspect required in nano-precipitates because thermally unstable precipitates are prone to coarsening and eventually reducing the strength of the steels. Shimizu et al. (2004) developed a technique to extremely refine the precipitates as well as improve the thermal stability of the refined precipitates by adding a proper amount of Ti and Mo to 0.04C–1.3Mn base steel composition. Table 2 shows the chemical compositions (in weight percents) of the examined NPSS in this study. It indicates that the NPSS examined here can be similar to that shown in Shimizu et al. (2004).

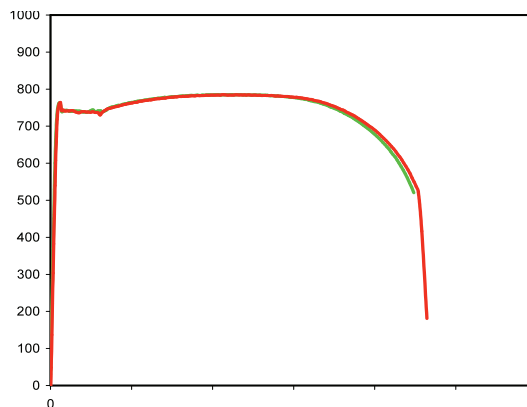


Figure 14. Stress-strain curves for NPSS.

Table 2. Chemical composition of NPSS.

C	Mn	P	S	Si	Cr	Ni
0.04	1.25	0.012	0.001	0.06	0.03	<0.01

Mo	Cu	Ti	V	Al	Co	Nb
0.18	0.01	0.08	0.015	0.048	0.006	0.011

For preliminary transmission electron microscopy (TEM) studies, a few samples were prepared with as-received NPSS. **Figure 15(a)** shows a TEM image of the grain size and shapes of the as-received NPSS. As shown in the figure, the grain size of the NPSS is approximately $1\mu\text{m}$. Here, the different colors of the grains are possibly due to the different grain orientations with respect to the direction of electron beam. **Figures 15(b) and 15(c)** show the TEM images of the precipitates found in the NPSS. As shown in these figures, only Mo precipitates could be found along the grain boundaries, whereas Ti precipitates could be found inside grains. Their sizes are approximately 10~20 nm. It was expected that well distributed nanometer size precipitates (~2-3nm) would be found inside the grains from TEM analysis as observed in Shimizu et al. (2004). However, those small precipitates were not identified in this preliminary test. To characterize the atomic-scale structure of the NPSS of interest, an X-ray diffraction experiment is considered for use. Molecular dynamics simulation is also considered for NPSS to obtain a more fundamental understanding of the nano-precipitates strengthening mechanisms and the influence of size and the inter-particle spacing of the precipitates on the strengthening effect.

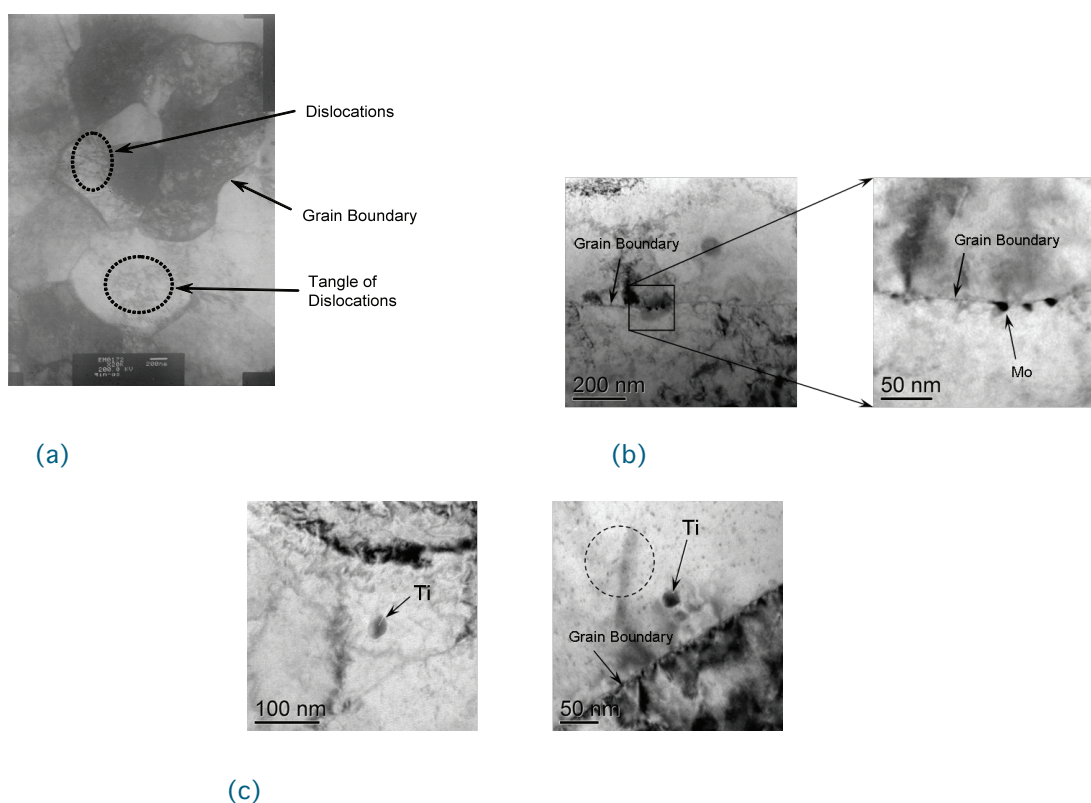


Figure 15. A TEM images of as-received NPSS.

Conclusions and Future Directions

This report summaries our technical accomplishments for FY09. This is the last year of our 4-year study on characterization of thermo-mechanical behaviors of advanced high-strength steels. Throughout the course of this project, we have investigated the formability and weldability of current generation AHSS under complex loading paths. We have developed a micro-structure based model framework and transformation kinetics model to simulate the constitutive relationships for 1st generation AHSS (dual phase [DP], transformation-induced plasticity [TRIP] and complex phase [CP]) under different loading conditions. These models are ready to be implemented in automotive forming and welding simulations to better quantify the effects of advanced high strength steels in the as-formed and as-welded body structures.

We also found that, for higher grades 1st generation AHSS (i.e., DP980, TRIP980), ductile failure is governed primarily by the deformation instability induced by the phase inhomogeneity between the hard and the soft phases. In other words, these results suggest that the conventional microvoids growth and coalescence is no longer the key failure driving mechanism for these steels.

In FY09, we have also assisted DOE in crafting a ‘Coherent Research Plan for the Development of 3rd Generation Advanced High Strength Steels’. The preliminary work we performed in FY09 on TWIP steel and nano-precipitate steel illustrate that multiple chemistry compositions and processing routes can be used in achieving the performance goals of the 3rd generation AHSS. Future work therefore lies in refining and improving these various approaches in making cost-effective 3rd generation advanced high strength steels for automotive applications.

Presentations/Publications/Patents

Choi KS, Liu WN, Sun X, Khaleel MA, Ren Y, and Wang YD. 2008. “Advanced Micromechanical Model for TRIP Steels with Application of In-Situ High-Energy X-ray Diffraction Method.” *Metallurgical and Materials Transactions A* 39:3089-3096.

Choi KS, Liu WN, Sun X, and Khaleel MA. 2009. “Influence of Martensite Mechanical Properties on Failure Mode and Ductility of Dual Phase Steels.” *Metallurgical and Materials Transactions A* 40:796-809.

Choi KS, Liu WN, Sun X, and Khaleel MA. 2009. “Micromechanics-Based Constitutive Modeling of TRIP Steel –Prediction of Ductility and Failure Modes under Different Loading Conditions.” *Acta Materialia* 57:2592-2604.

Choi KS, Soulami A, Liu WN, Sun X, and Khaleel MA. 2009. “Applicability of Micro-mechanics Model Based on Actual Micro-structure for Failure Prediction in DP Steels.” SAE Technical Paper 2009-01-0469. Presented in SAE 2009 World Congress, April 20-23, Detroit, MI.

Soulami A, Choi KS, Liu WN, Sun X, and Khaleel MA. 2009. “Characterization of the Fracture Toughness of TRIP 800 Sheet Steels Using Microstructure-Based Finite Element Analysis.” SAE Technical Paper 2009-01-0800. Presented in SAE 2009 World Congress, April 20-23, Detroit, MI.

Sun X, Choi KS, Liu WN, and Khaleel MA. 2009. “Predicting Failure Modes and Ductility of Dual Phase Steels Using Plastic Strain Localization.” *International Journal of Plasticity* 25: 1888-1909.

Choi KS, Liu WN, Sun X, Khaleel MA, and Fekete JR. 2009. “Influence of Manufacturing Processes and Microstructures on the Performance and Manufacturability of Advanced High Strength Steels (AHSS).” *Transactions of ASME, Journal of Engineering Materials and Technology* 131:#041205.

Soulami A, Choi KS, Liu WN, Sun X, Khaleel MA, Ren Y, and Wang YD. 2009. “Predicting Fracture Toughness of TRIP 800 Using Phase Properties Characterized by In-Situ High Energy X-Ray Diffraction.” Submitted for publication in *Metallurgical and Materials Transactions A*.

Sun X, Choi KS, Soulami A, Liu WN, and Khaleel MA. 2009. “On Key Factors Influencing Ductile Fractures of Dual Phase (DP) Steels.” *Materials Science and Engineering a* 526: 140-149.

Choi KS, Soulami A, Liu WN, Sun X and Khaleel MA. 2009. “Effects of Austenite Stability and Other Material Parameters on the behaviors of TRIP Steels.” In Preparation.

References

- Allain S. 2004. “*Multiscale Thermo-mechanical Characterization and Modeling of Deformation and Work-hardening of Austenitic Steels with High Manganese Content – Application to the TWIP Effect.*” Ph.D Thesis, INPL, France.
- Allain S, Chateau J-P, Bouaziz O, Migot S, and Guelton N. 2004. “Correlations between the Calculated Stacking Fault Energy and the Plasticity Mechanisms in Fe-Mn-C Alloys.” *Materials Science and Engineering A* 387-389:158-162.
- Choi KS, Liu WN, Sun X, and Khaleel MA. 2009. “Micromechanics-Based Constitutive Modeling of TRIP Steel –Prediction of Ductility and Failure Modes under Different Loading Conditions.” *Acta Materialia* 57:2592-2604.
- Merwin MJ. 2007. “Hot- and Cold-Rolled Low-Carbon Manganese TRIP Steels.” *SAE Technical Paper 2007-01-0336*. Society of Automotive Engineers, Warrendale, PA.
- Shimizu T, Funakawa Y, and Kaneko S. 2004. “*High Strength Sheets for Automobile Suspension and Chassis Use –Hogh Strength Hot-Rolled Steel Steel Sheets with Excellent Press Formability and Durability for Critical Safety Parts.*” JFE Technical Report No. 4, November.
- Sun X, Choi KS, Liu WN, and Khaleel MA. 2009. “Predicting Failure Modes and Ductility of Dual Phase Steels Using Plastic Strain Localization.” *International Journal of Plasticity* 25: 1888-1909.
- Yang YP, and Kim HO. 2008. “Shear fracture project update.” *Auto/Steel Partnership Shear Fracture Symposium*, September 10, Southfield, MI.

J. Characterization of Thermomechanical Behavior of Advanced High-Strength Steels (AHSS): Task 2—Weldability and Performance Evaluation of Welded AHSS Parts for Automotive Structures

Principal Investigator: Zhili Feng
Oak Ridge National Laboratory
1 Bethel Valley Road, Oak Ridge, TN 37831
(865) 576-3797; e-mail: fengz@ornl.gov

Participants:
Wan C. Woo, Ken Littrell, and Eliot Specht
Oak Ridge National Laboratory
John Chiang
Ford Motor Company
Min Kuo
ArcelorMittal Steel

Technology Area Development Manager: William Joost
(202) 587-6020; e-mail: william.joost@ee.doe.gov

Field Technical Monitor: C. David Warren
(865) 574-9693; e-mail: warrencd@ornl.gov

Contractor: Oak Ridge National Laboratory (ORNL)
Contract No.: DE-AC05-00OR22725

Objective

- Develop fundamental understanding and predictive capability to quantify the effects of welding and service loading on the structural performance of welded AHSS auto-body parts.
- Investigate welding techniques and practices to improve structural performance of AHSS welded auto-body components.
- Establish design guidelines and computer-aided engineering (CAE) methodology to assist auto-body structure design, optimization and prototyping for vehicle weight reduction and safety enhancement through knowledge-based selection and use of AHSS.

Approach

- Develop fundamental understanding of microstructure phase transformations of AHSS during welding through thermodynamic analysis, advanced microstructure characterization, and in situ neutron and synchrotron phase transformation measurement.
- Develop integrated thermal-mechanical-metallurgical predictive models to predict the microstructure and mechanical property gradients in the weld region that govern the performance of welded AHSS parts.

- Conduct comparative welding experiments on various AHSS to develop the correlations among the joint properties, welding process conditions, and steel chemistry.
- Characterize and rank the factors controlling the weld microstructures and weld joint performance.
- Investigate welding techniques for improved AHSS weld performance, and benchmark them against the current welding practices.
- Generate weld performance data including static strength, impact strength, and fatigue life as a function of welding processes/parameters and steel chemistry.
- Develop design guidelines and CAE methodology for AHSS to assist rapid structure design and prototyping.

Accomplishments

- Identified the fundamental metallurgical mechanisms causing the complex microstructure variations and the heat-affected zone (HAZ) softening phenomenon of current generation AHSS welds.
- Developed an integrated thermal-mechanical-metallurgical welding process model capable of simulating the microstructural changes and the softening in the HAZ of AHSS welds. Initial version of the integrated model has been licensed and transferred to the industry.
- Developed the correlation between the static structural performance and the microstructural changes of AHSS welds. A practical design parameter—joint efficiency—was introduced to quantify the effect of welding on the strength of AHSS welds.
- Revealed the influence of HAZ softening on the impact strength of AHSS joints.
- Demonstrated considerable fatigue life improvement by refining welding conditions.
- Developed a weld fatigue life prediction model relating the fatigue life of a weld joint to weld geometry and local weld properties.
- Applied in situ neutron and synchrotron diffraction experiments to understand the phase changes during welding of AHSS and the stress partitioning among different phases in transformation-induced plasticity (TRIP) steel.
- Developed close interactions with the industry including different Auto/Steel Partnership (A/SP) technical committees and the auto and steel companies to exchange research progress, to collaborate on related research projects, and to transfer and commercialize the technology developed in this project.
- Drafted a coherent R& D plan for the 3rd generation AHSS in support of the Lightweighting Materials Program thrust.

Future Direction

- Continue to investigate key factors controlling weld joint performance under static, fatigue, and impact loading conditions.
- Investigate the structural performance of AHSS weld joints under complex loading conditions (component level behavior).

- Continue to investigate welding techniques and practices to improve weld performance, especially the fatigue life and durability.
- Complete CAE analysis methodology to assist rapid design and prototyping of AHSS structures.
- Support the third generation AHSS initiative, focusing on new steel alloying and design concepts to avoid/minimize welding-induced thermal instability and microscopic deformation behavior of the new steels.

Introduction

This report describes an ORNL-Pacific Northwest National Laboratory (PNNL) collaborative research project on characterization of thermomechanical behavior of AHSS. This joint project aims at developing fundamental understanding and predictive modeling capability to quantify the effects of auto-body manufacturing processes (forming, welding, paint baking, etc.) and in-service conditions on the performance of auto-body structures made of AHSS. ORNL's research (designated as Task 2 in this project) focuses on welding AHSS and the influence of welding parameters on the structural performance of weld joints.

The specific relation of Task 2 to the mission of the DOE Lightweighting Materials program and the needs of the automotive industry for accelerated use of AHSSs for body structure lightweighting has been given in previous annual reports and will not be repeated here.

Task 2 has a technical steering committee with representatives from Chrysler, Ford, General Motors, A/SP technical committees, and steel companies.

We have made considerable progress since the start of the project toward the project goals of obtaining fundamental understanding of microstructural changes and their influence on the structural performance (static, fatigue, and impact) of AHSS welds and developing welding techniques/methods to enable the use AHSS in auto-body structures. The followings are the highlights and key findings from the previous years work.

- The static tensile strength of the lap weld joint made by the gas metal arc welding process (GMAW) increases as the base metal steel strength increases. However, the joint efficiency (the ratio of weld strength to the base metal strength) is influenced by the HAZ softening in the AHSS weld. Ultra-AHSS such as martensitic and boron steels have the most noticeable HAZ softening and thereby lower joint efficiency. The lower grade AHSS without HAZ softening exhibit high joint efficiency. Nevertheless, AHSS welds typically exhibit considerably higher absolute static strength than mild steel welds.
- Similar to the static tensile strength, the HAZ softening can have profound influence to the impact tensile strength, depending on the strength and chemistry of the AHSS.
- The HAZ softening phenomenon is fundamentally associated by the thermal instability of the hardened phases (such as martensite or bainite) subjected to the welding heat, the existence of the intercritical temperature range in Fe-C alloy, and the allotropic phase transformation mechanism employed in the current AHSS steelmaking practice.
- Microstructural changes in the weld region and the degree of HAZ softening have been quantified in an integrated thermal-mechanical-metallurgical weld process model. The initial version of this model has been licensed and transferred to industry collaborators of the project.
- The HAZ softening does not appear to be a major factor affecting the fatigue life of GMAW joints. However, AHSS welds do not exhibit improved fatigue life over the mild steel welds

when welded with practices commonly used for mild steels. New and/or improved welding practices specific for weld fatigue life enhancement are required to further realize the potential of AHSS for “down-gauging” (and thus “lightweighting”).

- It is feasible to improve the weld fatigue life of AHSS by manipulating welding procedures. This project has demonstrated that, by adjusting the welding parameters (within the process window acceptable to the auto industry), the weld geometry profile can be improved to reduce the stress concentration at the fatigue crack initiation site. This has resulted in drastic improvement of weld fatigue life, especially at the high-cycle fatigue regime that is mostly relevant to the durability of vehicles.
- A predictive model for fatigue life of AHSS gas metal arc welds has been developed. This model takes into account the effects of weld geometry and local mechanical properties in the weld toe and root regions. Overall, the model reasonably predicts the experimentally observed influences of steel grade (local mechanical property in the weld and HAZ) and the weld geometry for the steel grades investigated. With a few exceptions (e.g., hardened boron steel under high-cycle fatigue), the experiment data fall within a narrow band bounded by the 3x and 1/3x lines of the predicted data in the figure. The discrepancies between the model prediction and the testing results are on the same order as the scatter of the testing data.

The R&D efforts in FY 2009 focused on the following major activities.

In Situ Phase Transformation Study Using High-Energy X-Ray Synchrotron Source

The HAZ softening has profound influence on the static and dynamic performance of welded AHSS structures. Our study has shown that HAZ softening is fundamentally associated in the microstructural changes in the intercritical temperature range (i.e., between the A_1 and A_3 temperatures of the Fe-C phase diagram). However, our knowledge about the *non-equilibrium* phase changes in this temperature range under the fast heating and cooling conditions associated with welding is very limited. In this task, the kinetics (the start and finish temperature of phase transformation and the volume fraction of phases as a function of time and heating rates) of the non-equilibrium phase transformation processes was investigated using the high-energy X-ray synchrotron source at the Advanced Photon Source of Argonne National Laboratory.

A miniature programmable electric resistance-heating device was used to rapidly heat and cool the steel specimens to simulate the welding thermal cycles in the in-situ synchrotron experiment. Four types of steels (boron steel, DP980, TRIP700, and DR210) were studied. The experimental principles and setup are shown in Figure 1.

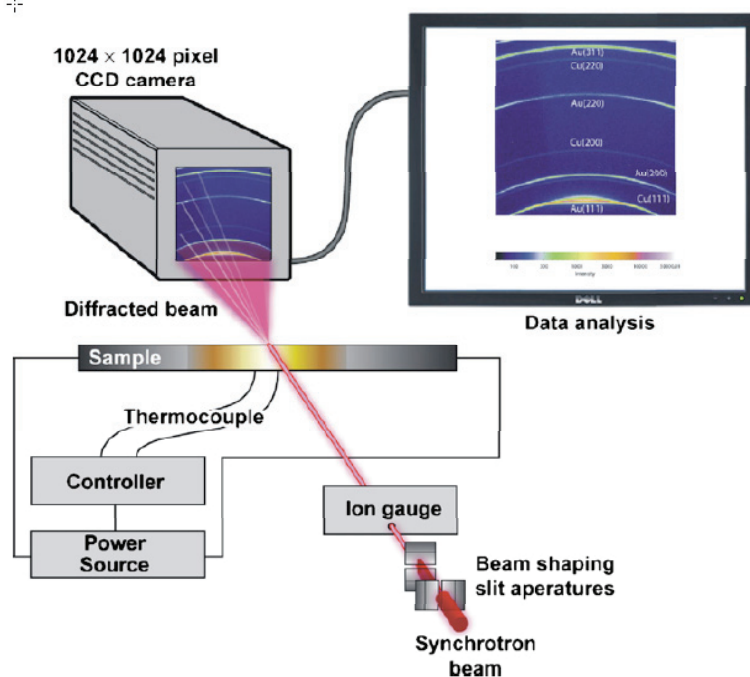
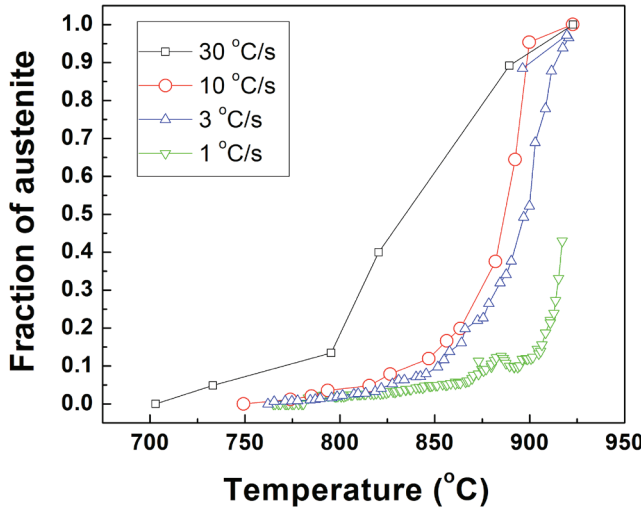


Figure 1. Synchrotron X-ray diffraction experiment for in-situ study of phase transformation kinetics of AHSS (after Elmer et al, 2007).

The in-situ synchrotron diffraction measurement focused on the on-heating phase transformation kinetics in the intercritical temperature range and its influence on the on-cooling phase transformation.

The kinetics of solid-state phase transformation was obtained from the diffraction peak analysis. Our study has revealed a noticeable dependency of phase transformation kinetics on the heating rate. In addition, aluminum-bearing TRIP steel showed very different phase transformation behavior than the other two AHSS.

Of particular importance is the discovery of the unusual on-heating austenite formation behavior. As the heating rate increases, the formation of the austenite during heating shifts to lower temperatures – the T_{A1} temperature (austenite formation starting temperature) decreases and the volume fraction of the austenite phase increases at a given temperature. Such behavior is illustrated in Figure 2 for DR210 steel. DP980 and the boron steel also exhibit the same behavior.



As the heating rate increases, the formation of the austenite during heating shifts to lower temperatures – the T_{A1} temperature (austenite formation starting temperature) decreases and the volume fraction of the austenite phase increases at a given temperature. Such behavior is illustrated in Figure 2 for DR210 steel. DP980 and the boron steel also exhibit the same behavior.

At first glance, the above synchrotron experiment results appeared to be counterintuitive to the generally accepted view of the formation of austenite. As a nucleation and growth process involving diffusion of carbon and other alloying elements, the formation of austenite on heating is expected to shift to higher temperatures as the heating rate increases.

Figure 2. Volume fraction of austenite formed on heating as function of heating rate. DR210 steel.

Further examination of the synchrotron diffraction data reveals that the lattice spacing of the newly formed austenite phase actually decreases in the intercritical temperature range before increases again during heating, as shown in Figure 3. This suggests that the partition of alloying elements such as carbon in the original microstructure of AHSS could play an important role during the *non-equilibrium* austenite formation process, as observed in the synchrotron experiments.

It should be noted that our above findings are preliminary. Additional confirmative experiments are necessary, as well as detailed microstructure analysis and study, to shed light on our discovery as it is expected to have far reaching impacts to the uses of the current generation AHSS and the development of future AHSS.

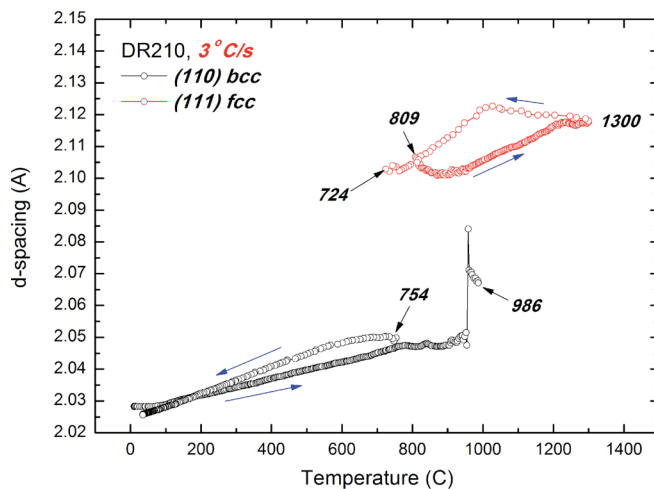


Figure 3. D-spacing change of DR210 steel during heating and cooling cycle. 3 °C/s. fcc is the austenite phase, and bcc the ferrite phase.

Thermal Stability of the Nano-Precipitate Strengthened Steels

The 3rd Generation AHSS Initiative for Automotive Applications provides a window of opportunity to explore new approaches in steel making. One such new technology is nano-precipitate strengthened steels (NPSS). NPSS achieves high strength (higher than 1000MPa) while maintain high ductility (20-40% elongation) by utilizing nano-sized precipitates in a single-phase matrix. Achieving the superior strength and ductility combination in NPSS requires the uniform distribution of nano-sized carbides, nitrides, or other types of nano-sized intermetallic particles. An important question concerning the NPSS is the thermal stability of these nano-sized strengthening precipitates - they must have sufficient stability during manufacturing and assembling processes especially during welding to eliminate or minimize the microstructure and property degradation.

An initial study of the thermal stability of the nano-precipitates in an experimental nano-precipitate strengthened steel was conducted in FY09. Microhardness mapping as well as microstructure characterization (optical, SEM, TEM) of the welds made from the nano-steel revealed that this experimental NPSS exhibits considerable improvement over DP980 (of similar strength as the experimental NPSS) in HAZ softening. The nano precipitates appeared to be stable in the intercritical temperature range during welding.

The thermal stability of the nano-precipitates was also studied using the recently upgraded, state-of-the-art, Small-Angle Neutron Scattering (SANS) facility at Oak Ridge National Laboratory. SANS provides an ideal technique to determine the changes in precipitate morphology in a statistically meaningful manner. The SANS results are shown in Figure 4. It reveals that the nano precipitates were quite stable up to the intercritical temperature. The average nano precipitate particle sizes become smaller in the coarse grain HAZ near the fusion line. Our initial study suggests the potential of nano precipitate strengthening mechanism in developing the 3rd generation AHSS.

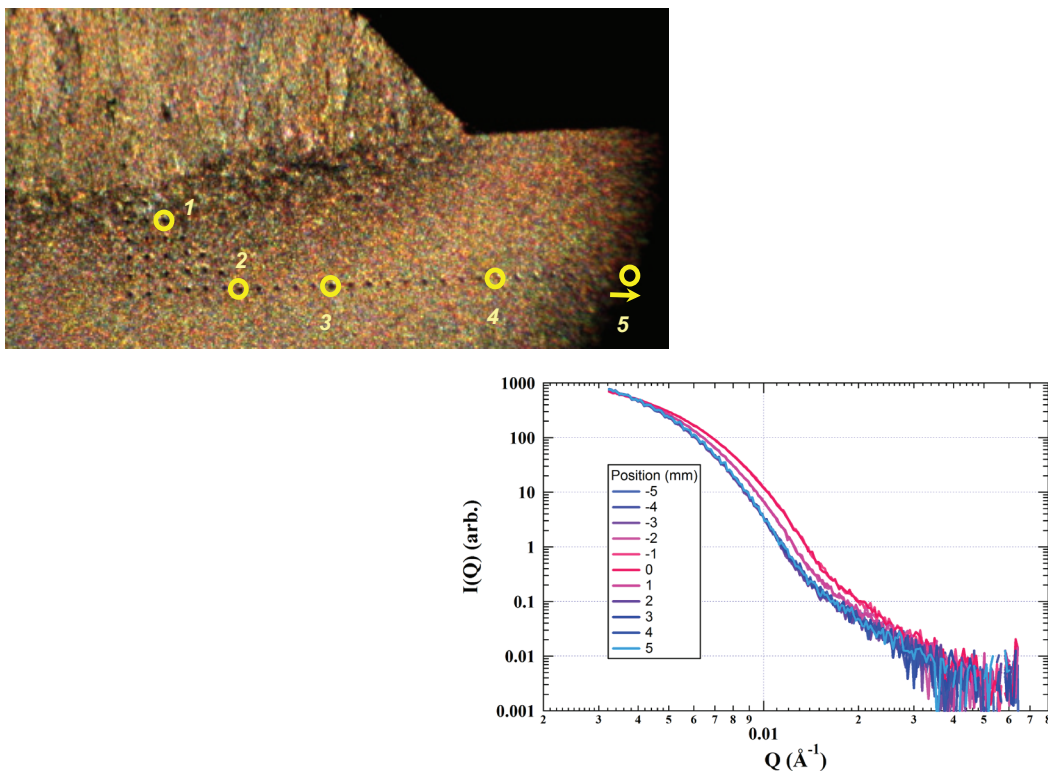


Figure 4. SANS results of nano precipitates at different locations of a gas metal arc welded NPSS. Location 1: near the weld fusion line, location 2: coarse grain HAZ, location 3: intercritical temperature region, location 4, below intercritical temperature, and location 5: base metal.

Plan for FY 2010

The R&D activities for FY2010 and beyond will be shifted to the development of the 3rd generation AHSS. The 3rd generation AHSS are expected to offer even greater potentials for weight reduction and safety enhancement with manufacturability and affordability acceptable in future generation vehicles. The target range of baseline properties (strength and ductility) of the 3rd generation AHSS would be such that the specific strength (strength-to-weight ratio) is on a par with those of Al alloys and Mg alloys, thereby eliminating the disparity in lightweighting.

Versatile strengthening mechanisms are available in steel-making (solid solution strengthening, precipitate strengthening, transformation strengthening, grain size refinement, and grain boundary strengthening). A fundamental challenge for development of the 3rd generation AHSS therefore lies in how to utilize one or more of these strengthening mechanisms cost-effectively. Equally important and challenging is that the 3rd generation AHSS must also possess robust manufacturability, i.e., formability and weldability, which is essential for their application in auto-body structures. A close partnership of universities and academia, national laboratories, and steel and auto industry will be essential in the development and technology transition of the 3rd generation AHSS, as shown in Figure 5.

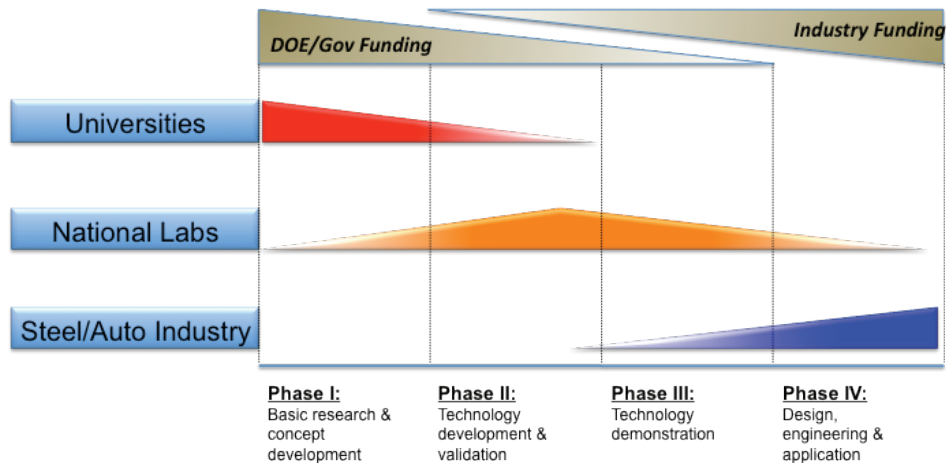


Figure 5. Partnership for 3rd generation AHSS development.

Presentations/Publications/Patents

Z. Feng, W. Zhang and S.A. David, "Predictive Model of Welding Induced Microstructure Changes in AHSS and Their Effects on Weld Performance," *International Auto Body Congress (IABC) 2009*, Nov 4-5, 2009, Troy, MI.

Y. Sang, C. Jiang, and Z. Feng, "Fatigue Life Prediction of Advanced High Strength Steel GMAW Joints Using Local Approach," *International Auto Body Congress (IABC) 2009*, Nov 4-5, 2009, Troy, MI.

W. Woo, E. Specht, Z. Feng, W. Zhang and X-L. Wang, "In situ x-ray synchrotron observations of steel phase transformation under non-equilibrium conditions," 139th Annual Meeting, TMS, Feb 14-18, 2010, Seattle, WA.

Acknowledgements

We would like to acknowledge the following individuals and A/SP committees who contributed to this project.

Chrysler: W. Marttila

Ford: J. Chiang, P. Geck

GM: S. Gayden, J. Bohr, C. Chen

Mittal Steel: M. Kuo

US Steel: M.F. Shi

Severstal N.A.: R.M. Iyengar, Y.-W. Wang

AK Steel: T. Montroy

Dofasco: W. Bernert

OTC: P. Mosquera

A/SP Joining Technologies Team

A/SP Sheet Steel Fatigue Committee

A/SP Lightweight Chassis Structure Team

K. Fundamental Study of the Relationship of Austenite-Ferrite Transformation Details to Austenite Retention in Carbon Steels

Principal Investigator: Michael L. Santella
Oak Ridge National Laboratory
1 Bethel Valley Road, Oak Ridge, TN 37831-6096
(865) 574-4805; e-mail: santellaml@ornl.gov

Technology Area Development Manager: Dr. Carol Schutte
(202) 287-5371; e-mail: carol.schutte@ee.doe.gov

Field Technical Monitor: C. David Warren
(865) 574-9693; e-mail: warrencd@ornl.gov

Primary Participants:
Eliot D. Specht
Oak Ridge National Laboratory

Contractor: Oak Ridge National Laboratory
Contract No.: DE-AC05-00OR22725

Objective

This project supports the development of the Generation III (Gen III) advanced high-strength steels (AHSS) through fundamental studies of the ferrite-austenite phase transformation during steel finishing operations and its relationship to stabilizing and retaining austenite in finished microstructures. This will be done using unique facilities like the Advanced Photon Source, available through the Department of Energy, Office of Science, to characterize in-situ the austenite-ferrite phase transformation behavior of carbon steels under the rapid heating/cooling conditions that typify modern sheet steel production. This behavior will then form the basis for determining the extent to which retained austenite can be increased in commercial and experimental low-carbon (< 0.2 wt%) steels.

Approach

The majority of the experimental part of this work will be done using the Advanced Photon Source to provide synchrotron radiation for high-speed diffraction. Diffraction patterns can be collected at rates of 1 every second, possibly even higher. Capabilities exist for integrating diffraction with rapid heating/cooling cycles. Control of temperatures and heating/cooling rates are sufficient for replicating most of the processing steps used to produce existing AHSS. Analysis of the diffraction data can determine volume fractions of the ferrite and austenite phases, their lattice parameters, and how they vary under dynamic temperature/time conditions.

Accomplishments

The ability to continuously measure phase fractions and lattice parameters by synchrotron diffraction during simulated steel heating/cooling process cycles was demonstrated.

Future Direction

Improvements to the experimentation used for the diffraction experiments will be made such as developing a procedure to minimize decarburization. Improvements to streamline data reduction and analysis techniques are also being addressed. Data from additional experiments on DP780 and the hot-stamp-boron steel will be analyzed for transformation behavior and retained austenite. Alloy compositions that promote higher amounts of retained austenite will be identified for preparation of lab-scale heats. These will be incorporated into future diffraction experiments.

Introduction

Project Background

Metals comprise about 80% of all the materials used for light vehicle construction, and, by a wide margin, the largest fractions of the metals are steels [Source: 2007 Great Designs in Steel presentations of R. A. Schultz and J. Schnatterly]. Steels represent about 62% of average vehicle weight. Of the various steel mill products used for auto construction about 70% of the total, or 839 kg of 1,970 kg average light vehicle weight, is supplied as flat-rolled carbon steel for chassis

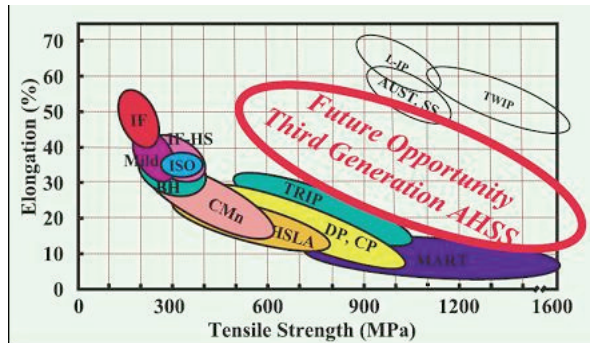


Figure 1. General variation of tensile elongation with strength showing how these properties characteristically balance in various grades of steel [Source: www.recycle-steel.org].

parts and body panels. The dominance of carbon steels, in terms of total vehicle weight, results from a variety of factors. The metallurgy of carbon steels creates broad boundaries for manipulating important properties such as strength and ductility as indicated in Figure 1. Carbon steels are relatively inexpensive and they have excellent recyclability. The recycle rate for automotive steels is about 100%. Source: www.recycle-steel.org.

The traditional sheet steels used for chassis and body constructions are the so-called “mild” steels. The combined interests of improving crashworthiness and reducing vehicle weights were at least partially responsible for the development of the first generation (Gen I) of advanced high strength steels (AHSS). Included in this group is the dual-phase (DP), complex-phase (CP), martensitic, and transformation-induced plasticity (TRIP) steels. A second generation (Gen II) of sheet steels was much more highly alloyed, and, therefore, more costly than the Gen I steels. This group included austenitic stainless steels (AUST, SS), steels strengthened by twinning-induced plasticity (TWIP steels), and other lightweight austenitic steels with induced plasticity (L-IP steels). What is now desired is a third generation of AHSS that borrows from previous alloy development efforts to achieve intermediate strengths and ductilities, as indicated in Figure 1, but at costs that would make acceptance for automotive construction feasible. Controlling cost will likely require that Gen III AHSS be no more than modestly alloyed compared to Gen I AHSS, and capable of being produced within existing steel mill infrastructures.

Approach

There are two temperature ranges where improved understanding is crucial to achieving the Gen III goals. One is the so-called intercritical temperature range. This is the range from about 700-850°C where, depending on chemical composition, the ferrite and austenite phases co-exist at equilibrium. The time and temperature of intercritical annealing during sheet production control both the relative fractions and chemical compositions of ferrite and austenite in the

microstructure. These factors combined with cooling rate will determine how the austenite behaves during subsequent cooling. Collectively, they determine whether austenite transforms to martensite, bainite, or ferrite, and whether any austenite is retained in the microstructure. The second critical range is from about 200-500°C where austenite can be maintained in a metastable condition due to the partitioning of alloying elements like carbon, manganese, and silicon. As is well known, retaining austenite can markedly improve ductility at high strength through the TRIP effect. Better fundamental understanding of austenite-ferrite transformations will enable a more scientific approach to improving properties through novel processing that can be achieved with existing infrastructure.

Technical Challenges

1. Making direct, *in-situ* observations of the time dependence of austenite-ferrite transformation behavior at elevated temperatures, during rapid heating/cooling, and during low temperature treatments designed to maximize retained austenite.
2. Measuring partitioning of carbon between austenite and ferrite during processing.
3. Understanding effects of critical alloying elements such as carbon, manganese, and silicon on transformation behavior and retention of austenite.

The technical activities of this task are complementary to and will be coordinated with those of Gen III AHSS projects funded to universities through the National Science Foundation (see X.Y1-Y10).

Materials and Experimental Details

Two uncoated high-strength steels are being used for initial experiments: the dual-phased steel, DP780 (ArcelorMittal), and hot-stamp boron (HSB) steel (sourced from a Swedish supplier, the parent of US Hardtech). The analyzed compositions of the steels are:

- DP780: Fe-0.11C-1.93Mn-0.24Si, wt%
- HSB steel: Fe-0.20C-1.26Mn-0.27Si-0.22Cr-0.002B, wt%

Specimens with dimensions of 5 mm x 1.25 mm x 110 mm were machined from sheets of both steels. The surfaces of these strips were ground by machining to remove oxides.

For diffraction experiments, the specimens are held in copper grips so that they function as resistors in an electrical circuit. A thermocouple is spot welded to the backside of each specimen at the location where they are impinged by x-rays. The thermocouple measures temperature ($\pm 0.2^\circ\text{C}$) and provides feedback to a controller that permits programming of temperature histories. The base of one side of the specimen holder is spring-loaded and mounted on bearings. This arrangement produces a slight tension force to permit the specimen to freely expand as it heats. The heating stage is mounted in a vacuum chamber that minimizes oxidation. Typically, there is no visible sign of significant oxidation after heating.

The incident x-rays are provided by the UNICAT X-33 bending magnet beamline at the Advanced Photon Source (Argonne National Laboratory, Argonne, Illinois). X-ray data were captured by a charge-coupled device (CCD) on which the diffracted beams were integrated over a 1 s exposure. Diffraction patterns are acquired at a maximum rate of about 1/s. The spot size of the incident x-ray beam is about 1 mm².

Data analysis begins by converting the two-dimensional images recorded by the CCD detector into one-dimensional plots of diffracted intensity versus crystal lattice spacing. The crystal

lattice spacing (d-spacing) uniquely identifies the presence of the austenite and ferrite phases in the steel specimens.. The one-dimensional plots were then analyzed for crystallographic texture effects, and ferrite and austenite phase volume fractions using published methods.

Results

Transformations and lattice parameters in DP780 were characterized for a specimen heated at 10°C/s to 800°C, held for 120 s, cooled to 460°C, held for 60 s, then free-cooled to room temperature. The results for intercritical annealing portion of this experiment are presented in [Figure 2](#) where the variation of specimen temperature is shown on top and the corresponding phase fractions are shown on the bottom. The first appearance of the austenite phase occurred during heating at 724°C. The specimen temperature overshoot the 800°C set point to reach a maximum of about 813°C, but this transient settled to the set point temperature in about 12 s. The austenite phase reached a maximum of about 66% and decreased during the isothermal hold at 800°C to 44%.

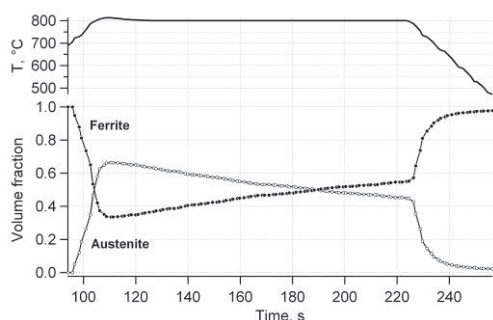


Figure 2. Temperature history (top) and associated ferrite-austenite transformation behavior (bottom) for DP780 heated directly to 800°C.

No austenite was detected in the DP780 specimen before heating/cooling. After the experiment, about 1% of austenite was retained in the microstructure.

The variation of the amount of austenite during the isothermal hold at 800°C was unexpected. The conventional view of the transformation behavior would indicate that austenite fraction would initially be less than the stable, equilibrium amount, but it would increase with holding time as carbides dissolved and alloying elements partitioned between the austenite and ferrite phases. At the end of the isothermal hold the expected amount of austenite was about 76%.

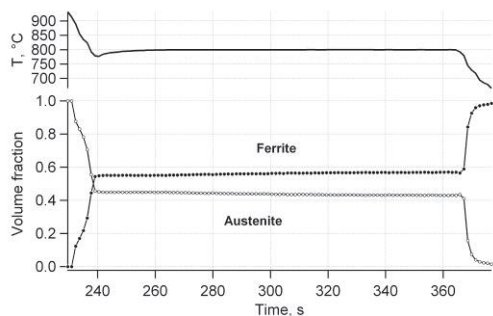


Figure 3. Temperature history (top) and associated ferrite-austenite transformation behavior (bottom) for DP780 heated to 970°C and then cooled to 800°C.

In a subsequent experiment, the DP780 steel was first heated to 970°C to promote dissolution of carbides and to cause complete transformation to the austenite phase. Following a 120 s hold at 970°C, the steel was cooled to 800°C, held there for 120 s, and then cooled to room temperature. These results are shown in [Figure 3](#). In this case, the amount of austenite rapidly decreased from 100% to 45% at the beginning of the isothermal hold period. During the isothermal hold the amount of austenite decreased slightly from 45-43%.

DP780, and those results are shown in [Figure 4](#). The predicted equilibrium amount of austenite at 800°C is 76%, about 30 percentage points higher than the amount measured by diffraction.

The second diffraction experiment suggests that the equilibrium amount of austenite in DP780 at 800°C is in the range of 43-45%. Thermodynamic calculations were used to corroborate the equilibrium phase fractions in

The difference between the diffraction results and the thermodynamic predictions was further investigated by reproducing the heating/cooling cycles used for the diffraction experiments in an independent experiment using a Gleeble testing machine. The Gleeble heats specimens resistively just as the heating stage used for the diffraction experiments. The Gleeble heating was also done in a vacuum chamber.

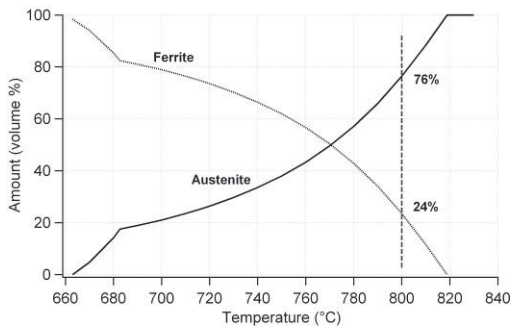


Figure 4. Predicted variations with temperature of ferrite and austenite fractions in DP780.

20%. The martensite transforms directly from austenite during quenching. These micrographs suggest that the phase fractions at 800°C were reasonably consistent with the equilibrium thermodynamic predictions of Figure 4. They also indicate there was no significant variation in the amount of austenite between 10-120 s. This observation is consistent with the diffraction results of Figure 3 although the amounts of the phases do not agree.

The continuing experiments emphasize resolving the inconsistency between phase fractions determined by synchrotron diffraction and those measured in independent experiments. Possible causes of disagreement include:

- Equilibrium is not being achieved in 120 s at 800°C.
- Decarburization is occurring during diffraction. This will locally decrease the carbon concentration which has a significant effect on phase fractions.
- Some step in the data analysis is not being handled accurately. Data analysis routines are being re-examined and validated.
- Other experimental issues related to heating stage are also being re-evaluated.

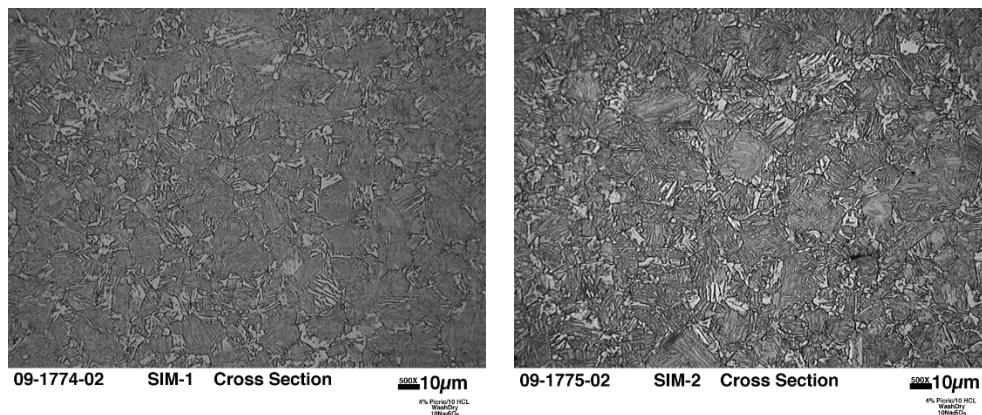


Figure 5. Optical microstructures of DP780 heated to 970°C, cooled to 800°C, then quenched after holding for 10 s (top) and 120 s (bottom).

The diffraction experiments were also used to determine the variations of ferrite and austenite lattice parameters, and an example after cooling from 970°C and isothermal holding at 800°C is presented as Figure 6. After the time mark of about 260 s the specimen temperature was constant. From that point until cooling began, the ferrite lattice parameter was approximately constant while that of austenite appeared to increase slightly. Analysis of these data is not complete, but it should be possible to use the lattice parameters to draw conclusions about

the partitioning of alloying elements between the phases. This could provide insights about stabilizing the austenite phase during cooling and retaining it to enhance the TRIP response during later deformation.

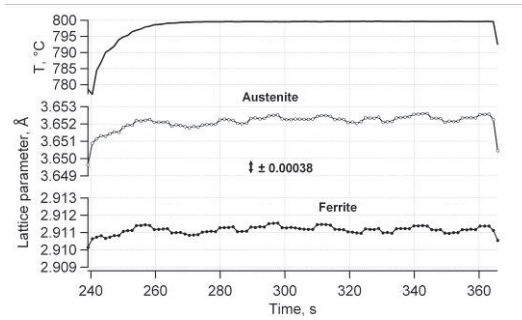


Figure 6. Variations of austenite and ferrite lattice parameters at 800°C.

Conclusions

Initial experiments demonstrate that phase fractions and lattice parameters can be continuously measured during heat treatments similar to those used in processing automotive sheet steels. However, inconsistencies were observed between phase fractions determined by diffraction and those measured by independent experiments. Analysis is continuing to resolve the differences and to extract additional information from the experimental diffraction data.

L. NSF Funding for the Development of 3rd Generation Advanced High-Strength Steels (ASP 280¹)

Principal Investigator: Ronald Krupitzer
American Iron and Steel Institute
2000 Town Center Drive, Suite 320
Southfield, Michigan 48075-1123
(248)945-4761; e-mail: krupitzerr@autosteel.org

Technology Area Development Manager: William Joost
(202) 287-6020; e-mail: william.joost@ee.doe.gov

Contractor: United States Automotive Materials Partnership (USAMP)
Contract No.: DE-FC05-02OR22910 through the National Energy Technology Laboratory

Objectives

Conduct the fundamental research required to develop a 3rd Generation Advanced High-Strength Steel (AHSS) that is higher in strength and more formable than currently available commercial grades of AHSS with the potential of being more cost effective than stainless steels and TWIP steels.

Approach

- Conduct fundamental steel research at Universities that can lead to the development of a cost effective family of 3rd Generation AHSS that can be applied for mass reduction in the auto body.
- Utilized National Science Foundation (NSF) processes to manage the research.
- Provide a portion of the funding (25%), through this project, for fundamental research required to develop a 3rd Generation AHSS.
- Additional funding will be provided directly by Department of Energy (DOE) (25%) and the NSF (50%).

Accomplishments

- NSF Advanced High-Strength Steel Workshop held October 22-23, 2006, Arlington, Virginia.
- NSF Advanced High-Strength Steel Proposal Panel Review held April 10-11, 2007, Arlington, Virginia. Eight proposals, from 30 submitted, were selected for funding using the NSF process and a budget allocation prepared by NSF. The research projects will be carried out over three years.
- NSF will notify the appropriate Principal Investigators and Universities of their grants and track and document the research projects following NSF standard practices.
- A NSF/DOE Steel Research Program Reviews were held on April 10, 2008 and May 12, 2009. Participants in both of these annual reviews included the University professors that are

conducting the NSF research, National Lab researchers working on steel research, CANMET steel researchers and personnel from NSF, DOE, and Auto/Steel Partnership (A/SP) member companies.

- An industry based steering committee has been formed.

Future Direction

- The industry based steering committee will work to provide the requested additional support to the researchers.
- A web-based site has been developed for researchers to store and share information.
- The third-year project review of the NSF/DOE Steel Research Program will be held on July 19-20, 2010.
- The second day of the July 2010 review will examine future work opportunities resulting from the projects.

Introduction

One of the tasks of the ASP240 Future Generation Passenger Compartment Project (FGPC) was to perform structural optimization with unrestricted strength limitations to define the upper strength bound for auto body steel for optimized mass reduction. Several areas of the body were found that would benefit from higher strength.

An additional 5 to 8% mass reduction is possible in those areas of the vehicle. Based on the specific areas of the body, estimates were made of the forming characteristic needed to make those types of parts. A window of opportunity was defined ranging from 600 MPa/40% elongation to 1600 MPa/20% elongation for a cost effective 3rd Generation Advanced High-Strength Steel (AHSS) family. It was recognized fundamental steel research would be required to develop steels in that property range. A collaborative effort by NSF, DOE, American Iron and Steel Institute (AISI) and Auto/Steel Partnership (A/SP) has been put together to fund eight university research proposals, using the NSF processes, to fund the supporting fundamental research to develop steels with the desired properties.

Objective

The objective of this project is to provide a portion of the funding (25%) for the fundamental research required to develop a cost effective family of 3rd Generation AHSS that can ultimately be applied for mass reduction in the auto body. Additional funding will be provided directly by DOE (25%) and NSF (50%). The research will be done utilizing the processes of the NSF. If the research is successful, it will provide the basis for the commercial development of cost effective 3rd Generation AHSS by the A/SP steel members.

Project Status

A NSF Advanced High-Strength Steel Workshop was held October 22-23, 2006, in Arlington Virginia. As a result of that workshop, the NSF requested proposals for basic research to support the development of a family of 3rd Generation AHSS. A NSF AHSS Proposal Panel Review was held April 10-11, 2007, in Arlington, Virginia. Eight proposals, from 30 submitted, were selected for funding, using the NSF process, and a budget allocation was prepared by NSF. The

research projects will be carried out over three years starting the academic year 2007-2008. The following table (Table 1) shows the Principal Investigators (PI), Institutions and Titles.

Table 1. Third Generation AHSS Research Institutions, Principal Investigators, and Topics

University	Professor	Topic
Carnegie Mellon University	Warren Garrison	AHSS through microstructure and mechanical properties
Case Western Reserve U.	Gary Michal	AHSS through C partitioning
Catholic University of America	Abu Al-Rub Rashid	AHSS through particle size and interface effects
Colorado School of Mines, Ohio State University	David Matlock (CSM) and Robert Wagoner (OSU)	Collaborative GOALI Project Formability and Springback of AHSS
Drexel University	Surya Kalidindi	FEM using crystal plasticity simulation modeling tools
Ohio State University	Ju Li	Multi-scale modeling of deformation for design of AHSS
University of Missouri-Rolla	David C. Van Aken	AHSS through nano-acicular duplex microstructures
Wayne State University	Susil K. Putatunda	High strength high toughness bainitic steel

An industry based steering committee has been formed with members from A/SP member companies. They include representatives from steel research centers, mills and automotive applications centers and advanced materials representatives from the automotive companies. The steering committee will help coordinate additional support for the NSF researchers and become the technology transfer interface for the research back into industry.

NSF/DOE Steel Research Program Reviews were held on April 10, 2008, in Southfield MI and May 12, 2009, in Livonia, MI, both in conjunction with AISI's Great Designs in Steel (GDIS) event held in both 2008 and 2009. GDIS provided the steel researchers the opportunity to see the need for a 3rd Generation AHSS. Overviews of each of the NSF sponsored research programs were presented. In addition, related research being conducted at Pacific Northwest National Laboratory, Oak Ridge National Laboratory and Canada's CANMET Laboratory was reviewed. Research representatives from the steel industry, advance engineering and research representatives from the automotive industry and staff from A/SP, AISI, NSF and DOE participated in the Southfield and Livonia reviews. There was active discussion during the reviews among the participants. Opportunities for future interactions among the attendees, areas needing additional support and gaps in the research were identified and are being addressed.

A web based system where information could be stored and shared became available in May 2008.

Conclusions

NSF has initiated the research contracts with the nine selected Universities. (Wayne State University was subsequently added to the full program after working on an exploratory research grant.) Reporting of the research will follow the normal processes of NSF for all nine universities.

Acknowledgments

The support and guidance of Dr. Mary Lynn Realff, Dr. Joyce Lynn Harrison, and Dr. Clark Cooper of the National Science Foundation and Dr. Joseph Carpenter and Mr. Will Joost of the Department of Energy is greatly appreciated.

Future Work

The industry based steering committee has provided additional support requested by the researchers. The next annual progress review of 3rd Generation AHSS research will be held on July 19-20, 2010, at AISI Facilities in Southfield MI. The intent of the annual reviews is to share progress, identify gaps in the research program and identify areas where additional support would be valuable. A web site debuted in May 2008 to store and share data amongst the researchers, and continues to be updated with progress reports and research information.

References

The NSF Report, “Advanced High Strength Steel Workshop Oct.22-23, 2006, Arlington, Virginia” by Professor Robert Wagoner, Department of Material Science and Engineering, Ohio State University, Columbus, OH.

¹Denotes project 280 of the Auto/Steel Partnership (A/SP), the automotive-focus arm of the American Iron and Steel Institute (AISI). See www.a-sp.org. The A/SP co-funds projects with the DOE through a Cooperative Agreement between DOE and the United States Automotive Materials Partnership (USAMP), one of the formal consortia of the United States Council for Automotive Research (USCAR), set up by Chrysler LLC, Ford Motor Company and General Motors Corporation to conduct joint, pre-competitive research and development. See www.uscar.org.

M. AHSS: A Multiresolution Analysis of the Particle Size and Interface Effects on the Strength and Ductility of Advanced High Strength Steels

Principal Investigator: Rashid K. Abu Al-Rub
Texas A&M University
3136 TAMU, College Station, TX 77843-3136
(979) 862-6603; e-mail: rabualrub@civil.tamu.edu

Technology Area Development Manager: William Joost
(202) 287-6020; e-mail: william.joost@ee.doe.gov

Contractor: Texas Engineering Experiment Station
Contract No.: NSF Grant – CMMI 0728032, jointly funded by NSF and DOE

Objective

- Identifying the role of dispersed micro and nano particles (inclusions) on enhancing the yield strength, ultimate strength, and ductility of AHSS (advanced high strength steels) reinforced with inclusions at decreasing microstructural length scales.
- Development of a multiresolution (multiscale) computational framework that can be used effectively in the design of AHSS with superior strength and ductility.

Approach

- Development of a robust multiresolution theoretical framework for the multi-scale modeling of inelastic deformation processes of evolving multi-phase AHSS.
- Development of a non-local strain gradient theory coupled with the developed multiresolution analysis.
- Implementing the developed theoretical models in a multi-scale hierarchical computational framework.
- Conducting a parametric study of the effect of microstructural features (e.g. particle size, interfacial properties, particle volume fractions and distribution) on the strength and ductility of AHSS.

Accomplishments

- A theoretical model based on nonlocal strain gradient plasticity has been developed and successfully validated.
- The model has successfully been implemented in the finite element program Abaqus.
- The model is used in predicting the increase in yield strength and strain hardening rates of AHSS with decreasing the particle (inclusion) size.
- It is found that optimizing the interfacial properties between the micro/nano particles and the metallic matrix has a significant effect on the yield strength of AHSS.

Future Direction

- Incorporating micro-damage nucleation and growth laws that can simulate micro and nano crack evolution within the matrix material of AHSS and at internal interfaces of second-phase materials and particles.
- Conducting a parametric study of the effect of microstructural features on the strength and ductility of AHSS.
- Draw conclusions about the main strengthening and damage mechanisms in AHSS.

Introduction

Advanced metal-matrix composites (AMMCs) (i.e. pure metals or metallic alloys with dispersed particles or inclusions at decreasing microstructural length scales ranging in size from few micrometers down to hundreds of nanometers) with mechanical and physical properties well in excess of those exhibited by conventional metal-matrix composites (i.e. pure metals or metallic alloys that consist of large particles, fibers, whiskers, etc) are of considerable economic, technological, and scientific interest and will contribute significantly to the heightened performance of structural components and systems in many industries. For example, with the introduction of stronger safety legislation and increased fuel prices, auto manufacturers are striving for increasing the car body stiffness for safety and lowering the body weight for fuel efficiency by designing new generation of advanced high strength steels (AHSS) embedded with metallic and/or ceramic particles of different sizes. [Figure 1](#) shows an AHSS embedded with inclusions at two distinct scales: primary particles (such as titanium nitrides) are typically on the order of several microns in size; and secondary particles (such as titanium carbides and manganese sulfides) are on the order of hundreds of nanometers in size.

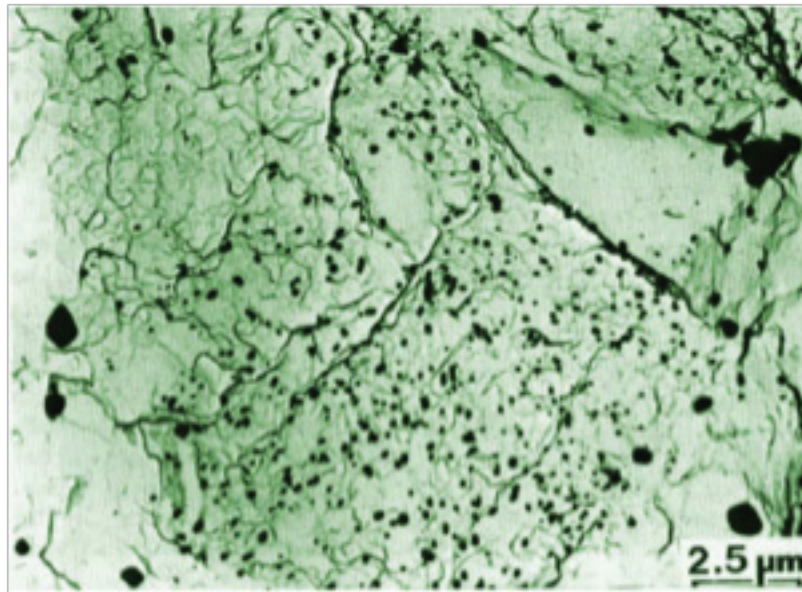


Figure 1. A TEM micrograph of the microstructure of an AHSS showing the different levels of dispersed small particles [1].

Generally, second phase particles play a dual role: (i) on one hand, depending on their size and interfacial hardening properties, they can significantly increase the strength and improve the plastic work-hardening behavior; (ii) on the other hand, depending on their strength and interfacial strength, particle cracking and/or interfacial debonding cause nucleation, growth,

and coalescence of micro-voids and micro-cracks, which eventually lead to damage induced-anisotropy and ductile failure. Many researchers have investigated the interfacial damage effects (see [2] for detailed literature review), whereas very few have researched the interfacial strengthening and hardening mechanisms due to varying the particle size and varying the particle-matrix interfacial properties. Therefore, the focus of this research is on the particle size and interfacial hardening effects in AMMCs. Several experimental works on particle-reinforced composites have revealed that a substantial increase in the macroscopic yield strength and flow stress can be achieved by decreasing the particle size while keeping the volume fraction constant (see [2] and [3] for detailed literature review). Therefore, there is a large need for the development of a mechanical theory that can accommodate size effects in AMMCs and can be used for bridging the length scales.

Theoretical modeling and multiscale computational simulations are necessary for the design of new generations of AMMCs. Therefore, it is imperative to develop a constitutive model and a multiscale framework that can be used successfully in incorporating the strengthening effects due to the reduction in particle (inclusion) size and the effects of the interfacial hardening by incorporating the particle-matrix interfacial mechanical properties (e.g. interfacial strength and hardening). Unfortunately, the classical continuum plasticity theories (e.g. von Mises or Drucker-Prager) are unable to predict the influence of particle size due to the absence of a microstructural length scale parameter in their constitutive equations [4]. Therefore, within a classical continuum mechanics framework, the mechanical properties of multi-phase materials only depend on the volume fraction of particles while the particle size is not accounted for. However, the mechanical properties of advanced materials, with a typical distance D between particles and particle size d , depend on how these geometrical parameters interfere with other characteristic distance such as the mean-free path of dislocations. Reducing the size of particles, while keeping the volume fraction constant, significantly improves the material macroscopic mechanical properties.

Approach

Since the increase in strength with decreasing scale can be related to proportional increase in the plastic strain gradients that evolve at the particle-matrix interfaces due to dislocation pileups, the gradient plasticity theory has been successful in addressing the size effect problem [5]. This success stems out from the incorporation of a microstructural length scale parameter through functional dependencies on the plastic strain gradient of nonlocal media. The gradient-dependent theory abandons the assumption that the stress at a given point is uniquely determined by the strain at this point only. It takes into account possible interactions with other material points in the vicinity of that point (i.e. nonlocality).

In the past decade, the physical basis of the gradient plasticity theory for metals has been founded on theoretical developments concerning geometrically necessary dislocations (GNDs) [6]. Standard micromechanical modeling of the inelastic material behavior of metallic single crystals and polycrystals is commonly based on the premise that resistance to glide is due mainly to the random trapping of mobile dislocations during locally homogeneous deformation. Such trapped dislocations are commonly referred to as statistically stored dislocations (SSDs), and act as obstacles to further dislocation motion, resulting in hardening. An additional contribution to the density of immobile dislocations and so to hardening can arise when the continuum length scale approaches that of the dominant microstructural features. An extensive review of the recent developments in gradient-dependent theory can be found in Voyiadjis and Abu Al-Rub [5].

As an initial effort, in order to include the size effect of dispersed particles within the AHSS matrix, a higher-order gradient plasticity theory has been developed within the laws of thermodynamics. This nonlocal theory takes into account the plastic strain gradient (i.e. heterogeneous distribution

of plasticity) around the second-phase inclusions. Also, the interfacial mechanical properties of the particle-matrix interface (e.g. interfacial yield strength and interfacial hardening) are explicitly incorporated in the formulated theory. Depending on the interfacial properties, the effect of hard, stiff, or soft inclusions are incorporated.

Also, in this theory, two plasticity yield conditions are formulated: one for the bulk (i.e. the matrix) and one for particle-matrix interface and grain boundaries. Therefore, two length scale parameters are incorporated. The bulk length scale parameter, l , is related to the average spacing between dislocations within the matrix material; whereas, the interfacial length scale, l_i , is related to the boundary layer thickness at the particle-matrix interface. Both length scales can be identified from nanoindentation tests.

Results

The formulated nonlocal strain gradient plasticity theory has been implemented in the commercial finite element program Abaqus through its user material subroutine UMAT and used to demonstrate the ability of the model in predicting particle size effects on the strength of AHSS. The direct and simple numerical implementation method for gradient-dependent theories as presented in [7] has been utilized for calculating the plastic strain gradients.

The implemented higher-order gradient plasticity is employed to handle size effects in advanced metal matrix composites with dispersed hard (e.g. ceramic), soft (e.g. metallic), or intermediate compliant inclusions (particles) under macroscopically uniform uniaxial σ_0 stress where d is the particle size (see Figure 2). For simplicity, the particles are assumed to be uniformly distributed and the matrix material is taken to be linearly hardening elasto-plastic.

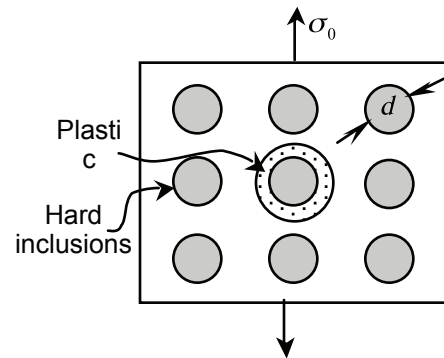


Figure 2. Plastic strain gradients are caused by evolution of geometrically necessary dislocations (GNDs) around spherical inclusions of size d under uniaxial loading.

Figures 3 and 4 show that the proposed nonlocal strain gradient plasticity is successful in predicting the inclusion size effect for a constant volume fraction unlike the classical plasticity theory. Moreover, it is shown that the proposed nonlocal strain gradient plasticity theory can predict an increase in the initial yield strength (i.e. onset of plasticity) and the strain hardening rate, where σ_y is the matrix size-independent yield strength and ϵ_y is the size-independent initial yield strain. This increase in the initial yield strength and strain hardening rates are shown for different particle sizes d (characterized by the ratio l/d where l is the material length scale). In other words, the smaller is the particle size and larger is the particle hardness; the larger is the ultimate strength. However, it is noteworthy that the above conclusions and observations are valid only in case the particle debonding and fracture effects are not considered. These effects will be incorporated in the subsequent development of the current study.

Moreover, the predicted particle size effect is shown for compliant particles (e.g. metallic particles) in Figure 3 and for stiff particles (e.g. ceramic particles) in Figure 4. Clearly one can

see that as the interfacial strength of the embedded particles increases the initial yield strength and strain hardening rates increase.

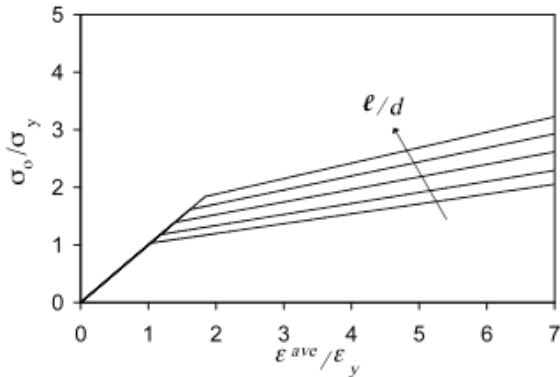


Figure 3. Normalized stress-strain relations for compliant inclusions.

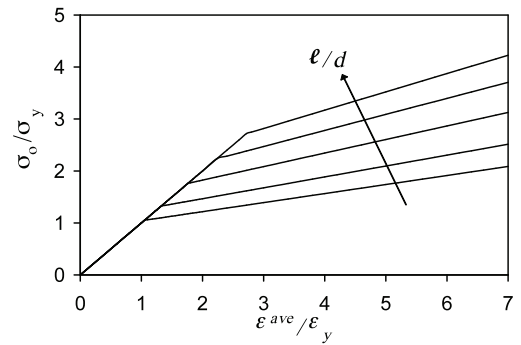


Figure 4. Normalized stress-strain relations for hard inclusions.

Conclusions

It is concluded that a nonlocal strain gradient plasticity theory can be used to qualitatively predict the particle size effect in AHSS reinforced with particles (inclusions) at decreasing microstructural length scales. These particles can range in size from few hundreds of nanometers to few microns. It is shown that as the particle size decreases or particle hardness increases both the onset of plasticity (yield strength) and strain hardening rate (or ultimate strength) increases. This is a crucial conclusion for the design of AHSS with improved yield and ultimate strengths. Also, it is concluded that for rigid particles, the bulk (i.e. the metal matrix) length scale controls the particle size effect whereas for soft and intermediate particles the interfacial length scale controls the particle size effect.

However, these conclusions are only valid in case both debonding and fracture of particles are not considered. Future extensions of the current study will consider damage evolution in the matrix, particle, and particle debonding which are very important to validate the aforementioned conclusions and for assessment of the effect of particle size and hardness on the ductility of AHSS.

Moreover, future work will be concerned with incorporating the formulated nonlocal strain gradient plasticity theory in a multi-scale hierarchical computational framework ranging from the nano scale to the macro scale. This is important to study the effect of each scale on the other and how the microstructural changes within each scale affect the overall macroscopic strength and ductility of AHSS or low-density materials. Furthermore, phase transformation of austenite to the hard phase martensite will also be incorporated into the proposed multiscale framework. One of the important aspects of this study that will be investigated thoroughly is the calibration, validation, and verification of the proposed theoretical models and computational tools. The proposed frameworks will be validated and verified against available experimental results for specific material systems or microstructures.

Presentations

1. Abu Al-Rub, R.K., "On the Higher-Order Nonlocal Gradient Plasticity for Modeling Size Scale Effects," In. Symposium on Micro-plasticity and Homogenization (in honor of Prof. Ohno), Plasticity 2010, St. Kitts, Jan. 3-8, 2010 (Key-note Lecture).

2. Abu Al-Rub, R.K., "Prediction of Scale-Dependent Strength and Hardening Rates in Metallic Thin Films: Intrinsic and Extrinsic Size Effects," In. 2009 ASME International Mechanical Engineering Congress and Exposition, Lake Buena Vista, Florida, November 13-19, 2009.
3. Abu Al-Rub, R.K., "Nonlocal Interfacial Gradient Plasticity Governs Scale-Dependent Yield Strength and Strain Hardening Rates in Nanostructured Metals," In. 2009 ASME International Mechanical Engineering Congress and Exposition, Lake Buena Vista, Florida, November 13-19, 2009.
4. Abu Al-Rub, R.K., "Modeling the Particle Size and Interfacial Hardening Effects in Metal Matrix Composites with Dispersed Particles at Decreasing Microstructural Length Scales," In. 2009 ASME International Mechanical Engineering Congress and Exposition, Lake Buena Vista, Florida, November 13-19, 2009.
5. Abu Al-Rub, R.K., Faruk, A.N.M., "Multiresolution Analysis of Size-Scale Effects in Metal/Metal Alloys with Dispersed Particles at Decreasing Microstructural Length Scales," In. 10th US National Congress on Computational Mechanics, Columbus, Ohio, July 16-19, 2009.
6. Abu Al-Rub, R.K., Kim, S.-M., "Predicting Mesh-Independent Ballistic Limits for Heterogeneous Targets by a Nonlocal Damage Computational Framework," In. The 2009 Joint ASCE-ASME-SES Conference on Mechanics of Materials, Blacksburg, Virginia, June 24-27, 2009.
7. Abu Al-Rub, R.K., "Interfacial Plasticity Governs Strength Size-Scale Effects in Micro/Nanostructured Metals," In. 50th AIAA/ASME/ASCE/AHS/ASC Structures, Structural Dynamics and Materials Conference, AIAA 2009, Session on Impact and Shock Response, Palm Springs, California, May 4-7, 2009.
8. Abu Al-Rub, R.K., Kim, S.-M., "Nonlocal Microdamage Models for Mesh-independent Predictions of Ballistic Limits in High Velocity Impacts," In. 50th AIAA/ASME/ASCE/AHS/ASC Structures, Structural Dynamics and Materials Conference, AIAA 2009, Palm Springs, California, May 4-7, 2009.

Publications

1. Abu Al-Rub, R.K., Voyiadjis, G.Z., and Aifantis, E.C. "On the thermodynamics of higher-order gradient plasticity for size-effects at the micron and submicron length scales," *International Journal of Materials and Product Technology*, Vol. 34, No. 1/2, pp. 172-187, 2009.
2. Abu Al-Rub, R.K., Kim, S.-M. "Predicting mesh-independent ballistic limits for heterogeneous targets by a nonlocal damage computational framework," *Composites: Part B*, Vol. 40, No. 6, pp. 495-510, 2009.
3. Abu Al-Rub, R.K. "Modeling the particle size and interfacial hardening effects in metal matrix composites with dispersed particles at decreasing microstructural length scales," *International Journal for Multiscale Computational Engineering*, Vol. 7, No. 4, pp. 329-350, 2009.
4. "The micro and nano indentation hardness of metallic materials," *International Journal of Materials and Structural Integrity*, Vol. 4, No. 2-3, 2010.
5. Graham, M.A., Grasley, Z.C., Abu Al-Rub, R.K., "The effect of atomic force microscope probe size on nanoindentation," *International Journal of Materials and Structural Integrity*, Vol. 4, No. 2-3, 2010.
6. Abu Al-Rub, R.K., "Modeling size effects in micro/nano-systems by including interfacial effects in a gradient plasticity framework," *International Journal of Materials and Structural Integrity*, Vol. 4, No. 2-3, 2010.

7. Abu Al-Rub, R.K., Kim, S.-M., “Nonlocal microdamage models for mesh-independent predictions of ballistic limits in high velocity impacts,” In. Collection of Technical Papers- AIAA/ASME/ASCE/AHS/ASC Structures, Structural Dynamics and Materials Conference, AIAA 2009.
8. Abu Al-Rub, R.K., “Interfacial plasticity governs strength size-scale effects in micro/nanostructured metals,” In. Collection of Technical Papers- AIAA/ASME/ASCE/AHS/ASC Structures, Structural Dynamics and Materials Conference, AIAA 2009.

References

1. Baker, M.A., 2004. Proceedings of the International Conference on Advanced High Strength Sheet Steels for Automotive Applications. Association for Iron and Steel Technology, Warrendale, PA, USA.
2. Abu Al-Rub, R.K., 2009. Modeling the particle size and interfacial hardening effects in metal matrix composites with dispersed particles at decreasing microstructural length scales. *International Journal for Multiscale Computational Engineering*, 7(4), 329-350.
3. Abu Al-Rub, R.K., 2008. Interfacial gradient plasticity governs scale-dependent yield strength and strain hardening rates in micro/nano structured metals. *International Journal of Plasticity*, 24, 1277-1306.
4. Voyiadjis, G.Z., Abu Al-Rub, R.K., 2009. *Nonlocal Continuum Damage and Plasticity: Theory and Computation*. World Scientific Publishing Co Pte Ltd., UK.
5. Arsenlis, A., Parks, D.M., 1999. Crystallographic aspects of geometrically-necessary and statistically-stored dislocation density. *Acta Materialia* 47, 1597-1611.
6. Abu Al-Rub, R.K. and Voyiadjis, G.Z., 2005. A direct finite element implementation of the gradient plasticity theory. *Int. J. Numer. Meth. Engng.* 63, 603–629.

N. A Study of the Effects of Microstructure on the Mechanical Properties and Failure Mechanisms of Advanced High Strength Steels

Principal Investigator: Warren M. Garrison Jr.
Carnegie Mellon University
5000 Forbes Avenue
Pittsburgh, PA 15213
(412) 268-3593; e-mail: wmg@andrew.cmu.edu

Technology Area Development Manager: William Joost
(202) 287-6020; e-mail: william.joost@ee.doe.gov

Contractor: Carnegie Mellon University; Pittsburgh, Pennsylvania
Award Number: National Science Foundation Award CMMI 0726949

Objectives

- To understand the effect of complex, multi-phase microstructures on the mechanical behavior and formability of advanced high strength sheet steels.
- To investigate the effect of void nucleation resistance at inclusion particles on the mechanical behavior and formability of high strength sheet steels.

Approach

- Develop microstructures consisting of lower bainite mixed with 0%, 25%, and 50% ferrite and assess the mechanical behavior and formability of these microstructures.
- Develop microstructures consisting of martensite mixed with 0%, 25%, and 50% ferrite and assess the mechanical properties and formability of these microstructures and compare the behavior of these martensite structures with those of the lower bainite structures.
- Prepare heats of steel which are identical except for the sulfide type with one sulfide type having low resistance to void nucleation and the other sulfide type being resistant to void nucleation. Sulfide particles which have a low resistance to void nucleation are achieved by gettering the sulfur as particles of manganese sulfide. Sulfide particles which are very resistant to void nucleation are achieved by gettering the sulfur as particles of titanium carbosulfide.
- This project has been coordinated with the US Steel research center in Pittsburgh. They have prepared all of the heats but one and have worked the experimental heats into one half inch plate and into sheet. Presentations have been given at the US Steel research center on the effects of gettering the sulfur as inclusions resistant to void nucleation that is gettering the sulfur as particles of titanium carbosulfide, on toughness and possibly on formability.

Milestones, Metrics and Accomplishments

- Defined four steel compositions to be used in investigating mixtures of lower bainite and ferrite and mixtures of martensite and ferrite on mechanical behavior and formability.

- Defined two steel compositions to be used to assess void nucleation resistance of inclusions on mechanical behavior and formability.
- Melted the four heats of the compositions selected to examine the effects of mixtures of lower bainite and ferrite and mixtures of martensite and ferrite on mechanical behavior and formability. Portions of these four heats have been processed to one half inch thick plate and to sheet material. This was done at US Steel research facilities in Pittsburgh.
- Prepared four heats to examine the effect of inclusion void nucleation resistance on mechanical behavior and formability. The first such heat was prepared to have inclusions which were not resistant to void nucleation. Portions of this heat have been rolled to half inch plate and other portions to sheet. However, two heats were made in succession to getter the sulfur as particles of titanium carbosulfide. Neither heat was successful due to calcium contamination with the result the sulfur was gettered as particles of calcium sulfide and such particles are not resistant to void nucleation. A third heat was prepared in which titanium additions were made to getter the sulfur as particles of titanium carbosulfide. This heat was prepared by vacuum induction melting followed by vacuum arc remelting at Carpenter Technology. US steel's research center has rolled this material to one half inch plate and to sheet.
- Have obtained the hardness, Charpy impact energy and all tensile properties including the uniform elongation as a function of annealing temperature for the four alloys being used to assess the effect of mixed microstructures on mechanical behavior and formability. We have found that for certain annealing temperatures for all four of these alloys there are certain annealing temperatures which have a very high uniform elongation which is characteristic of a high work hardening capacity and good formability.
- For the heat prepared to getter the sulfur as particles not resistant to void nucleation we have determined the inclusion volume fraction, sizes and spacings and chemistry. These sulfides were primarily calcium sulfide. Void generation studies were carried out and it was found these inclusions were not resistant to void nucleation. In addition, the Charpy impact energy and tensile properties were determined. It is felt that this heat can be used as the material with inclusions not resistant to void nucleation.

Future Directions

- Need to complete our study of the effect of annealing temperature on the tensile properties of the four alloys being used to assess the effects of complex microstructures on mechanical behavior and formability.
- Need to determine the microstructures developed in the four alloys being used to assess the effect of complex microstructures on formability as a function of annealing temperature.
- Need to quantify the sulfide type in the third heat prepared in an attempt to produce a material in which the sulfur is gettered as particles of titanium carbosulfide. We believe this third heat should be successful in gettering sulfur as particles of titanium carbosulfide because we have made such heats previously at Carpenter Technology and these heats were successful. Then we need to determine the inclusion volume fraction, inclusion size and spacing for this heat. Then we need to carry out a study of void nucleation for this heat.
- Need to carry out studies of formability using the sheet material produced for the six heats.

Introduction

The purpose of this work is to examine the effects of heat treatment and composition on the microstructure and mechanical properties of high strength steels with the ultimate goal of producing microstructures which would have ultimate tensile strengths of at least 1200 MPa and which would be suitable for use in automotive applications, especially for steel sheet to be used in forming operations.

There are several factors to consider in assessing the formability of steel. The first is that the work hardening capacity and characteristics be sufficient to ensure formability in the sense that strain localization and/or local thinning does not take place in the forming process; thus, the strains which can be tolerated prior to local thinning increase with work hardening rate[1]. The uniform strain is often taken as measure of this characteristic, thus high uniform strains are desired in steels which are intended for applications in which they must be formed. The second is that the material has sufficient ductility that fracture does not take place during the forming operation. The latter characteristic is important because it has been found that as the strength levels of steels for forming applications are increased there is a tendency for fracture to take place before the forming operation is complete, at least for some forming operations[2-7]. Thus, not only are the work hardening characteristics important, in that the work hardening rates should be high and remain high even at large strains, but that resistance to fracture should also be high. Thus in assessing sheet materials for forming using a tensile test, one would want both high uniform strains and high true strains to fracture. That is, the behavior of the material after necking is also of importance. Coupled with the requirements for high formability there are interests in steels of higher strength in order to reduce weight and the ability of the structures produced of these materials to absorb energy under impact conditions [8].

Our approach is strongly influenced by two papers concerning transformation induced plasticity (TRIP) [2-5, 9-15] steels developed for steel sheet applications. These TRIP steels contain several microstructure features, including ferrite, bainite, martensite, and retained austenite which, through control of composition and heat treatment, is mechanically stable. In the TRIP steels developed for sheet applications it is believed that the carefully controlled transformation of the retained austenite to a high carbon martensite during deformation is critical to achieving high rates of work hardening and high uniform strains which are important to good formability. The first paper is a note by Bhadeshia[16] which was inspired by a paper by Jacques et al[17]. Jacques et al found that one could obtain excellent uniform elongations in multiphase steels which did not contain silicon or aluminum to promote the existence of mechanically stable retained austenite which is free from carbide formation. Badheshia suggested, based on these results, that the 8 to 15 volume % retained austenite commonly found in TRIP steels contributed about 2% to a total uniform elongation of say 25%. Badheshia suggested that the high work hardening rates in the multiphase steels typical of TRIP steels might be instead due to a mixture of soft and hard phases. In his discussion, Badheshia suggested that the high work hardening rates might be associated with initial deformation of the ferrite which would not work harden at a high rate but at some point the as-quenched martensite in the microstructure would start to deform and the high work hardening rate of the as-quenched martensite is what determines the high work hardening rate of the structure and the high uniform elongations. (The high work-hardening rate of as-quenched martensite is related to not only the distribution of the carbon [18] in the martensite but also, we believe, to the amount of retained austenite in the as-quenched martensite). The second paper is one by Lee et al [19] in which void generation in multi-phase steels was investigated. They found that voids are generated during plastic deformation not only at inclusions and carbide particles but at interfaces between strong and weak microstructural elements; for example, voids could be generated at interfaces between ferrite and martensite. The rate at which voids are formed during deformation can have important consequences in terms of tensile ductility and possibly on formability. The slower the rate at which voids are generated can improve tensile ductility. The rate of void generation will be influenced by the rate at which the volume fractions of voids increases and by the strain

at which voids are nucleated. The goals would be to minimize the volume fraction of voids at each point of the deformation process and to make void nucleation as difficult as possible.

As a consequence of these observations, we view the proposed work to be primarily an examination of the effects of complex, multiphase microstructures on strength, work hardening behavior, and ductility or toughness. In the end, of course, the objective would be to examine the formability of such steels, particularly in applications where ductility as measured by say, the true strain to fracture in a tensile test, or toughness, are important. Two microstructures will be examined: dual phase steels in which we can control (through control of heat treatment and composition) the amounts of ferrite, martensite and retained austenite, and TRIP steels. Thus, we would be examining the effects of mixtures of ferrite and martensite or of ferrite and bainite on mechanical behavior. In both systems we have the possibility of introducing different amounts of retained austenite. In this work we will adhere to one melt practice and aim to maintain a constant inclusion type(s) and inclusion volume fraction. We also propose a separate study of the effect of inclusion resistance to void nucleation on formability. We have found that by getting the sulfur as particles of titanium carbosulfides one can increase the fracture toughness and Charpy impact energy in some steels by more than a factor of two [20,21]. This is because the particles of titanium carbosulfide are very resistant to void nucleation [20, 21]. It is our thesis that by getting the sulfur as particles of titanium carbosulfide one can improve the toughness of steels used in automotive sheet which would improve energy absorption in a crash and that one can also improve formability by making the inclusions very resistant to void nucleation [22-24].

Objectives

The primary objective of this work is to understand the effects of complex, multi-phase microstructures on the mechanical properties of such steels. Specifically, we are assessing the effect of ferrite in combination with either a martensitic structure or with a bainitic microstructure on mechanical properties. We will be comparing the properties of bainitic structures and martensitic structures that contain the same amounts of ferrite. Furthermore, at each ferrite level the bainitic and martensitic structures should have very similar strength levels. The mechanical properties of interest will be the tensile properties, including strength, work hardening behavior, the associated uniform strain, the tensile ductility, which is taken as the true strain to fracture. An important issue is the strain to fracture after reaching the uniform strain. Also, the toughness of the microstructures will be assessed and formability assessed, primarily for forming operations in which ductility and or toughness appears to be an issue. This work will be done using materials which should have the same inclusion characteristics.

To obtain these mixed microstructures consisting of martensite and ferrite we have begun by annealing the steels selected for this work over a wide range of temperatures to obtain mixtures of ferrite and austenite and then quench so that the austenite remaining would transform to martensite. To obtain the mixed microstructures of lower bainite and ferrite we will begin again by annealing over a wide range of temperatures to obtain mixtures of ferrite and austenite and then quench to a temperature above the martensite start temperature to transform as much of the austenite to lower bainite as possible.

In addition, we will explore the effect of the void nucleation resistance of inclusions on tensile properties and toughness of low-alloy martensitic steel and assess the effect of inclusion void nucleation resistance on formability.

Chemistries and Processing of the Experimental Heats

Heats of the four compositions selected to examine the effects of multi-phase microstructures have been prepared and worked to one half inch plate and to sheet. These general compositions of the four materials are MP1, MP2, MP3, and MP4. The specific heat designations for these four heats are D, B, C and A, respectively. All four of the heats contain about 0.2 wt. % carbon and 4 wt. % manganese. Heat D contains no addition of aluminum or silicon while heat B contains an addition of 1.5 wt. % aluminum, heat C contains an addition of 1.5 wt. % silicon and heat A contains an addition of 3 wt. % silicon. In addition it was our goal to prepare two low alloy heats in which one heat would contain sulfide particles not resistant to void nucleation; this would be the composition M1 in Table 1. Heat E was melted and found to contain calcium sulfide particles not resistant to void nucleation. The composition M2 was intended to be identical to heat M1 except that in the composition M2 the sulfur would be gettered as particles of titanium carbosulfide and would be resistant to void nucleation. However, our first and second heats of the M2 composition were unusable as the sulfur was gettered in both heats as particles of calcium sulfide. We have prepared a third heat of the M2 composition. We believe that in this heat, heat H in Table 1, the sulfur will have been gettered as particles of titanium carbosulfide. This remains to be determined however. All of these heats, except for heat H, were melted by vacuum induction melting at the US Steel research center. All heats were worked to one half inch plate and sheet at the US Steel research center.

Table 1. Compositions of Experimental Heats in wt. %

Alloy	Heat ID	C	Mn	Ni	Cr	Mo	Ti	Al	Si	P	S	O ₂	N ₂
MP1	D	0.188	3.84	<0.002	0.01	0.002	<0.002	0.021	0.015	0.005	0.0037	0.0021	0.0041
MP2	B	0.183	3.73	<0.002	0.01	0.021	<0.002	1.437	0.021	0.005	0.0024	0.0033	0.0041
MP3	C	0.197	4.22	<0.002	0.011	0.003	<0.002	0.030	1.46	0.005	0.0031	0.0013	0.0056
MP4	A	0.205	4.27	<0.002	0.010	0.003	0.002	0.033	2.84	0.004	0.0025	0.0027	0.0055
M1	E	0.180	0.49	3.01	0.98	0.24	<0.002	0.031	1.98	0.003	0.0027	0.0015	0.0018
M2	F	0.158	0.007	2.93	0.97	0.25	0.038	0.025	1.95	0.002	0.0034	0.0013	0.0014
M2B	G	0.15	-	3	1	0.25	0.025	-	-	-	-	-	-
M2C	H	0.15	-	3	1	0.25	0.025	-	-	-	-	-	-

Results for the Multi-Phase Alloys

Our first step was to anneal all of the four alloys at temperatures for which we believed the alloys would be completely austenitic and for temperatures for which we believed the annealing temperature would be in the two phase, $\alpha+\gamma$, field. To do this we began with using Thermo-Calc to determine the phase diagrams relevant to our compositions. The Thermo-Calc results were supplemented by determinations of the austenite start temperatures, austenite finish temperatures and Martensite start temperatures which were done by heating and cooling samples in a Gleeble at the US Steel research center.

Based on these results we selected a series of annealing temperatures for each alloy. The annealing temperatures selected were as follows. For the alloy D the temperatures selected were 900°C, 800°C, 780°C, 760°C, 740°C, 720°C, 700°C, 680°C and 660°C. For the alloy C, which contains 1.5 wt. % silicon, the temperatures selected were 950°C and then temperatures from 900°C to 660°C in steps of 20°C. For the alloy A, which contains 3 wt. % silicon, the temperatures selected were 1000°C, 950°C and then temperatures from 900°C to 700°C in steps of 20°C. For the alloy B, which contains 1.5 wt. % aluminum, the temperatures selected were 1000°C, 950°C and then temperatures from 920°C to 740°C in steps of 20°C. It is believed that at higher temperatures selected for each alloy the structures would be completely austenitic and the structures achieved after quenching from these higher temperatures would

be completely Martensitic. After an annealing treatment the samples were oil quenched and then tempered at 200°C to make any retained austenite as mechanically stable as possible. Our objective was then to determine for each alloy and the selected annealing temperatures the microstructure, the hardness, the Charpy impact energy and the tensile properties.

The Rockwell A hardness is plotted as a function of annealing temperature for the four alloys in Figure 1.

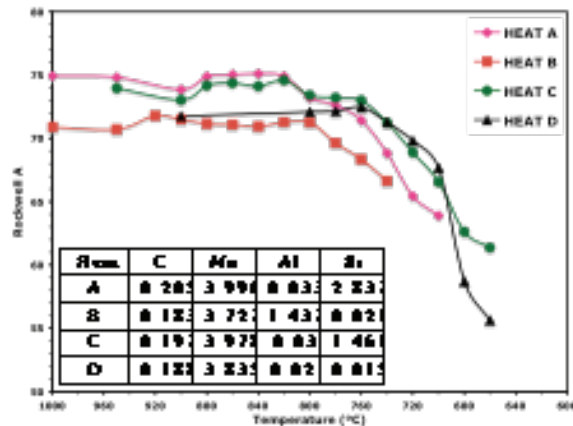


Figure 1. The Rockwell A hardness plotted as a function of annealing temperature for the four multi-phase alloys.

For all four alloys the hardness remains relatively constant as the annealing temperature is decreased until the annealing temperature reaches a critical value which depends on the composition. Once the annealing temperature is reduced to below a certain temperature the hardness decreases with decreasing annealing temperature.

The Charpy impact energy is plotted as a function of annealing temperature for the four multi-phase alloys in Figure 2.

The Charpy impact energy of alloy D which is not modified by silicon or aluminum additions is about 57 J for annealing temperatures from 900°C to 760°C. However, the Charpy impact energy decreases as the annealing temperature is lowered and reaches a minimum of 26 J after annealing at 720°C. The Charpy impact energy increases as the annealing temperature is decreased further. The fracture surfaces of the Charpy impact specimens of alloy D obtained for annealing temperatures of 900°C through 700°C indicate a predominantly quasi-cleavage and/or cleavage fracture mode.

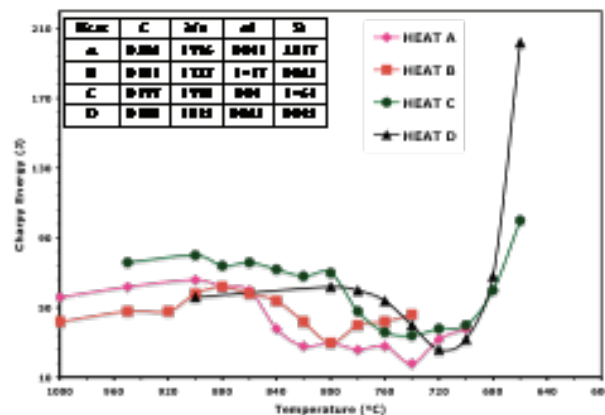


Figure 2. The Charpy impact energy of the four multi-phase alloys plotted as a function of annealing temperature.

The Charpy impact energy of alloy C which contains 1.5 wt. % silicon is 80 J after annealing at 900°C. At this temperature the alloy should be completely austenitic and the microstructure after quenching and tempering should be lath martensite with a small amount of retained

austenite. The Charpy impact energy then decreases with decreasing annealing temperature and reaches a minimum of 34 J on annealing at 740°C. The Charpy impact energy increases with decreasing annealing temperature as the annealing temperature is further decreased. The fracture mode of alloy C after annealing at 900°C was ductile as was the fracture mode after annealing at 800°C. As the annealing temperature is decreased to 780°C the fracture mode is mixed, being primarily ductile but some regions of quasi-cleavage fracture. As the annealing temperature is decreased further the fracture mode is always mixed with regions of both ductile fracture and quasi-cleavage fracture. After annealing at 740°C where the Charpy impact energy was at a minimum the fracture mode was primarily quasi-cleavage but there were regions of ductile fracture.

The Charpy impact energy of alloy B which contains 1.5 wt. % aluminum is 42 J and 48 J, after annealing at 1000°C and 950°C, respectively. The austenite finish temperature for this alloy was about 935°C so after annealing at 1000°C and 950°C the microstructure of this alloy should be martensitic with a small amount of retained austenite. For annealing temperatures from 900°C to 840°C the Charpy impact energies were about 57 J. These annealing temperatures are all below the austenite finish temperature so the microstructures should consist of martensite and some ferrite. All of these Charpy impact energies are greater than the Charpy impact energies achieved after annealing at 1000°C and 950°C. The Charpy impact energy decreases after annealing at 820°C and reaches a minimum of 30 J on annealing at 800°C. As the annealing temperature is decreased further the Charpy impact energy increases with decreasing annealing temperature. The fracture surfaces of alloy B for all annealing temperatures from 1000°C to 800°C where the Charpy impact energy reached a minimum of 30 J contained regions of both ductile fracture and of quasi-cleavage fracture. The maximum Charpy impact energy for alloy B was after annealing at 880°C and it was 62 J and it was for this annealing temperature that the amount of quasi-cleavage fracture was the smallest.

The Charpy impact energy of alloy A which contains 3 wt. % silicon was 66 J after annealing at 900°C. The Charpy impact energy decreases with decreasing annealing temperature and reaches a minimum of 18 J after annealing at 740°C. Annealing at lower temperatures results in increases in the Charpy impact energy. The fracture mode for Charpy impact specimens annealed at 900°C exhibited ductile fracture. The fracture mode exhibited for lower annealing temperatures were not ductile and seemed to be a form of very fine scale quasi-cleavage fracture.

In terms of Charpy impact toughness all four of these alloys exhibit reasonable toughness on annealing at the highest temperatures. However, all four alloys exhibit similar behavior in that the Charpy energy decreases as the annealing temperature is decreased and reaches a minimum value at some annealing temperature and then as the annealing temperature is further decreased the Charpy impact energy begins to increase with decreasing annealing temperature. Further, the fracture surfaces associated with the minimum Charpy impact energies were characterized by quasi-cleavage fracture or a fracture which exhibits a mixture of quasi-cleavage and some ductile fracture. The effect of annealing temperature on the Charpy impact energy and fracture mode was qualitatively the same for all four of the alloys. At this point we do not understand the microstructural origins for the effect of annealing temperature on the Charpy impact energy. This effect of annealing temperature on the Charpy impact energy is very similar to the effect of annealing temperature on the true strain to fracture obtained for the tensile specimens.

The tensile properties of the four multi-phase alloys are plotted as function of annealing temperature in Figures 3 through 6. In [Figure 3](#) the yield strengths are plotted as a function of annealing temperature. In [Figure 4](#) the ultimate tensile strengths are plotted as a function of annealing temperature. In [Figure 5](#) the true strains to fracture are plotted as a function of annealing temperature. In [Figure 6](#) the uniform strains are plotted as a function of annealing temperature.

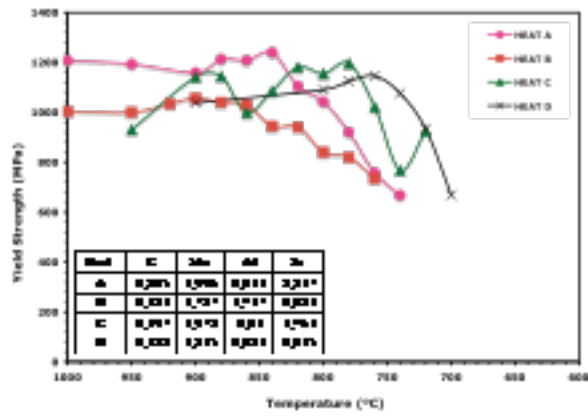


Figure 3. The yield strengths of the four multi-phase alloys plotted as a function of annealing temperature.

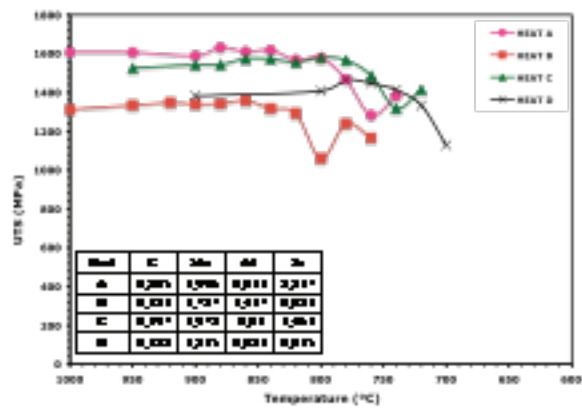


Figure 4. The ultimate tensile strengths of the four multi-phase alloys plotted as a function of annealing temperature

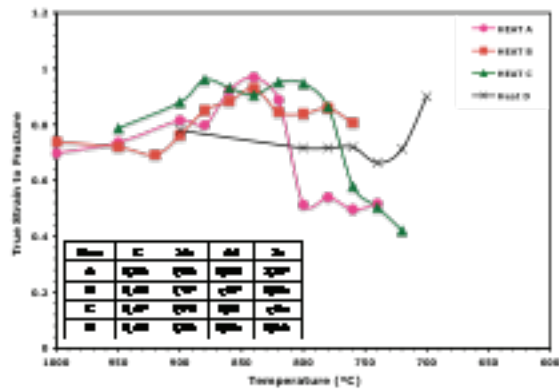


Figure 5. The true strain to fractures of the multi-phase alloys plotted as a function of annealing temperature.

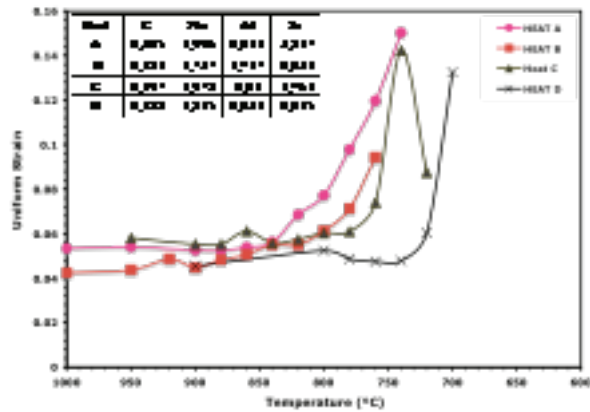


Figure 6. The uniform strains of the four multi-phase alloys plotted as a function of annealing temperature.

The most important results given in Figures 3 through 6 are the following. For all four alloys, there is an annealing temperature at which there is a maximum in the uniform strain. Usually the uniform strain can be taken as a measure of the work hardening capacity. Therefore one would expect these alloys to exhibit their best formability at the annealing temperatures at which the uniform strains are a maximum. The maximum uniform strains are at annealing temperatures at which the ultimate tensile strength is still relatively high. However, the annealing temperatures at which the maximum uniform strains are the highest tend to be annealing temperatures at which the true strains to fracture and the Charpy impact energy are low. However, the high maximum uniform strains achieved for the three multi-phase alloys A, D and B, the three multi-phase alloys alloyed with silicon or aluminum, are observed at ultimate tensile strengths ranging from 1200 MPa to almost 1400 MPa which suggests these three alloys when annealed at the temperature at which the uniform strain is a maximum might have good formability at these strength levels.

Results Obtained for Effects of Void Nucleation Resistance

The two alloys first prepared to investigate the effect of void nucleation resistance of inclusions on formability and toughness were alloys E and F. Alloy E contained 0.5 wt. % manganese and it was anticipated the sulfides in this heat would be MnS and particles of MnS are not resistant to void nucleation. The alloy F contained no manganese but was modified by an addition of 0.04 wt. % titanium and it was anticipated that the sulfides in this heat would be particles of titanium carbosulfide which are resistant to void nucleation. These alloys were heat treated by austenitizing at 900°C, oil quenching and then tempering at 200°C. Alloy E had a yield strength of 1086 MPa, an ultimate tensile strength of 1401 MPa, a true strain to fracture of 0.99 and a Charpy impact energy of 124 J. Alloy F had a yield strength of 1111 MPa, an ultimate tensile strength of 1404 MPa, a true strain to fracture of 1.08 and a Charpy impact energy of 113 J. The inclusions in both heats were analyzed. The sulfides in heat F were found to be calcium sulfides. The study of void nucleation in heat E showed that voids were nucleated in a tensile specimen at a true stain of about 0.3 which is lower than the void nucleation strain when the sulfur is gettered as particles of manganese sulfide [20]. Thus heat E seems to be a reasonable material to use when the resistance to void nucleation at the inclusions is low. Heat F was found to contain not titanium carbosulfides but calcium sulfides as was the case for heat G. We have made a fourth heat, heat H, in which it is believed the sulfur will be gettered as particles of titanium carbosulfide. We have just begun to collect mechanical property and inclusion data for this heat.

Conclusions

At this point it would appear that each of multi-phase alloys exhibits a peak in the uniform strain at some annealing temperature. The microstructures of greatest interest from the standpoint of improved formability at high strength levels would be the microstructures associated with this peak in the uniform strain. Our intention is complete the study in order to precisely determine the temperature at which the uniform is a maximum for each of the alloys and then to try to quantify the microstructures for the annealing temperatures where the maximum uniform strains are observed for each of the alloys.

While we still believe strongly that strong void nucleation resistance will result in high toughness sheet steels and improved formability we need to prove this. We have a good heat in which the inclusions are not resistant to void nucleation. However, we need to characterize the most recent heat in which we have attempted to get the sulfur as particles of titanium carbosulfide. It is believed this heat will prove successful but we need to characterize this heat from the standpoint of mechanical properties and inclusion type and volume fraction and to then carry out for this heat a study of void nucleation at the inclusion particles.

Presentations/Publications/Patents

Warren M. Garrison, Jr., A Discussion of the Effects of Gettering Sulfur as Particles as Particles of Titanium Carbosulfide on toughness, Ductility and Formability, Presented at the US Steel research and Technology Center, April 20, 2009, Pittsburgh, PA.

Warren M. Garrison Jr., A Study of the Effects of Microstructure on the Mechanical Properties and Failure Mechanisms of Advanced High Strength Steels, Presented at the AISI review of projects on Advanced High Strength Steels, May 12, 2009.

Warren M. Garrison Jr., Anthony Rollett and Aditya Aryasomayajula, The Effects of Annealing in the $\alpha+\gamma$ Field on the Tensile Properties and Charpy Impact Energy of a 0.2C-4Mn Steel With and Without Aluminum and Silicon Additions, Poster Presentation at the 2009 NSF Engineering Research and Innovation Conference, Honolulu, Hawaii, June 21-26, 2009.

Warren M. Garrison Jr., Anthony Rollett and Aditya Aryasomayajula, The Effects of Annealing in the $\alpha+\gamma$ Field on the Tensile Properties and Charpy Impact Energy of a 0.2C-4Mn Steel With and Without Aluminum and Silicon Additions, Conference Proceedings of the 2009 NSF Engineering Research and Innovation Conference, Honolulu, Hawaii, June 21-26, 2009.

References

W.F. Hosford and R.M. Caddell. *Metal Forming: Mechanics and Metallurgy*, Prentice-Hall, Englewood Cliffs, N.J., 1983, p. 299.

K. Sumimoto, J. Sakaguchi, T. Iida and T. Kashima, Stretch-flangeability of High-strength TRIP Type Bainitic Sheet Steel, *ISIJ international*, Vol. 40, 2000, p. 920.

K. Sumimoto, A. Kanda, R. Kikuchi, S. Hasimoto, T. Kashima and S. Ikeda, Ductility and Formability of Newly Developed High Strength Low Alloy TRIP-aided Sheet Steels with Annealed Martensite Matrix, *ISIJ international*, Vol. 42, 2002, p.910.

K. Sugimoyo, B. Yu, Y. Mukai and S. Ikeda, Microstructure and Formability of Aluminum Bearing TRIP-Aided Steels with Annealed Martensite Matrix, *ISIJ international*, Vol. 45, 2005, p.1194.

- K. Yamazaki, M. Oka, H. Yasuda, Y. Mizuyama and H. Tsuchiya, Recent Advances in Ultrahigh-Strength Sheet Steels for Automotive Structural Use, Nippon Steel Technical Report No. 64, January 1995, p. 37.
- Y.J. Park, A.P. Coldren and J.W. Morrow, Effect of Martensite Bands and Elongated Manganese Sulfide Inclusions on the Formability of Dual-Phase Steels, Proceedings on the Conference on the *Fundamentals of Dual Phase Steels*, held at Chicago, 1981, p. 485.
- A. Nishimoto, Y. Hosoya and K. Nakaoka, Relation Between Hole Expansion Formability and Metallurgical Factors in Dual-Phase Steel Sheets, Proceedings on the Conference on the *Fundamentals of Dual Phase Steels*, held at Chicago, 1981, p.447.
- C.D. Horvath and J.R. Fekete, Opportunities and Challenges for Increased Usage of Advanced High Strength Steels in Automotive Applications, International Conference on Advanced High Strength Sheet Steels for Automotive Applications Proceedings, Winter Park, Colorado, 2004, p.3.
- J. Van Slycken, P. Verleysen, J. Degrieck, L. Samek and B.C. De Cooman, High-Strain-Rate Behavior of Low-Alloy Multiphase Aluminum and Silicon Based Transformation Induced Plasticity Steels, Metall. and Mat. Transactions A, Vol. 37A, 2006, p. 1527.
- S. Traint, A. Pichler, K. Hauzenberger, P. Stiaszny and E. Werner, Influence of Silicon, Aluminum Phosphorus and Copper on the Phase Transformations of Low Alloyed TRIP Steels, Steel Research, Vol. 73, 2002, p. 259.
- T. Lung, J. Drillet, A. Couturier and C. Olier, Detailed Study of the Transformation Mechanisms in Ferrous TRIP Aided Steels, Steel Research, Vol. 73, 2002, p. 218.
- H. Matsuda, F. Kitano, K. Hasegawa, T. Urabe and Y. Hosoya, Metallurgy of Continuously Annealed High Strength TRIP Steel Sheet, Steel Research, Vol. 73, 2002, p. 211.
- B. Ehrhardt, T. Gerber and T.W. Schaumann, Approaches to Microstructural Design of TRIP and TRIP Aided Cold Rolled High Strength Steels, International Conference on Advanced High Strength Sheet Steels for Automotive Applications Proceedings, Winter Park, Colorado, 2004, p.39.
- K. Sugimoto, S. Hashimoto and S. Ikeda, Ultra High Strength Low Alloy TRIP-Aided Sheet Steels With Bainitic Ferrite Matrix, International Conference on Advanced High Strength Sheet Steels for Automotive Applications Proceedings, Winter Park, Colorado, 2004, p.63.
- Y.R. Cho, S.K. Kim, H.N. Han, Y.S. Jin and J.H. Jung, Development of Hot Rolled High Strength TRIP Steel With a Tensile Strength of 780MPa Grade, International Conference on Advanced High Strength Sheet Steels for Automotive Applications Proceedings, Winter Park, Colorado, 2004, p.71.
- H.K.D.H. Bhadeshia, TRIP-Assisted Steels?, ISIJ international, Vol. 42, 2002, p.1059.
- P.J. Jacques, E. Girault, Ph. Harlet and F. Delannay, The Developments of Cold-rolled TRIP-assisted Multiphase Steels. Low Silicon-assisted Multiphase Steels, ISIJ international, Vol. 41, 2001, p. 1061.
- M. Saeglitz and G. Krauss, Deformation, Fracture, and Mechanical Properties of Low-Temperature-Tempered Martensite in SAE 43xx Steels, Metall. and Mat. Transactions A, Vol. 28A, 1997, p.377.

S.B. Lee, J.G. Speer and D.K. Matlock, The Influence of Phase Distributions and Interfaces on Fracture and formability of High Strength Sheet Steels, International Conference on Advanced High Strength Sheet Steels for Automotive Applications Proceedings, Winter Park, Colorado, 2004, p. 383.

J. L. Maloney and W.M. Garrison Jr., The Effect of Sulfide Type on the Fracture Behavior of HY180 Steel, Acta Materialia, Vol. 53, 2005,p. 533.

L.E. Iorio and W.M. Garrison Jr., The Effects of Titanium Additions on AF1410 Ultra-high Strength Steel. Metallurgical and Materials Transactions A, Vol. 37A, 2006, p. 1165.

Z. Narciniak and K. Kuczynski, Limit Strains in the Processes of Stretch-Forming Sheet Metal, Int. J. Mech. Sci. Vol. 9, 1967, p. 609.

J.H. Schmitt and J.M. Jalinier, Damage in Sheet Metal Forming-I. Physical Behavior, Acta Metall.,Vol. 30, 1982, p. 1789.

J.H. Schmitt and J.M. Jalinier, Damage in Sheet Metal Forming-II. Plastic Instability, Acta Metall.,Vol. 30, 1982, p. 1799.

O. Advanced High Strength Steels: Development of Novel Finite Element Simulation Tools that Implement Crystal Plasticity Constitutive Theories Using an Efficient Spectral Framework

Principal Investigator: Surya R. Kalidindi
Drexel University
Department of Materials Science and Engineering;
Philadelphia, PA 19104
(215) 895-1311; e-mail: skalidin@coe.drexel.edu

Technology Area Development Manager: William Joost
(202) 287-6020; e-mail: william.joost@ee.doe.gov

Contractor: Drexel University
Contract No.: National Science Foundation Award CMMI 0727931

Objective

- Develop spectral crystal plasticity based finite element tools for simulating deformation processing operations and final mechanical performance of AHSS components. A salient feature of these tools is that they can be executed with computational times that are comparable to the tools currently used by the industry, which largely employ phenomenological material models.
- Systematically introduce the inherent complexities of the physics of plastic deformation at multiple length scales in the spectral crystal plasticity framework. The goal is to start with crystallographic slip and then proceed to deformation twinning. From the perspective of length scales, the goal is to start with grain-scale deformation and then proceed to incorporating explicitly the mechanics of dislocation networks.
- Develop computationally efficient spectral approaches for higher-order homogenization theories that utilize local spatial correlations for a rigorous quantification of the interactions at the lower length scales in the material.
- Critical validation of the tools and methodologies developed in this work by comparisons with experiments and numerical predictions obtained by other approaches.

Approach

- Capture solutions at the lower length scales in an efficient spectral database. Although building the database requires substantial effort, it is a one-time activity. Once an appropriate database is built, all subsequent computations requiring solutions at the lower length scales can be accomplished with minimal computational effort and resources.
- Explore the use discrete Fourier transforms (DFTs) for building such databases, as they offer tremendous computational efficiency.

Accomplishments

- In last year's effort, we have demonstrated that it is possible to speed up the crystal plasticity calculations in cubic metals that deform by crystallographic slip by two orders of magnitude using a compact database of DFTs. In the current year, we have extended this framework to include elastic deformations (in addition to purely plastic deformations considered before) and have developed an analytical Jacobian needed for the development of a UMAT in ABAQUS. We are currently now implementing all of these new developments from our work into a new spectral crystal plasticity UMAT that is expected to be several orders of magnitude faster than any of the ones being used today.
- In last year's effort, we have formulated a new spectral for capturing higher-order structure-performance-structure evolution linkages at the lower length scales. In this year's effort, we have demonstrated the accuracy of this new approach to plastic deformation in a two-phase composite. Furthermore, we have demonstrated that this approach produces linkages that can be executed with minimal computational resources that are orders of magnitude lower than what is required to produce the same results from a micro-mechanical finite element model.

Future Direction

- Demonstrate the implementation of spectral crystal plasticity tools developed for metals deforming by crystallographic slip in a finite element code used in simulating metal forming operations. In particular we will focus our efforts on DEFORM and ABAQUS.
- Extend the spectral linkages to incorporate deformation twinning and phase transformations.
- Extend the spectral linkages to include grain-scale interactions using our newly developed framework.

Introduction

Crystal plasticity theories [1-6] are used extensively in understanding and predicting the evolution of the underlying microstructure (mainly texture related aspects) and the concomitant anisotropic stress-strain response in polycrystalline metals subjected to finite plastic strains. Such physics-based constitutive theories are highly desirable for conducting more accurate simulations of various metal manufacturing/fabrication processes, since they provide better understanding and predictions of the material behavior [7-9]. The crystal plasticity computations, however, typically demand significant computational resources because of the low value of strain rate sensitivity parameter in the rate-dependent crystal plasticity formulations [1] (which makes the resulting system of algebraic equations numerically extremely stiff). Moreover, in any simulation of a forming operation on polycrystalline metals, the same set of stiff equations needs to be solved for a large number of constituent grains at every integration point in the finite element mesh for every trial time step. This is the main deterrent in implementing the crystal plasticity models in finite element modeling framework for simulating deformation processing operations typically employed by the metal working industry.

In recent work [10-11], we have developed computationally efficient representations for the essential functions capturing the solutions to the conventional crystal plasticity theory in fcc metals subjected to arbitrary deformation paths. More specifically, we have built new Discrete Fourier Transforms (DFTs)-based spectral databases for the stresses, the $\sigma'_{ij}(\mathbf{g}, \mathbf{L})$, lattice rotations $\mathbf{W}_{ij}^*(\mathbf{g}, \mathbf{L})$, and the total slip rate $\sum_{\alpha} |\dot{\gamma}^{\alpha}|(\mathbf{g}, \mathbf{L})$, where \mathbf{g} is the crystal lattice orientation and \mathbf{L} is the applied velocity gradient tensor. In any given time step in the simulation of the

deformation process, these functions are then used to compute all of the needed microscale and macroscale field quantities that would be typically computed by the traditional crystal plasticity approach. The domain of these functions was defined to be the product space comprising all possible crystal orientations and all possible isochoric deformation modes.

In this work [12], we have developed a new spectral database for deformation of BCC metals with 48 slip systems (which is much higher than the 12 slip systems operating in fcc metals). We found that only a limited number of the dominant DFTs were adequate to recover the functions of interest on their entire respective domains. More interestingly, we noticed that the new DFT-based spectral database for BCC crystals is more compact compared to our earlier FCC database. Furthermore, we demonstrate in this work the use of these databases in the fast computation of yield surfaces predicted by the Taylor-type model for polycrystalline cubic metals.

Development of higher-order models requires a more sophisticated approach that partitions the imposed deformation on the polycrystal to each of the constituent grains while taking into account the details of its neighborhood. With the goal of extending the spectral crystal plasticity framework to include details at lower length scales as well as higher-order interactions, we have formulated a novel spectral approach for addressing the localization relationship among the constituent grains. In this report, we have demonstrated the applicability of this new approach by successfully applying it to a two-phase composite undergoing plastic deformation.

Spectral Databases for BCC metals

Following the approach described in our earlier work [13-14], we have developed a new spectral database for deformation of BCC metals with 48 slip systems [12]. The families of potential slip systems for the BCC crystals were assumed to include $[110] \langle 111 \rangle$, $[112] \langle 111 \rangle$, and $[123] \langle 111 \rangle$. It is typically observed that only a small fraction of the DFTs are numerically significant compared to the others. The numbers of numerically significant DFTs (henceforth referred to as dominant DFTs) varied for the different field variables. For example, it has been found that the average error when using 500 dominant DFTs was less than 2% for all of the functions involved. It was also observed that the errors for the DFT-based spectral databases for BCC metals were lower than the corresponding errors reported in our earlier work on FCC metals [10]. We attribute the more compact representation of the functions for BCC crystals to the availability of many more potential slip systems, compared to the FCC crystals. The availability of the larger number of slip systems results in the functions of interest becoming more uniform in their respective domains, and therefore needs lesser numbers of dominant DFTs to achieve the desired accuracy.

The new BCC spectral database developed here was validated by comparing the predictions of the stress-strain curves and the deformed textures against the corresponding predictions from the classical Taylor-type model for different deformation processes with different initial textures. As an example, the predicted texture and stress-strain curves for a polycrystalline IF steel deformed by simple shear to a shear strain of $\gamma = 0.6$ using the conventional Taylor-type model and the newly developed DFT spectral approach in this work are shown in Figure 1. The initial texture in the sample was captured using a set of 1200 discrete crystal orientations [15]. The DFT-based predictions used 500 dominant DFTs for the stress, the shearing rate, and the lattice spin components. It is clear that the DFT-based databases developed here for BCC crystals produce excellent predictions, and these are obtained at a significant faster computational speed. The simulation time was 130 s for the conventional Taylor-type calculations, and only 2.9 s for the spectral approach using dominant DFTs. All of the computations reported in this work were performed on a regular Pentium 4 desktop PC.

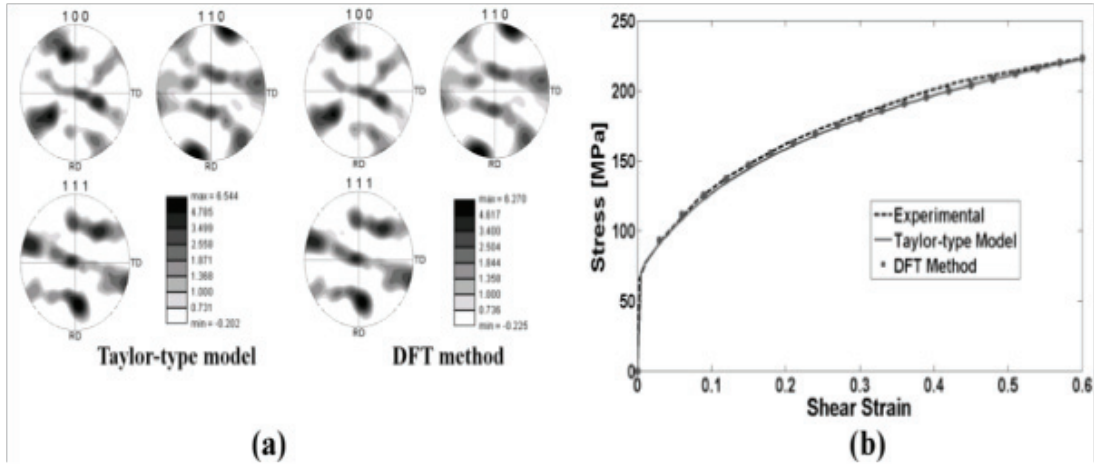


Figure 1. Comparison of the predictions from the spectral method (using 500 DFTs for the stress, the shearing rate, and the lattice spin components) against the corresponding predictions from the conventional Taylor-type model for simple shear of IF steel: (a) pole figures, and (b) stress-strain curves, including the experimental result [15].

Computation of Yield Surfaces

The delineation of the anisotropic yield surface in stress space using the Taylor-type crystal plasticity theories is computationally very expensive. We describe here a new efficient method for the fast computation of the yield surface in the five-dimensional deviatoric stress space using the DFT-based databases for both FCC and BCC metals. This new approach exploited our spectral representations of the texture [11](Kalidindi, Knezevic et al. 2009) and the stress function and their orthogonal properties. In this method, the volume-averaged value of the local stress tensor in the constituent crystal of the polycrystalline aggregate was efficiently evaluated using the orthogonal properties of the DFTs as:

$$\bar{\sigma}'_q = s|\dot{\epsilon}|^m \text{sgn}(\dot{\epsilon}) \frac{1}{N_g N_\theta} \sum_{\mathbf{k}} \sum_{\mathbf{n}} \tilde{F}_{\mathbf{k}} C_{\mathbf{k}\mathbf{n}} e^{\frac{2\pi i \mathbf{n} \cdot \mathbf{c}}{N_\theta}} \quad (1)$$

where $\bar{\sigma}'_q$ denotes the components of the volume averaged deviatoric stress tensor for certain deformation mode θ , enumerated by q , $\tilde{F}_{\mathbf{k}}$ and $C_{\mathbf{k}\mathbf{n}}$ denote the DFTs for the orientation distribution function (ODF) and the stress function respectively. It should be noted that the spectral representations of the ODF and the stress functions do not implicitly assume any sample symmetry. Consequently, the yield surface can be constructed for any texture in the sample, without the need to invoke any simplifying assumptions of sample symmetry.

The approach described above has been used successfully to construct the complete five-dimensional yield surface for both FCC and BCC polycrystalline materials at extremely fast computational speeds. Figure 2 represents a selected projection of the five-dimensional yield surface computed here for IF-steel using 500 dominant DFTs. The material was assumed to possess a random texture described by a set of 1000 discrete crystal orientations. In order to check the accuracy of the yield surface, we compare in Figure 3 the $(\sigma_{11}, \sigma_{22})$ section of the IF-steel yield surface computed using 500 dominant DFTs against the one computed using the conventional approach. It is clear that the DFT-based computations are in excellent agreement with the conventional computations.

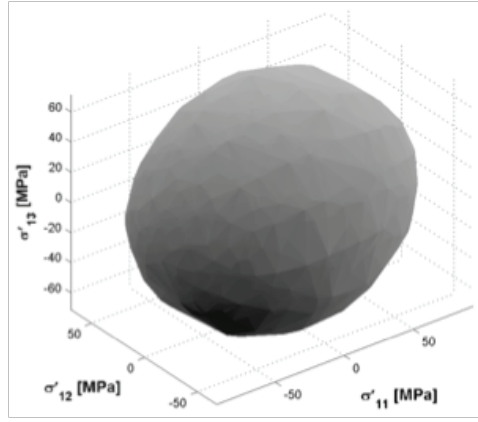


Figure 2. Three-dimensional projection of the yield surface computed using the spectral methods described in this work for IF-steel with a random texture.

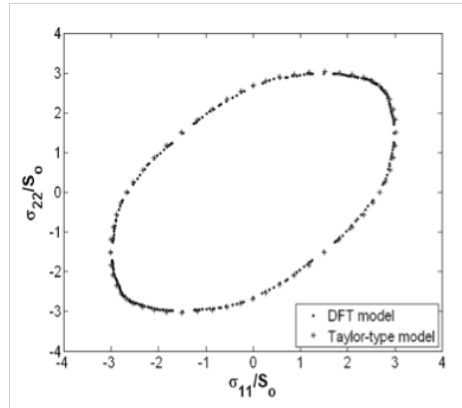


Figure 3. The predicted $(\sigma_{11}, \sigma_{22})$ yield locus for IF-steel using the DFT-based spectral approach and the conventional approach. Both computations are based on the Taylor-type model

Computation of Jacobian

The computation of the Jacobian is required for incorporation of our spectral crystal plasticity approach with any implicit finite element code. The Jacobian matrix is used in a Newton-Raphson iterative method for revising the estimated displacements such that the corresponding stresses are likely to better satisfy the principle of virtual work at the end of the increment. It should be noted the Jacobian matrix plays an important role in the rate of convergence of the solution to the global equilibrium equations, but has no effect on the accuracy of the solution. The Jacobian established here is based on the following definition of the Jacobian in ABAQUS which is required for implementing a “user material” subroutine, UMAT:

$$\mathbf{J} = \frac{\partial \Delta \boldsymbol{\sigma}}{\partial \Delta \mathbf{E}} \quad (2)$$

where $\Delta \boldsymbol{\sigma}$ and $\Delta \mathbf{E}$ are the increments in the stress and strain tensors, respectively.

The deviatoric stress tensor in the spectral approach is defined in the principal frame of the stretching tensor, \mathbf{D} , as

$$\boldsymbol{\sigma}_{rq}^D(\theta, g^p) = s|\dot{\epsilon}|^m \text{sgn}(\dot{\epsilon}) \frac{1}{N_{gp} N_\theta} \sum_k \sum_n C_{kn} e^{\frac{2\pi i k r}{N_{gp}}} e^{\frac{2\pi i n q}{N_\theta}} \quad (3)$$

where θ denotes the deformation mode, and g^p indicates the crystal lattice orientation defined with respect to the principal frame of \mathbf{D} . The stress function can be transformed to the sample frame by a coordinate transformation law for second-rank tensors using a set three Euler angles,

$\mathbf{g}^D = (\varphi_1^D, \Phi^D, \varphi_2^D)$, that describe the eigenvector matrix of \mathbf{D} . We have been able to derive an analytical expression for the Jacobian by expanding it using the chain rule as:

$$\mathbf{J}_{ik} = \frac{\partial \Delta \boldsymbol{\sigma}_i}{\partial \Delta \mathbf{E}_k} = \frac{\partial \boldsymbol{\sigma}_i}{\partial \mathbf{D}_j} \frac{\partial \mathbf{D}_j}{\partial (\mathbf{E}_t)_k} = \quad (4)$$

$$\begin{aligned} & \left[\left(\frac{\partial \boldsymbol{\sigma}_i}{\partial |\mathbf{D}|} \Big|_{\theta, \text{tr}(\mathbf{D}), \varphi_1^D, \Phi^D, \varphi_2^D} \frac{\partial |\mathbf{D}|}{\partial \mathbf{D}_j} \right) + \right. \\ & \left(\frac{\partial \boldsymbol{\sigma}_i}{\partial \text{tr}(\mathbf{D})} \Big|_{\theta, |\mathbf{D}|, \varphi_1^D, \Phi^D, \varphi_2^D} \frac{\partial \text{tr}(\mathbf{D})}{\partial \mathbf{D}_j} \right) + \\ & \left(\frac{\partial \boldsymbol{\sigma}_i}{\partial \theta} \Big|_{|\mathbf{D}|, \text{tr}(\mathbf{D}), \varphi_1^D, \Phi^D, \varphi_2^D} \frac{\partial \theta}{\partial \mathbf{D}_j} \right) + \\ & \left(\frac{\partial \boldsymbol{\sigma}_i}{\partial \varphi_1^D} \Big|_{\theta, |\mathbf{D}|, \text{tr}(\mathbf{D}), \Phi^D, \varphi_2^D} \frac{\partial \varphi_1^D}{\partial \mathbf{D}_j} \right) + \\ & \left(\frac{\partial \boldsymbol{\sigma}_i}{\partial \Phi^D} \Big|_{\theta, |\mathbf{D}|, \text{tr}(\mathbf{D}), \varphi_1^D, \varphi_2^D} \frac{\partial \Phi^D}{\partial \mathbf{D}_j} \right) + \\ & \left. \left(\frac{\partial \boldsymbol{\sigma}_i}{\partial \varphi_2^D} \Big|_{\theta, |\mathbf{D}|, \text{tr}(\mathbf{D}), \varphi_1^D, \Phi^D} \frac{\partial \varphi_2^D}{\partial \mathbf{D}_j} \right) \right] \frac{\partial \mathbf{D}_j}{\partial \Delta \mathbf{E}_k} \end{aligned}$$

We then proceeded to derive an expression for each of the terms in Eq. (4). We have validated our expressions by comparing the values produced from our derived analytical expressions with those computed numerically by slightly perturbing the independent variable in each expression.

We are now ready to proceed with the implementation of the spectral crystal plasticity framework into the finite element code ABAQUS in form of a user material subroutine, UMAT.

Higher-Order Spectral Linkages

The framework described above addresses crystal plasticity for a single crystal. It is easily implemented in a Taylor model for polycrystals where it is assumed that all constituent crystals experience the deformation. However, in most AHSS, there is a need for higher-order models that account for grain interactions. The most successful approach for accurately capturing the grain interactions in a polycrystal involves the use of finite element models. However, this is impractical for simulating forming operation on AHSS, because it would entail executing micromechanical finite element models on representative volume elements of polycrystals at each integration point in the macroscale forming simulation.

In this work we employ a completely different approach to address this challenge. We focus our efforts on developing a new framework for harvesting efficiently the essential knowledge contained in the results obtained from micromechanical finite element models and store this knowledge in an easily accessible database. This approach is developed by applying established methods in non-linear system theory and informatics.

We start with a discrete representation of the microstructure where the spatial domain is binned into a uniform grid of spatial cells (or voxels) that are enumerated by a three-dimensional vector \mathbf{s} whose components take only integer values. Let \mathbf{S} and $|\mathbf{S}|$ represent the complete set of all spatial cells and the total number of spatial cells, respectively, in the given dataset. The microstructure datasets typically identify the local state in each cell. The set of all distinct local states that are possible in a given material system is referred to as the local state space. In this work, the local state space of interest is also assumed to be tessellated into individual bins and enumerated by $h=1,2,\dots,H$. The variable $m_{\mathbf{s}}^h$ then defines the volume fraction of local state h in

the spatial cell s . Based on this definition of the discretized microstructure variable, it is easy to establish the following properties [16]:

$$\sum_{h=1}^H m_s^h = 1, \quad m_s^h \geq 0 \quad \frac{1}{|S|} \sum_{s \in S} m_s^h = v^h \quad (5)$$

where v^h denotes the volume fraction of local state h in the complete microstructure dataset.

Let p_s denote the local response variable in the spatial bin of interest, s . This could represent any local response of interest such as stress, strain, or strain rate. Let \bar{p} represent the volume averaged value of the response for the entire microstructure. Drawing on analogues in systems theory, the localization of the response variable in the microstructure can be expressed as a series of higher-order convolutions between the microstructure signal and the response signal as

$$\frac{p_s}{\bar{p}} = \left(\sum_{h=1}^H \sum_{t \in S} \alpha_t^h m_{s+t}^h + \sum_{h=1}^H \sum_{h'=1}^H \sum_{t \in S} \sum_{t' \in S} \alpha_{tt'}^{hh'} m_{s+t}^h m_{s+t+t'}^{h'} + \dots \right) \quad (6)$$

where α_t^h and $\alpha_{tt'}^{hh'}$ are referred to as the first-order and second-order influence coefficients, respectively. The values of these coefficients are expected to be completely independent of the microstructure coefficients m_s^h .

Note that in writing Eq. (6) we are treating the spatial distributions of both the microstructure variable and the response variable as digital signals. For example, when we subject a representative volume element (RVE) of a material structure to a specific macroscale loading condition (say tensile stress) and simulate the internal stress field in the RVE using a finite element model, we obtain a very large dataset that can be treated as a digital signal. In current practice, we do not utilize these datasets very efficiently. Often, we extract only a limited number of predictions (e.g. effective macroscale properties, hot spots in stress fields) and throw away much of the rest of the information contained in the dataset. However, there exist underlying correlations (i.e. knowledge) implicit in these datasets that would efficiently capture the underlying physics in the system. Such correlations should be local for a given boundary condition. Although Eq. (6) was established based on analogues in systems theory, it is gratifying to note that the exact same expression can be derived following the statistical continuum mechanics theories developed by Kroner [17].

We have previously demonstrated that it is possible to establish highly accurate localization relationships by calibrating the series expansions of Eq. (6) to results obtained from finite element (FE) models. The main difficulty with Eq. (6) is that all of the influence coefficients are fully coupled. The focus in our work has been mainly on the first-order terms. Eq. (6) takes a much simpler form when transformed into the discrete Fourier transform (DFT) space, where it can be recast as

$$P_k = \left[\left(\sum_{h=1}^H \beta_k^{h*} M_k^h \right) + \right. \quad (7)$$

$$\left. \left(\sum_{h=1}^H \sum_{h'=1}^H \sum_{r \in S} \beta_{kr}^{hh'} M_r^{h'} M_{k-r}^h \right) + \dots \right] \quad (8)$$

$$\beta_k^h = \mathfrak{F}_k(\alpha_t^h), P_k = \mathfrak{F}_k(p_s/\bar{p}), M_k^h = \mathfrak{F}_k(m_s^h)$$

where (\mathfrak{S}_k) denotes the multi-dimensional DFT operation with respect to the spatial variables s or t , and the star in the superscript denotes the complex conjugate. The simplification in Eq. (7) compared to Eq. (6) is a direct consequence of well-known convolution properties of DFTs. Note that the number of coupled first-order coefficients in Eq. (7) is only H , although the total number of first-order coefficients still remains as $|S|H$. Because of this dramatic uncoupling of first-order coefficients into smaller sets, it becomes fairly easy to estimate the values of influence coefficients β_k^h by calibrating them to results from FE models.

It is emphasized here that establishing β_k^h is a one-time computational task for a selected composite material system, because these coefficients are expected to be independent of the morphology of the microstructure (defined by m_s^h). As such, they offer a compact representation of the underlying knowledge regarding the localization of the selected response variable for all possible topologies that could be defined in the given composite material system. The simplicity of Eq. (7) also presents a computationally efficient procedure for computing the spatial distribution of the selected response variable for any microstructure dataset, after the corresponding influence coefficients are established and stored. However, it should be noted that the influence coefficients are expected to be strongly dependent on the imposed boundary conditions, i.e. they need to be established separately for all boundary conditions of interest. We are currently developing novel strategies for expressing the functional dependence of the influence coefficients on the imposed boundary conditions.

In order to explore the viability of this approach, we explored the application of this novel framework to the rate-independent rigid-plastic deformation of a two-phase representative volume element (RVE), with no strain hardening. In future work, we will extend this to crystal plasticity. In this first example, the two phases are assumed to exhibit isotropic plasticity with yield strengths of 200 MPa and 250 MPa, respectively. The stress-strain relationships for both phases are assumed to be described by the Levy-Mises equations as

$$\dot{\boldsymbol{\varepsilon}} = \lambda \boldsymbol{\sigma}' \quad (9)$$

where $\dot{\boldsymbol{\varepsilon}}$ is the symmetric strain rate tensor, $\boldsymbol{\sigma}'$ is the symmetric deviatoric Cauchy stress tensor, and λ is a proportionality parameter that can be related to the yield strength of the material, the equivalent plastic strain rate and the equivalent stress. The goal of the localization expression in this example is to compute the local strain rate field in the RVE of the two-phase composite. For simplicity, we initially demonstrate the establishment of the localization relationship for the case of an applied isochoric simple compression strain rate tensor on the RVE at the macroscale.

For this example, the local state space is comprised of two isotropic phases ($H=2$), where $h=1$ identifies the first local state (phase) and $h=2$ the second one. We assume each cell of the tessellated spatial domain to be completely filled with either of the two local states. Thus, the microstructure variable m_s^h takes on values of zeros or ones. Based on equations (6) and (7), the first-order localization linkage for the present problem can be expressed in the DFT space as

$$\mathfrak{S}_k(\dot{\boldsymbol{\varepsilon}}_s) = \left[\sum_{h=1}^{H=2} \beta_k^{h*} M_k^h \right] \dot{\boldsymbol{\varepsilon}}, \quad (10)$$

where $\dot{\boldsymbol{\varepsilon}}_s$ represents the local strain rate in the spatial bin s , and $\dot{\boldsymbol{\varepsilon}} = \mathbf{0.02s}^{-1}$ is the macroscopically imposed strain rate in the e_1 direction on the RVE.

As described earlier, the values of the influence coefficients are established by calibrating against datasets produced by FE models on selected microstructures. In our work, we discovered that “delta” microstructures, consisting of one element of one phase surrounded completely by another phase, are very convenient for the calibration process and produce the best estimates

for β_k^h . In a two-phase composite, it is possible to define only two distinct delta microstructures, and both of these were used in the calibration process for this problem. All of the FEM results used in this study were generated using the commercial software ABAQUS®, where each RVE contained 804,357 (93x93x93) cuboid-shaped three-dimensional eight-noded solid elements. The macroscale simple compression strain rate was imposed on the finite element mesh as a periodic uniform boundary condition. The values of β_k^h were established as the best-fit values for the FE results on the two delta microstructures described above, using standard linear regression analyses methods.

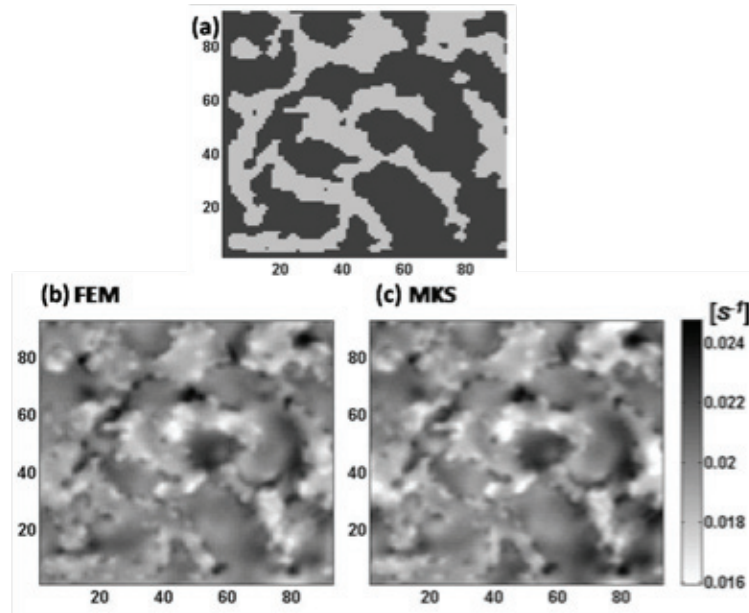


Figure 4. Comparison of the contour maps of the local $\dot{\epsilon}_{11}$ component of the strain rate tensor for a 3-D microstructure. The middle section of the 3-D RVE used in the calculation is shown at the top (a), while the predicted strain rate contours by the FE method (b) and the MKS established in this work (c) are shown below. Both phases are assumed to exhibit isotropic plasticity with yield strengths of 200 MPa and 250 MPa, respectively. The macroscopic simple compression strain rate applied is 0.02s^{-1} .

The established β_k^h coefficients constitute the materials knowledge systems (MKS) for the case study presented. In fact, the strain rate field for any other RVE comprising any spatial arrangements of the same constituent phases, subjected to the same simple compression loading condition, can be easily computed using Eq. (10). As a critical validation of this concept, we explore the application of the MKS established here to a random microstructure of the selected two phases. We selected a random microstructure for our validation here because their rich diversity of local neighbourhoods produce the most heterogeneous microscale strain rate fields in the composite, and therefore offer an excellent opportunity to evaluate the localization relationships most critically. We note that we have successfully applied the MKS developed here to a large number of microstructures, although only one example is described here in detail. Figure 4 compares the local $\dot{\epsilon}_{11}$ component of the strain rate field for the selected random microstructure using both the FE analysis and the MKS approach developed in this work.

The average error between the predictions shown in Figure 4 from the MKS approach described here and the FEM analysis is only 2.2%. The FE analyses could not be performed on a regular desktop PC. It was executed on an IBM e1350 supercomputing system (part of The Ohio Supercomputer Center), and required 94 processor hours. In contrast, the MKS method took only 32 seconds on a regular laptop (2GHz CPU and 2GB RAM).

Conclusions

In this study, we have further established and validated a new spectral crystal plasticity database using discrete Fourier transforms (DFTs) for BCC metals with 48 slip systems. It was seen that a small number of dominant DFTs is enough to capture the dependence of the stresses, the lattice spins, and the strain hardening in individual crystals on their lattice orientation and the applied deformation modes. Furthermore, a new efficient approach was developed for the fast computation of the yield surfaces in the five-dimensional deviatoric stress space for both BCC and FCC metals using the Taylor-type crystal plasticity models. It was demonstrated that it is possible to construct the entire five-dimensional yield surface at extremely fast computational speeds.

We have developed novel FFT (Fast Fourier Transforms)-based algorithms for data-mining local structure-response-structure evolution linkages from large numerical datasets produced by micromechanical finite element models. The viability of this new approach was demonstrated with a case study involving two constituents exhibiting isotropic plasticity. It was noted that the first-order influence coefficients adequately captured the localization relationships in spite of the non-linearity inherent to the phenomena.

Publications

M. Knezevic, H. F. Al-Harbi and S. R. Kalidindi, Crystal Plasticity Simulations Using Discrete Fourier Transforms, *Acta Materialia*, 2009. 57(6): p. 1777-1784.

H. F. Al-Harbi, M. Knezevic and S. R. Kalidindi, Spectral Approaches for the Fast Computation of Yield Surfaces and First-Order Plastic Property Closures for Polycrystalline Materials with Cubic-Triclinic Textures. *Computers, Materials, & Continua (CMC)*, 2010, accepted.

S. R. Kalidindi, S. R. Niezgoda, G. Landi, S. Vachhani, T. Fast, A novel framework for building materials knowledge systems, *Computers, Materials, & Continua (CMC)*, 2010, under review.

References

1. Asaro, R.J. and A. Needleman, Texture development and strain hardening in rate dependent polycrystals. *Acta Metallurgica et Materialia*, 1985. 33(6): p. 923-953.
2. Bronkhorst, C.A., S.R. Kalidindi, and L. Anand, Polycrystalline plasticity and the evolution of crystallographic texture in FCC metals. *Philosophical Transactions of the Royal Society of London Series A-Mathematical Physical and Engineering Sciences*, 1992. 341(1662): p. 443-477.
3. Kalidindi, S.R., C.A. Bronkhorst, and L. Anand, Crystallographic Texture Evolution in Bulk Deformation Processing of Fcc Metals. *Journal of the Mechanics and Physics of Solids*, 1992. 40(3): p. 537-569.
4. Delannay, L., S.R. Kalidindi, and P. Van Houtte, Quantitative prediction of textures in aluminium cold rolled to moderate strains. *Materials Science and Engineering A*, 2002. 336(1-2): p. 233-244.
5. Van Houtte, P., L. Delannay, and S.R. Kalidindi, Comparison of two grain interaction models for polycrystal plasticity and deformation texture prediction. *International Journal of Plasticity*, 2002. 18(3): p. 359-377.
6. S. R. Kalidindi, A.B., and R. Doherty, Detailed Analysis of Plastic Deformation in Columnar Polycrystalline Aluminum Using Orientation Image Mapping and Crystal Plasticity Models.

Proceedings of the Royal Society of London: Mathematical, Physical and Engineering Sciences., 2004.

7. Raabe, D., Z. Zhao, and F. Roters, A finite element method on the basis of texture components for fast predictions of anisotropic forming operations. *Steel Research*, 2001. 72(10): p. 421-426.
8. Raabe, D., Y. Wang, and F. Roters, Crystal plasticity simulation study on the influence of texture on earing in steel. *Computational Materials Science*, 2005. 34(3): p. 221-234.
9. Hosford, W.F. and R.M. Caddell, *Metal forming mechanics and metallurgy*. 1993: Prentice-Hall, Inc.
10. Knezevic, M., H.F. Al-Harbi, and S.R. Kalidindi, Crystal plasticity simulations using discrete Fourier transforms. *Acta Materialia*, 2009. 57(6): p. 1777-1784.
11. Kalidindi, S.R., et al., Representation of the orientation distribution function and computation of first-order elastic properties closures using discrete Fourier transforms. *Acta Materialia*, 2009. 57(13): p. 3916-3923.
12. Hamad F. Al-Harbi, M.K., and Surya R. Kalidindi Spectral Approaches for the Fast Computation of Yield Surfaces and First-Order Plastic Property Closures for Polycrystalline Materials with Cubic-Triclinic Textures *Computers, Materials, & Continua (CMC)*, 2010. accepted.
13. Kalidindi, S.R., H.K. Duvvuru, and M. Knezevic, Spectral calibration of crystal plasticity models. *Acta Materialia*, 2006. 54(7): p. 1795-1804.
14. Knezevic, M., S.R. Kalidindi, and D. Fullwood, Computationally efficient database and spectral interpolation for fully plastic Taylor-type crystal plasticity calculations of face-centered cubic polycrystals. *International Journal of Plasticity*, 2008. 24(7): p. 1264-1276.
15. Peeters, B., et al., Work-hardening/softening behaviour of b.c.c. polycrystals during changing strain paths: I. An integrated model based on substructure and texture evolution, and its prediction of the stress-strain behaviour of an IF steel during two-stage strain paths. *Acta Materialia*, 2001. 49(9): p. 1607-1619.
16. Adams, B.L., X. Gao, and S.R. Kalidindi, Finite approximations to the second-order properties closure in single phase polycrystals. *Acta Materialia*, 2005. 53(13): p. 3563-3577.
17. Kröner, E., Statistical modeling, in *Modeling small deformation in polycrystals*, J. Gittus and J. Zarka, Editors. 1986, Elsevier: New York. p. 229-291.

P. Advanced High Strength Steels through Paraequilibrium Carbon Partitioning and Austenite Stabilization

Principal Investigator: Gary M. Michal
Case Western Reserve University
Department of Materials Science and Engineering
Cleveland, OH 44106
(216) 368-5070; e-mail: gmm3@case.edu

Co-Principal Investigator: Arthur H. Heuer
Case Western Reserve University
Department of Materials Science and Engineering
Cleveland, OH 44106
(216) 368-3869; e-mail: ahh@case.edu

Technology Area Development Manager: William Joost
(202) 287-6020; e-mail: william.joost@ee.doe.gov

Contractor: Case Western Reserve University
Contract No.: CMMI 0727583

Objective

- The development of a third generation of advanced high strength steel (AHSS) possessing:
- Strength and ductility combinations exceeding those of ferritic first generation AHSS.
- The ability to be manufactured much more economically than austenitic second generation AHSS.
- Establish a steel chemistry that fulfills the three transformational characteristics required to achieve a double stabilization thermal processing scheme:

The steel can be completely austenitized at 900°C.

- The hardenability of the steel is great enough that the bainite transformation can be avoided during a liquid metal quench to 450°C.
- Carbide formation is suppressed during aging somewhere in the range of 300 to 500°C during which carbon will partition from the martensite phase to the austenite phase.

Approach

- The strength/ductility goal of a third generation AHSS can be achieved by employing a microstructure comprised of martensite and a significant volume fraction of austenite.
- The austenite must have sufficient stability such that it transforms to martensite only at progressively higher levels of strain, so that the work hardening rate of the steel increases in a continuous fashion.
- A high volume fraction of austenite must be obtained within the constraints of:
A carbon content low enough that weldability is not severely compromised.

The alloy levels in the steel do not greatly increase its price.

The processing route for the steel is consistent with current sheet steel commercial production practice.

- Use of a double stabilization thermal processing scheme to increase the amount of austenite:

The steel will be held for a brief time at approximately 450°C for its first stabilization.

The second stabilization will be an aging of the steel at a temperature at which carbides will not form while carbon partitions from the martensite phase to the austenite phase.

Accomplishments

- Initial use of the thermal processing facility that was constructed during the first year of this project was a series of direct quench heat treatments.

Candidate steels were held at 900°C for 60 seconds then quenched into water.

The vol. pct. of austenite that was present at 900°C and the vol. pct. retained austenite and the hardness at room temperature were measured using SEM, X-ray and Vickers hardness analyses.

- A series of interrupted quench heat treatments was performed.

Candidate steels were held at 900°C for 60 seconds, quenched into molten tin at 450°C for 5 seconds then air cooled.

The vol. pct. retained austenite and hardness at room temperature were measured using X-ray and Vickers hardness analyses.

- Two series of double stabilization heat treatments were performed.

Candidate steels were held at 900°C for 60 seconds, quenched into molten tin at 450°C for 5 seconds, quenched into molten Wood's metal at 192 or 267°C and then were aged to promote carbon partitioning at temperatures between 325 and 375°C for times ranging from 15 to 120 seconds.

The vol. pct. retained austenite and hardness at room temperature were measured using X-ray and Vickers hardness analyses.

- Modeling with Thermo-Calc software was used to establish the levels of manganese, carbon, aluminum and silicon in steel that will allow its complete transformation to austenite at 900°C.

Two additional candidate steel chemistries were selected based upon the results of the modeling effort.

Steel D: 4 wt. pct. manganese, 0.30 wt. pct. carbon, 1.90 wt. pct. silicon, 0.70 wt. pct. aluminum.

Steel E: 4 wt. pct. manganese, 0.25 wt. pct. carbon, 1.40 wt. pct. silicon, 0.70 wt. pct. aluminum.

Future Direction

- Perform additional double stabilization heat treatments with steels 4B and 6B.
Select a final quench temperature to yield an optimum vol. pct. austenite to be exposed to carbon partitioning aging cycles.
Change specimen geometry from coupons to one with a reduced gage section appropriate for tensile testing.
- Conduct tensile tests of select steels that have been subjected to optimum double stabilization heat treatments.
- Have AK Steel Corporation-Research complete the processing of the second group of candidate steels
Perform direct and indirect quench heat treatments.
Conduct double stabilization heat treatments.
- Prepare thin foil samples and conduct transmission electron microscopy (TEM) analyses of the retained austenite contained in select samples.

Introduction

Efforts are aimed at the development of a third generation of advanced high strength steel (AHSS) with strength and ductility combinations exceeding those of ferritic first generation AHSS and that can be manufactured much more economically than austenitic second generation AHSS. The strength/ductility goal of a third generation AHSS can be achieved by employing a microstructure comprised of martensite and a significant volume fraction of austenite. The austenite must have sufficient stability to transform to martensite only at progressively higher levels of strain, so that the work hardening rate concurrently increases in a continuous fashion. The key to viable third generation AHSS is obtaining a high volume fraction of such austenite within the constraints of a carbon content low enough to not severely compromise weldability, of alloy levels that do not greatly increase the cost of the steel, and of a processing route consistent with current sheet steel production practice.

A key component of the project is exploiting a double stabilization thermal processing scheme to increase the amount of austenite. Candidate steels will be held for a brief time at approximately 450°C which will comprise the first stabilization step. The second stabilization will be an aging of the steel at a temperature at which carbides will not form while carbon partitions from the martensite phase to the austenite phase. An initial undertaking was the design and construction of a thermal processing facility. Such a facility enables steel strip to track the rapid temperature changes associated with a double stabilization thermal cycle. A second project task was the design and production of the first series of candidate heats of steel.

The thermal processing facility was put into operation in February, 2009 and the initial group of three steel chemistries was produced by AK Steel Corporation – Research. The thermal processing facility and the initial group of experimental steels are described along with the results of heat treatment cycles applied to determine the extent of austenitization and the efficacy of the thermal stabilization steps applied to the three steel chemistries. A modeling effort using Thermo-Calc software was initiated to define the combined effect of the alloying elements carbon, manganese, silicon and aluminum on the ability of candidate steels to be fully austenitized at 900°C. The results of that modeling effort also are presented herein.

Thermal Processing Requirements

The core design requirement for the thermal processing facility was to be able to achieve the thermal cycle illustrated in Figure 1. The thermal cycle contains four brief isothermal holds corresponding to 1.) austenitization, 2.) initial quench and stabilization, 3.) final quench, and 4.) carbon partitioning for final stabilization. The hold times at the four relevant temperatures are anticipated to vary from as little as 5 seconds to several minutes. The demand for rapid temperature changes associated with movement from one isothermal hold to another prompted the use of liquid media to establish the isothermal hold temperatures. For austenitization, the chosen temperature has been 900°C and the medium is a neutral salt. For the initial quench and also the carbon partitioning the temperatures used have been 300 to 500°C and the medium is liquid tin. For the final quench, the temperature has been in the range of 150 to 300°C and the medium is liquid Wood's metal.

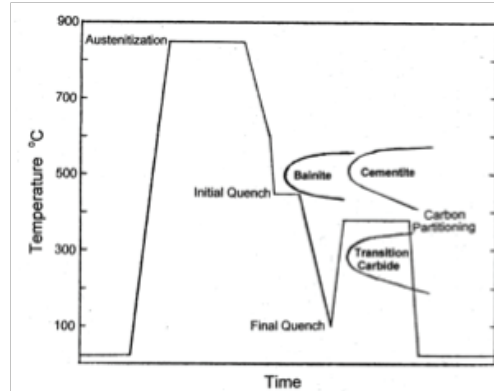


Figure 1. A schematic representation of a double stabilization thermal cycle.

Four crucible furnaces were purchased to establish the core of the thermal processing facility. Funding for the furnaces was obtained through a grant from the Ohio Department of Development. The austenitization furnace is equipped with an Inconel 625 alloy cylindrical crucible 190 mm (7.5 inch.) deep with an inside diameter of 102 mm (4 inch.). The other three furnaces contain KIMAX® cylindrical crucibles 184 mm (7.25 inch.) deep with an inside diameter of 83 mm (3.25 inch.). Each furnace has a primary control thermocouple and a second overtemperature control thermocouple. A third thermocouple is inserted directly into the liquid media in each crucible. These latter four thermocouples and a set of two thermocouples constructed with very fine chromel-alumel wires for an extremely fast response time will all be read with an eight place analog to digital board with output to a laptop computer for data display and storage. The set of fast response thermocouples are embedded into test samples.

Candidate Steels Chemistry

The chemical compositions of the first group of candidate steels were strongly influenced by the requirements of the double stabilization thermal cycle. To maintain a completely austenitic microstructure during cooling to the initial quench temperature demands that the steel have sufficient hardenability to avoid the formation of bainite as shown schematically in Figure 1. To enhance hardenability boron was chosen as an alloying element in all of the candidate steels. In order to reliably achieve boron levels of 0.001 to 0.003 wt. pct. titanium also must be added to the steel to prevent the formation of BN. Manganese increases the hardenability of steel. Conventional steel making practices limit the manganese content to a maximum of 2 wt. pct. That level of manganese provides substantial hardenability and was chosen as a baseline value for the candidate steels. A manganese content of 4 wt. pct. was chosen for a more highly alloyed heat. To suppress the formation of carbides during the carbon partitioning isothermal hold the candidate steels must contain ample concentrations of silicon, or aluminum. The decision was made to make a combined addition of silicon and aluminum to the candidate

steels at concentrations commonly used for electrical steel grades. The chosen alloying levels for the silicon and aluminum were nominally 2 wt. pct. and 1.5 wt. pct., respectively.

Carbon is the alloying element that has by far the greatest potency with respect to increasing the stability of the austenite phase and the strength of the martensite phase. Carbon also is a very low cost alloying element. The primary restraint to having high carbon contents in candidate alloys is provided by a loss of weldability. To maintain good spot welding performance sheet steels typically have less than 0.1 wt. pct. carbon. Other forms of welding steel can tolerate carbon contents several times that value. The decision was made to have nominally 0.3 wt. pct. carbon in the most highly alloyed candidate steel and half that level of carbon in the baseline candidate steel. As carbon partitions from martensite to austenite, the austenite's resistance to transformation to martensite increases and the strength of the martensite decreases. To bolster the strength of the martensite phase, the decision was made to add nominally 0.5 wt. pct. chromium to the highly alloyed candidate steel. As an example of the effect of chromium, the tensile strength of martensite containing 0.02 wt. pct. carbon has been shown to increase from 525 to 625 MPa due to an increase in its chromium content from essentially zero to 0.5 wt. pct. [1]

A total of three candidate steel chemistries were selected for initial preparation and evaluation. The chemical compositions of these first three candidate alloys are listed in [Table 1](#).

Table 1. Proposed Chemical Compositions in Wt. Pct. for the Initial Candidate Steels

Alloy	C	Mn	Si	Al	S	P	B	Cr
A	0.13/0.17	1.95/2.05	2.00/2.30	1.50/1.70	0.015 max	0.010 max	0.001/0.003	0.12 max
B	0.18/0.22	1.95/2.05	2.00/2.30	1.50/1.70	0.015 max	0.010 max	0.001/0.003	0.12 max
C	0.28/0.32	3.90/4.10	2.00/2.30	1.50/1.70	0.015 max	0.010 max	0.001/0.003	0.45/0.55

Production of Laboratory Heats of Steel

AK Steel Corporation-Research produced four laboratory induction air melted heats of steel using high purity materials. Each heat yielded one 14 Kg (30 lbs) ingot 9.5 X 9.5 X 19 cm (3.75 X 3.75 X 7.5 inch.) in size. One heat of the baseline (A) and one heat of the intermediate (B) alloy chemistries were melted. Two heats of the highly alloyed (C) chemistry were melted. To prevent excessive oxidation and losses during melting, the liquid steel surface was shrouded with argon.

Ingots from this first group of candidate steels were processed by hot rolling and coil simulation cooling to form a series of hot bands. Hot bands were subjected to cold reductions of 67% to a final thickness of 1.02 mm (0.040 inch) using a laboratory cold mill.

Resulting Fully Processed Steels

Chemical compositions obtained from cold rolled samples derived from all six hot bands are listed in [Table 2](#). The sum total of the cropping, machining, sectioning, and descaling applied to the original 13.6 Kg (30 lbs) ingots resulted in a yield of the final cold rolled steel of about 24%, i.e., 3.2 Kg (7 lbs). Each hot band produced approximately 0.2 m² (310 inch²) of cold rolled steel 1.02 mm (0.040 inch) thick. That amount of steel provided an ample number of test coupons to enable exploration of an extensive range of time/temperature parameters associated with double stabilization thermal cycles.

Table 2. Chemical Compositions in Wt. Pct. of the Cold-Rolled Initial Candidate Steels

Hot Band	C	Mn	P	S	Si	Ni	Cr	Cu	Mo	N	Nb	V	Ti	Al	B
3A	0.10	2.16	<0.002	0.0008	1.15	0.004	<0.002	<0.002	<0.002	0.0049	<0.002	0.002	0.003	1.48	0.0018
3B	0.092	2.17	<0.002	0.0008	1.17	0.002	<0.002	<0.002	<0.002	0.0046	<0.002	0.002	0.003	1.48	0.0016
4B	0.26	4.12	0.002	0.0008	1.12	0.002	0.47	<0.002	<0.002	0.0080	<0.002	0.002	0.002	1.58	0.0014
5A	0.25	1.95	0.002	0.0007	1.08	0.002	0.013	<0.002	<0.002	0.0055	<0.002	0.002	0.002	1.46	0.0016
5B	0.25	1.95	0.002	0.0008	1.06	0.003	0.014	<0.002	<0.002	0.0039	<0.002	0.002	0.002	1.44	0.0015
6B	0.29	3.99	0.002	0.0008	1.11	0.002	0.48	<0.002	<0.002	0.0047	<0.002	0.002	0.002	1.50	0.0011

Direct Quench Heat Treatments

The intent of the first series of heat treatments was to determine the amount of austenite that was present in each of the candidate steels after a 60 second hold at 900°C. After being held in a molten salt bath, samples of each steel were directly quenched into water. The water quench transformed most of the austenite created at 900°C to martensite. An SEM image of the microstructure of steel 6B after austenitization followed by a water quench is shown in Figure 2(a). The microstructure is comprised of martensite and retained austenite containing isolated, irregularly shaped grains of ferrite that are in darker contrast. SEM images of the microstructures of steels 4B, 5A and 3A after an equivalent heat treatment cycle are shown in Figures 2(b), (c) and (d), respectively. These steels have progressively lower carbon contents and their microstructures contain successively higher volume fractions of ferrite. A point counting procedure was employed to determine the vol. pct. ferrite present after austenitization at 900°C for 60 seconds based upon SEM images of steels 5A, 5B, 4B and 6B.

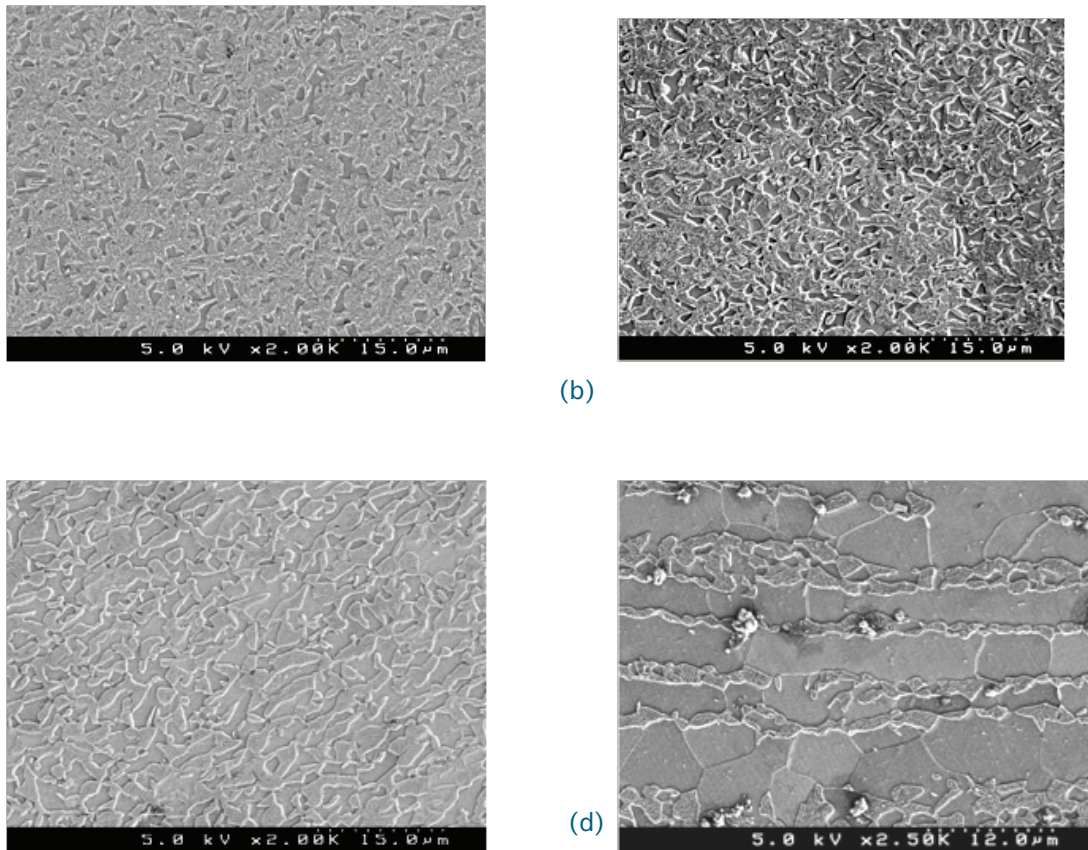


Figure 2. SEM image of steel (a) 6B (b) 4B (c) 5A (d) 3A after a direct quench heat treatment.

The resulting values listed in Table 3 show that the steels with nominally 2 wt. pct. manganese and 0.25 wt. pct. carbon yielded 54 vol. pct. austenite while those with nominally 4 wt. pct. manganese and 0.28 wt. pct. carbon achieved 77 vol. pct. austenite. The relatively high silicon and aluminum levels in the steels imposed a severe restriction on the amount of austenite that could be formed at 900°C in the 0.10 wt. pct. carbon steel 3A.

Table 3. Vol. Pct. of Ferrite Contained in Several Candidate Steels after a Direct Quench Heat Treatment

Candidate Steels	5A	5B	4B	6B
Vol. Pct. Ferrite	46%	47%	24%	23%

Vickers hardness tests were conducted on each of the candidate steels after they were subjected to the direct quench heat treatment. A 50 g load was employed in all cases. The average hardness value measured and its standard deviation are listed in Table 4. For comparative purposes, the hardness of the steels in their non-heat treated, as-cold-rolled condition also is contained in Table 4. The highest carbon content steels, i.e., 6B and 4B, had a sufficient volume fraction of martensite with a high enough carbon content that their hardness increased substantially due to the direct quench heat treatment. The intermediate carbon content steels with nominally 2 wt. pct. manganese, i.e., 5A and 5B, had enough martensite with an adequate carbon content that their hardness increased modestly due to the direct quench heat treatment. The lowest carbon content steels, i.e., 3A and 3B, had very low martensite contents resulting in their hardness decreasing due to the direct quench heat treatment.

Table 4. Vickers Hardness 50g Load

Steel	As-Cold-Rolled	Direct Quench	Interrupted Quench
3A	410±30	440±40	450±40
3B	400±20	390±50	420±40
5A	450±10	470±20	490±40
5B	470±10	500±20	450±40
4B	440±30	660±30	700±50
6B	480±20	590±20	630±40

The direct quench in water to room temperature, i.e., 20°C would not be expected to transform all of the austenite created at 900°C to martensite [2]. Some retained austenite should be present among the martensite. The direct comparison method was employed in conjunction with x-ray diffractometry to determine the volume percent retained austenite in each of the candidate steels after they were subjected to the direct quench heat treatment [3]. Measured retained austenite levels for the various steels are listed in Table 5. The amount of retained austenite scales directly with the combined carbon and manganese contents of the steels, i.e., their MS temperatures. The high carbon and manganese content steels, 4B and 6B, have nominally 4 volume pct. retained austenite and the low carbon and manganese content steels, 3A and 3B, have nominally less than 1 volume pct. retained austenite.

Table 5. Volume Percent Retained Austenite

Steel	Direct Quench	Interrupted Quench
3A	0.6	1.4
3B	1.0	1.3
5B	2.2	5.2
4B	4.5	5.7
6B	3.8	11.1

Interrupted Quench Heat Treatments

The aim of the second series of heat treatments was to reveal how much retained austenite could be achieved in the candidate steels after they were subjected to the first thermal stabilization step. The first thermal stabilization step was incorporated into interrupted quench heat treatments. The as-cold-rolled steels were held in molten salt at 900°C for 60 seconds, quenched into molten tin at 450°C for 5 seconds, and then allowed to air cool to room temperature. The short hold time at 450°C was designed to prevent transformation of

austenite to bainite. Examination of the microstructures of the steels after interrupted quench heat treatments found that the ferrite phase fraction and disposition were virtually identical to those produced by the direct quench heat treatments. That observation serves as proof that whatever ferrite was present after the 60 seconds hold at 900°C, it was retained to the same extent by the direct quench and interrupted quench heat treatments.

A 50 g load was employed for Vickers hardness tests conducted on each of the candidate steels after they were subjected to the interrupted quench heat treatments. The average hardness value measured and its standard deviation also are listed in Table 4. The interrupted quench hardness levels are quite similar to those found in the same steel after direct quench heat treatments. Interrupted quench steel has the potential for more extensive autotempering of its martensite and additional retained austenite compared to its direct quench state. Neither of those effects appears to have significantly changed the hardness of the steels.

Measured retained austenite levels of the various steels subjected to the interrupted quench heat treatment also are listed in Table 5. In all cases the interrupted quench heat treatments yielded a higher volume pct. retained austenite compared to that measured in the same steel after a direct quench heat treatment. The high carbon and manganese content steel 6B exhibited a very high retained austenite level of 11.1 volume pct. after an interrupted quench heat treatment.

Double Stabilization Heat Treatments

Two series of double stabilization heat treatments have been performed with select candidate steels. The initial step in all of the dual stabilization heat treatments was a hold in molten salt at 900°C for 60 seconds for the as-cold-rolled steels followed by quenching into molten tin at 450°C for 5 seconds. The subsequent quench into Wood's metal was design to transform 50 or 75 vol. pct. of the austenite to martensite before steel was subjected to an isothermal carbon partitioning aging. The temperature of the Wood's metal required to transform the desired vol. pct. of austenite to martensite was calculated based upon the M_s temperature of each steel corresponding to its chemical composition. The Koistinen-Marburger equation was used to establish the final quench temperature in the Wood's metal based upon an α value of -0.011, the M_s temperature of the steel and the final austenite vol. pct. specified. The steels 4B and 6B were used for the two series of double stabilization heat treatments. To achieve 25 and 50 vol. pct austenite in the microstructures that were then subjected an isothermal carbon partitioning aging final quench temperatures of 192 and 267°C, respectively, were employed. At each of the two levels of austenite, the steels were aged at three different temperatures and at each temperature for three different periods of time. **Tables 6 and 7** list the carbon partitioning aging temperatures and times employed for the two series of double stabilization heat treatments applied to steel 6B along with the corresponding vol. pct. retained austenite and hardness levels achieved.

Table 6. After Double Stabilization Heat Treatments: Vol. Pct. Retained Austenite and Vickers Hardness 50g Load for Steel 6B Quenched to Have 25 Vol. Pct. Austenite

Carbon Partitioning		Austenite (Vol. Pct.)	Vickers Hardness
Temperature (°C)	Time (s)		
325	15	9.0	590
	30	8.0	620
	60	7.7	640
350	15	8.4	580
	30	9.8	580
	60	9.1	570
375	15	11.2	570
	30	12.6	550
	60	11.4	570

Table 7. After Double Stabilization Heat Treatments: Vol. Pct. Retained Austenite and Vickers Hardness 50g Load for Steel 6B Quenched to Have 50 Vol. Pct. Austenite

Carbon Partitioning		Austenite (Vol. Pct.)	Vickers Hardness
Temperature (°C)	Time (s)		
325	15	7.0	630
	30	7.2	650
	60	8.9	620
350	15	6.9	640
	30	5.8	640
	60	5.8	640
375	30	4.7	530
	60	2.7	540
	120	1.9	550

Modeling

Both aluminum and silicon are strong ferrite stabilizers. These elements also suppress carbide formation and enable the second thermal stabilization step of carbon partitioning from the martensite phase into the austenite phase to take place. It is anticipated that the best combination of mechanical properties will occur in steel with a martensite/austenite matrix with little, or no, ferrite present. To create such a microstructure requires that the steel be completely austenitic when held at 900°C for 60 seconds. Thermo-Calc software version R was used to explore what levels of aluminum and silicon could be tolerated in steel while maintaining the requirement of complete austenitization at 900°C. The base chemistry chosen was iron with 4 wt. pct. manganese. The software was used to determine the minimum temperature for complete austenitization of steels with both carbon contents of 0.1, 0.2, or 0.3 wt. pct. and an array of aluminum and silicon concentrations.

Figure 3 illustrates the major findings of the modeling effort. The maximum wt. pct. of aluminum and silicon are plotted for steels with carbon contents of 0.1, 0.2 or 0.3 wt. pct. subject to the condition that the steel must be able to completely transform to austenite at 900°C. The most highly alloyed steel in the first series of experimental heats was 6B with nominally 0.3 wt. pct. carbon, 4 wt. pct. manganese, 1.5 wt. pct. aluminum and 2 wt. pct. silicon. That steel could only tolerate 1 wt. pct. aluminum if the other three alloying elements were kept constant in order to attain complete austenitization at 900°C.

Second Group of Candidate Steels

Based upon the findings of the Thermo-Calc modeling aimed at establishing the levels of manganese, carbon, aluminum and silicon in a steel that will allow complete transformation to austenite at 900°C, two additional heat chemistries were selected. Both steels will have nominally 4 wt. pct. manganese and a lesser amount of aluminum of nominally 0.70 wt. pct. compared to a value of 1.5 wt. pct. aluminum in the first group of candidate steels. The more highly alloyed steel “D” will have nominally 0.30 wt. pct. carbon and 1.9 wt. pct. silicon. The leaner alloyed steel “E” will have nominally 0.25 wt. pct. carbon and 1.4 wt. pct. silicon. The chemical compositions of the two steels in the second group of candidate steels are listed in Table 8. AK Steel Corporation- Research is in the process of producing laboratory induction air

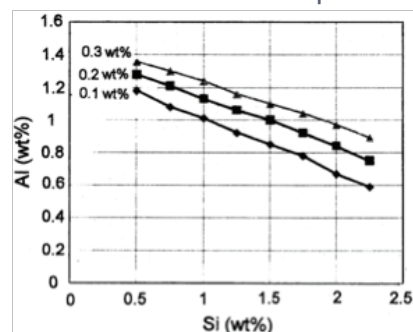


Figure 3: Maximum aluminum and silicon contents for 4 wt. pct. manganese steel that can be fully austenitized at 900°C as a function of its carbon content.

melted heats of each of the two steels. The ingots of each of the steels from this second group of candidate steels will be processed by hot rolling, coil simulation cooling and cold rolling to yield sheet nominally 1 mm thick that has been cold reduced approximately 67 pct.

Table 8. Proposed Chemical Compositions in Wt. Pct. for the Second Group of Candidate Steels

Alloy	C	Mn	Si	Al	S	P	B	Cr
D	0.28/0.32	4.00/4.25	1.80/2.00	0.65/0.75	0.002 max	0.003 max	0.001/0.003	0.45/0.55
E	0.23/0.27	4.00/4.25	1.30/1.50	0.65/0.75	0.002 max	0.003 max	0.001/0.003	0.45/0.55

Discussion

The volume fraction of austenite, f_A , in a steel can be predicted based upon the phenomenological equation 1 proposed by Koistinen and Marburger [4].

$$f_A = \exp [\alpha(MS-T)]$$

In equation 1 α is a constant with a negative sign and MS is the martensite start temperature. The volume fraction of austenite decreases exponentially as the undercooling below MS increases. Brook et al. [5] showed that α can vary from -0.008 to -0.013 depending upon alloy composition. An empirical formula for the effect of alloying elements that are relevant to the candidate steels in this study is presented in equation 2 [6,7].

$$M_S(^{\circ}\text{C}) = 539 - 423[\text{wt.\%C}] - 30.4[\text{wt.\%Mn}] - 7.5[\text{wt.\%Si}] + 30[\text{wt\%Al}]$$

The M_S temperature calculated for each candidate steel, based upon their chemical compositions as listed in Table 2, is displayed in Table 9. Using the calculated MS temperatures equation 1 was employed with an α value of -0.011 to estimate the volume fraction of austenite that would be retained at 20°C for the candidate steels. The predicted volume pct. of retained austenite is listed for each steel in Table 9.

Table 9. M_S Temperature and Predicted Volume Percent Retained Austenite

Steel	M_S ($^{\circ}\text{C}$)	Retained Austenite (Volume Pct.)
3A	459	0.8
3B	462	0.8
5B	402	1.5
4B	330	3.3
6B	318	3.8

Good agreement is observed between the predicted values for retained austenite contained in Table 9 and the measured volume pct. of retained austenite listed in Table 8 for the steels that were subjected to direct quench heat treatments. That result is fortuitous because the predictions of equation 1 are based upon the nominal alloy chemistry and the inherent assumption that the microstructure is completely austenitic at temperatures above M_S . The fraction of microstructure that was austenite was less than unity at 900°C for all of the candidate steels. As such, the potential volume percent of retained austenite must be discounted accordingly. The presence of ferrite at 900°C indicates that carbon partitioning occurred and enriched the austenite in carbon. The higher carbon content of the austenite would lower its M_S temperature which in turn would increase the potential volume pct. of retained austenite. The lower starting volume fraction of austenite and the carbon enrichment of the initial austenite have opposite effects upon the potential volume pct. of retained austenite. These effects appeared to have nearly canceled each other resulting in measured retained austenite levels that match well the predictions derived from Equation 1.

Conclusions

Direct quench heat treatments have shown that a range of volume fractions of austenite are generated among the initial series of candidate steels when held at 900°C for 60 seconds. Increased levels of retained austenite were achieved by employing the first proposed thermal stabilization step as part of a series of interrupted quench heat treatments. Double stabilization heat treatments have been able to substantially increase the vol. pct. of retained austenite to a level as high as 12.6. Thermo-Calc based modeling has been used to select two additional candidate steel chemistries that will enable the steels to completely transform to austenite when held at 900°C.

Presentations/Publications/Patents

1. G. M. Michal, 'AHSS through Paraequilibrium Carbon Partitioning and Austenite Stabilization', Special seminar at AK Steel Corporation - Research, Middletown, Ohio, August 30, 2007
2. G. M. Michal and A. H. Heuer, 'Increasing the Austenite Content of AHSS by Dual Stabilization Processing', MS&T'07 Conference and Exhibition, Detroit, Michigan, September 17, 2007
3. G. M. Michal, 'AHSS through Carbon Partitioning', NSF/DOE Steel Research Program Review, Southfield, Michigan, April 10, 2008.
4. G. M. Michal and A.H. Heuer, 'Use of Dual Stabilization Thermal Processing to Increase the Austenite Content of AHSS,' MS&T'08 Conference and Exhibition, Pittsburgh, Pennsylvania, October 6, 2008.
5. G. M. Michal, 'AHSS through Carbon Partitioning', NSF/DOE Steel Research Program Review, Livonia, Michigan, May 12, 2009.
6. G. M. Michal and A.H. Heuer, 'Increasing the Austenite Content of AHSS through Dual-Stabilization Thermal Processing' MS&T'09 Conference and Exhibition, Pittsburgh, Pennsylvania, October 28, 2009.

References

1. E.G. Bain and H.W. Paxton, Alloying Elements in Steel, ASM, Metals Park, OH, pp. 125-128, 1966.
2. C.L. Magee, "The Nucleation of Martensite", in Phase Transformations, ASM, Metals Park, OH, pp. 115-156, 1979.
3. B.L. Averbach and M. Cohen, "X-ray Determination of Retained Austenite by Integrated Intensities", Transactions AIME, Vol. 176, pp. 401-415, 1948.
4. D.P. Koistinen and R.E. Marburger, "A General Equation Prescribing the Extent of the Austenite-Martensite Transformation in Pure Iron-Carbon Alloys and Plain Carbon Steels", Acta Metallurgica, Vol. 7, pp. 59-60, 1959.
5. R. Brook, A.R. Entwisle and E.F. Ibrahim, "The Effect of Chemical Composition on the Shape of Martensite Transformation Curves", Journal of the Iron and Steel Institute, Vol. 195, pp. 292-298, 1960.

6. J. Mahieu, J. Maki, B.C. DeCooman and S. Claessens, "Phase Transformation and Mechanical Properties of Si-Free CMnAl Transformation-Induced Plasticity-Aided Steel", *Metallurgical and Materials Transactions A*, Vol. 33A, pp. 2573-2580, 2002.
7. Dong-Woo Suh, Seong-Jun Park, Chang-Hoon Lee and Sung-Joon Kim, "Microstructure and Mechanical Behaviors of 0.1C-13Mn Metastable Austenitic Steel", *Metallurgical and Materials Transactions A*, Vol. 40A, pp. 264-268, 2009.

Q. Development of a High Strength High Toughness Ausferritic Steel

Principal Investigator: Susil K. Putatunda
Chemical Engineering and Material Science,
Wayne State University; Detroit, MI 48202
Phone: (313) 577-3808; e-mail: sputa@eng.wayne.edu

Technology Area Development Manager: William Joost
(202) 287-6020; e-mail: william.joost@ee.doe.gov

Contractor: Wayne State University
Contract No: NSF 0854962

Objective

- The primary objective of this investigation was to develop a new ausferritic steel with simultaneous high yield strength, ductility and fracture toughness by applying the novel concept of adiabatic deformation and two-step austempering process.
- The secondary objective was to examine the influence of austempering temperature on the microstructure and mechanical properties of this new steel.

Approach

In this investigation a new low alloy steel has been designed and austempered by single step austempering process. The alloy steel has been designed such that its M_s (martensite start) temperature is sufficiently low. The steel with the following composition has been designed for this investigation. (C=0.20%, Si=1.7%, Cr=1.0%, Mn=0.80%, Ni=2.0%, Nb=0.06%, V=0.06%, Mo=0.20% with S and P less than 0.1%.

Inclusion of high silicon helped in the prevention of cementite formation during the transformation to upper bainite. The addition of chromium helped in reducing graphitization and improving hardenability. This also depressed the M_s temperature. The carbon content has been selected as 0.20% to retain sufficient ductility in the as cast and hot rolled condition. Carbon also helps to depress the upper to lower bainite boundary transition line. This allowed us to initially quench the steel to a lower austempering temperature and thus achieve refinement of bainitic ferrite-austenite structure. Addition of a small amount of molybdenum helped to attain high hardenability in the steel.

Accomplishments

- A new, low alloy, low carbon steel with high silicon content has been developed.
- By austempering this steel in the temperature range of 260°C - 400°C considerable strength, toughness, and ductility was produced.
- After austempering this steel in the temperature range of 260°C - 400°C, a mixed microstructure consisting of bainitic ferrite and austenite was obtained in this steel. However presence of some martensite was also observed.

- Very high fracture toughness of 114 MPavm was obtained in this steel after austempering at 260°C.
- This steel is an inexpensive alternate to maraging steel in applications requiring very high fracture toughness.
- This steel has good ductility, very good strength and fracture toughness. Therefore, it can be used in automotive components to reduce weight and increase fuel efficiency.

Future Directions

In future we propose to apply adiabatic deformation and a novel concept of two step austempering in this steel. Applying adiabatic deformation and two step austempering will result in an extremely fine scale microstructure (nano scale region) and very high carbon in the austenite. Further, higher density of nucleation at the same growth rate will cause the austempering reaction (stage 1) to occur very fast i.e. the end point of reaction one will be achieved quickly. The purpose of step austempering is to momentarily force the material into the lower bainitic region to increase nucleation and we intend to raise the temperature of transformation into the upper bainitic region to grow the ferrite austenite structure. In our opinion single step austempering will not produce as finer structure as the two step austempering. When we do the initial quench to a temperature just above the M_s temperature of the steel, we expect to be in the region below the Bainitic nose of the IT diagram. Therefore, we do not expect significant amount of lower bainite to be formed in the material.

Thus the overall new process will include the following steps:

1. Heat up the material to an initial austenitizing temperature (T_1) (i.e. just below and above A_1)
2. Enclose in an insulated chamber with heated rolls maintained at the same temperature.
3. Adiabatically deform it by rolling to a final temperature (T_2) (i.e. about 871°C)
4. This will be followed by two step austempering i.e. immediate quenching to first austempering temperature T_3 in a salt bath (above M_s Temperature) and then raising the temperature of the salt bath to the final austempering temperature (T_4) and holding and finally air cooling .

This processing will result in steel with very fine scale ausferritic microstructure (nano scale region) and will also result in exceptional combination of mechanical and physical properties.

Introduction

The primary focus of this investigation was to create a high strength, high toughness ausferritic steel. This was achieved by austempering a low carbon low alloy steel with high silicon content. Steels with ausferritic structure have several advantages including high strength, high toughness and high ductility as compared to HSLA steel. In conventional steels generally the fracture toughness decreases as yield strength increases. On the other hand the fracture toughness will be high when the yield strength is low. Thus the combination of high strength and high fracture toughness cannot easily be obtained in most conventional steels. In this investigation, new ausferritic steel with simultaneous high yield strength and high fracture toughness was developed. This novel steel was synthesized using the concepts of Austempered Ductile Cast Iron (ADI) [1-4] technology.

Austempering reaction in steel

When steel is austempered at temperatures below the nose of the TTT (Time Temperature and Transformation) curve, a structure is produced in which ferrite and iron carbide are not lamellar. This transformation product is called bainite. Bainite in steel has a needle-like (acicular) microstructure. Whereas pearlite is nucleated by iron carbide [5,6] and is accompanied by the subsequent formation of ferrite, bainite is nucleated by ferrite, followed by the precipitation of iron carbide. This process leads to the dispersion of iron carbide in a ferrite matrix. With a lower transformation temperature, the distribution of carbide is finer and the ferrite needles are thinner [7,8]. This product is called lower bainite. The transformation product at relatively higher temperatures consists of lath or plate shaped ferrite units arranged in packets and interlath carbide precipitates. This product is called upper bainite [9]. In steel, lower bainite produces higher yield strength but lower toughness. While the austempering reaction in ADI is a two-step reaction process, it is a one-step reaction process [7,8] in the case of steel. During austempering in steel, austenite directly decomposes into acicular ferrite and carbide (bainite). Austempering of steel offers the advantages of increased ductility, reduced distortion, and a short overall time cycle to harden thoroughly. Generally, upper bainitic temperatures are above 316°C (600°F) in the case of steels and cast iron. Temperatures between 232°C (450°F) to 316°C (600°F) are the lower bainitic temperature range.

However, when steels containing sufficient silicon or aluminum (exceeding 2.0%) are austempered in the upper bainitic temperature range, a unique microstructure similar to ADI [10-22] develops in these steels. The carbon that is partitioned in to residual austenite does not precipitate but remains stable to ambient temperature. The microstructure obtained consists of fine plates of bainitic ferrite separated by carbon enriched region of austenite. This structure is called ausferrite. The potential advantages of this mixed micro structure can be listed as follows:

- Cementite is responsible for initiating fracture in high-strength steels. Its absence is expected to make the microstructure more resistant to cleavage failure and void formation.
- The bainitic ferrite is almost free of carbon, which substantially strengthens the ferrite [10].
- The microstructure derives its strength from the fine grain size of the ferrite plates, which are less than 1µm in thickness. It is the thickness of these plates, which determines the mean free slip distance, so that the effective grain size is less than a micrometer. This cannot be achieved by any other commercially viable process. Grain refinement is the only method available for simultaneously improving the strength and toughness of steels.
- The ductile films of austenite, which are intimately dispersed between the plates of ferrite, have a crack blunting effect. They further add to toughness by increasing the work of fracture as the austenite is induced to transform to martensite under the influence of the stress field of a propagating crack. This is the TRIP, or transformation-induced plasticity effect.
- The diffusion of hydrogen in austenite is slower than in ferrite. The presence of austenite can therefore improve the stress corrosion resistance.
- Steels with the bainitic ferrite and austenite microstructure can be obtained without the use of expensive alloying elements. All that is required is that the silicon or aluminum concentration should be large enough to suppress the cementite formation.

In spite of these appealing features, the microstructure does not always give the expected combination of strength and toughness. This is because the relatively large blocky regions of austenite between the sheaves of bainite readily transform into high-carbon martensite under the influence of stress. This untempered, hard, and coarse martensite regions severely embrittle the steel. Therefore we argue that if the austenitic and ferrite can be made in very fine-grained structure and austenite sufficiently enriched with carbon so that its M_s (Martensite

Start) temperature is sufficiently depressed [39-41] then, the strength and other mechanical properties will increase significantly.

This investigator has developed a novel concept of adiabatic deformation and two step austempering process to produce extremely fine scale microstructure consisting of ferrite and austenite in steels. This is expected to produce an exceptional combination of strength, ductility and fracture toughness in ausferritic steels.

Results

This project started on June of 2009 after receiving fund from NSF. The NSF grant number of the study was CMMI 0854962. We melt cast and hot rolled, a low alloy and low carbon steel. After hot rolling, annealing the steel was austenitized at 926°C for 2 hours and then austempered at several temperatures between 260°C and 398°C. **Figure 1** shows the typical microstructure of the steel in as cast condition. **Figure 1B** shows the microstructure of the steel after austempering at 371°C. This microstructure shows a fine scale ausferritic structure i.e. a mixture of ferrite and high carbon austenite. X-ray diffraction confirmed the microstructure consisting of ferrite and high carbon austenite. **Table 1** reports the mechanical properties of the steel including the fracture toughness. We obtained exceptionally high yield strength and very high fracture toughness (114 MPa√m, comparable to Maraging Steel) in this material after austempering at 260°C. The ductility of the material is also good. We also measured ferrite and austenite content. **Table 2** reports the ferrite and austenite content and the ferritic cell size in this material. A very fine scale ferritic microstructure was obtained in the steel. Thus we have already established the proof of principle of this project. We now propose to apply the novel concept of adiabatic deformation and two step austempering in this steel to produce extremely fine (nearly nano crystalline) microstructure with austenite and ferrite together with very high carbon content in austenite. We expect to have properties significantly higher than Maraging Steels after this process. As mentioned earlier, such high strength high toughness steel will have major applications in defense, automotive and other manufacturing industries because it will result in significant weight savings.

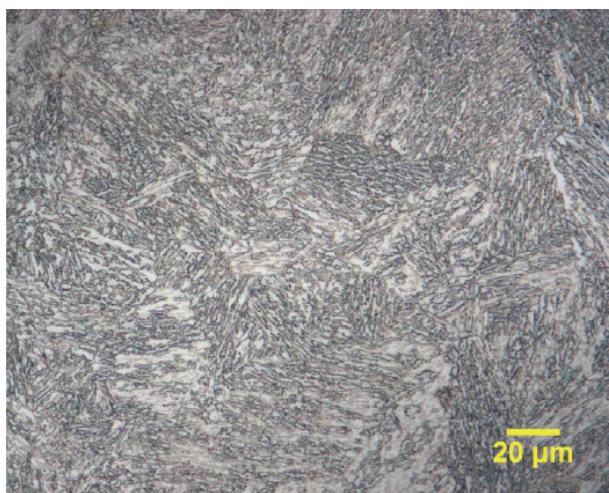


Figure 1A. Microstructure of the steel in as-cast condition

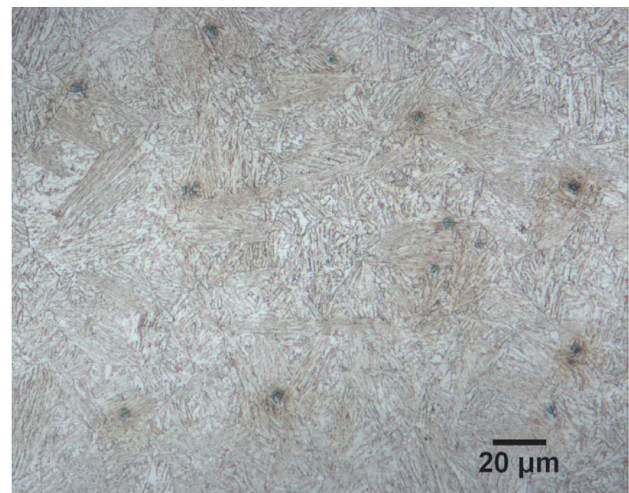


Figure 1B. Microstructure of the steel after austempering at 371°C condition

Once this steel of above composition has been developed we will concentrate on developing other ausferritic steels with lower carbon content and different alloying composition using the same basic principle i.e. designed with a lower M_s temperature and processed by adiabatic deformation and two step austempering.

Table 1. Effect of Austempering Temperature on the Mechanical Properties of the Steel

Austempering Temp (°C)	Yield Strength (MPa)	Ultimate Tensile Strength	Ductility(% elongation)	Fracture Toughness (MPa√m)
As cast	732	1198	5.5	53.9
260	1197	1411	3.6	114.0
315	1156	1411	3.7	109.4
371	991	1319	4.32	76.8
398	853	1302	4.8	54.0

Table 2. Effect of Austempering Temperature on Volume Fraction of Austenite and Ferritic Cell Size

Austempering Temp (°C)	Retained Austenite (%)	Carbon Content (wt%)	Ferritic Cell Size (nm)
260	3.15	1.36	19.98
315	2.57	1.27	19.54
371	4.50	1.26	21.04
398	5.40	1.19	21.60

Conclusions

A new, low alloy, low carbon steel with high silicon content has been developed. By Austempering this steel in the temperature range of 260°C - 400°C considerable strength and ductility was produced in the sample. After Austempering this steel in the temperature range of 260°C - 400°C, a mixed microstructure consisting of bainitic ferrite and austenite was obtained in this steel. The steel had properties comparable to maraging steel. Adiabatic deformation produced very fine scale ferrite and austenite.

Presentations/Publications/Patents (to date from the project)

- Three Papers were presented at M.S and T conferences in 2007 (Detroit), 2008(Pittsburgh) and 2009(Pittsburgh)
- Two papers have been published in Materials Science and Engineering A (Vol. A 513 pp 329-339, 2009) and Materials Science Forum(Vol. 638 pp 3453-3458, 2010)
- One patent application has been filed with U.S. Government in 2009 (under consideration)

References

1. J. Dodd, "High Strength, High Ductility Ductile Irons," Modern Casting, Vol.68, No.5, pp. 60-66 (1978)
2. R.B. Gundlach and J.F. Janowak, "Development of a Ductile Iron for Commercial Austempering," AFS Transaction, Vol.94, pp. 377-388 (1983)
3. S. K. Putatunda and P.P. Rao, "Influence of Microstructure on Fracture Toughness of Austempered Ductile Cast Iron," Metallurgical and Materials Transaction, Vol 28A. No.7, pp. 1457-1470, July 1997.
4. S.K. Putatunda, R. Gupta and P.P. Rao, "Influence of Austempering time and temperature on Fracture Toughness of Austempered Ductile Iron," Microstructural Sciences, ASM International, Vol.24, pp.103-110, (1996).

5. R.E.Reed Hill “Physical metallurgy principles 2 nd Edition, D. Van Nostrand Company New York, 1973.
6. D.A.Porter and K.E.Easterling” Phase Transformations in Metals and alloys” Chapman and Hall, 2nd Edition, 1992.
7. P.G.Shewmon “Phase Transformations in Metals,” McGraw Hill, 1986.
8. W.F.Smith “ Structure and Properties of Engineering Alloys,” McGraw Hill (1981).
9. B.P.J. SandVik “Bainitic Transformation in High Silicon Steel” Metallurgical Transactions, Vol A13,pp 777-787, 1982.
- 10.H.D.K.H. Bhadeshia “Bainite in Steels” Second Edition, The University Press, Cambridge, IOM communication Ltd., London, pp 373-375, 2001.
- 11.J.Aranzabal et al “Influence of Heat Treatment on the Microstructure of an Austempered Ductile Iron,” Materials Science and Technology, Vol 20, pp. 36-46, 1994.
- 12.S.K.Putatunda “Development of a High Carbon and High Silicon Steel”, Journal of Materials Processing and Technology, pp 335-358, August 2001.
- 13.S.K.Putatunda “Fracture Toughness of a High Carbon and High Silicon Steel” Materials Science and Engineering, Vol A297, pp 31-43, January 2001.
- 14.H.K.D.H Bhadeshia et all “Very strong low temperature Bainite” Material Science and Technology, Vol. 18, pp 279 – 284 , March 2002.
- 15.S.K. Putatunda and P.P. Rao, “Comparative Study of Fracture Toughness of Austempered Ductile Iron With Upper and Lower Ausferritic Microstructure,” Materials Science and Technology, Vol 14, pp 1257-1263, December, 1998.
- 16.P.P.Rao and S.K. Putatunda “Investigations on Fracture Toughness of Austempered Ductile Iron Alloyed with Chromium”, Materials science and Engineering, Vol A346, pp 254-265, 2003.
- 17.P.P. Rao and S.K. Putatunda “Dependence of Fracture Toughness of Austempered Ductile Cast Iron on Austempering Temperature” Metallurgical and Materials Transaction, Vol 29A, pp 3005-3016, December 1998.
- 18.S. Yazdani and A.Firouzi “ Influence of heat treatment on fatigue behavior of a Cu-Ni alloyed Austempered ductile iron” Material Science Forum, Vols. 426-432, pp 925-930, 2003
- 19.K.L.Harynen, D.J.Moore and K.B.Rundman, “Tensile Properties and Microstructure of a Clean Austempered Ductile Iron”, AFS Transaction, Vol 98, pp. 471, 1990.
- 20.A.S.H.Ali, K.I.Uzlov, N. Darwish and R. Elliot “Austempering of a Low Manganese Ductile Iron, Part 4 Relationship between Mechanical Properties and Microstructure”, Materials Science and Technology, Vol 70, pp. 35-48, 1994.
- 21.S.K. Putatunda and P. Gadicherla “Influence of Austenitizing Temperature on Fracture Toughness of a low manganese Austempered Ductile Cast Iron “ Materials Science and Engineering, Vol A268, pp 15-31, August 1999.
- 22.S.K.Putatunda “Development of Austempered Ductile Cast Iron (ADI) with Simultaneous High Yield Strength and Fracture Toughness by a Novel Two-step Austempering Process”, Materials Science and Engineering, Vol A 315, pp. 70-80, September (2001).

R. Development of Nano-acicular Duplex Steels

Principal Investigator: David C. Van Aken
Missouri University of Science and Technology Materials Science and Engineering
1400 N. Bishop, Rolla, MO 65409-0340
(573) 341-4717; e-mail: dcva@mst.edu

Co-Principal Investigator: Julia E. Medvedeva
Missouri University of Science and Technology Physics
1315 N. Pine St., Rolla, MO 65409-0640
(573) 341-4789; e-mail: juliaem@mst.edu

Co-Principal Investigator: Von L. Richards
Missouri University of Science and Technology Materials Science and Engineering
1400 N. Bishop, Rolla, MO 65409-0340
(573) 341-4730; e-mail: vonlr@mst.edu

Technology Area Development Manager: William Joost
(202) 287-6020; e-mail: william.joost@ee.doe.gov

Contractor: Missouri University of Science and Technology
Contract No.: National Science Foundation Award CMMI-0726888

Objective

- Develop a third generation advanced high strength steel (AHSS) that is both lighter and stronger than current automotive steels. The new steel is to be stronger than first generation AHSS that are based upon ferritic microstructures and less expensive than the high manganese, austenitic grades known as second generation AHSS.
- Improve automotive crashworthiness by producing a microstructure that is similar to acicular $\alpha+\beta$ Ti alloys that have high fracture toughness. The new steel will be a duplex microstructure of acicular ferrite and austenite.
- Develop a physics based understanding of phase stability with respect to alloying. Use first principle calculations to determine appropriate alloy additions to strengthen the austenitic phase. This knowledge can then be used in the formulation of steel alloys to produce nano-scale acicular ferrite microstructures.
- Develop an acoustic emission facility for studying bainitic phase transformation.

Approach

To address the questions related to the structural, electronic, and magnetic properties of steels, we will perform a thorough density functional investigation of the electronic structure, magnetic properties, and stability for α (bcc) and γ (fcc) Fe phases, their solid solutions with interstitial carbon and substitutional manganese, as well as for cementite with 2p and 3p impurities. A projector augmented wave (PAW) method as implemented in the Vienna ab initio simulation package (VASP) within the generalized gradient approximation (GGA) will be used. We considered the octahedral interstitial sites for carbon which are the most preferable in both bcc and fcc Fe phases, and the nearest substitutional positions of manganese. In cementite, to determine the most energetically preferable location of the 2p or 3p impurity (N, O, B or Si, Al, S, P), we

compare the formation energies of either carbon or iron substitution by the impurity. For all the structures investigated, we optimized the lattice parameters and the internal positions of all atoms in the supercells via the atomic force and the total energy minimization.

The solution enthalpy is calculated as $\Delta H_s = E(\text{Fe}_3\text{C}) - E(\text{Fe}_3) - E(\text{C})$ for carbon and $\Delta H_s = E(\text{Fe}_3\text{MnC}) - E(\text{Fe}_3\text{C}) + E(\text{Fe}) - E(\text{Mn})$ for manganese, where supercells were taken with the same magnetic states and $E(\text{C})$, $E(\text{Fe})$ and $E(\text{Mn})$ are the total energies of carbon as graphite, iron and α -Mn, respectively.

Steelmaking will be performed at Missouri University of Science and Technology with the aim of producing steel microstructures similar to the acicular $\alpha + \beta$ titanium alloy, which has high fracture toughness. Of particular interest will be alloys containing manganese, aluminum, and silicon, where the addition of aluminum and silicon promote the formation of bainitic ferrite, but discourage the formation of cementite. Aluminum has the added benefit of lowering the overall density of the steel. Initial steel heats will be used to verify the thermo-chemical database for FeMn-Al-Si-C steel compositions using FactSage (a free energy minimization modeling program). Alloy and phase composition studies will then be performed to narrow the range in steel compositions explored.

Accomplishments

- Demonstrated through calculations that neither manganese nor nitrogen at 3 at.% concentration changes the ground magnetic state of γ -Fe. This is similar to γ -Fe with carbon as reported previously. Thus, not only carbon, but also nitrogen frustrates the ideal magnetic order in antiferromagnetic state by spin flip of the nearest planar Fe atoms and makes them ferromagnetically coupled in the octahedron Fe₆N.
- Established that there is a strong tendency for the formation of Mn-C pairs, which corresponds to the lowest energy as compared to the other possible Mn locations with respect to C. The Mn and Fe atoms in Fe₅MnC octahedrons are shifted outward from carbon atom by 6-8 %. Further, the second Mn atom prefers to occupy the apical position, thus, forming a 180° Mn-C-Mn complex.
- Found that the most favorable position for both Si and Al substituted for iron atoms in austenite is site 2 (second coordination sphere with respect to carbon). The predicted by the calculations distribution of Al and C in austenite exactly corresponds to the structure of κ -carbide.
- Missouri S&T produced five lightweight steels that met mechanical property goals for a third generation AHSS with compositions (in weight percent) ranging from Fe-13.5-15.4Mn-2.383.53Al-1.4-2.9Si-0.06-0.23C.
- Demonstrated that FactSage (a free energy minimization modeling program) did not accurately predict the stabilization of austenite at typical hot working temperature for automotive steels.
- Target microstructures having acicular ferrite were obtained by inoculation with nonmetallic inclusions having good lattice registry with ferrite.
- Developed alloys containing acicular ferrite and retained austenite displaying TRIP-/TWIP-like behavior during mechanical testing. Demonstrated that alloys containing ϵ -martensite and retained austenite display only TRIP-like mechanical behavior.

Future Direction

Ferrite and austenite Fe-Mn-N alloys. We will continue our systematic comparative investigations of the electronic structure, magnetic properties and stability of α - and γ -Fe with interstitial nitrogen and substitutional manganese. The main objectives are (i) to determine the ground states of the Fe-N, and Fe-Mn-N phases with small manganese and nitrogen concentrations, (ii) to find their energetically-preferable spatial distribution and (iii) to understand how these impurities affect the lattice parameters, local crystal structure, magnetic interactions and phase stability. The results will be compared to those obtained for Fe-Mn-C alloys.

Austenite Fe-Mn-(C,N)-(Al,Si) alloys. We will continue to study the distribution of the light impurities (N, C) with respect to the substitutional 3d (Mn) or 3p (Al, Si) atoms, as well as the distribution of the latter two with respect to each other. For each composition, several magnetic structures will be considered and the formation energies will be accurately determined.

Two to four experimental heats will be produced with standard steelmaking practices like Cawire treatment and Ar-stirring in the furnace to reduce the inclusion density in Alloy 1. We will study the effects of a reduced amount of inclusions on the nucleation of acicular ferrite and mechanical properties.

Three to five experimental heats will be produced to observe the effect of carbon content on mechanical behavior during tensile testing. These steels will be hot rolled to produce sheet product and metallurgically characterized.

The effect of aluminum on mechanical behavior and microstructure will be investigated by producing two to four experiment heats. The steel will be used in acoustic emission experiments to determine the effect of aluminum on the martensite start temperature.

The role of displacive relaxation and strength in the transformation of the parent phase will be examined using acoustic emission. Initial studies will examine the melting of indium inclusions embedded in aluminum. Inclusions that are embedded within crystalline grains are known to require superheating prior to melting, since the melting is inhibited by the addition pressure produced by the matrix confining the volume expansion. Acoustic emission studies of the bainitic reaction will be conducted using the Fe -2.1Mn -4Co -1.2Si -0.6C -0.2Mo steel produced at Missouri S&T.

Introduction

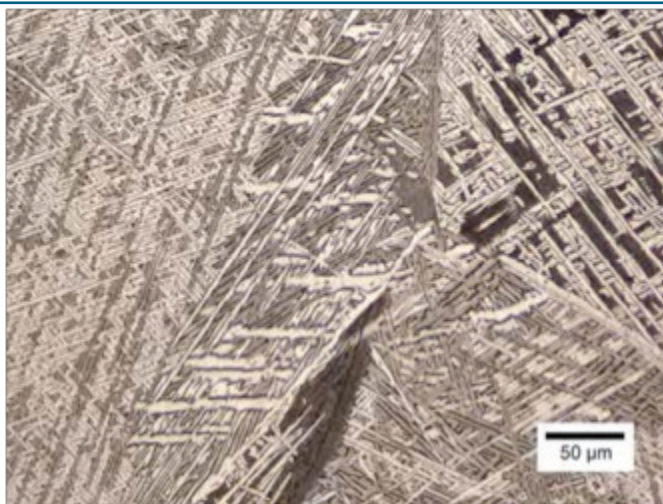


Figure 1. A titanium $\alpha+\beta$ microstructure of acicular α plates with retained β developed for high toughness.

Recent developments in steels have resulted in first generation advanced high strength steels (AHSS) with ferritic microstructures and second generation high strength steels with austenitic microstructures. The aim of ongoing research at Missouri S&T is to develop steels with duplex ferrite and austenite microstructures that will be analogous to acicular microstructures developed in $\alpha + \beta$ titanium alloys, which have high fracture toughness (see [Figure 1](#)).

The proposed steels will have strengths greater than first generation advanced high strength steels, but cost less than the ultra high manganese second generation austenitic steels TWIP and L-IP (see [Figure 2](#)). The

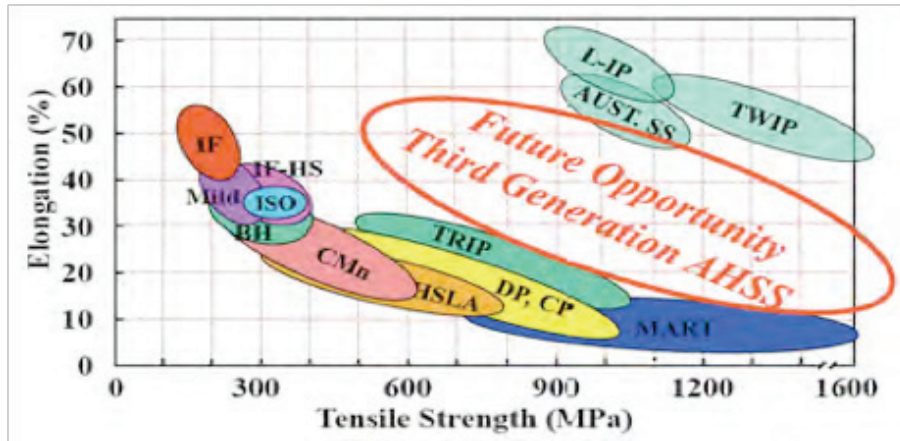


Figure 2. Property distribution plot for third generation advanced high strength steels (AHSS).

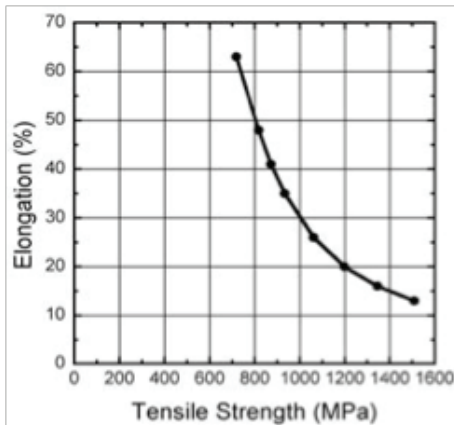


Figure 3. Predicted strength and elongation properties for combinations of martensite and austenite. It was assumed ultimate tensile strength of austenite and martensite was 640 MPa and 2000 MPa with elongations of 0.6 and 0.08, respectively [2].

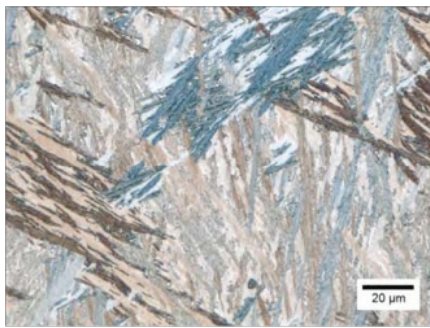


Figure 4. A basket weave microstructure produced by austempering a Fe-0.63C-3.99Co-2.1Mn-1.35Si-0.34Cr-0.21Mo-0.61Al steel at 300°C for 3 days. The scale of bainitic ferrite produced was measured by x-ray diffraction to be 10-20 nm and Rockwell C hardness value was 43, but the amount of retained austenite was less than 10%. Nital etch and imaged with cross polarized light and $\frac{1}{4}$ wavelength filter.

proposed third generation steels will have nanometer size acicular ferrite microstructures with metastable austenite that create steels both high in strength and toughness. These steels are expected to maintain steel as the preeminent high strength structural material in designing low weight automobiles with exceptional crash worthiness.

Matlock and Speer have applied Mieliko's model [1] to demonstrate the property goals set for third generation AHSS can be accomplished with a combination of martensite and austenite [2]. It should be noted that nanoscale ferrite as observed in some bainitic steels have strengths approaching that of martensite.

Hard bainitic structures have been studied by Garcia-Mateo et al. [3]. A "basketweave" microstructure similar to the acicular microstructures in $\alpha + \beta$ titanium alloys as shown in Figure 1 can be produced by isothermal transformation. The bainitic steel shown in Figure 4 was austenitized at 920°C and isothermally transformed at 300°C for 3 days. A low isothermal transformation temperature assists in strengthening the austenite, which reduces the ferrite sub-unit size [4]. Cobalt was added in an effort to increase the rate of bainitic transformation [5]. While hard bainitic steels produced promising nanoscale microstructures, the high cost of cobalt makes hard bainitic steel impractical for automotive applications.

Cobalt and aluminum are the only additions that increase the rate of bainitic transformation [5]; and thus, Missouri S&T alloy development has focused on aluminum additions. Aluminum along with silicon also raises the enthalpy of formation for cementite to make formation of cementite less favorable [6]. Retention of austenite will depend upon the suppression of cementite formation. Along with stabilizing ferrite and suppressing cementite formation, aluminum reduces the density of steel. Manganese will reduce density to a lesser extent, but is beneficial in stabilizing austenite as aluminum content is increased.

The complex structural and magnetic phase diagram of iron makes it challenging to determine the effect of impurities on the microstructure of steel as well as its electronic structure, which is critical for the fundamental understanding of the observed macroscopic properties.

A physics-based approach to alloy design is being pursued to understand the role of Mn, Al and Si in the defect formation with interstitial atoms. Systematic calculations of the electronic structure and lattice distortions are being performed using the highly precise first-principles full potential linearized augmented plane wave method (FLAPW) with the structure optimization capabilities. This will allow us to calculate the dependence of the lattice parameters on carbon and nitrogen concentrations for austenite and ferrite. The interaction between solutes and interstitials will be the most important part of our investigations. The total and formation energy calculations will allow us to analyze the possibility of clustering and the effect of solutes on the diffusion of interstitial impurities (C, N, and B).

Electronic structure, magnetic properties and stability of austenite Fe-Mn-N alloys.

Using first-principles approach – the projector augmented waves (PAW) method as implemented in the Vienna ab-initio simulation package (VASP) – we determined the ground states for Fe-N and Fe-Mn-N phases with small manganese and nitrogen concentration (3 at.%) and found how nitrogen and manganese affect the lattice parameters, local crystal structure, magnetic interactions and phase stability. The lattice parameters and the internal positions of all atoms in the supercells were optimized by the atomic forces and total energy minimization. We performed calculations for the nonmagnetic, ferromagnetic, single-layer antiferromagnetic (AFM) and double-layer antiferromagnetic (AFMD) states. The latter is a good collinear approximation for spiral magnetism. The cubic symmetry and collinear magnetism are incompatible and, we studied the tetragonal structures to elucidate the effect of tetragonality, which we obtained to be lower in energy than the corresponding cubic phases by 30-45 meV/atom.

Based on the results obtained, we conclude that neither manganese nor nitrogen at 3 at.% concentration changes the ground magnetic state of γ -Fe, which remains AFMD (see Table I). (This is similar to γ -Fe with carbon as reported previously). We predict that the local magnetic order is strongly affected by nitrogen, which favors ferromagnetic coupling of the nearest Fe atoms and leads to the local instability of nearest iron and manganese magnetic moments. For AFM magnetic structure, we demonstrate that the moments of four planar Fe atoms have opposite spins with respect to the other Fe atoms in the layer (Table I). Thus, not only carbon, but also nitrogen frustrates the ideal magnetic order in antiferromagnetic state by spin flip of the nearest planar Fe atoms and makes them ferromagnetically coupled in the octahedron Fe₆N.

Traditionally, the transition from AFM to FM state with an increase of carbon concentration in Fe is explained by the volume expansion associated with the presence of interstitial C. To separate the role of the Fe-C interaction from the volume effect, we compared the magnetic ordering in the fully-optimized structure with carbon to the one obtained for a modeled (hypothetical) structure without the carbon atom, but with the same expanded lattice (i.e., with Fe-Fe distances fixed). While only one stable magnetic state exists in γ -Fe with 3 at.% carbon (with the Fe spins flipped with respect to the Fe in the layer), we found two nearly degenerate states in the case when carbon is omitted: one corresponds to the flipped Fe spins and the other, with a lower energy, to the unflipped spins on the nearest iron atoms. Therefore, volume expansion favors ferromagnetic ordering, but it is carbon or nitrogen that stabilizes the short-range ferromagnetic coupling (local ferromagnetic regions near the impurity) in the AFM state.

Magnetism plays a critical role in the phase stabilities and transitions in steels: it affects the thermodynamic properties such as the mixing enthalpies, structural parameters as well as

elastic properties and deformation behavior. In particular, the magnetic interactions determine the temperature of austenite-to-ferrite transformation and also are important for martensitic transformations in steel because the solubility of impurities depends on the local magnetic coupling. Recently, it was demonstrated experimentally that stabilization of ferritic and austenitic structures in steels occurs by short range ferromagnetic correlations. Our theoretical results reveal that light impurities (carbon, nitrogen) cause the short-range FM coupling and that the AFM-FM transition in fcc Fe occurs in a discontinuous way through the local magneto-volume instability. Further investigations (e.g. systematic studies of other interstitial and substitutional impurities) are required in order to understand the microscopic mechanisms responsible for the experimentally observed behavior. (A detailed plan of future work is given above.)

Table 1. Lattice parameters, total energy difference ΔE between phases and local magnetic moments m in γ -Fe, γ -Fe-N and γ -Fe-Mn-N

	FM/HS	AFM	AFMD
γ -Fe			
a , Å	3.43	3.42	3.46
c/a	1.17	1.07	1.08
ΔE , eV/atom	19	17	0
$m(\text{Fe})$, μB	2.4	1.6	2.0
γ -Fe ₃ 2N			
a , Å	3.46	3.47	3.48
c/a	1.16	1.05	1.08
ΔH , eV/atom	19	15	0
$m(\text{FeI})$, μB	2.1	1.5 \uparrow	1.4 \uparrow , 2.1 \downarrow
$m(\text{FeII})$, μB	2.0	1.1 \downarrow	1.9 \uparrow
γ -Fe ₃ 1MnN			
a	3.471	3.476	3.485
c/a	1.145	1.049	1.085
ΔH , meV/atom	25	14	0
$m(\text{Mn})$, μB	-2.56	1.40 \uparrow	1.54 \uparrow
$m(\text{FeI})$, μB	2.24	1.51 \uparrow	-2.08 \downarrow
$m(\text{FeII})$, μB	2.00	1.00 \downarrow	1.66 \uparrow

Conclusions

Density functional theory calculations were performed to study the structure and magnetic properties of ferrite and austenite Fe with 3 at. % nitrogen (carbon) and manganese impurities.

We find that impurities affect the local magnetic interactions significantly. The states with opposite manganese magnetic moments are quasi-degenerate in bcc Fe-Mn alloy, whereas octa-site carbon stabilizes ferromagnetic coupling of the nearest manganese atom with the Fe host. For the first time we demonstrate that the antiferromagnetic (AF) fcc Fe-N and Fe-Mn-N alloys are intrinsically inhomogeneous magnetic systems. Nitrogen frustrates the local magnetic order by reorientation of magnetic moments of the nearest Mn and Fe atoms, and favors their ferromagnetic coupling. Based on our results we believe that the AF-FM transition caused by impurity (nitrogen, carbon) concentration occurs in a discontinuous way through the local magnetovolume instability.

References

N.I. Medvedeva, D. Van Aken, J.E. Medvedeva, "Magnetism in bcc and fcc Fe with carbon and manganese", submitted for publication.

S. Sheet Formability and Springback of Advanced High Strength Steels

Principal Investigator: David K. Matlock
Advanced Steel Processing and Products Research Center
George S. Ansell Department of Metallurgical and Materials Engineering
Colorado School of Mines
Golden, CO 80401
(303)273-3775; e-mail: dmatlock@mines.edu

Co-Principal Investigator: John G. Speer
Advanced Steel Processing and Products Research Center
George S. Ansell Department of Metallurgical and Materials Engineering
Colorado School of Mines
Golden, CO 80401
(303)273-3897; e-mail: djspeer@mines.edu

Co-Principal Investigator – GOALI Partner: James G. Schroth
General Motors R & D Center
30500 Mound Road
M/C 480-106-212
Warren, MI 48090-9055
(586)986-0977; e-mail: james.g.schroth@gm.com

Principal Investigator – Partner University: Robert H. Wagoner
Department of Materials Science and Engineering
The Ohio State University
2041 College Road
Columbus, OH 43210
(614)292-2079; e-mail: wagoner.2@osu.edu

Technology Area Development Manager: William Joost
(202) 287-6020; e-mail: william.joost@ee.doe.gov

Contractor: Colorado School of Mines
Contract No.: National Science Foundation Award CMMI -0729114

Objectives

- Identify new processing routes and microstructures which lead to economical steels with properties characteristic of third generation AHSS.
- Experimentally and theoretically evaluate properties of new AHSS materials.

Approach including industrial partner/collaborator and path to technology transfer and commercialization

- Utilize theoretical predictions developed by the authors and others to predict ideal microstructures that lead to potential strength/ductility combinations characteristic of the third generation AHSS.

- Evaluate and develop novel laboratory processing methods to produce materials with controlled variations in phase volume fractions, distributions, and properties.
- Produce sample material for use in this project as well as in the companion springback study at Ohio State University (a partner with CSM through the NSF GOALI program).
- Experimentally evaluate the mechanical properties, including formability, of the experimental steels.
- Compare experimentally measured properties to predictions of the theoretical models.
- For materials which appear promising based on laboratory data, assess potential paths to process materials on a larger scale.

Milestones, Metrics, and Accomplishments

- Supported Senior Design Project at the Colorado School of Mines. The project entitled “Advanced High Strength Sheet Steels for Automotive Technology” evaluated the quenching and partitioning process developed by Speer and Matlock and was completed during the spring semester, 2009.
- Reviewed the research program and results during the semi-annual review meetings (March and September) of the Advanced Steel Processing and Products Research Center at the Colorado School of Mines.
- Processed materials following the methodology outlined in the report below and obtained mechanical property data.
- Initiated the development of a formative review article on current status of international research on AHSS.

Future Direction

- Complete the international review article and submit for publication.
- Complete the evaluation of the microstructures and properties of heat treated Mn steels and prepare summary paper for publication.
- Develop laminated materials with alternating controlled microstructural layers consisting of austenitic and either ferritic or martensitic microstructures.
- Expand model development for predicting microstructures and properties of multi-phase steels.
- Evaluate the mechanical properties of the layered materials and interpret based on predictions of a refined composite model.

Introduction

During this project period, the literature review has been expanded, evaluation of high manganese alloys has been initiated, and a draft of a formative review has been prepared. The PhD graduate student, Mr. Paul J. Gibbs, initiated his graduate studies in August, 2008 after completing his BS in Metallurgical and Materials Engineering at the Colorado School of Mines in May, 2008. The project was budgeted for three years and NSF funded the project over 4 years. In this

report, the backgrounds for the project is highlighted along with the materials and processing approaches that have been identified for the first phase of the research program. A detailed methodology to increase austenite stability through manganese (and carbon) partitioning is presented. The basis for this approach is illustrated.

Background

Recent research has shown that, in order to produce the new AHSS sheet steels, unique processing schemes will be required. It is anticipated [1-3] that these steels will be initially based on modifications to routes currently employed to produce dual phase (DP) and transformation-induced plasticity (TRIP) steels. To produce materials with the desired final properties, several microstructural features must be simultaneously and independently controlled. These include: number of constituents (e.g. phases) and constituent volume fractions, sizes, and distributions, along with the mechanical properties (e.g. strength and strain hardening behavior) of the individual constituents.

A methodology to assess the effects of microstructural variables in new AHSS grades has been demonstrated [2, 3] based on the composite model approach of Mileiko [4]. **Figure 1** compares predicted effects of systematic microstructural variations, obtained by increasing the martensite volume fraction (up to 70 pct), in hypothetical two-component composite materials comprised of either ferrite and martensite or stable austenite and martensite [2,3]. These predictions are superimposed on a strength-ductility map often used to compare sheet steel properties [1] and which identifies property bands associated with ferrite-based First and austenitic Second Generation AHSS families. For these calculations, specific properties for each phase were assumed based on trends in literature data. Predictions utilized a composite model for two ductile constituents assuming iso-strain [2]. Figure 1 shows that the properties of a wide variety of sheet steel families, including the First Generation AHSS steels, are reasonably predicted with a two-component ferrite-based system and that steels in the desired Third Generation band may be modeled by various combinations of martensite with stable austenite. Later calculations based on metastable austenite have shown that the resulting composite properties depend sensitively on austenite stability against deformation-induced transformation to martensite [3].

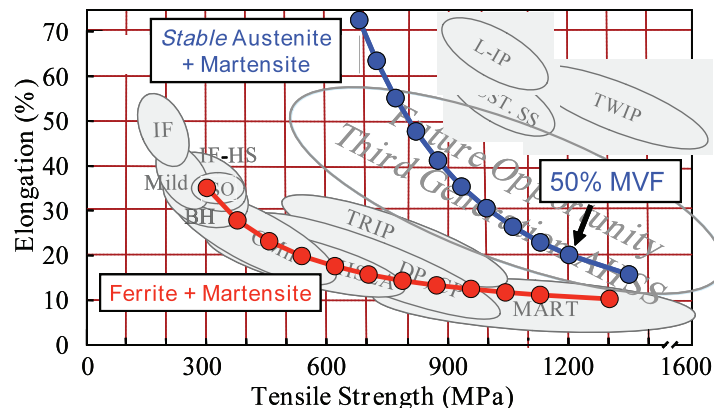


Figure 1. Predicted [2,3] strength/ductility combinations for two hypothetical steel families with systematically varied martensite volume fractions with property bands for various classes of conventional and AHSS steels [1]. Predictions shown are for composites consisting

The analysis summarized in Figure 1 successfully predicted strength-ductility properties for existing ferritic-based steels from low strength interstitial free (IF) to high strength martensitic steels and provides insight in to the requirements for the Third Generation AHSS. It appears clear that the Third Generation of AHSS will consist of complex microstructural combinations, with significant use of both high strength constituents (e.g. martensite, bainite, ultrafine grained

ferrite, etc) and high ductility constituents with significant strain hardening capacity (e.g. austenite with controlled stability against deformation induced transformation to martensite) [2,3]. Contemporary processing methodologies present several potential avenues to be developed to produce these microstructures.

Several production methodologies and resulting microstructures have been identified as candidates for new AHSS grades and these include:

- Modified processing to produced enhanced DP steels
- Use of low temperature processing to enhance ultra fine bainite formation
- Modified thermal processing utilizing rapid heating and cooling equipment
- Incorporation of modified TRIP alloys and processing histories.
- Use of the unique quenching and partitioning (Q&P) process
- Modified second generation steels to lower cost (e.g. lower manganese twinning induced plasticity steels (TWIP).
- Use of processing histories to stabilize austenite through manganese partitioning.

A comprehensive and formative literature review detailing methodologies used in the processing of these steels and resulting mechanical properties has been drafted and will be submitted for publication in the spring of 2010 [5]. This review paper will serve to focus research efforts and to highlight some of the areas for future development in the Third Generation AHSS. One important and promising area that has been identified is the use of processing histories to stabilize austenite through controlled manganese partitioning [6-12]. In the following sections manganese partitioning, a method to precondition austenite prior to thermal processing, is outlined and used to predict potential microstructures characteristic of high strength AHSS steels. It is envisioned that this methodology can be used to produce steels with properties characteristic of the third generation band shown in Figure 1.

Outline of Methodology to Precondition Austenite

The selection of steel alloy compositions is a balance between potential microstructures that can be generated and the cost of additional alloying elements. Manganese can fully stabilize austenite in steels with additions between 15-20 wt pct in bulk alloys as has been done with the development of TWIP steels [13] characteristic of Second Generation AHSS shown in Figure 1. However, this high level of alloying is generally cost prohibitive and leaner compositions are desired. Additionally, very high manganese additions potentially pose serious processing impediments such as manganese vaporization and mold erosion during casting as well as challenges in rolling and annealing. Through alloy design and heat treat selection it should be possible to use Mn partitioning to produce lower alloy steels with reasonable volume fractions of austenite containing high Mn contents and improved stability against transformation to martensite on quenching or during deformation. Bulk alloy additions between 2 and 7 wt pct manganese in representative low carbon steels are of interest to develop heat treatments with the goal to precondition the austenite for improved stability. Significant manganese enrichment in intercritical austenite should be possible while avoiding some of the potential complications of richer alloys.

To utilize the lower alloy steels to produce complex microstructures with significant amounts of Mn-stabilized austenite, a preconditioning heat treatment step is required. The methodology used for developing an austenite preconditioning treatment can be divided into two distinct steps: alloy and temperature selection based on thermodynamic predictions; and the development of

a heat treatment based on kinetic diffusion models with the consideration of cooling conditions based on assumed final chemical compositions. In the following sections, the design approach to predicting alloy compositions, process temperatures, and process times of interest are illustrated. This analysis is based on a set of experimental high manganese steels produced by Merwin and which were used, without a preconditioning heat treatment step, in several recent studies [6-9]. The compositions of these steels are outlined in Table 1 [6-9] and in the subsequent discussion; each steel will be identified by its Mn content.

Table 1. Idealized compositions for preconditioning experiments, [6-9]

Steel Designation	C	Mn	Si
5.2Mn	0.10	5.18	0.12
5.8Mn	0.095	5.80	0.13
7.1Mn	0.099	7.09	0.13

Alloy Theory and Preconditioning Temperature Selection

Using the bulk compositions listed in Table 1 and the ThermoCalc™ thermodynamic simulation program, the amount of intercritical austenite as a function of annealing temperature for the alloys in Table 1 was calculated and the results plotted in Figure 2a. Increasing the bulk alloy Mn content increases the amount of intercritical austenite at any particular temperature (e.g. at 600°C, an increase of Mn from 5.2 to 7.1 wt pct results in an increase in austenite from 25.6 to 42.4 pct). ThermoCalc™ was also used to predict the equilibrium compositions of the austenite at the intercritical annealing temperatures, and Figure 2b shows these results plotted for the 5.8Mn steel. With a decrease in annealing temperature from 700 to 500°C, the Mn content in the austenite present at the intercritical temperature increases from 6.6 to 21 wt pct. The amount of carbon in the austenite goes through a maximum at approximately 590°C, this maximum content reflects the presence of cementite (Fe_3C) below the peak temperature.

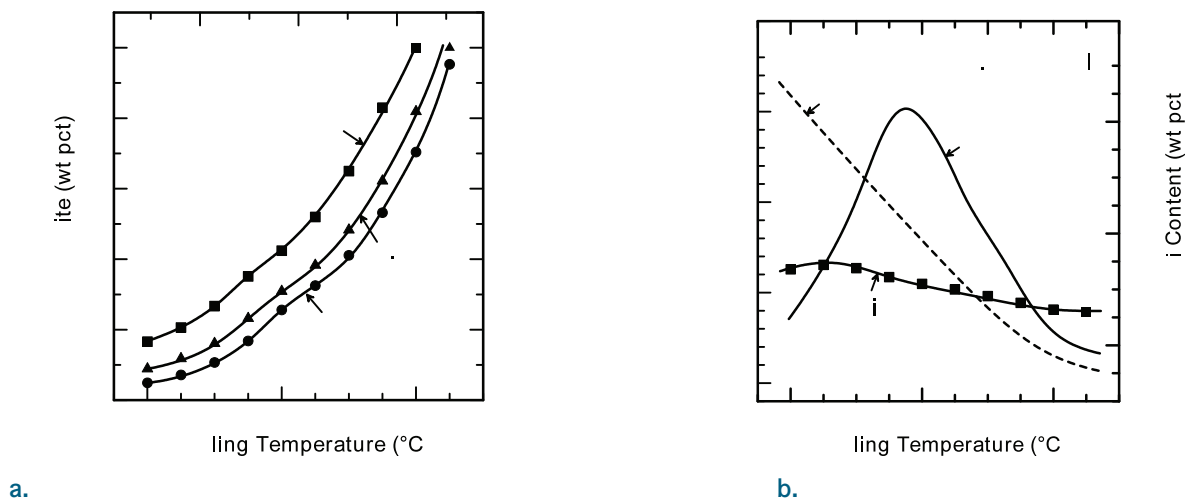


Figure 2. Predicted austenite amount as a function of annealing temperature for all three experimental alloys (a) and (b) predicted intercritical austenite compositions as a function of annealing temperature for the 5.8-Mn steel [15].

The data presented in Figure 2 can be used to identify potential intercritical annealing temperatures and possible austenite compositions for microstructures of interest. From the earlier modeling work [2,3], it was determined that retained austenite contents of at least 20 volume pct. at room temperature would be desired in potential candidate materials for Third Generation AHSS. Using the 5.8Mn steel as an example, Figure 2a shows that an annealing temperature of at least 575 °C would be required. Correspondingly, if a criterion of at least 10

wt pct Mn in austenite is set to maximize austenite stability to room temperature, then Figure 2b shows that annealing temperatures below 625°C are required for the 5.8Mn steel. Combining these two observations results in a window of potential annealing temperatures for which the microstructures of interest could be generated. The next step is to investigate, with diffusion calculations, the practicality of a potential partitioning heat treatment in the indicated heat temperature range to obtain desirable Mn enrichment of austenite.

Heat Treatment Development

Manganese is a substitutional alloying element on the iron lattice of a steel structure. This results in a generally low diffusion rate, especially in the close packed austenite phase. Since manganese enrichment of austenite during a preconditioning intercritical anneal is dependent on long range manganese diffusion from ferrite to austenite, generalized diffusion calculations can be used to predict annealing times. Relative diffusion distances were calculated for the two phases in the temperature ranges of interest based on the thermodynamic predictions. This was accomplished by using the equation:

$$x = P \times \sqrt{D \times t}$$

where x is the diffusion distance, P is a constant related to the solution of the error function and the symmetry of the problem and taken here to be 1.41, D is Mn diffusivity in the phase of interest, and t is the annealing time. The results of these calculations over the temperature range of 550 to 650°C are presented in Figure 3 for the 5.8Mn steel.

The calculations summarized in Figure 3 show that bulk manganese diffusion in ferrite is practical to distances of approximately 5 μm for the highest temperature case (i.e. 650°C). However, the diffusion distances in austenite are restricted to very short scales, approximately 1 μm , even at the upper temperature limit. Distances of this magnitude can be obtained by utilizing a starting microstructure of martensite, where the lath width would control the critical distance for Mn partitioning.

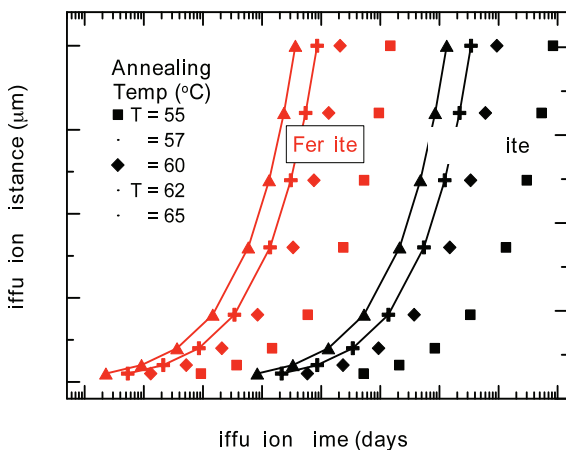


Figure 3. Calculated diffusion distances versus time for intercritical annealing temperatures in the range of 550 to 650 °C; manganese diffusion in ferrite and austenite [16-18].

Partitioning could be enhanced if the development of a cold worked martensitic starting structure prior to intercritical annealing is considered. The introduction of high diffusivity paths via the introduction of cold work could decrease the diffusion times by enhancing Mn transport in ferrite. This analysis reveals that starting microstructures other than martensite (bainite or ferrite-pearlite structures) would require significantly longer diffusion times, in some cases on the order of tens of years, to attain any significant manganese partitioning to the intercritical austenite.

Assuming that the intercritical treatment is successful in generating high manganese preconditioned austenite, the manganese will retard the high temperature transformations allowing austenite to be stable at room temperature. The limit of the austenite stability can be approximated by assuming instantaneous quenching from the intercritical temperature to room temperature, the degree of cooling below the martensite start temperatures will dictate the amount of retained austenite. The predicted martensite start temperatures, as calculated by the Andrews equation [19] for the predicted compositions in Figure 2b, are shown in Figure 4. It can be seen that the martensite start temperature decreases to a value below room temperature for equilibrium intercritical austenite compositions corresponding to a 600°C annealing temperature. If austenite of this

composition were quenched to room temperature rapidly enough to prevent high temperature transformation products (e.g. bainite, pearlite, and primary ferrite) then all of the intercritical austenite would be present at room temperature. For annealing temperatures above 600°C there is insufficient manganese and carbon present in the austenite to fully stabilize it to room temperature; however some fraction of the intercritical austenite will be retained as long as the quench temperature is above the martensite finish temperature. Additionally, the relative austenite stability for various partitioning temperatures can be inferred from this comparison.

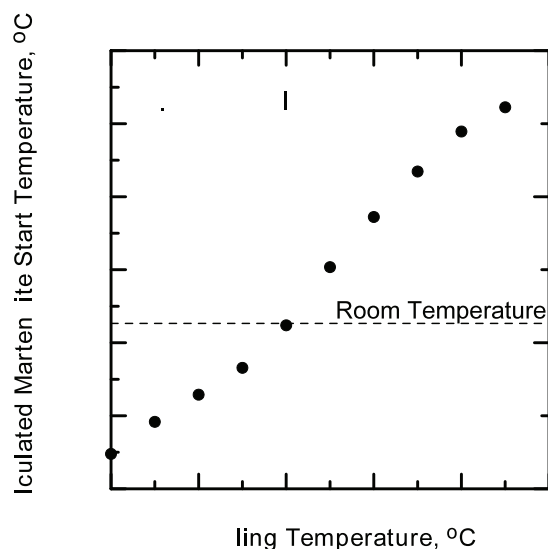


Figure 4. Predicted dependence of the martensite start temperatures as a function of intercritical annealing temperature for the calculated compositions shown in Figure 5; calculations based on the Andrews equation [19].

Applications of Manganese Partitioning

To test the applicability of the Mn partitioning treatment outlined above, a set of experimental heat treatments has been performed following the methodology. Three laboratory processed cold-rolled steels, with basic compositions listed in Table 1, were intercritically preconditioned in 25°C increments between 575 and 675°C for one week. The resulting temperature-dependent microstructures are composed of intercritical ferrite, martensite, and retained austenite. Mechanical properties of the steels are being assessed with tensile testing and vary with microstructure, depending on phase fractions present, from low strength moderate ductility to very high strength relatively limited ductility. Annealing between 600 and 650°C produced unique combinations of high strength-ductility and display deformation behaviors with decreasing yield to ultimate tensile strength ratios with increasing annealing temperature. These conditions also resulted in inverse strain hardening immediately after yielding. The mechanical property results are correlated to the microstructural constituents and the mechanical stability of the retained austenite. The results of these experiments are being compiled for presentation and publication at MS&T 2010 [20].

Summary and Conclusions

The preconditioning treatment outlined here allows for the systematic development of steel alloys and heat treatment methodologies. By combining this method with the presented model for strength and ductility processing routes to generate microstructures of interest for the Third Generation AHSS may be developed. This has been done for the three steel compositions listed in Table 1 and heat treatments have been performed. Additional, work has been initiated to refine the preconditioning model and to develop new experimental steel grades to test the

feasibility of the proposed methodology to AHSS. Additionally a review paper of current Third Generation AHSS principles has been compiled in draft form and will be submitted for publication shortly [5].

Presentations/Publications/Patents

1. March 17, 2009: “Design Principles for the Third Generation Advanced High Strength Steel,” by Paul Gibbs, a special presentation to the sponsors of the Advanced Steel Processing and Products Research Center.
2. May 12, 2009: Sheet Formability and Springback of Advanced High Strength Steels,” at the Auto/Steel Partnership/DOE/NSF Seminar in Livonia, MI (with J.G. Speer).
3. June 23, 2009: “AHSS: Sheet Formability and Springback of Advanced High Strength Steels: Austenite Preconditioning as an Approach to Enhance Formation of Retained Austenite in Advanced High Strength Steels,” 2009 National Science Foundation (NSF) Civil, Mechanical and Manufacturing Innovation (CMMI) Engineering Research and Innovation Conference, Honolulu, Hawaii. (with Paul. Gibbs, John Speer, John Schroth, and Robert Wagoner as co-authors).
4. September 15, 2009, Henry Fountain article “Many Faces, and Phases, of Steel in Cars” in New York Times with direct reference to the Third Generation AHSS. David Matlock and James Schroth are cited directly describing AHSS applications and development [21].
5. September 19, 2009: “Applications for Neutron Scattering at ASPPRC to Evaluate AHSS: A Report on the 2009 Los Alamos Neutron Science Center (LANSCE) Neutron Scattering School,” by Courtney Nowill and Paul Gibbs, a special presentation to the sponsors of the Advanced Steel Processing and Products Research.
6. September 20, 2009: “Design Principles for the Third Generation Advanced High Strength Steel,” Paul Gibbs, a special presentation to update progress and present current results to the sponsors of the Advanced Steel Processing and Products Research.
7. November 19, 2009: “Perspectives on Global Steel Product Developments,” Special lecture on AHSS as part of the Ispat-Industries, Mumbai, India, invited educational series.
8. D.K. Matlock and J.G. Speer, “Third Generation of AHSS: Microstructure Design Concepts,” Microstructure and Texture in Steels and Other Materials, ed. by A. Haldar, S. Suwas, and D. Bhattacharjee, Springer, London, 2009, pp. 185-205.
9. J.G. Speer and D.K. Matlock, “Progress in the Global Development of the Quenching and Partitioning Process,” Proceedings of the 17th International Federation for Heat Treatment and Surface Engineering (IFHTSE) Congress, ed. T. Maki, the Japan Society for Heat Treatment, Kobe, Japan, Vol. 49, Special Issue 2009, Vol. 2, pp. 415-422.
10. David K. Matlock, Paul J. Gibbs, John G. Speer, Robert H. Wagoner, and James G. Schroth, “Austenite Preconditioning as an Approach to Enhance Formation of Retained Austenite in Advanced High Strength Steels,” Proceedings NSF CMMI Research and Innovation Conference, Honolulu, Hawaii, June 22-25, 2009, published by NSF, Washington, DC, paper for Grant no. 0729114, 8 pages.
11. R. H. Wagoner, L. Suna, J.H. Sunga, J.H. Kimb, H. Limb, J. G. Schroth, and D. K. Matlock, “Draw-bend and Springback of Advanced High Strength Steels and Related Constitutive Model,” Proceedings NSF CMMI Research and Innovation Conference, Honolulu, Hawaii, June 22-25, 2009, published by NSF, Washington DC, paper for Grant no. 0727641, 7 pages.

References

1. "Third Generation Advanced High Strength Steel [AHSS]" Research and Development Solicitation, AISI, Washington, DC, 2006.
2. D.K. Matlock and J.G. Speer, Proceedings of the 3rd International Conference on Structural Steels, ed. by H.C. Lee, The Korean Institute of Metals and Materials, Seoul, Korea, 2006, pp. 774-781.
3. D.K. Matlock and J.G. Speer, Proceedings International Conference on Microstructure and Texture in Steels, ed. by A. Haldar, Springer-Verlag, London, 2009, pp. 185-205.
4. S.T. Mleiko, J. of Mat. Sci., vol 4, 1969, pp. 974-977.
5. E. De Moor, P.J. Gibbs, J.G. Speer, J.G. Schroth, D.K. Matlock, "Strategies for Third Generation Advanced High Strength Steel Development," for submittal to Iron and Steel Technology, 2010.
6. M.J. Merwin, Proc. of Mater. Sci. and Tech. 2007, Sept. 16-20, 2007, Detroit, MI, pp. 515-563, 2007.
7. M.J. Merwin, Proc. Of THERMEC 2006, Mater. Sci. Forum, Vols. 539-543, pp. 4327-4332, 2007.
8. M.J. Merwin, Proc. Of SAE Intl. World Congress & Exhibition, April 2007, Innovations in Sheet Steel Products and Processing, SAE Paper No. 2007-01-0336.
9. M.J. Merwin, Iron & Steel Tech., Vol. 5, No, 10, 2008.
10. R.A. Grange, and R.L. Miller, United States Patent, 4,047,979, September 13, 1977.
11. R.L. Miller, Metall, Trans. A, Vol. 3, pp. 905-912, 1972.
12. D.K. Matlock, P.J. Gibbs, J.G. Speer, R.H. Wagoner, and J.G. Speer, Proc. Of 2009 NSF Engineering Research and Innovation Conf. July 2009, Honolulu HI, 8 pages.
13. G. Frommeyer, U. Brück, and P. Neumann, ISIJ Int., vol. 43, no. 3, pp. 438-446, 2003.
14. M.J. Merwin, Proceedings of Steel Properties and Applications Conference, edited by L.C. Oldham, AIST, Warrendale, PA, 2007, pp. 1017-1038.
15. Thermo-Calc 3.1.1.2, Computer Software. Thermo-Calc Software AB, PC 2004.
16. N. Pussegoda, W.R. Tyson, P. Wycliffe, G.R. Purdy. Metall Trans A, vol 15A, 1984, pp. 1499-1502.
17. Smithells Metals Reference Book. ed. by W.F. Gale and T.C. Totemeier. 8th ed. 2004. Kidlington: Elsevier Inc.
18. A. Hoshino and T. Araki, Trans. Nat. Res. Inst. Metals, 1971, vol. 13, 99.
19. K.W. Andrews, JISI, vol. 203, 1965, pp. 721-727.
20. P.J. Gibbs, E. De Moor, M.J. Merwin, J.G. Speer, D.K. Matlock, "Long Time Intercritical Heat Treatment in Manganese TRIP Steels" Submitted to MS&T 2010
21. H. Fountain, "The Many Faces, and Phases, of Steel," The New York Times, September 15, 2009, nat. ed, D1+.

T. Sheet Formability and Springback of Advanced High Strength Steels

Principal Investigator: Robert H. Wagoner

Affiliation: George R. Smith Chair and Professor, Department of Materials Science and Engineering, Department of Mechanical Engineering, The Ohio State University
484 Watts Hall, 2041 N. College Rd, Columbus, OH 43210
(614) 292-2079; e-mail: wagoner.2@osu.edu

Co-Principal Investigator – GOALI Partner: James G. Schroth

Staff Research Engineer, General Motors R & D Center
30500 Mound Road, M/C 480-106-212, Warren, MI 48090-9055
(586) 986-0977; e-mail: james.g.schroth@gm.com

Principal Investigator – Partner University: David K. Matlock

Advanced Steel Processing and Products Research Center
Department of Metallurgical and Materials Engineering, Colorado School of Mines
Golden, CO 80401
(303) 273-3775; e-mail: dmatlock@mines.edu

Technology Area Development Manager: William Joost

(202) 287-6020; e-mail: william.joost@ee.doe.gov

Contractor: The Ohio State University Research Foundation

Contract No.: National Science Foundation Award CMMI-0727641

Objectives

- Identify the origins of unpredicted sheet forming failures (“shear fracture”) of Advanced High Strength Steels (AHSS).
- Develop a draw-bend fracture test (DBF) to reproduce shear fractures and measure formability under conditions similar to industrial practice but with laboratory precision.
- Improve the accuracy of springback prediction for AHSS.
- Develop a new theoretical material model incorporating what has been phenomenologically called “variable modulus” effects in the literature.
- Educational Program: attraction of promising and diverse students to related technical areas at both undergraduate and graduate levels.

Approach

- Devise advanced constitutive equations, implement in Finite Element Method
- Measure and simulate the failure and springback in draw bend tests
- GM-OSU collaboration to transfer fundamental springback and formability advances to commercial software and analysis

Milestone, Metrics and Accomplishments

- A novel H/V constitutive equation incorporating strain, strain rate and temperature effects was developed, tested, and published. It predicts necking and failure with much more accuracy than any existing constitutive model.
- Novel draw-bend formability (DBF) test was developed using dual displacement control. It provides better reproducibility and consistency than other such methods.
- DBF tests and corresponding thermo-mechanical FE models were developed and used successfully to predict “shear fracture” without damage mechanics. Part of this work has been published, other publications are in preparation.
- Identified the principal cause of “shear fracture” of AHSS as high deformation-induced heating at industrial strain rates; it is related to the very large energy absorption of these alloys. A secondary cause for some microstructures is internal fracture and damage, but this was observed only for isolated alloys and batches.
- Solved the long-standing problem of “variable modulus” effects and their role in springback prediction error by formulating a unique Quasi-Plastic-Elastic (QPE) model.
- The QPE model was used to simulate draw-bend tests and correctly predicted the springback. This work is in progress, but current results appear very promising.

Future Direction

- Apply the thermo-mechanical model to real parts using isothermal commercial software and shell elements.
- Compare the experimental data with simulation results of QPE model for complex sheet forming process.

Introduction

Advanced high strength steels (AHSS) offer impressive combinations of strength and ductility that can reduce the mass and improve the crash worthiness of sheet-formed automotive parts and vehicles. However, manufacturing automotive parts with AHSS have imposed many challenges: springback, edge cracking, early fracture (i.e. shear fracture), high residual stress, die wear, and high load capacity for press [1-2]. Among them the early fractures and springback have been critical barriers for the wide spread of AHSS [3-4]. One estimate says that springback related costs for well established materials amounts to \$50 million/year for only the U.S. automotive industry.

In this report, the different types of material failure, which were controlled by bend ratio, drawing speed ratios, and strain rate, were investigated in draw bend fracture tests for AHSS and deformation-induced heat was recorded to study the influence of thermo effect. Also, a novel H/V Model based on the tensile data of uniform strain range was developed and adopted to predict the AHSS failure without damage mechanics. On the other hand, a new Quasi-Plastic-Elastic (QPE) model, in which the evolution of Young’s modulus and Bauschinger effect were considered, was introduced and conducted to predict springback in draw bend tests by using FEM code. The prediction results were compared with the classical Chaboche model and secant modulus model.

1. A plastic constitutive equation [5]

An empirical 1D plasticity constitutive form describing the flow stress as a function of strain, strain-rate, and temperature has been developed, fit to data for three dual-phase (DP) steels, and compared with independent experiments outside of the fit domain.

Dubbed the “H/V model” (for “Hollomon / Voce”), the function consists of three multiplicative functions describing (a) strain hardening(f), (b) strain-rate sensitivity(g), and (c) temperature sensitivity(h) shown as:

$$\sigma = \sigma(\varepsilon, \dot{\varepsilon}, T) = f(\varepsilon, T) \cdot g(\dot{\varepsilon}) \cdot h(T)$$

Neither the multiplicative structure nor the choice of functions (b) or (c) is novel. The novel strain hardening function, (a), is proposed as:

$$f(\varepsilon, T) = \alpha f_H + (1 - \alpha) \cdot f_V$$

$$\begin{cases} f_H = H_{HV} \varepsilon^{n_{HV}} \\ f_V = V_{HV} (1 - A_{HV} e^{-B_{HV} \varepsilon}) \end{cases}$$

The strain hardening function has two novel features: 1) it incorporates a linear combination coefficient, α , that allows representation of Hollomon (power law) behavior ($\alpha = 1$), Voce (saturation) behavior ($\alpha = 0$) or any intermediate case ($0 < \alpha < 1$), and 2) it allows incorporation of the temperature sensitivity of strain hardening rate in a natural way by allowing α to vary with temperature (in the simplest case, linearly). This form therefore allows a natural transition from unbounded strain hardening at low temperatures toward saturation behavior at higher temperatures, consistent with many observations.

Hollomon, Voce, H/V models and others selected as representative from the literature were fit for DP590, DP780, and DP980 steels by least-squares using a series of tensile tests up to the uniform strain conducted over a range of temperatures. Jump-rate tests were used to probe strain rate sensitivity. Figure 1 shows one example of the fit results. The three forms are almost identical in the fit range, but the difference is getting bigger as the strain increases. Biaxial hydraulic bulge test results confirm the H/V model’s prediction in large strain area.

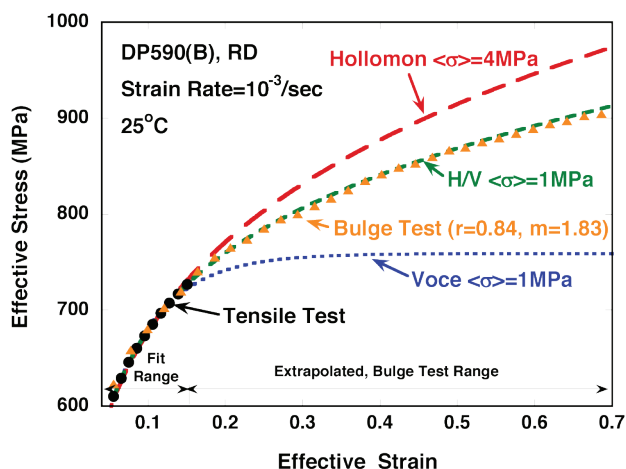


Figure 1. Large strain verification of H/V model [6].

The selected laws were then used with coupled thermo-mechanical finite element (FE) modeling to predict behavior for tests outside the fit range: non-isothermal tensile tests (Figure 2) beyond the uniform strain at room temperatures and isothermal tensile tests (Figure 3) beyond the uniform strain at several temperatures (Table 1). The agreement was best for the H/V model, which captured strain hardening at high strain accurately as well as the variation of strain hardening with temperature.

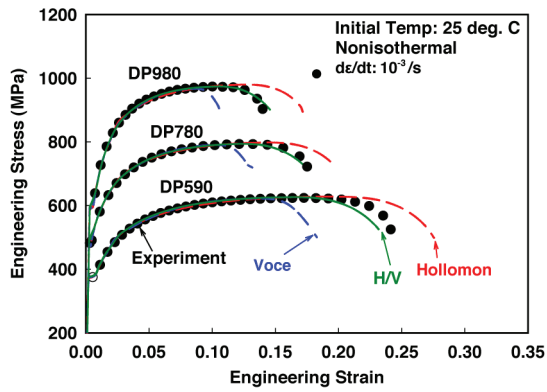


Figure 2. Comparison of nonisothermal tensile test data and FE simulation using selected constitutive models.

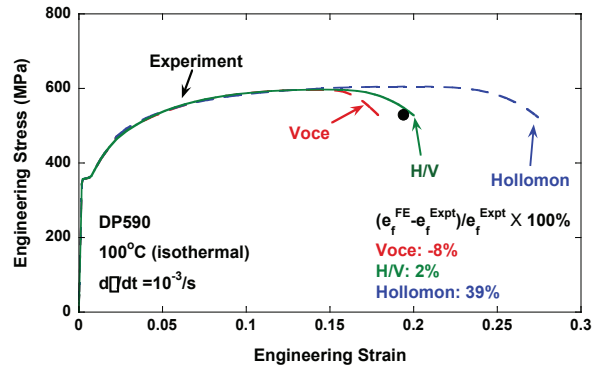


Figure 3. Comparison of isothermal tensile test data and FE simulation using selected constitutive models for DP590.

Table 1. Difference^a of total elongations of isothermal tensile tests conducted at 25, 50, and 100 °C and FE simulations for various constitutive models.

	$\alpha(T)=1$	$\alpha(T)=0$	H/V
DP590	23%	19%	3%
DP780	21%	22%	5%
DP980	29%	23%	6%
Avg.	24%	21%	5%

^a Computed by $(e_{f,FE} - e_{f,exp}) / e_{f,exp} \times 100(\%)$ where $e_{f,FE}$ is the predicted elongation at the time step when the predicted load matches the measured load at $e_{f,exp}$. The percentage error shown in the table is the average of the absolute values of these percentage errors for three temperatures: 25, 50, and 100 °C.

The agreement of FE predictions up to the tensile failure strain illustrates the critical role of deformation-induced heating in high-strength / high ductility alloys, the importance of having a constitutive model that is accurate at large strains, and the implication that damage and void growth are unlikely to be determinant factors in the tensile failure of these alloys.

The new constitutive model may have application for a wide range of alloys beyond DP steels, and it may be extended to larger strain rate and temperature ranges using alternate forms of strain rate sensitivity and thermal softening appearing in the literature.

2. Draw-Bend Fracture (DBF) Test [7]

Sheet forming failures of dual-phase (DP) steels occur unpredictably in regions of high curvature and with little apparent necking. Such failures are often referred to as “shear fractures”. In order to reproduce such fractures in a laboratory setting, and to understand their origin and the inability to predict them, a novel draw-bend formability (DBF) test was devised using dual displacement rate control (Figure 4).

DP steels from several suppliers, with tensile strengths ranging from 590 to 980 MPa, were tested over a range of rates and bend ratios (R/t) along with TRIP (Transformation Induced Plasticity) steel for comparison.

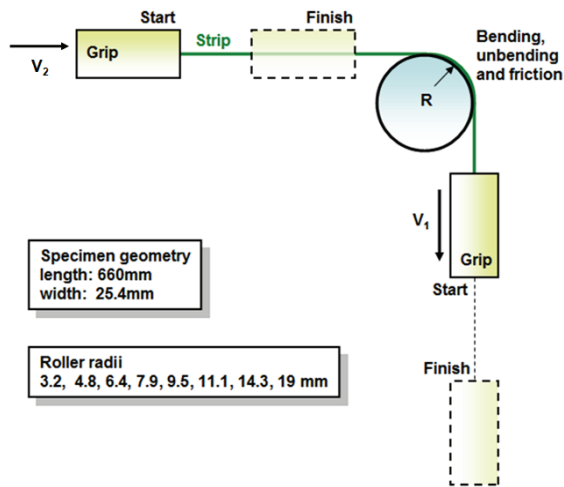


Figure 4. Schematic of draw-bend formability (DBF) test and the boundary conditions for the new dual-displacement controlled test (V_1 , V_2 , $V_2/V_1 = \alpha$, a constant).

The new test reliably reproduced three kinds of failures identified as Types I, II, and III, corresponding to tensile failure, transitional failure, and shear fracture, respectively (Figure 5). Especially, type II is unlikely to occur in typical industrial forming, where tight-radius features are usually very long relative to the sheet thickness and die radius.

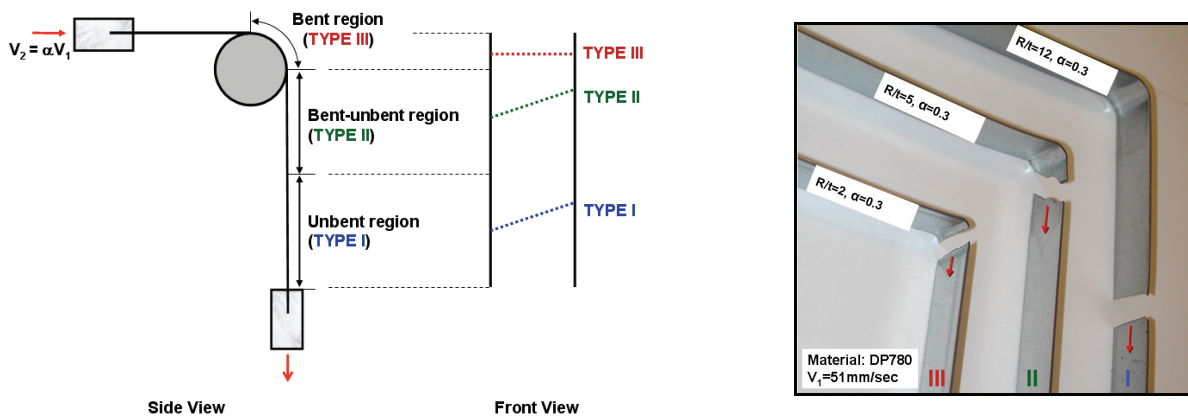


Figure 5. Examples of three types of fracture types with the dual displacement rate controlled test.

The type of failure depends on R/t and strain rate. Two critical factors influencing the lack of accurate failure prediction were identified. The dominant one is deformation-induced heating, which is particularly significant for advanced high strength steels because of their high heat dissipation. Temperature rises of up to 100°C were observed. This factor causes reduced formability at higher strain rates, and a transition in failure from Type I to Type III (Figure 6).

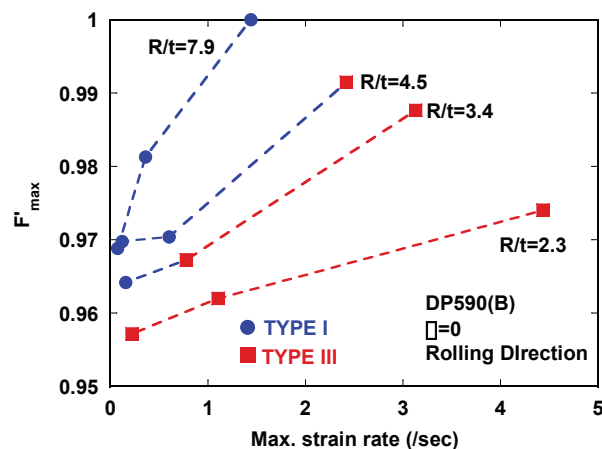


Figure 6. Fracture map of DP980, (b) F'_{max} vs. strain rate

The second factor is related to microstructural features. This was observed in only one material in one test direction (one DP980 (D) in the transverse direction). Alternate measures for assessing the formability of materials, including the effect of bending, were introduced and compared. They can be used to rank the formability of competing materials and to detect processing problems that lead to unsuitable microstructures.

3. A new model for springback prediction (Quasi-Plastic-Elastic model)

The evolution of Young’s modulus undergoing unloading-loading processes of DP980 is shown in Figure 7. It presents that the tangent unloading modulus is linear at the beginning and then decreased to a lower value. The similar phenomenon can also be observed in the reverse loading process. The calculated elastic strain error according to using traditional constant Young’s modulus during unloading process is between 20% and 30%. In order to predict springback accurately, Quasi-Plastic-Elastic (QPE) model was developed to describe this variation of Young’s modulus of Dual Phase Steels during metal sheet forming processes.

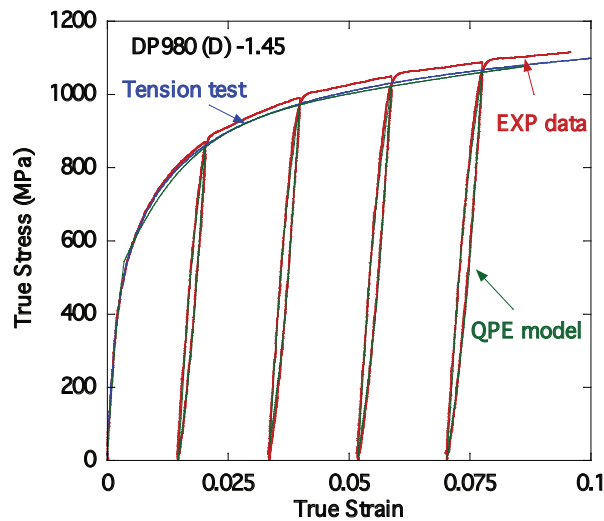


Figure 7. Unloading-loading test and QPE model for DP980

Two surfaces were introduced in QPE model: the inner surface f_1 and yield surface f_2 which is always outside the inner surface, with the magnitude R_1 and R_2 , respectively.

The material behaves according to a classical (linear) elastic principle inside the inner surface f_1 , which follows

$$d\sigma = C_0 : d\varepsilon_e$$

where C_0 and ε_e are the constant elastic modulus and elastic strain, respectively.

When the stress state is on the inner surface, $f_1=0$ and $\partial f_1 / \partial \sigma : d\sigma > 0$, the inner surface evolves inside the yield surface (the outer surface) f_2 . The dissipated energy is produced in this process; however, no plastic strain is introduced in order to distinguish it from plastic behavior. This dissipation-related strain is defined as Quasi-Plastic-Elastic (QPE) strain ε_{QPE} which is reversible and has the same direction as elastic strain but does not make any contribution to the stress. Both elastic and QPE strain are produced in this process. The relationship between stress and strain within QPE state is expressed as

$$d\sigma = C_0 : d\varepsilon_e = C(\varepsilon, \varepsilon_{QPE}) : d\varepsilon$$

$$d\varepsilon = d\varepsilon_e + d\varepsilon_{QPE}$$

where $C(\varepsilon, \varepsilon_{QPE})$ is the QPE modulus. It is assumed that the material is isotropic and the proposed QPE Young's modulus $E(\varepsilon, \varepsilon_{QPE})$ is exponential decay function in terms of total strain and QPE strain.

When the inner surface f_1 contacts the yield surface f_2 at the corresponding stress point $\bar{\sigma}$, and $\partial f_1 / \partial \sigma : d\sigma > 0$, plastic flow occurs and two surfaces are tangent at the loading point and then move together according to the classical Chaboche model. In plasticity, we have

$$d\sigma = C_0 : d\varepsilon_e = C' : (d\varepsilon - d\varepsilon_p)$$

$$d\varepsilon = d\varepsilon + d\varepsilon_{QPE} + d\varepsilon_p$$

where ε_p is the plastic strain and C' is the QPE modulus in plastic state.

For curve fitting the unloading-loading process, the least square method was used to determine the parameters of QPE model and it is shown that QPE model matches well with the experimental results of Young's modulus variation for DP980 in Fig. 7.

4. Simulation of springback in draw bend tests

Numerical simulations of a few draw-bend tests, for springback prediction, were carried out using a three-dimensional solid model (ABAQUS element C3D8R) with 5 layers through the sheet thickness. The specimen is 710mm length and 25.4 mm width. The back force was set to 60% and 80% of the 0.2% offset yield stress and the specimen was drawn to a distance 127mm at the rate of 25.4mm/s. At the end of test, the specimen was released and the springback angle was recorded to indicate the magnitude of the springback. An R/t ratio (roller radius/ specimen thickness) of 4.38 was used. A friction coefficient between the specimen and roller was taken as 0.04 in the simulations.

Figure 8 and Figure 9 compared QPE model, Chaboche model and secant modulus model with experimental results for the springback angles. The QPE model gave the best prediction in three models. The results indicated that Chaboche model much underestimated the effect of springback and the secant modulus model overrated it.

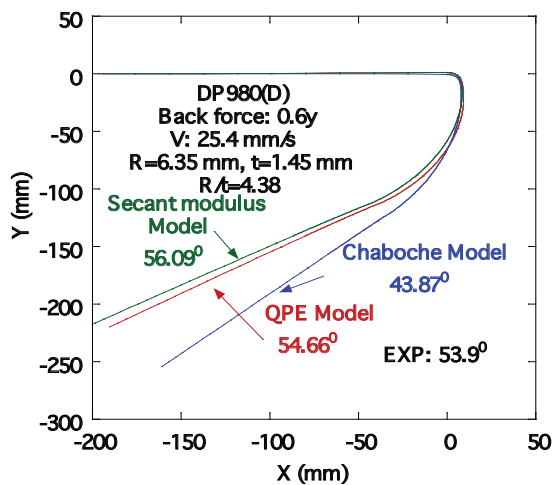


Figure 8. Springback prediction for the QPE model, Chaboche model and secant modulus model (0.6y).

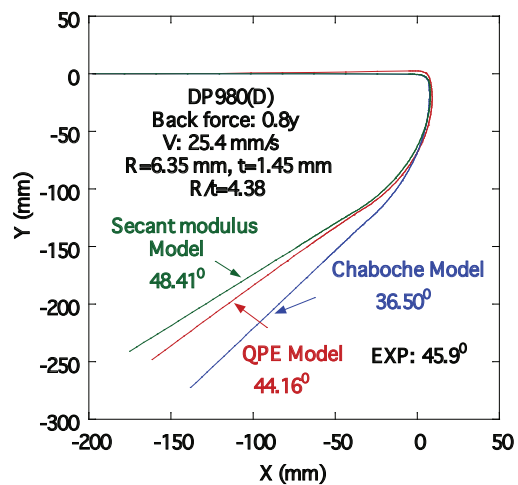


Figure 9. Springback prediction for the QPE model, Chaboche model and secant modulus model (0.8y).

Conclusions

- The origin of the unpredicted “shear fracture” of AHSS has been identified. The differences between predicted failures and actual behavior are predominantly related to ignoring deformation-induced heating in these strong, ductile alloys.
- A secondary effect is related to unfavorable microstructures in isolated batches of sheet, particularly for principal straining in the transverse direction.
- A novel displacement-controlled draw-bend test reproduces shear and tensile failures reproducibly and serves as a basis for evaluating the formability limited by both failure modes.
- A new constitutive equation, deemed the H/V Model, relates flow stress to strain, strain-rate, and temperature. For AHSS, the strain hardening rate varies significantly with temperature, which is critical to predicting formability.
- Thermo-mechanical finite element models with solid elements have been developed using the H/V Model and are capable of predicting shear and tensile failures with good accuracy. Remaining differences are attributable to fracture / damage rather than standard plastic localization.
- A firm mechanical basis incorporating “variable modulus” (also called “microplastic effects” in the literature) has been established. Deemed the Quasi-Plastic-Elastic (QPE) model, it introduces a third component of strain that is recoverable (elastic-like) but energy dissipative (plastic-like) and in a natural way produces nonlinear loading and unloading curves following stress/strain path changes.
- The QPE Model matches experimental results for “variable modulus” well and promises to improve the prediction of springback significantly.

Publications

1. H. Lim, M. G. Lee, Ji Hyun Sung and R. H. Wagoner, “Time-dependent Springback” , International Journal of Material Forming, Apr. 3, 2008.
2. R. Padmanabhan, Ji Hyun Sung, H. Lim, M. C. Oliveira, L. F. Menezes and R. H. Wagoner, “Influence of Draw Restraining Force on the Springback in Advanced High Strength Steels”, International Journal of Material Forming, Vol. 10, pp. 1-4, 2008.
3. R.H. Wagoner, A. Madeshia, Ji Hyun Sung, J. H. Kim, “Plasticity and Failure of Advanced High Strength Steel”, presented in Plasticity 2009, Jan. 3 – 9, St. Thomas, USA.
4. Wagoner, R.H, Kim, J.H. and Ji Hyun Sung, “Formability of advanced high strength steels”, International Journal of Material Forming 2, pp.359-362, 2009.
5. Ji Hyun Sung, J.H. Kim, and R.H. Wagoner, “A plastic constitutive equation incorporating strain, strain-rate, and temperature”, accepted to International Journal of Plasticity, Mar. 2009.
6. Ji Hyun Sung, J.H. Kim and R.H. Wagoner, “Draw-bend fracture of dual-phase steels”, (in preparation).
7. J. H. Kim, Ji Hyun Sung and R.H. Wagoner, “Finite element simulation of shear failure of advanced high strength steels”, (In preparation)

Presentations

1. Ji Hyun Sung, Ji Hoon Kim and R.H. Wagoner, "Constitutive Equation of AHSS", presented in NADDRG 2008, May 14-15, 2008, Windsor, CANADA.
2. Ji Hoon Kim, Ji Hyun Sung and R.H. Wagoner, "Finite Element Simulation of DP590 Draw-Bend Tests", NADDRG 2008, May 14-15, 2008, Windsor, CANADA.
3. Li Sun, Ji Hoon Kim and R.H. Wagoner, "Non-Proportional Hardening of Dual Phase Steels and Its Constitutive Representation", presented in IDDRG 2009 proceedings, pp.119-130, June 1-3, Golden, CO, USA.
4. H. Kim, A. Bandar, Y. Yang, Ji Hyun Sung and R.H. Wagoner, "Failure analysis of advanced high strength steels(AHSS) during draw bending", presented in IDDRG 2009 proceedings, pp.449-460, June 1-3, Golden, CO, USA.
5. J. H. Kim, Ji Hyun Sung, R.H. Wagoner, "Thermo-mechanical FEM of draw-bend formability tests", presented in IDDRG 2009 proceedings, pp. 503-512, June 1-3, Golden, CO, USA.
6. Ji Hyun Sung, J.H. Kim, and R.H. Wagoner, "Accurate constitutive eq. for dual-phase steels", presented in IDDRG 2009 proceedings, pp. 165-176, June 1-3, Golden, CO, USA.
7. H. Wagoner, Ji Hyun Sung, J. H. Kim: "The Formability of Dual-Phase Steels", Proc. 2009 International Symposium on Automobile Steel (ISAS09), Dalian, China, September 5-8, 2009.
8. R. H. Wagoner, Li Sun, Ji Hyun Sung, Ji Hoon Kim, H. Kim, J. G. Schroth and D. K. Matlock, "Draw-bend and Springback of Advanced High Strength Steels and Related Constitutive Model", NSF CMMI Grantee Conference, June 22 - 25, 2009, Honolulu, HI
9. Ji Hyun Sung, J.H. Kim, and R.H. Wagoner, "Sheet formability of advanced high strength steels", presented in NSF CMMI GRANTEE CONFERENCE 2009, June 22-25, Honolulu, HI, USA.

References

1. Demeri, M.Y., Forming of advanced high strength steels, in ASM handbook, S.L. Semiatin, Editor. 2006, ASM International: Materials Park, OH, USA.
2. Horvath, C.D. and J.R. Fekete. Opportunities and challenges for increased usage of advanced high strength steels in automotive applications. in International conference on advanced high strength steels for automotive applications. 2004. Golden, CO, USA: Association of Iron and Steel Engineers.
3. Wagoner, R.H., Advanced High-Strength Steels: Fundamental Research Issues, R.H. Wagoner, Editor. 2006, National Science Foundation, Department of Energy, Auto-Steel Partnership: Arlington, VA, USA.
4. Wu, J., et al., A failure criterion for stretch bendability of advanced high strength steels. SAE International, 2006: p. 2006-01-0349.
5. Sung, J.H., J.H. Kim, and R.H. Wagoner, A plastic constitutive equation incorporating strain, strain-rate, and temperature. Int J Plasticity (accepted on March 2010), 2010.
6. Wagoner, R.H., J.H. Sung, and J.H. Kim. The formability of dual-phase steels. in 2009 International Symposium on Automotive Steel (ISAS09). 2009. Dalian, China.
7. Sung, J.H., J.H. Kim, and R.H. Wagoner, Draw-bend fracture of dual-phase steels. 2010. (In Preparation).

U. Materials Design for Steel Alloys in the Southern Regional Center for Lightweight Innovative Designs (SRCLID)

Principal Investigator: Seong-Gon Kim
Associate Professor, Physics and Astronomy
Hilbun Hall, Rm 237
Mississippi State University (MSST), P.O. Box 5405
Mississippi State, MS 39762-5405
(662) 325-8031; e-mail: kimsg@hpc.msstate.edu

Technology Area Development Manager: Dr. Carol Schutte
(202) 287-5371; e-mail: carol.schutte@ee.doe.gov

Project Manager: Magda Rivera
e-mail: magda.rivera@netl.doe.gov

Participants: M. F. Horstemeyer, Hongjoo Rhee, Sungho Kim

Contractor: Mississippi State University
Contract No.: DE-FC-26-06NT42755

Objective

- Design a new high-strength steel alloy with improved strength and ductility for automotive applications.
- Identify the fundamental mechanisms at a quantum mechanical and a micromechanical level that determine overall strength and ductility of steel alloys.
- Investigate the interaction among different phases of high-strength steel alloys.
- Investigate the effect of micro-alloying elements to the material properties of high-strength steel alloys.
- Investigate the effect of various strengthening mechanisms to the material properties of high-strength steel alloys.

Approach

- We use a hierarchical multiscale methodology to investigate the effect of nanoscale precipitates and additives to the overall strength and ductility in steel alloy design for automotive applications.
- Critical issues being addressed include: selection of key micro-alloying elements, interaction of precipitate and matrix phases, and ultimately composition-structure-property relationship.
- At electronic level, quantum mechanical first-principles simulations based on Density Functional Theory (DFT) will be performed.
- At the atomistic level, accurate atomistic simulations will be performed using Modified Embedded Atom Method (MEAM) and force-matching-embedded-atom-method (FMEAM) potentials.

- Large scale atomistic simulations will be conducted to study the effect that size, shape, and volume fraction of different inclusion particles have on the material properties of steel alloys.
- Results will be used to guide quantitative alloy composition designs to improve strength and ductility of steel alloys.

Accomplishments

- The objectives were met by accomplishing the following:
- Performed the full spin-polarized density functional theory (DFT) calculations on Fe ferrite phase to correctly account for the ferromagnetism in Fe atoms.
- Developed a new multi-objective optimization methodology as a robust procedure to construct reliable and transferable interatomic potentials for steel alloy systems.
- Applied the multi-objective optimization (MOO) procedure to construct reliable interatomic potentials for Fe, C, Fe-C, V, and Fe-V using the modified-embedded-atom-method (MEAM).
- Established a basic framework for the accelerated development of reliable and efficient interatomic potentials for other combination of alloy systems.
- Performed DFT calculations on cementite Fe-C alloy phase and optimized the structure.
- Investigated the microalloying effect of vanadium on steels using DFT methods.
- Conducted fundamental materials/mechanical properties characterization and microstructure characterization on advanced high strength steel (AHSS) alloy samples obtained from POSCO, performed thermomechanical treatment, and investigated the effect of bake-hardening.
- Established close collaborative relationships with industrial partners including POSCO, SAC, Inc., and Wade Service.

Future Direction

- Construct and validate reliable interatomic potentials to model various phases of high-strength steel alloys
 1. Determine MEAM potentials for Si, N, Mn, and V
 2. Determine MEAM potentials for various combinations of elements for steel alloys (Fe-C-V, Fe-C-Si, Fe-C-Si-Mn, etc.)
- Perform electronic and atomistic simulations to obtain the electronic, structural, and mechanical properties of the main phases of steel alloys.
 1. Alpha-ferrite, cementite, martensite, etc.
 2. DFT and MEAM calculations
- Perform electronic and atomistic simulations to investigate the interactions between main phases of high-strength steel alloys.
 1. Alpha-ferrite, cementite, martensite, etc.
 2. DFT and MEAM calculations

- Perform electronic and atomistic simulations to investigate the effect of microalloying of high-strength steel alloys.
 1. Vanadium (V), Titanium (Ti), etc.
 2. DFT and MEAM calculations
 3. Diffusion; effect on dislocation mobility; interaction with grain boundaries
- Perform heat treatment (i.e., intercritical annealing followed by quenching), structure observation, and mechanical tests on DP steels to characterize the effect of martensite volume fraction and carbon content in matrix martensite on the mechanical behavior of AHSS.

Introduction

Despite their desirable material characteristics, high-strength steels have limited fabrication capability because they inherently resist deformation and wear the tooling. Therefore, we have the challenge and opportunities to perform compositional design of high-strength steel alloys in a manner that lowers mass, increases strength, retains workability, and generates required strength after the fabrication step.

Potential components for lightweight and ultra-strength materials are the front end, power train, instrument panels, the chassis system, and car bodies including door panels, for example. We propose to perform compositional design of steel alloys to lower these barriers with a better understanding of the quantum-mechanical and atomistic structure of various constituent composite crystal structures and their interactions, the influence of alloying additions, and the effects of thermomechanical treatments on wrought materials during and after processing. Ductility of materials can be improved by alloying and by the resulting activation of slip systems. We will investigate the origin of these alloying effects by using first-principles methods such as Density Functional Theory (DFT). We will focus on understanding the extent to which these effects are governed primarily by electronic structure or crystallography.

Computational Approach

We use a hierarchical, multiscale methodology to investigate the effect of nanoscale precipitates and additives to the overall strength and formability in steel-alloy design for automotive applications. In a hierarchical, multiscale framework, numerical methods are run independently at disparate length scales. Then, a bridging methodology such as statistical-analysis methods, homogenization techniques, or optimization methods are used to distinguish the pertinent cause-effect relations at the lower scale to determine the relevant effects for the next higher scale (E and Engquist (2003)). We will adopt the strategy developed by Horstemeyer and his co-workers who used ISVs as a top-down hierarchical approach to bring the pertinent nanoscale, microscale, and mesoscale phenomena into the macroscale (2003) and Olso (1998).

Critical issues being addressed include: selection of key combination of precipitates and matrices, interaction of precipitate and matrix phases, and, ultimately, composition-structure-property relationship. At the electronic level, quantum-mechanical first-principles simulations will be performed to investigate the interfacial interactions between matrix and the primary and the secondary precipitates. All first-principles, total-energy calculations and geometry optimizations are performed within DFT using Blöchl's all-electron projector augmented wave (PAW) method (Blochl (1994)) as implemented by Kresse et al. (1996). For the treatment of electron exchange and correlation, we generally use the local density approximation (LDA) (Perdew and Zunger (1981)) and sometimes the generalized gradient approximation (GGA) (Perdew et al. (1996))

depending on the accuracy required. At the atomistic level, accurate atomistic simulations will be performed using efficient and reliable empirical interatomic potentials such as the modified-embedded-atom method (MEAM) (Baskes (1992)) or force-matching embedded-atom method (FMEAM) (Li et al. (2003)) potentials. The interatomic potentials are constructed by optimizing the potential parameters to reproduce various experimental materials properties and atomic-force data from DFT calculations. Large-scale, atomistic simulations will be conducted to study the effect that size, shape, and volume fraction of different precipitates have on the thermomechanical properties of steel alloys. Many factors that govern the yield, hardening, and fracture behavior of solids, such as, crack-tip propagation, dislocation nucleation, dislocation motion, and the interaction of dislocations with grain boundaries will be investigated through these simulations. Results will be used to guide quantitative alloy composition designs to improve strength and formability of steel alloys. For more detailed description of experimental and computational approach, see 2007 Annual Report (Kim et al. (2007)).

Experimental Approach

In order to design a novel AHSS alloy with improved strength and ductility, the effects of various phases, novel additives, heat treatment, and manufacturing processes on the materials and mechanical properties of the AHSS are investigated. The overall chemical analysis of the base-alloys is performed by using a spectrometer. The quantitative as well as qualitative chemical compositions of each phase present in the alloys are individually analyzed by an energy dispersive x-ray (EDX) spectroscopy technique. Microstructures of the alloys are investigated by an optical microscope and a scanning electron microscope (SEM). Conventional hardness tests are conducted to gain overall properties of the alloys, while nanoindentation tests are performed to obtain micromechanical properties of various phases found in the alloys.

A small amount of sample is manufactured and supplied by the industrial partners, and the model validation by various experiments is carried out. The main objective of experimental study on the base-alloys (e.g. AHSS) is to carry out systematical research on the strain rate dependence of strengthening mechanisms. In order to achieve this goal, the effectiveness of different metallurgical strengthening mechanisms in the quasi-static regime was quantified. That in the automotive high strain rate regime will be quantified during phase II research. The base alloys in the present research were commercial grade dual phase (DP) steels provided by an industrial partner (POSCO, South Korea). Data obtained from such experiments will be provided to atomistic simulation and modeling research to develop third generation AHSS. The base-alloys in this research, DP steels, are characterized by a ferrite matrix with small islands of martensite [IISI06]. The hard martensite phase provides substantial strengthening while the soft ferrite matrix gives good ductility and formability. The favorable combination of strength and ductility coupled with a relatively simple chemical composition and manufacturing process make DP steels very attractive for automotive applications as a structural material for weight reduction and formability. The DP steels exhibit higher initial work hardening rate, higher ultimate tensile strength, and lower yield strength/tensile strength ratio than the similar yield strength HSLA steels.

Computational Results

MEAM potentials for Fe-C alloys

We developed a new MEAM potential for Fe-C alloys using a multi-objective optimization procedure (Kim et al. (2009)) based on the MEAM potentials for pure Fe and C (Baskes (2009)). **Figure 1** shows the cohesive energy of Fe-C alloy systems in the B1 and L12 crystal structures as a function of the nearest neighbor distance. Our results show that the MEAM potential for

Fe-C alloy system reproduces DFT calculations reasonably accurately for these two structures over a wide range of nearest neighbor distances.

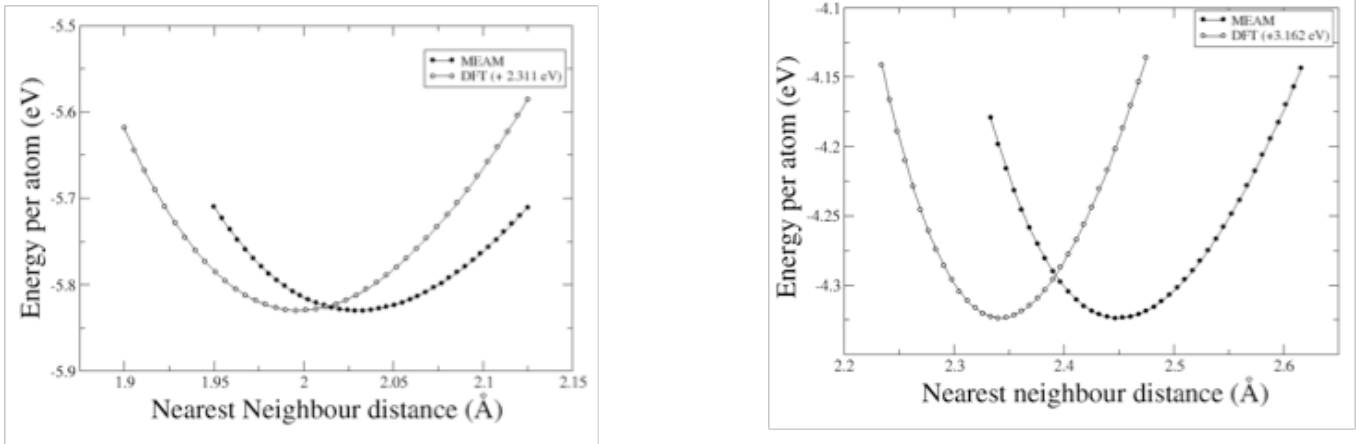


Figure 1. The cohesive energy of Fe-C alloy systems as a function of the nearest neighbor distance in Å. (a) FeC in B1 crystal structure and (b) FeC in L12 crystal structure. The result by MEAM potential (filled circles) are compared with those of the DFT calculations (open circles).

To further test the validity of our alloy potential, we computed several physical properties of Fe-C alloy systems and compared them with DFT values. We found that the new Fe-C MEAM potential demonstrates excellent agreement with DFT calculations for many important physical quantities. Particularly, our Fe-C potential reproduces the heat of formation results from DFT calculations accurately for three of the main crystal structures of Fe-C alloy system. Furthermore, the order of stability between two interstitial C defects in Fe is correctly reproduced by the new Fe-C potential.

Diffusion of V in ferrite

Vanadium is one of the most important microalloying elements for steels. We used DFT to study the effect of V atoms in ferrite. Since vacancies are readily available in the ferrite phase of most AHSS alloys, we consider the diffusion of Fe and V atoms assisted by vacancies. The Fe atom in the center of Figure 2(a) moves to the adjacent vacancy via the intermediate structure shown in Figure 2(b). Likewise, the V atom in the center of Figure 2(c) moves to the vacancy via the intermediate structure in Figure 2(d).

The energy barriers for migration of Fe and V atoms in the presence of Fe vacancies are

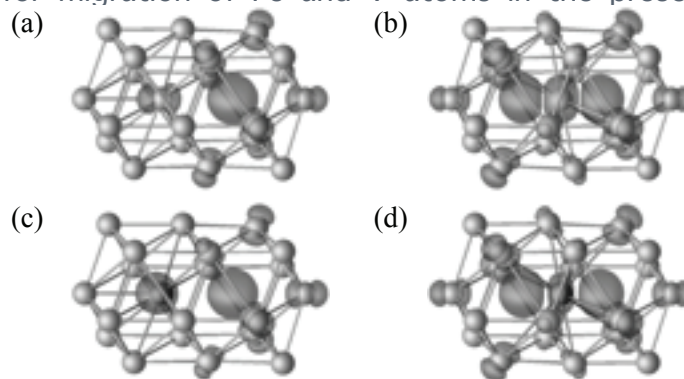


Figure 2. Diffusion of Fe vacancy and V substitutional defect in ferrite. (a) Fe vacancy, (b) an intermediate state of Fe atom diffusion, (c) V substitutional defect, and (d) an intermediate structure of V diffusion. Semitransparent balloons represent the isosurfaces of electron charge densities relative to that of perfect ferrite crystal. Fe (V) atoms are represented by lighter (darker) spheres.

calculated as shown in Figure 3. The migration energy for a V atom is about 0.17 eV lower than that of a Fe atom. Furthermore, low migration energy of V atom (0.55 eV) indicates that V atoms move around fairly easily in ferrite phase of the steels.

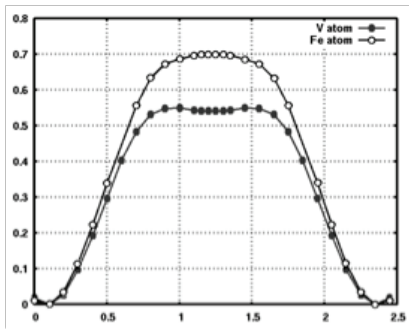


Figure 3. The relative total energies of V atom (circles) and Fe atom (diamonds) diffusion in ferrite. All relative energy values are computed relative to the total energy of their respective initial configurations.

Diffusion of V in cementite

We use the DFT method to investigate microalloying in the cementite (Fe_3C) phase. First, we studied the vacancy-assisted diffusion of Fe atoms from various atomic positions as summarized in Figure 4. Our results indicate that Fe (V) atom can diffuse to a vacancy with the energy barrier of 0.76 (0.73) eV, which are low enough to allow the diffusion of Fe or V atoms at room temperature.

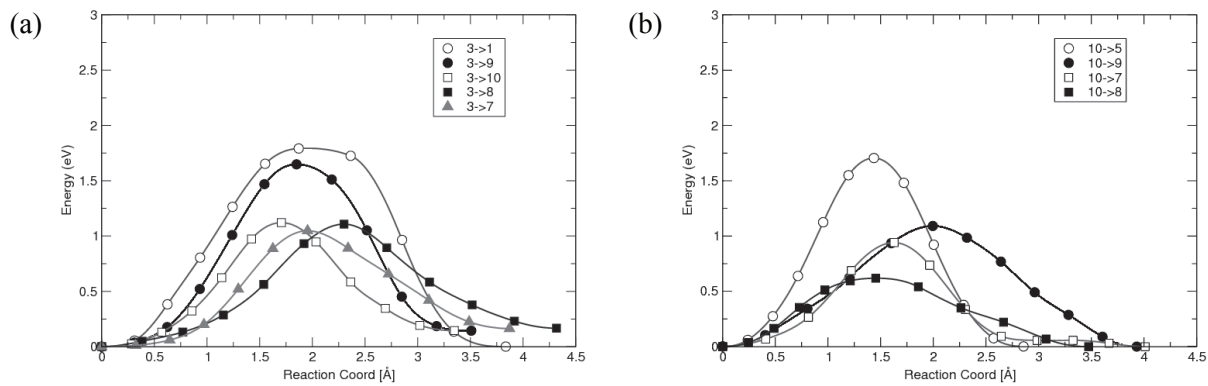


Figure 4: The relative total energies of (a) Fe and (b) V atom during vacancy-assisted diffusion in cementite.

Peierls stress in steel alloys

The strength and ductility of advanced high-strength steel alloys are determined mainly by the properties and behavior of dislocations. The micro-alloying element V makes the steel alloy stronger and interacts with dislocations present in the material. The interaction between V and dislocations affects the plastic properties of the advanced high-strength steels. These interactions are investigated through large scale simulations using empirical interatomic potentials. As the first step to study the effect of micro-alloying elements on the dynamics of dislocations, we compute the Peierls stress in the available slip systems in ferrite.

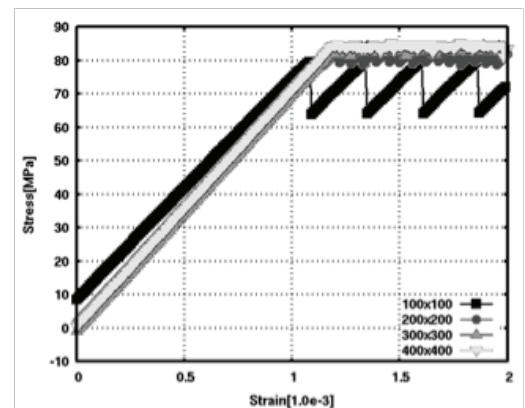


Figure 5: The stress-strain plots in different system sizes 100x100, 200x200, 300x300, and 400x400 Å in perfect $\frac{1}{2}\langle 111 \rangle$ edge dislocation lying along a $\langle 112 \rangle$ direction in a $\{110\}$ slip plane in a BCC iron crystal.

The incremental shear strains are applied in x -direction on x - z planes around an edge dislocation lying in z -direction until the measured stress reach maximum at Peierls stress and the dislocation starts to move (Osetsky and Bacon (2003)). The periodic boundary conditions are applied in x and z directions. Figure 5 shows the size effect of stress-strain calculation in perfect $\frac{1}{2} \langle 111 \rangle$ edge dislocation lying along the $\langle 112 \rangle$ direction in a $\{110\}$ slip plane in a BCC iron crystal using the EAM interatomic potential for Fe by Mendeleev et al. (2003). The Peierls stress converges nicely to 83 MPa as the system size increases.

There are many slip systems in BCC ferrite crystals. When the applied stress reaches the Peierls stress value, a dislocation responds by moving along one of the crystallographic planes of the Burgers vector closest to the maximum resolved shear stress (MRSS) plane. The MRSS's in different slip systems are compared in Figure 6. The slip system $\frac{1}{2} [111] (110)$ has the lowest Peierls stress and dominantly affects the plastic properties in iron polycrystals.

The core structure and other properties of dislocation depend highly on the stacking fault energies. The optimum structure of a dislocation is determined by stacking fault energies in various configurations. Understanding the stacking fault energies is important in studying the behavior of dislocations. The generalized stacking fault energy curves are shown in Figure 6 in two different slip systems using density functional theory (DFT) calculations and the Embedded Atom Method (EAM).

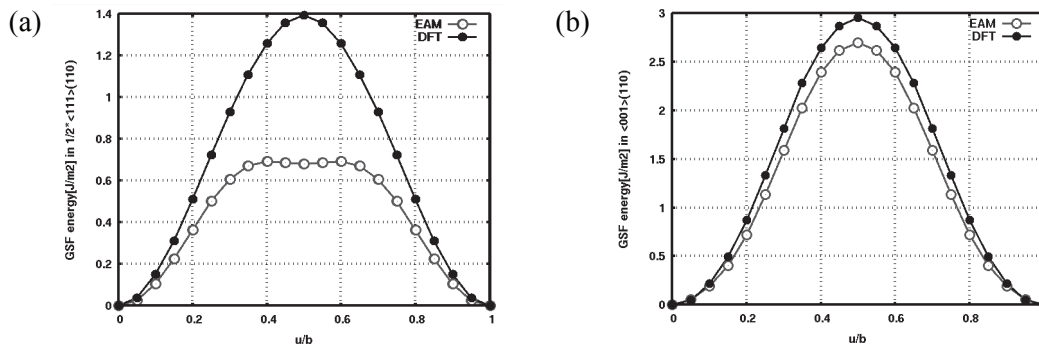


Figure 6. The generalized stacking fault energy curves using DFT and EAM in perfect (a) $\frac{1}{2} \langle 111 \rangle$ and (b) $\langle 001 \rangle$ edge dislocations lying along a $\langle 112 \rangle$ and $\langle 1-10 \rangle$ directions in a $\{110\}$ slip planes respectively in a BCC iron crystal.

Experimental Results

DP590 grade steel, one of the widely used DP steels in automobile structural parts, obtained from an industrial partner (POSCO, South Korea) was used in this study. Our previous research on the DP steel alloy revealed that the combination of formability and strength makes bake hardenable DP steels good options for drawn or stretched applications where resistance to dents and palm printing is important in applications such as hoods, doors, fenders, and deck lids. DP steels exhibit a high uniform and total elongation and lower yield strength to tensile strength ratio (YS/TS) compared to conventional high strength steels. These characteristics provide improvements in both formability and structural performance in automotive components. An added focus of the present research is to study the effect of controlled constituent phase distribution on the strength-ductility combination of DP steels for developing tailorable 3rd generation advanced high strength steels (AHSS). We have been investigating the role of microstructure on the strength-ductility combination of DP steels. Various combinations of microstructure, grain size, phase volume fraction, and phase distribution will be acquired by carrying out different heat treatment schedules. Various heat treatments including intercritical annealing followed by quenching in different quenching media, structure observation, and mechanical tests on DP 590 grade dual phase steel samples have been carried out to characterize the effect of martensite volume fraction and carbon content in matrix martensite on the mechanical behavior of AHSS. In addition, similar heat treatments on a different grade of AHSS, such as transformation

induced plasticity (TRIP) steel alloys, will be carried out to investigate the effect of phase transformation of constituent phase (i.e., retained austenite to martensite) and volume fraction on the mechanical behavior of AHSS. The results will enable the prediction of optimum strength-ductility combination of AHSS for desired components of automotive applications.

In order to investigate the effects of modified microstructure on the mechanical behavior of AHSS, various heat treatment conditions were implemented to gain different martensite volume fraction, C content in martensite, ferrite grain size, etc. Metallographic specimens were sectioned as 1x1 in² size samples from a 3mm-thick DP 590 grade steel plate. The first set of heat treatments was carried out on prepared DP 590 steel specimens after fully austenizing the specimens at 925°C and then annealing at different temperatures of 720, 760, and 800°C in a muffle furnace followed by quenching in different quenching media of oil, water, and ice-brine. Other sets of heat treatments with varying heat treatment conditions (e.g., direct annealing without fully austenizing, double annealing, post-process heat treatments, etc.) will also be performed in the near future.

Heat treated samples were ground, mechanically polished, and etched in a 2% nital to reveal general microstructure. Typical microstructures and hardness values obtained after such heat treatments at different annealing temperatures and quenching media are depicted in Figure 7. Microstructure observation results revealed typical ferrite and martensite dual phase with varying phase volume fractions with respect to different annealing temperatures and cooling rates.

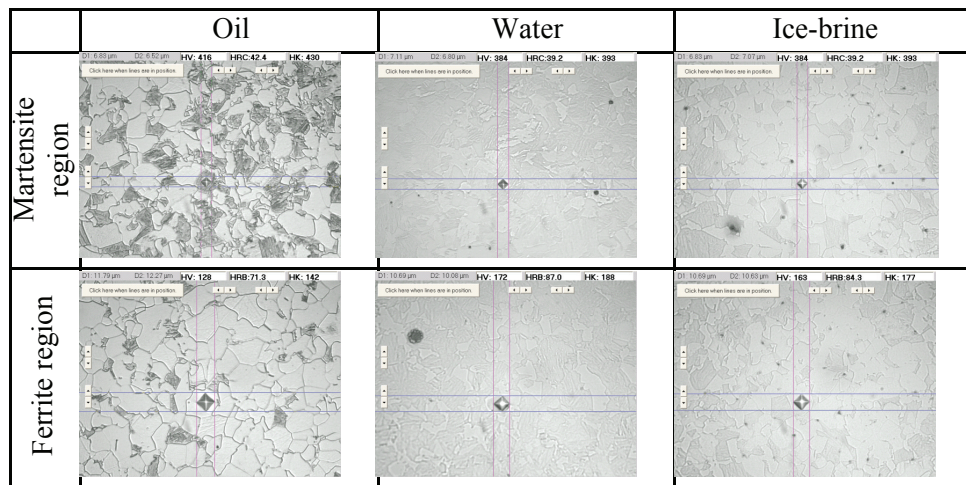


Figure 7. Typical microstructures and hardness values obtained after austenizing at 925 °C and then 720 °C annealing followed by quenching at different quenching media.

Figure 8(a) provides the area volume fractions of martensite and ferrite phases measured by using the in-house image analyzer software after heat treatments obtained from above microstructural images. The amount of martensite phase slightly increased with increasing annealing temperature for a given cooling rate. They also increased with increasing cooling rate for all annealing temperature ranges. However, no significant changes in phase volume fractions are noted between water and ice-brine quenching due to similar hardenabilities of this material in those quenching media.

Microindentation tests were carried out to obtain micromechanical properties of different phases found in the material by using a Vickers hardness tester. Overall hardness and hardness values of each phase were measured and the results are depicted in Figure 8(b). In this test set-up, overall hardness values were measured by indenting on the regions including both martensite and ferrite phases, whereas hardness values of each phase were obtained by indenting on the regions only containing individual phase. Not surprisingly, the martensite phase possessed

much higher hardness values compared to ferrite phase. Overall hardness values showed a similar trend to the results obtained from Figure 8(a). This implies that the volume fraction of constituent phases in DP steels plays an important role on the mechanical behavior of such material. Mechanical tests—including tensile tests after implementing aforementioned heat treatments—will be carried out to study the effects of modified microstructures on the mechanical behavior of DP steels. Effects of modified microstructures on the bake hardenability of DP steels will also be investigated.

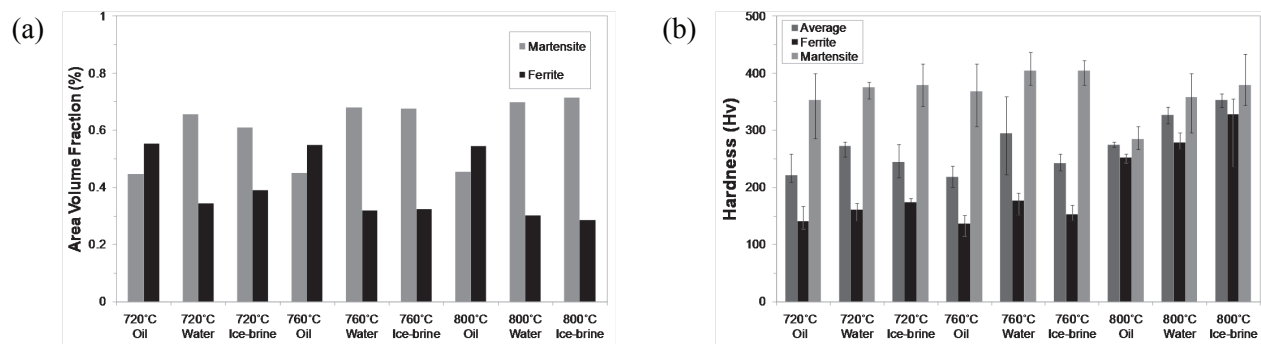


Figure 8. Comparisons of martensite and ferrite (a) area volume fractions and (b) hardness values after performing heat treatments at different annealing temperatures and quenching media.

Conclusions

The goal of this project is to investigate the effect of nanoscale precipitates and novel additives to the overall strength and formability of advanced high strength steel alloys. Quantum mechanical first-principles simulations based on DFT were performed on the main phases of AHSS to investigate the microalloying effect. The diffusion of V atoms assisted by Fe vacancies in the ferrite phase and cementite phase is simulated and the migration energies are obtained. We found that V atoms move easily in ferrite. We also calculated the formation energies of various defects relevant to microalloying of V atoms in cementite. We characterized materials and mechanical properties of AHSS alloys using dual-phase (DP) steels. We also performed thermomechanical treatment and investigated the effect of pre-strain on bake-hardening of DP steels.

Presentations/Publications/Patents

Seong-Gon Kim, M. F. Horstemeyer, M. I. Baskes, Masoud Rais-Rohani, Sungho Kim, B. Jelinek, J. Houze, Amitava Moitra, and Laalitha Liyanage, “*Semi-empirical Potential Methods for Atomistic Simulations of Metals and Their Construction Procedures*,” J. Eng. Mater. Technol., 131 (4), 041210 (2009).

Jeff Houze, Sungho Kim, Moitra Amitava, B. Jelinek, Sebastien Groh, M. F. Horstemeyer, Erdem Acar, Masoud Rais-Rohani, and Seong-Gon Kim, “*A multi-objective optimization procedure to develop modified-embedded-atom-method potentials*,” Preprint, <http://arxiv.org/abs/0708.0075>

L. Liyanage, Amitava Moitra, J. House, Sungho Kim, Seong-Gon Kim, and M. F. Horstemeyer, “*A modified embedded-atom-method potential for Fe-C alloy systems*,” In preparation.

J. House, Sungho Kim, Amitava Moitra, L. Liyanage, Seong-Gon Kim, and M. F. Horstemeyer, “*The vacancy-assisted diffusion of V atoms in cementite: An ab-initio study*,” In preparation.

Seong-Gon Kim, "Materials Design for Steel Alloys by Multiscale Modeling", Keynote Speech at 45th Steel Technology Symposium, POSCO, Kwangyang, KOREA, July 17, 2008.

Sungho Kim, Jeffrey Houze, Seong-Gon Kim, Mark Horstemeyer, "Vanadium diffusion in ferrite," APS 2009 March meeting, Pittsburgh, PA, Mar. 16-20, 2009.

References

Baskes, MI. 1992. *Modified Embedded-Atom Potentials for Cubic Materials and Impurities*. Phys Rev B 46:2727.

Baskes, MI. *Modified Embedded-Atom Potentials for Fe*. Unpublished.

Blöchl, PE. 1994. *Projector Augmented-Wave Method*. Phys Rev B 50:17953.

E, W and Engquist, B. 2003. *Multiscale Modeling and Computation*. Notices of the AMS 50:1062-1070.

Horstemeyer, M and Wang, P. 2003. *Cradle-to-Grave Simulation-Based Design Incorporating Multiscale Microstructure-Property Modeling: Reinvigorating Design with Science*. J Comput Aided Mater Des 10:13-34.

International Iron & Steel Institute. *Advanced High Strength Steel (AHSS) Application Guidelines*. September 2006.

Kim, SG; Horstemeyer, MF; Baskes, MI; Rais-Rohani, M; Kim, S; Jelinek, B; Houze, J; Moitra, A; and Liyanage, L. 2009. *Semi-Empirical Potential Methods for Atomistic Simulations of Metals and Their Construction Procedures*. J Eng Mater Technol 131(4):041210 [9 pages].

Kim, SG; Horstemeyer, MF; German, R; Rhee, H; and Kim, S. 2007. *Task 2: Materials Design for Steel Alloys*. DOE FY 2006-2007 Annual Report, Chap. 4. p. 52-62.

Kresse, G and Furthmüller, J. 1996. *Efficient Iterative Schemes for Ab Initio Total-Energy Calculations Using a Plane-Wave Basis Set*. Phys Rev B 54:11169.

Li, Y; Siegel, DJ; Adams, JB; and Liu, WY. 2003. *Embedded-Atom-Method Tantalum Potential Developed by the Force-Matching Method*. Phys Rev B 67:125101.

Mendelev, MI; Han, S; Srolovitz, DJ; Ackland, GJ; Sun, DY; and Asta, M. 2003. *Development of New Interatomic Potentials Appropriate for Crystalline and Liquid Iron*. Phil Mag 83:3977.

Olson, G. 1998. *Systems Design of Hierarchically Structured Materials: Advanced Steels*. J Comput Aided Mater Des 4:143-156.

Osetsky, YN and Bacon, DJ. 2003. *An Atomic-Level Model for Studying the Dynamics of Edge Dislocations in Metals*. Modeling Simul Mater Sci Eng 11:427-46.

Perdew, JP; Burke, K; and Ernzerhof, M. 1996. *Generalized Gradient Approximation Made Simple*. Phys Rev Lett 77:3865.

Perdew, JP and Zunger, A. 1981. *Self-Interaction Correction to Density-Functional Approximations for Many-Electron Systems*. Phys Rev B 23:5048.

V. Nonlinear Strain Paths Project

Project Investigator: Thomas B. Stoughton, Ph.D.
General Motors Corporation
GM Research & Development Center, MC 480-106-359
30500 Mound Road
Warren, MI 48090-9055
(586) 986-0630; e-mail: thomas.b.stoughton@gm.com

Project Investigator: Cedric Xia, Ph.D.
Ford Motor Company, Mail Drop 3135 - RIC
Research and Advanced Engineering Laboratory
P.O. Box 2053
Dearborn, MI 48121-2053
(313) 845-2322; e-mail: zxia@ford.com

Project Investigator: Chang-Qing Du, Ph.D.
Chrysler Corporation
ASME Stamping Technology Center, CIMS 482-60-05
800 Chrysler Drive
Auburn Hills, MI 48326
(248) 576-5197; e-mail: cd4@chrysler.com

Project Technical Administrator: Manish Mehta, Ph.D.
National Center for Manufacturing Sciences
3025 Boardwalk
Ann Arbor, MI 48108-3266
(734) 995-4938; e-mail: manishm@ncms.org

Technology Area Development Manager: William Joost
(202) 287-6020; e-mail: joseph.carpenter@ee.doe.gov

Field Technical Manager: Philip S. Sklad
(865) 574-5069; e-mail: skladps@ornl.gov

Contractor: U.S. Automotive Materials Partnership
Contract No.: DE-FC05-02OR22910

Objective

- The project aims to deliver a comprehensive set of experimental data and associated predictive models for the Advanced High-Strength Steels (AHSS) under nonlinear strain path deformations. The models include constitutive behavior, forming limit and fracture criteria for stamping/hydroforming simulations and vehicle crashworthiness simulations.
- In the ultimate application of this technology, the developed and validated models will (a) Enable efficient vehicle design for more weight reduction opportunities to take advantage of the rapid hardening behavior of AHSS; and (b) Enable the acceleration of AHSS usage by reducing the cost and time for AHSS manufacturing.

Approach

- The collaborating partners include Chrysler Group LLC , Ford Motor Company, General Motors Company, US Steel and ArcelorMittal Steel, and over its 36-month duration, up to a dozen test laboratories, finite element modeling (FEM) software vendors and stamping technology vendors, all facilitated and coordinated by the National Center for Manufacturing Sciences (NCMS) which serves as Technical Project Administrator. The project team will consult as needed with experimental researchers and metallurgists at the National Institute of Standards and Technology (NIST).
- This project seeks to develop, validate and implement a set of predictive models including constitutive behavior, forming limits and fracture criteria for vehicle manufacturing and performance simulations. The approach is to first identify the gaps between prediction and experiment under nonlinear deformation conditions; and then quantify the effect under the variations of deformation conditions encountered through the life of automotive sheet metal products from the stamping plant to the vehicle services. Based on the correlation results, the project will identify the best available advanced constitutive, forming limits and fracture models applicable to nonlinear deformation of sheet steels. The best models from the validation will then be implemented in production software for stamping and crashworthiness.
- The project has three major tasks, each involving an order of magnitude increase in the test matrix compared to linear testing requirements. Data collection tasks will take full advantage of recent advances in Digital Image Correlation (DIC) technology in the experiments. DIC is an optical method that employs tracking & image registration techniques for accurate 2D and 3D measurements of deformations, displacement and strain from the digital images.
- The LS-DYNA engineering package was the team's reference modeling package for demonstrating and evaluating new technology advances and material models resulting from the characterization of nonlinear strain paths in AHSS.
- The main project deliverables include:
 1. A comprehensive database of orientation-dependent uniaxial tension behavior for yield, transient hardening and fracture under uniaxial and equi-biaxial pre-straining.
 2. A comprehensive database of biaxial transient hardening behavior under continuous strain path change conditions.
 3. A transient hardening model validated from experimental data and implemented in production software LS-DYNA for stamping and crash simulations.

Accomplishments

- The team held its Kickoff Meeting on September 29, 2009 to to formally execute the Statement of Work, beginning with development of consensus approaches for designing and refining experimental techniques. A top priority is to develop a Request for Proposal document for soliciting quotes from material test vendors.
- Other accomplishments will be reported in future progress reports.

Future Direction

- Accompanying the technology development, a benefit analysis will also be performed to estimate the weight-save potential of anticipated technology advances in stamping and crash simulation models.

Introduction

The project aims to deliver a comprehensive set of experimental data and associated predictive models for the Advanced High-Strength Steels (AHSS) under nonlinear strain path deformations. The models include constitutive behavior, forming limit and fracture criteria for stamping/hydroforming simulations and vehicle crashworthiness simulations. The materials of focus are DP600 and DP780 grades, with DDQ and BH210 as baseline comparisons. Exploratory work will also be done on DP980 and TRIP780 grades.

The developed and validated models will (1) enable efficient vehicle design for more weight reduction opportunities to take advantage of the rapid hardening behavior of AHSS; and (2) enable the acceleration of AHSS usage by reducing the cost and time for AHSS manufacturing.

Current product performance simulations such as crashworthiness generally assume that the vehicle body parts are un-deformed at the start of the simulation with a uniform thickness for a given part. However, in reality they already underwent significant deformation during stamping/hydroforming and were also bake-hardened during the paint process in case of dual-phase steels and BH steels. Consequently, the steel parts will not be responding the same way as if they were still virgin materials due to the strain hardening and bake hardening of the material and non-uniform thickness distribution resulted from forming. Furthermore, the deformation paths will generally have abrupt changes from that during stamping. It is, thus, critical to incorporate the prior manufacturing effects such as forming and bake-hardening into product performance simulations with reliable constitutive and fracture models.

This project seeks to develop, validate and implement a set of predictive models including constitutive behavior, forming limits and fracture criteria for vehicle manufacturing and performance simulations. The approach is to first identify the gaps between prediction and experiment under nonlinear deformation conditions; and then quantify the effect under the variations of deformation conditions encountered through the life of automotive sheet metal products from the stamping plant to the vehicle services. Based on the correlation results, the project will identify the best available advanced constitutive, forming limits and fracture models applicable to nonlinear deformation of sheet steels. The best models from the validation will then be implemented in production software for stamping and crashworthiness.

W. Lightweight Front Suspension

Principal Investigator: Bart DePompolo
United States Steel Corporation
Automotive Product Technology
5850 New King Court
Troy, Michigan 48090
(248) 267-2756; e-mail: badepompolo@uss.com

Principal Investigator: Rich Salmon
General Motors Corporation
BFO Control Arms & Lateral Links
30001 Van Dyke Avenue
Warren, Michigan 48090
(586) 492-3814; e-mail: richard.j.salmon@gm.com

Technology Area Development Manager: William Joost
(202) 287-6020; e-mail: william.joost@ee.doe.gov

Contractor: U.S. Automotive Materials Partnership
Contract No.: DE-FC26-02OR22910

Objective

The project objective is to develop cost effective designs and manufacturing processes to enable light weight as-formed steel front lower control arm (sheet and forged alternatives) for a MacPherson Strut suspension system that meet the following criteria without adversely impacting performance.

- Structural performance equivalent to the current production (baseline) aluminum front lower control arm(LCA).
- Mass equivalent to the forged aluminum baseline LCA.
- Cost at 30% less than the forged aluminum baseline LCA.
- Must meet available package constraints.
- Complete technical assessment of suspension corrosion requirements and performance.

Approach

The team will design two steel Lower Control Arms to meet the general requirements of the MacPherson front suspension package of the baseline vehicle. The two solutions will be a sheet steel solution and a forged steel solution with attached ball joints. The designs must include:

- FE and CAD models that are readable in Catia and UG.
- Complete static and dynamic load analysis and performance assessment.
- Complete cost estimate of current production aluminum and steel solutions for production volumes of 30,000, 100,000, and 250,000 vehicles/year for six years.
- Progress and final reports as required by USAMP and A/SP.

Milestone, Metrics and Accomplishments

The project officially started on August 4, 2009 and has progressed rapidly with the following milestones.

- Request for quotes were submitted, compiled and reviewed on August 4, 2009.
- Vendor selection was completed on August 12th. The Project Team awarded the bid to Multimatic, which demonstrated a superior proposal with respect to meeting program deliverables, cost and in-kind cost contribution.
- Supplier kick-off meeting was held on September 14, 2009. The Project Team and Multimatic reviewed the project objectives and addressed open issues raised by the team and the supplier.
- An Initial Concept Review meeting with the supplier was held on October 13, 2009. Multimatic summarized input data and provided some preliminary designs concepts.
- A Design Review meeting was held on November 11, 2009.

Future Direction

The project will be meeting monthly with the supplier (see meeting schedule below) to review progress, identify issues and initiate corrective actions to make sure that the final control arm designs meet the project objectives.

- December: Design approval
- January: Final design review
- February: Close Project

The Project Team is compiling competitive data from the A/SP Benchmarking Project Team's A2MAC1 database to determine an industry baseline for lightweight control arm design comparison. The database will also be used to determine if there is justification for like programs on other suspension components.

Introduction

The American Iron and Steel Institute (AISI) and the Auto-Steel Partnership (A/SP) have completed numerous demonstration projects in the automotive body-in-white system that routinely show at least 25% weight savings with the use of AHSS when compared to traditional steel designs. As important as weight savings is in the automotive body and closures, weight savings in the chassis and suspension systems is just as valuable. In fact the reduction of unsprung mass benefits both the fuel efficiency and vehicle handling characteristics.

The purpose of this six month project is to develop steel intensive front lower control arm (FLCA) designs (one in sheet steel and one in bar steel) that meet the mass and performance of the base-line forged aluminum design at 30% less cost, and offer significant weight reduction when compared to traditional steel and cast iron designs.

Discussion

Today's automotive suspension structures revolve around architectures and materials that have been in use for many years. Unlike body structures, little work has been undertaken to optimize the mass and performance of steel suspension structures/components through the use of advanced high strength steels and the use of new design and manufacturing concepts. For this reason, the Auto/Steel Partnership (A/SP) has formed the Lightweight Front Suspension Team. This initial project, developed by the team, is to develop two lightweight steel intensive FLCA designs.



Figure 1. Chevy Malibu Forged Aluminum Front Lower Control Arm.

The baseline FLCA design is the current production Chevrolet Malibu/Buick Lacrosse aluminum cast/forged component design, see Figure 1. The concept study will develop innovative steel designs, with sufficient use of leading edge technology to achieve the greatest mass reduction while obtaining manufacturing feasibility. The design must provide efficient cost, weight and performance solutions using new steel technologies.

The current Chevy Malibu /Buick Lacrosse control arm is a challenging baseline component as it is one of the lightest weight designs as shown in the benchmarking study (Figure 2).

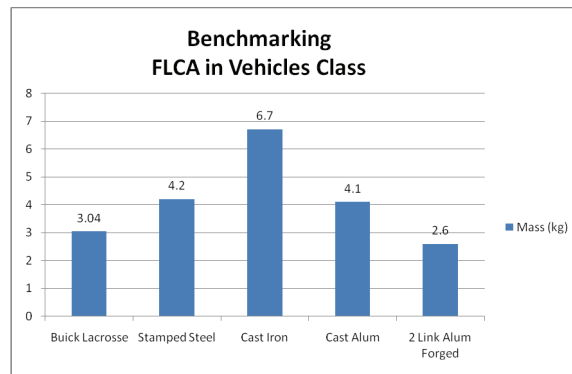


Figure 2. Front Lower Control Arm Benchmarking Study.

The Project is structured in three phases, which consist of design, cost estimating and technology transfer.

Phase 1: Design Optimization. Through a clean sheet redesign, the goal is to obtain two steel intensive designs and design iterations: one using sheet steel and the other bar steel (forged). While these steel intensive designs will not be designed to meet the requirements of the specific vehicle, the methodology and principles must be robust enough to be applicable across the family of mid-size vehicles.

Phase 2: Cost Estimate: The successful supplier must provide a cost estimate of the baseline design and both steel solutions.

Phase 3: Communications. The goal is to transfer the technology developed in the Project to OEM and Tier 1 chassis/suspension structure designers.

Phase 1: Design Optimization Status

The project officially started on August 4, 2009. A request for quotes was solicited to identify vendors capable of designing, modeling, estimating manufacturing costs and predicting corrosion behavior for stamped and forged steel FLCA designs. Eight quotes were reviewed on August 12, 2009 followed by vendor selection. Multimatic was selected as the best vendor capable of meeting the stringent team requirements.

A vendor kick-off meeting was held on September 14, 2009 where the project timing and schedule were established. On October 13, 2009 the Project team met with Mulitmatic to review initial design concepts, identify any issues and confirm design and performance targets. The team also reviewed competitive control arm designs and concluded that the program objectives of creating steel control arms of equivalent weight and less cost than forged aluminum control arms were reasonable.

On November 11, 2009 the team met with Multimatic to review the initial stamped and forged steel control arm designs. The preliminary designs, based on current component performance requirements, were close to target the 1.942 kg and indicate that the weight target is reasonable. Additional design iterations to the refine the models are needed and will be reviewed in December.

Phase 2: Cost Estimate Status

This phase is scheduled for January, 2010.

Phase 3: Communications Status

This phase is scheduled for February, 2010.

Conclusions

Initial design direction has been established as of the writing of this report. The initial design review, combined with an in-depth analysis of existing front lower control arms contained within the A2MAC1 database, conducted by the University of Michigan's Transportation Department, suggests that the project objectives to produce stamped and forged steel control arms that are of equivalent weight and lower cost to aluminum forgings are achievable. Remaining work is to finalize the design, estimate the manufacturing costs and complete the corrosion assessment.

Presentations, Publications and Patents

Bart DePompolo, USS "Lightweight Suspension" *Presented at the 2009 DOE Project Review Meeting on October 28, 2009 in Southfield, Michigan*

X. Precision Flow Form Application Development

Principal Investigator: Todd Cleaver
Tech Knowledge
29415 East River Road
Grosse Ile, Michigan 48138
(734) 675-5562; e-mail: Todd@TechKnowledgeAMD.com

Technology Area Development Manager: William Joost
(202) 287-6020; fax: (202) 586-2476; e-mail: william.joost@ee.doe.gov

Contractor: U.S. Automotive Materials Partnership
Contract No.: DE-FC26-02OR22910

Objectives

The objective of this project is to develop and demonstrate the Precision Flow Form Process of forming steel components to replace cast iron components, reducing weight by over 50% with equal or reduced manufacturing costs and significantly reduced tooling costs. The target component is a differential case housing.

Approach

Designed experiments will focus on developing the precision flow forming of distortion free, functional cases and on a distortion free welding process. The statement of work contains 9 tasks and three gates:

- Launch and define metrics of success and test criteria to prove the concept.
- Design differential case and tooling and perform finite element analyses to assure a quality product.
- Build tools.
- Acquire materials including differential case components (gears, washers, pins, etc.).
- Develop precision flow form process and conduct designed experiments to result in distortion free functional components.
- Develop distortion free welding process.
- Assemble precision flow formed cases with new welding process.
- Validate the new cases successfully meet test criteria.
- Information dissemination and reporting.

It is planned to do the development work at Linamar, a recognized leader in the application of flow form technology in North America and a supplier of differential cases as well. They have excellent state-of-the-art development and tooling facilities in Guelph, Ontario ideal for this project.

Milestone, Metrics and Accomplishments

Milestones:

- Gate 1: Based on the completed FEA and designs, is success achievable?
- Gate 2: Are distortion free flow formed differential case sets suitable for welding and validation testing?
- Gate 3: Is a suitable distortion free weld process available to successfully assemble the differential cases?

Metrics:

- The team is defining the metrics of success and gate metrics as part of Task 1.

Accomplishments:

- The project Kick-Off meeting occurred September 22, 2009. Thirteen companies were represented at the kick-off, as well as, representatives of the American Iron and Steel Institute.

Future Direction

The team will execute the statement of work with the intent of achieving each gate. The immediate task is the definition of metrics of success and test criteria for each gate and to prove the concept.

Introduction

Flow forming is one of several types of metal spinning techniques used to produce round sheet metal products. Metal spinning has been known and evolving for centuries. All metal spinning processes use the same basic tools to shape metal. These tools include: a lathe-type spinning machine, rollers and a mandrel.

The work piece, or blank, is normally a flat metal disc or pre-form that is clamped between the mandrel and the machine's tail stock. Rollers are used to apply pressure to the rotating blank forcing it, in successive passes, to take the shape of the mandrel which is made to the inside dimensions of the part.

Flow forming, a more recent advancement in the technology, elevates metal spinning to a higher plateau. It differs dramatically from other types of spinning in that, rather than shaping the metal by bending or compressing it, the metal is shaped by being forced to flow along the mandrel. Because of the high forming pressures involved, temperatures at the roller-work piece interface typically are 1000 degrees Fahrenheit or higher, causing the metal to soften and flow; hence the name flow forming. Because the process changes the structure of the metal, drastic reductions in wall thickness can be achieved along with very fine accuracy.

In recent years, CNC (computer numerical control) technology has increased the uses of flow forming for many of the reasons that made it attractive for machining centers. Closed-loop control of the forming forces yields closer tolerances, consistent repeatability and more complex forming geometries than those available previously.

Virtually any ductile metal may be flow formed, from aluminum or stainless steel, to high-strength, high-temperature alloys. Work hardening of the metal during flow forming refines and elongates grain structure of the work piece, resulting in increases in tensile and yield strengths

and hardness. Thus stronger, lighter-weight designs can be produced with less material, and in some cases with the substitution of lower cost materials. By controlling the roller tool configuration and feed rate, surface finishes as fine as 6 micro inches are possible. This can completely eliminate the need for costly secondary finishing operations.

Flow forming has been used successfully in the auto industry to produce clutch components with weight and cost advantages. Significant cost and weight opportunities can be achieved in other components as well, such as differential cases, if it can be demonstrated that the flow forming technology can deliver close tolerances with steel blanks of thicknesses over 10mm (current state-of-the-art.). The combination of recent improvements in machine and control capabilities coupled with new control strategies and roller designs may deliver differential cases at net shape with weight savings of over 50% at a net cost savings as compared to the current cast iron.

This proposed project is structured to develop the new Precision Flow Form Process (PFF) and demonstrate that weight savings can be achieved. The weight savings will result from:

- The work hardened steel of the PFF process is much stronger than the cast iron resulting in thinner cross sections.
- The cast iron case has both thin and thick sections because of castability requirements whereas the PFF case can be of more uniform thickness throughout.
- The weldability of the PFF steel components eliminates the large flanges required for bolting in the cast iron version. (This would eliminate the weight of the high strength bolts as well.).
- A study will be included to determine the potential manufacturing cost benefits in both operating and tooling costs. The cost savings offsets to the forming process costs result from:
- Far less machining will be required with the PFF process because it is a precision net-shape component especially on the mandrel surface. The cast iron design requires significant internal surface machining with unique, expensive tooling.
- There will be no threaded holes in the flanges to machine because the PFF design will be welded.
- The cost of mandrels and rollers is much less than casting tooling and much quicker to manufacture and launch.
- Other benefits to the PFF process versus the cast iron process include:
- Less steel off-all generated versus cast gates, runners and risers (less material to recycle).
- Less machining chips and supporting coolant and chip handling.
- Less machining facilities and tooling.
- Net shape and consistent wall thickness improves housing balance and improves NVH
- Higher strength of steel material potentially allows for same torque in smaller package.

American Iron and Steel Institute (AISI) and Ford have done concept feasibility work on the PFF technology for a heavy duty F series truck application. The study associated with this work indicated an estimated weight savings for the differential case of 59% in a bolted design (direct replacement for the cast design). In a welded design the weight savings would have been even higher and a half pound of bolts could have been eliminated as well. In addition, the potential existed to reduce the package size to deliver the same torque or increase the torque in the same package size.

This initial attempt identified some hurdles to be overcome. The Ford heavy duty F series application used a high strength steel and with the added work hardening and flowing of metal to the flange, the material became too brittle and failed at that area. The anticipated design for this project will be with milder steel and no heavy bolted flange, so this issue should not reoccur. The excessive work to move material to the flange end also resulted in high internal stresses which resulted in some distortion during the machining of openings in the case. These stresses should be significantly reduced in the proposed design.

Main Section

As the project kicked off on September 22, 2009, there are no findings to report. The team is currently defining the metrics of success and test criteria for successful passage of project gates and final validation of the PFF concept.

Conclusions

The project has been launched successfully and conclusions will be reported as the project progresses.

Presentations/Publications/Patents

Kami Buchholz, writer, "Steely Visions of Lightweight Parts" *Published in Automotive Engineering International, October 2009*